Dynamics of synapse function during postnatal development and homeostatic plasticity in central neurons

Kevin Fu-Hsiang Lee

Thesis submitted to the
Faculty of Graduate and Postdoctoral Studies
in partial fulfillment of the requirements
for the Doctorate in Philosophy in Neuroscience

Department of Cellular & Molecular Medicine

Faculty of Medicine

University of Ottawa

Table of Contents

Page	Title
ix	**Acknowledgments**
xii	**Abstract**
xv	**Copyright Authorizations**
1	**General Introduction**
7	Excitatory synapses are formed on dendritic spines at principal cells of the brain
15	Hebbian synaptic plasticity
19	Homeostatic synaptic plasticity
23	Dendrites exhibit cable properties and passively filter synaptic potentials
25	Active dendrites and neuronal information processing
29	Neural connectivity: structure relates to function at multiple spatial scales
32	Postnatal development and the functional organization of synaptic connectivity
36	**Preface to Manuscripts**
	Manuscripts
37	Manuscript I – Examining form and function of dendritic spines
55	Manuscript II – Differential subcellular targeting of glutamate receptor subtypes during homeostatic synaptic plasticity
94	Manuscript III – Tuning into diversity of homeostatic synaptic plasticity
114	Manuscript IV – A unique mechanism of NMDA spike initiation supports a distinct role in synaptic input integration
121	Manuscript V – Spatiotemporal transformations of local calcium dynamics during clustered synapse development
155	**General Discussion**
167	**Concluding Remarks**
168	**References**

Page Title

Appendices

188 Appendix A – An iterative test for multiplicative scaling

Instructions and analysis codes for use in MATLAB

189 Appendix B – Analysis work-flow for frame scan calcium imaging

i. Identifying regions of interest (ROIs)
ii. Data extraction using ImageJ
iii. Data processing using MATLAB

194 Appendix C – Analysis work-flow for line scan calcium imaging

Instructions and analysis codes for use in MATLAB

202 Appendix D – Synaptic weight clustering analysis

Analysis codes written for use in MATLAB

i. Fraction of silent synapses analysis (segment strength)
ii. Synaptic weight variance analysis (weight variability)
iii. Synaptic weight-matching analysis (spatial bounds)

218 Appendix E – Modeling synapse development in computer simulations

i. A Markov chain model
ii. A spiking neuron model

245 Appendix F – Integrate-and-fire model of STDP

i. Course report for NSC8104 (Computational Neuroscience)
ii. MATLAB code for integrate-and-fire model of STDP

278 Appendix G – Supplemental Data for Manuscript V

i. Supplemental Figures
ii. Supplemental Experimental Procedures

List of Figures

Page

44 Biochemical compartmentalization in dendritic spines

53 Dissociation of spine size and synaptic strength

68 Multiplicative scaling of CA1 pyramidal neurons in response to prolonged TTX treatment

70 Recruitment of higher conductance synaptic AMPARs following prolonged TTX treatment

71 Increased surface expression of GluA1 and the emergence of inwardly rectifying AMPARs at SC-synapses following prolonged TTX treatment

74 Synaptic incorporation of GluA2-lacking AMPARs in CA1 pyramidal neurons following prolonged TTX treatment

79 Homeostatic upregulation of surface NMDARs in CA1 pyramidal neurons in response to prolonged TTX treatment

81 Homeostatic shift in synaptic NMDAR subunit composition in response to prolonged TTX treatment

83 Cell-wide homeostatic upregulation of GluA2-lacking AMPARs in response to prolonged TTX treatment

87 GluN2A-NMDARs are specifically targeted to synapses in response to prolonged TTX treatment

88 Differential subcellular targeting of glutamate receptor subtypes during HSP

101 Diversity of Homeostatic Synaptic Plasticity (HSP)

128 2P imaging of synaptic calcium signals during postnatal development

131 2P glutamate uncaging at individual dendritic spines triggers regenerative dendritic calcium signals during early postnatal development

133 Pharmacological dissection of synaptic calcium signal propagation

135 Calcium release from intracellular stores is a major determinant of NMDAR-dependent calcium kinetics at developing dendritic spines

138 Effect of spine morphology on calcium propagation

140 NMDAR-dependent CICR encodes spatiotemporal features of synaptic inputs

145 Clustered synaptic weights during synapse development

List of Appendix Figures

Page

Appendix E – Modeling Synapse Development

219 The dendritic space

220 The local spatial influence

221 Validating the developmental trajectory of the model with experimental data

222 P-value matrix, simulated data compared to experimental data

224 Poisson inputs delivered to the spiking neuron model

225 Graded influence of backpropagating action potentials (bAP) along the proximal-distal axis of the model neuron

226 The local plasticity signal along dendrites

227 Spiking model synapse development parameter space

228 Dynamic behaviour of the spiking neuron model

229 Evolution of synaptic weights under different plasticity parameters

230 Comparing overall synaptic weight distributions between experiment and model at a developmental epoch of 20% silent synapses

231 The clustering index

232 The clustering index comparison between experiment and model

Appendix F – Integrate-and-fire model of spike-timing dependent plasticity

251 Dynamic membrane voltage fluctuations and action potential discharge in an Integrate-and-Fire (IF) neuron model

253 Spike-timing dependent plasticity synaptic modification rule

257 STDP induces synaptic competition and generates stable bimodal distributions of synaptic weights

257 Initial attempts at replicating the model of Song et al. (2000) failed

259 Initial attempts at replicating the model of Song et al. (2000) failed

260 Success in replicating the core STDP model of Song et al. (2000)

262 Success in replicating the core STDP model of Song et al. (2000)

Appendix G – Supplemental Data for Manuscript V

278 Spinogenesis and synapse development during the second and third postnatal weeks

280 Two-photon (2P) glutamate uncaging and calcium imaging

283 Spatial spread of calcium signals originating at dendritic spines

285 Summary data (mean ± SEM) for spine calcium transients recorded in CPA (>1 hr pretreatment)

287 The relationship between spine morphology and spine calcium behaviour

289 Activation of NMDAR-mediated CICR by spatially-clustered glutamate uncaging and spike-pairing at young dendrites

290 Probing the functional development of dendritic spines by measure AMPA/NMDA ratios with 2P glutamate uncaging

List of Abbreviations

2P	two photon
AMPA	α-amino-3-hydroxy-5-methyl-4-isoxazolepropionic acid
APV	2-amino-5-phosphonopentanoic acid
ATP	adenosine triphosphate
bAP	back-propagating action potential
CA1, CA3	Cornu Ammonis areas 1 and 3 of the hippocampus
CaM	calmodulin
CaMKII/IV	calcium/calmodulin-dependent kinase II
CNQX	6-cyano-7-nitroquinoxaline
CPA	cyclopiazonic acid
CTL	control
CICR	calcium-induced calcium release
DIC	differential interference contrast
EPSP	excitatory postsynaptic potential
EPSC	excitatory postsynaptic current
eEPSC	evoked EPSC
ER	endoplasmic reticulum
eYFP	enhanced yellow fluorescent protein
FRAP	fluorescence recovery after photobleaching
FWHM	full-width at half maximum
GABA	γ-amino butyric acid
GDP	giant depolarizing potential
GFP	green fluorescent protein
GluA(1-4)	AMPA receptor subunit 1-4
GluN(1-2)	NMDA receptor subunit 1-2
GPCR	G-protein coupled receptor

GTP	guanosine triphosphate
HSP	homeostatic synaptic plasticity
IV	current-voltage
LGN	lateral geniculate nucleus of the thalamus
LTP	long term potentiation
LTD	long term depression
MCPG	α-methyl-4-carboxyphenylglycine
mEPSC	miniature EPSC, ‘minis’
NBQX	2,3-dioxo-6-nitro-1,2,3,4-tetrahydrobenzo[f]quinoxaline-7-sulfonamide
NMDA	N-methyl-D-aspartate
NMJ	neuromuscular junction
PKA	protein kinase A
PMCA	plasma membrane calcium ATPase
PP1	protein phosphatase 1
PSD	postsynaptic density
sEPSC	spontaneous EPSC
SERCA	smooth endoplasmic reticulum calcium ATPase
STDP	spike timing dependent plasticity
TBOA	threo-β-Benzyloxyaspartic acid
TeTX	tetanus toxin light chain
TTX	tetrodotoxin
VGCC	voltage-gated calcium channel
VGSC	voltage-gated sodium channel
WT	wild-type

Acknowledgments

Over the past six years, I have been fortunate to have the freedom to exercise creativity and ingenuity to navigate the global scientific enterprise using cutting-edge technologies, investigating what I believe to be one of the most intriguing topics in biology today – the brain. More importantly, the richness of my experiences in these past years extends beyond mere academic inquiries. Akin to wandering the woods in wonder of the majesty of nature, exploring new cities and meeting interesting people, or becoming captivated by the plot of a great novel, for me, graduate school has been one fantastic adventure. Certainly, my development as a writer and speaker and my accumulation of scientific knowledge are all important treasures that I have gained, but I have learned many less discernable, though intrinsically important, lessons along the way. The challenges were often daunting, the road was rocky and my footing was often uncertain, as experimental plans were under almost perpetual change. These experiences made me acutely aware of my strengths and weaknesses and, importantly, summoned a drive to persevere and perpetually strive toward self-improvement. The collective abrasion of these tribulations have honed, polished and sharpened my capacities as an attentive student of life in the world. Today, I am endowed with a sense of holistic accomplishment and fulfillment, and I am inclined to believe that there are few other opportunities that could have offered me this.

It is only partially tongue-in-cheek in saying that I would not be here without my parents, Felix and Amy. They have provided me with an incredibly supportive and loving childhood, and instilled in me the value of education. As I progressed through primary and secondary school and entered university, they offered the utmost support and guidance, and to this day, are steadfast in expressing their pride in my accomplishments. My parents have selflessly devoted themselves to creating a better life, generating greater opportunities, for me and my siblings than they

themselves had, and I intend to carry forward these same values and goals if one day I am blessed with the responsibilities of parenthood. My parents have equipped me with all the tools, road maps, and physical and mental nutrition to thrive, and all of it was delivered with the warmest love a son could ever fathom – and I love and thank them for that. As a big brother, I have learned many intangibles that have powerfully shaped who I am today. My siblings, Karah, Kasha and Kurtis have challenged me in the most important ways through the most important years of my personal growth and development, and I am thankful to know that they will always be my strongest pillars of support.

I am forever grateful to Dr. Jean-Claude Béïque for extending to me the unique opportunity to be his first graduate student and trainee. It is most terrifying to recall that our first encounter was a spontaneous conversation at lunch during the Faculty of Medicine's graduate recruitment day in February 2009 – had either of us chosen different seats, I likely would not be writing these words today. Dr. Béïque is a great mentor and a source of immense inspiration. He encourages a culture of free thought and creativity, thereby fostering an environment suited to the genesis of ideas, big and small, to which I owe much of my intellectual development. Dr. Béïque's inclination to camaraderie and friendship is perhaps one of the key ingredients to the jovial and enjoyable environment of the laboratory. I have always admired, and have been utterly amazed at, how relaxed he can be, never hesitating to take the time to exchange stories and laughs despite looming deadlines and an ever mounting workload. This is a personality trait that has illuminated important perspective when I encountered my own difficult and busy times. I do not hesitate to contend that few students are as fortunate to have a mentor and role model as great as Jean-Claude Béïque.

Finally, it is with deep appreciation that I salute my friends and colleagues in the lab – in particular, Cary Soares, who also joined the lab in 2009. Cary is a great scientist, ardent thinker and above all, a great friend. It has been a remarkable collaborative scientific experience over the years – I like to imagine that we had our very own 'Hodgkin and Huxley' or 'Neher and Sakmann' dynamic in the lab. Perhaps the most valuable spinoff from our relationship in the lab is the incredible network of friends we have established together outside the lab. Undoubtedly, one's social support system is integral for maintaining a healthy balance of work and play, and I am fortunate to know that I will continue to cherish the stabilizing weight of these friendships in balance of my academic career for many years to come.

Finally, I should acknowledge the Canadian Institutes of Health Research (CIHR) for Master's Award funding and the Ontario Ministry of Training, Colleges and Universities for scholarship support through the completion of my doctoral studies via the Ontario Graduate Scholarships (OGS) and Queen Elizabeth II Graduate Scholarships in Science and Technology (QEIISST) programs. These government sponsored studentships are of the utmost importance in cultivating innovation in Canada's centers for higher learning. Although these public investments, to some, may appear to have intangible returns during difficult fiscal times, I urge policy makers and public leaders to have the wisdom and vision to recognize that these relatively small investments are indispensable for supporting the intrinsic utilitarian goodness in driving intellectual advancement.

Abstract

The majority of fast excitatory neurotransmission in the brain occurs at glutamatergic synapses. The extensive dendritic arborisations of pyramidal neurons in the neocortex and hippocampus harbor thousands of synaptic connections, each formed on tiny protrusions called dendritic spines. Spine synapses are rapidly established during early postnatal development – a key period in neural circuit assembly – and are subject to dynamic activity-dependent plasticity mechanisms that are believed to underlie neural information storage and processing for learning and memory. Recent decades have seen remarkable progress in identifying diverse plasticity mechanisms responsible for regulating synapse structure and function, and in understanding the processes underlying computation of synaptic inputs in the dendrites of individual neurons. These advances have strengthened our understanding of the biological mechanisms underlying brain function but, not surprisingly, they have also raised many new questions. Using a combination of whole-cell electrophysiology, 2-photon imaging and glutamate uncaging in rodent brain slice preparations, I have helped to document the subtype-specific regulation of glutamate receptors during a homeostatic form of synaptic plasticity at CA1 pyramidal neurons of the hippocampus, and have discovered novel synaptic calcium dynamics during a critical period of neural circuit formation. First, we found that during a homeostatic response to prolonged inactivity, both AMPA and NMDA subtypes of glutamate receptors undergo a switch in subunit composition at synapses, but exhibit a divergence in their subcellular localization at extrasynaptic regions of the plasma membrane (this work was published in the Journal of Neuroscience in 2013). In separate series of experiments using 2-photon calcium imaging, I discovered a functional coupling between NMDA receptor activation and intracellular calcium release at dendritic spines and dendrites that is selectively expressed during a critical period of synapse formation. This synaptic calcium

signaling mechanism enabled the transformation of distinct spatiotemporal patterns of synaptic input into salient biochemical signals, and is thus apt to locally regulate synapse development along individual dendritic branches. Consistent with this hypothesis, I found evidence for non-random clustering of synapse development between neighboring dendritic spines. Together, these experimental results expand the current understanding of the dynamics of synapse function during homeostatic plasticity and early postnatal development.

Les synapses glutamatergiques soutiennent la majorité de la neurotransmission excitatrice rapide du cerveau. Des milliers de ces synapses, localisées sur de minuscules saillies appelées épines dendritiques, décorent les vastes arborisations dendritiques des neurones pyramidaux du néocortex et de l'hippocampe. Ces synapses sont formées tôt lors du développement postnatal et sont soumises à des mécanismes dynamiques de plasticité qui sous-tendent, croit-on, les capacités d'apprentissage et de mémoire du cerveau. Les dernières décennies ont vu des progrès remarquables dans l'identification de divers mécanismes de régulation de la structure et de la fonction des synapses sur différentes échelles de temps, et dans la compréhension des processus qui régissent l'intégration des inputs synaptiques au niveau des dendrites individuelles. Ces progrès ont renforcé notre compréhension des éléments fondamentaux régissant la fonction cérébrale et ont ouvert de nouvelles voies d'investigations neurophysiologiques. En utilisant une combinaison d'électrophysiologie cellulaire, d'imagerie à deux-photons et de photolibération de glutamate sur des neurones pyramidaux de la région CA1 de l'hippocampe de rats, j'ai contribué à la découverte et à la caractérisation de nouvelles régulations des récepteurs du glutamate durant la plasticité synaptique homéostatique. J'ai également découvert un nouveau type de dynamique de calcium synaptique relié à une organisation spatiale du développement des synapses pendant

une période critique de l'ontogénie des circuits neuronaux. Dans la première étude, nous avons constaté que lors d'une plasticité de type homéostatique induite par une inactivité prolongée, les récepteurs de glutamate de types AMPA et NMDA sont soumis à un changement important dans la composition de leurs sous-unités. De plus, nous avons observé un ciblage différentiel de ces récepteurs vers des compartiments subcellulaires spécifiques des neurones. Dans une série d'expériences séparée utilisant l'imagerie calcique à deux-photons, j'ai découvert un couplage fonctionnel durant le développent entre l'activation des récepteurs NMDA et une libération de calcium intracellulaire qui envahit tant les épines dendritiques que les dendrites. J'ai également trouvé que ce mécanisme de signalisation de calcium synaptique transforme des motifs spatiotemporels d'activités synaptiques spécifiques en signaux biochimiques post-synaptiques de manière à potentiellement réguler l'organisation spatiale des synapses durant le développement. Conformément à cette hypothèse, j'ai observé des manifestations fonctionnelles claires de regroupement dans l'espace de synapses de forces similaires le long de branches dendritiques individuelles. Ensemble, ces résultats expérimentaux élargissent notre compréhension actuelle de de la fonction des synapses durant la plasticité homéostatique ainsi que durant le développement postnatal du cerveau. En étudiant les mécanismes neurophysiologiques de base, il sera possible d'avoir un aperçu plus profond du fonctionnement du cerveau et de ses pathologies.

Copyright Authorizations

Manuscript I was published in the Hindawi journal *Neural Plasticity* in 2012:

Lee KF, Soares C, Béïque JC. Examining form and function of dendritic spines. Neural Plast. 2012; 2012:704103. doi: 10.1155/2012/704103. Epub 2012 Apr 17. PMID: 22577585

"All articles published in Hindawi journals are released under a "Creative Commons Attribution License" enabling the unrestricted use, distribution, and reproduction of an article in any medium, provided that the original work is properly cited which means that authors of the article, along with any interested reader, are free to view, print and download any articles published in the journal." (Personal communication with Sara Ammar, Editorial Office, Hindawi Publishing Corporation)

Manuscript II and IV were published in the *Journal of Neuroscience* in 2012 and 2013, respectively:

Soares C, Lee KF, Nassrallah W, Béïque JC. Differential subcellular targeting of glutamate receptor subtypes during homeostatic synaptic plasticity. J Neurosci. 2013 Aug 14; 33(33):13547-59. doi: 10.1523/JNEUROSCI.1873-13.2013. PMID: 23946413

Lee KF. A unique mechanism of NMDA spike initiation supports a distinct role in synaptic input integration. J Neurosci. 2012 Feb 29;32(9):2913-14. doi: 10.1523/JNEUROSCI.6318-11.2012. PMID: 22378866

According to *The Journal of Neuroscience* permissions policy:
"Authors need NOT contact the journal to obtain rights for any non-commercial reuse their own material so long as authors provide attribution to the place of original publication and, for the first six months after publication, refrain from making the work publicly available. Authors are automatically granted permission to:

- Reuse the article in print collections of their own writing.
- Present a work orally in its entirety.

- Use an article in a thesis and/or dissertation.
- Reproduce an article for use in the author's courses.
- Reuse a figure, photo and/or table in future non-commercial works."

Manuscript III was published in the Elsevier journal *Neuropharmacology* in 2014:

Lee KF, Soares C, Béïque JC. Tuning into diversity of homeostatic synaptic plasticity. Neuropharmacology. 2014 Mar;78:31-7. doi: 10.1016/j.neuropharm.2013.03.016. Epub 2013 Mar 27. PMID: 23541721

Under the International Association of Scientific, Technical & Medical Publishers' STM Permissions Guidelines, to which Elsevier is a signatory:
"Authors publishing in Elsevier journals retain wide rights to continue to use their works to support scientific advancement, teaching and scholarly communication. An author can, without asking permission, do the following after publication of the author's article in an Elsevier-published journal…
… - include the article in full or in part in a thesis or dissertation"

General Introduction

The brain is arguably the most complex system in the known universe, and is often touted as the 'last frontier' and one of the greatest mysteries in science today. At the core of this mystery is the question of how the myriad of processes in the brain enable animals to interact and survive in their environments. As humans, we know that this mystery extends far beyond the processing of senses and the coordination of behavioral responses. We consciously experience the world, perceiving our environments with deep emotional capacity and can calculate and plan our actions with extraordinary precision. We learn about and interact with our environments through symbolisms and can manipulate these symbols across many layers of abstraction. How is it that our brain endows us with the ability to be conscious, to perceive, to feel? Although these are lofty academic questions, there are practical reasons for gaining a better understanding of how the brain functions, reasons that are firmly rooted in the prevalence and diversity of neuropsychiatric disease plaguing millions of people today. The experiences we have and the memories we forge arguably comprise the essence of life. To the unfortunate many in the world, however, something in the way the brain carries out its duties goes awry, leading to incapacitating intellectual disability, uncontrollable psychosis, and deep depression, to name only a few debilitating symptoms. By developing a better understanding of the basic biological mechanisms that underlie normal brain function, we will glean important insights into the nature of neuropsychiatric disease, and hopefully begin to develop ever more efficacious therapies for mental illness. To put this in perspective, I use this analogy when speaking to friends and family about brain research: "you can't fix a car without first understanding how the pieces, the nuts and bolts, make the car run". In this line, the challenge to understand the "nuts and bolts" of the brain is the overarching goal of the neuroscience research community.

Arguably some of the most important insights in neuroscience have come with the development and refinement of experimental methods and instruments to study live nervous tissue. The earliest known experiments were performed by the Dutch scientist Jan Swammerdam in the 17th century, who established a preparation of frog muscle with its attached its nerve to show that 'irritation' of the nerve resulted in muscle contraction. This work was furthered by Italian researchers led by Luigi Galvani a century later, but it was not until the mid-1800s that instruments developed to show that electrical currents were conducted by the live tissue. Through the early-to-mid 1900s, the invention of intracellular electrodes and the voltage-clamp technique enabled Hodgkin and Huxley to document the ionic basis of membrane excitability and action potential generation in the giant squid axon. Verkhratsky and colleagues have written a recent informative review describing these and other key events in the history of electrophysiology (Verkhratsky et al., 2006). Although these early experiments in live tissue seeded the technological and theoretical foundations for understanding signal transduction in the nervous system, the birth of modern 'neuroscience' is generally attributed to the work of Ramon y Cajal, in the late 19th century. Cajal pioneered the view that the brain is composed of an immense number of individual microscopic components – neurons – which transmit information through the brain by communicating with one another at synapses, and he made the prescient hypothesis that these connections between neurons could serve as sites for information storage. Now, over a century later, these ideas have solidified into a major pillar for our understanding of neuronal transmission of information in the brain.

Chemical synaptic transmission, as it is known in the central nervous system today, was a concept famously contested by John Eccles, who at first held the notion that synaptic transmission was purely electrical in nature (Eccles, 1946, 1949, 1982), despite being a key

contributor to earlier work first indicating that that synaptic transmission may be chemical in nature (Eccles et al., 1941; Eccles and Kuffler, 1941). The controversy over whether synaptic transmission was chemical or electrical became known as the 'soup versus spark' debate, where Eccles' ideas regarding electrical transmission were challenged by Stephen Kuffler and Bernhard Katz. Kuffler argued that the time delay behavior and graded amplitudes of end-plate potentials aligned better with the actions of a chemical transmitter, likely acetylcholine (Fatt, 1949), rather than direct electrical transmission (Kuffler, 1942b, a). Bernhard Katz and his colleagues provided significant support to the actions of a chemical transmitter by demonstrating the unitary nature of endplate potentials at the neuromuscular junction (NMJ) (Fatt and Katz, 1952; Delcastillo and Katz, 1954; Katz and Miledi, 1965), ultimately culminating in what is now known as the 'quantal theory' of vesicular neurotransmission (Kandel et al., 2000). With time, through experiments using intracellular microelectrodes (Brock et al., 1952; Eccles et al., 1954), Eccles eventually became convinced of the role of acetylcholine as the chemical transmitter at the NMJ. Presently, it is now textbook knowledge that synaptic transmission, the primary mode of rapid signal transduction through the nervous system, involves both electrical and chemical events (Kandel et al., 2000). In short, action potentials traveling along axons trigger release of neurotransmitters at their terminals. Neurotransmitter release is quantal in nature (*i.e.,* one vesicle at a time) and is dependent on calcium influx into the axon terminal (Katz and Miledi, 1967, 1968, 1969, 1970). Neurotransmitter molecules released by the axon terminal diffuse across the synaptic cleft to activate postsynaptic receptors to induce excitatory or inhibitory potentials in target cells. This sequence of events is rapid, occurring within only a few milliseconds. In essence, synapses serve as relay stations whereby electrical signals are transformed into chemical signals, and then back into electrical signals, thus mediating the

forward propagation of information through neural circuits. Although electrical synapses do exist in the central nervous system, in the form of gap junctions (Connors and Long, 2004), these types of synapses will not be discussed here.

The seminal work on synaptic transmission at the squid giant synapse, NMJ and various spinal neurons (Kuffler, 1942b, a; Brock et al., 1952; Fatt and Katz, 1952; Delcastillo and Katz, 1954; Eccles et al., 1954; Katz and Miledi, 1965; Bloedel et al., 1966; Katz and Miledi, 1967, 1969; Kuno and Miyahara, 1969a, b) provided a major conceptual platform for an explosion of experimental work leading to the current wealth of information on the diversity of chemical synaptic transmission in the central nervous system. It is now well understood that, while acetylcholine is the primary neurotransmitter in the periphery and glycine is a primary inhibitory transmitter in the brainstem and spinal cord, in the brain, glutamate is the primary excitatory neurotransmitter and gamma amino butyric acid (GABA) mediates fast inhibitory transmission (Kandel et al., 2000). Both of these rapid transmitter systems in the brain depend on the same principles of calcium-dependent vesicular release mechanisms in early experiments as described above (Kandel et al., 2000; Sudhof, 2004). It is important to appreciate that the balance between excitation and inhibition is essential to the rhythms that underlie brain function (Kandel et al., 2000; Buzsaki and Wang, 2012), and that substances such as serotonin, dopamine and norepinephrine are only a few of the many neuromodulatory transmitters that play crucial roles in these processes (Kandel et al., 2000; Marder et al., 2014). Given the immense size and scope of the research fields on each neurotransmitter, I will not attempt to provide a comprehensive account of 'neurotransmission' *per se*, but will instead center this thesis on fast excitatory synapses, for which glutamate is the neurotransmitter (Krnjevic and Phillis, 1963).

A surge in research on glutamate receptors began in the 1990's, owing in large part to the first cloning of a glutamate receptor (Hollmann et al., 1989) and the application of patch-clamp electrophysiology methods enabling high resistance, low noise electrophysiological recordings of single channels (Neher and Sakmann, 1976; Neher et al., 1978). Although there is a wide diversity in glutamate receptor classes, existing in both ionotropic (pore-forming) and metabotropic (G-protein coupled receptors), the two principle glutamate receptors at central synapses are the AMPA and NMDA subtypes (see (Traynelis et al., 2010) for an authoritative review). Kainate receptors are also expressed in the brain, although their function is less well understood. AMPA and NMDA receptors are tetrameric assemblies: AMPARs exist as different combinations GluA1-4 subunits, while NMDARs contain two obligatory GluN1 subunits plus additional two GluN2(A-D) and/or GluN3(A-B) subunits (Traynelis et al., 2010). AMPARs are often called the 'workhorse' of the synapse because they are responsible for the majority of synaptic conductance at resting membrane potentials (*i.e,* subthreshold synaptic transmission). In contrast, NMDARs conduct ionic currents only upon membrane depolarization due to a voltage-dependent block by magnesium ions at the channel pore (Mayer et al., 1984; Nowak et al., 1984). Thus, by responding to coincident pre- and postsynaptic depolarization, NMDARs are considered to be 'coincidence detectors' of activity. Importantly, NMDARs are permeable to calcium (Mayer and Westbrook, 1987) – a key signaling molecule involved in several aspects of synapse regulation. AMPA and NMDARs are present at both synaptic and extrasynaptic locations, diffuse laterally in the plasma membrane to varying degrees (Choquet and Triller, 2003; Groc et al., 2004; Triller and Choquet, 2005), and are dynamically regulated and stabilized at synapses in a subunit-dependent manner (Traynelis et al., 2010). The dynamic regulation of glutamate receptors at synapses constitutes a central mechanism for synaptic plasticity, that is,

the ability for synapses to alter their function in response to various patterns of activity (Malenka and Bear, 2004).

The most intensely studied forms of synaptic plasticity are long term potentiation and long term depression (LTP and LTD, respectively), which have been studied in detail for more than four decades and provide the current theoretical foundation for understanding information storage (and thus, learning and memory) at the cellular level (Malenka and Bear, 2004). Beyond LTP and LTD, however, it is well appreciated that synapse function is influenced and altered by a multitude of other factors such as homeostatic mechanisms that operate across broader temporal windows (Turrigiano, 2008), underscoring the staggering complexity in the orchestration of brain function. Given the central role of synapses in transmitting information throughout the nervous system, elucidating the mechanisms that dynamically regulate synapse function is imperative for understanding the brain in both health and disease.

Here in this thesis, I will focus on the structural and functional dynamics of glutamatergic synapses in the contexts of homeostasis and postnatal development. This General Introduction is intended to serve as a guide through a series of published review papers where I discussed these topics, as well as two original research papers that contribute new knowledge to the field (one published and one in revision). These manuscripts are not presented in chronological order, but are instead arranged for optimal continuity between topics. This introduction will begin with a brief overview of the structure and function of individual synapses before outlining the two dominant mechanisms that regulate synapse function, namely, Hebbian and homeostatic forms of synaptic plasticity. Finally, I will extend the discussion outward in scope to the functional organization of synaptic connectivity along dendrites, introducing how microscopic nuances in connectivity patterns can powerfully influence neuronal input-output functions. This final

perspective on synaptic connectivity is central for contextualizing the data described in the final manuscript, which contains the major original research findings obtained during my doctoral studies (Manuscript V, in revision).

Excitatory synapses are formed on dendritic spines at principal cells of the brain

Pyramidal neurons are principal cells in the cortex and hippocampus and use the neurotransmitter glutamate to mediate fast excitatory neurotransmission. Individual pyramidal neurons are endowed with thousands of glutamatergic synapses, highlighting the remarkably dense and complex network of synaptic connectivity that comprises excitatory neural circuits (Spruston, 2008). One characteristic feature of glutamatergic synapses on pyramidal neurons is that they are formed onto tiny femtolitre-sized dendritic protrusions called dendritic spines (Cajal, 1888; Alvarez and Sabatini, 2007; Bhatt et al., 2009; Colgan and Yasuda, 2014), where a postsynaptic density harbors a high concentration of neurotransmitter receptors. Since not all neurons types exhibit dendritic spines, there has been considerable speculation regarding the functional role of dendritic spines. One simple and well-accepted notion is that dendritic spines increase the synaptic surface area of neurons, allowing for increased synapse number and therefore increased capacity for information processing and storage. Indeed, differences in spine density on pyramidal neurons have been hypothesized to reflect varying degrees of computational demands in different cortical regions (Elston, 2000). In recent decades, spurred by advances in laser scanning microscopy, we have begun to better understand the role of dendritic spines as not only physical scaffolds for synaptic transmission, but also as biochemical and electrical compartments that are capable of undergoing functional alterations through activity-dependent changes in morphology (Alvarez and Sabatini, 2007; Bhatt et al., 2009; Colgan and Yasuda, 2014).

Dendritic spines are morphologically heterogeneous. There have been many attempts in past decades to formulate classification schemes, methods and nomenclatures to refer to, and analyze, spine morphology (Harris and Stevens, 1989; Harris et al., 1992; Benavides-Piccione et al., 2002; Koh et al., 2002; Portera-Cailliau et al., 2003; Rodriguez et al., 2008; Shi et al., 2009; Son et al., 2011; Risher et al., 2014). These efforts have been complicated by the inability to compare between light microscopy and electron microscopy due to the diffraction-limited resolution of standard laser-scanning microscopes, distortions due to the planar visualization of spines positioned in three-dimensional space, and intrinsic differences in the various neuronal preparations (dissociated cultures versus slice preparations). It has even been suggested that differences in slice preparation methods may influence spine morphology (Kirov et al., 1999; Kirov et al., 2004b), thus confounding experimental results and making between-study comparisons exceedingly difficult. As such, it is perhaps more useful to apply a reduced classification scheme outlining more generalized spine morphologies for simplicity. Here, I will refer to three major spine morphologies: *i*) thin/filipodia spines that are slender finger-like structures; *ii*) stubby spines, which are stud-like protrusions with a wide base projecting from the parent dendrite; and *iii*) mushroom spines, which resemble mushrooms (as the name implies), with a slender stem-like spine neck and bulbous spine head. These three morphological categories undoubtedly overlook important structural details of spines that can now be resolved by super-resolution imaging techniques (Adrian et al., 2014; Takasaki and Sabatini, 2014; Tonnesen et al., 2014), but nevertheless will be sufficiently useful for discussion within the scope of this thesis.

During embryonic and postnatal development, pyramidal neurons in the cortex and hippocampus exhibit rapid dendritic outgrowth and the emergence of dendritic spines from an

initially aspiny (spine-lacking) state (Pokorny and Yamamoto, 1981a; Michel and Garey, 1984; Murphy and Magness, 1984; Zecevic et al., 1989; Harris et al., 1992; Bourgeois and Rakic, 1993; Kirov et al., 2004a). Early in spine development, most dendritic spines are seen as thin/filipodia or stubby spines and gradually mature into mushroom spines with age. At the same time, synaptic AMPA and NMDAR populations are dynamically regulated (Ben-Ari et al., 1997; Molnar et al., 2002; Hanse et al., 2013; Lohmann and Kessels, 2014). The canonical model of spine synapse development begins with the emergence of filipodial or stubby spines that are initially devoid of AMPARs but contain NMDARs (so-called "silent" synapses). Synapses that lack AMPARs are considered "silent" since they conduct little to no synaptic current near resting membrane potential (Isaac et al., 1995; Liao et al., 1995; Durand and Konnerth, 1996). With time, these immature spine synapses transition into mature mushroom spines that contain both AMPA and NMDARs (Kerchner and Nicoll, 2008; Hanse et al., 2013). The acquisition and retention of AMPARs at spines therefore outlines the functional strengthening of synapses during development concomitant with a shift toward mushroom spine morphologies. Consistent with expected manifestations of these correlated changes in synapse structure and function during development, ultrastructural studies using immune-gold labeling of AMPARs show a correlation between spine volume and AMPAR content (Baude et al., 1995; Kharazia and Weinberg, 1999; Takumi et al., 1999). Together, these structure-function correlations at dendritic spines indicate that activity-dependent mechanisms involved in functional synaptic plasticity are closely tied to mechanisms that regulate spine structure (*i.e.,* 'structural plasticity'). The development of two-photon (2P) laser-scanning microscopy techniques at the turn of the millennium has empowered researchers to closely examine the relationship between form and function at dendritic spines.

In 2004, using 2P photolysis of caged-glutamate ("glutamate uncaging") to stimulate single dendritic spines, Matsuzaki and colleagues demonstrated that concurrent functional *and* structural changes take place at individual spines in response to plasticity-inducing stimuli (Matsuzaki et al., 2004). Specifically, it was found that LTP at individual spines involved not only an increase in the amplitude of AMPAR-mediated currents, but also sustained increases in dendritic spine volume. These conclusions have since been verified by other groups (Harvey and Svoboda, 2007; Lee et al., 2009; Lee et al., 2010; Hill and Zito, 2013) to the effect that spine growth alone has been used as an all-optical proxy of synaptic potentiation. While these are not the first demonstrations that morphological changes accompany synaptic plasticity (Yuste and Bonhoeffer, 2001), they provide the most conclusive evidence at single spine resolution. In a manner closely reflecting the bidirectional nature of synaptic plasticity, synapse weakening appears to be coupled to spine shrinkage and even elimination (Okamoto et al., 2004; Zhou et al., 2004; Oh et al., 2013). More recent studies using super-resolution imaging techniques combined with glutamate uncaging have unveiled finer details regarding spine structural plasticity, demonstrating dynamic changes at the nanometer scale that could not previously be resolved with standard 2P microscopy (Frost et al., 2012; MacGillavry and Blanpied, 2013; Takasaki and Sabatini, 2014; Tonnesen et al., 2014; Wijetunge et al., 2014). Together, this work underscores a mechanistic link between structural and functional plasticity of dendritic spines, but what is the significance of altering dendritic spine structure and how do these changes influence synapse function?

Synaptic strengthening and weakening (*i.e.,* LTP and LTD) are mechanisms that intuitively modulate the routing of information transmission between neurons (introduced in more detail in the following section). As such, the consequences of this 'functional' plasticity are

perhaps more obvious than those resulting from changes in spine morphology via 'structural' plasticity mechanisms. However, it has become clear that dendritic spine structure can significantly influence both the biochemical and electrical behavior of the spine, and may therefore exert changes to synapse function over broad time scales. For example, dendritic spines form distinct structural compartments that physically segregate individual synapses, and their morphology may determine the diffusion of molecules within the spine head, enabling them to serve as micro-domains for biochemical reactions. This chemical compartmentalization has been revealed by analyzing the spatial profile of evoked synaptic calcium signals in spines (Muller and Connor, 1991; Mainen et al., 1999; Majewska et al., 2000b; Majewska et al., 2000a; Noguchi et al., 2005; Grunditz et al., 2008) or by measuring intracellular diffusion of fluorescent dyes or proteins using fluorescence recovery after photobleaching (FRAP) or photoactivation techniques (Svoboda et al., 1996; Bloodgood and Sabatini, 2005; Tonnesen et al., 2014). Moreover, studies using targeted fluorescence-labeling techniques have shown striking differences in the subcellular mobility of various molecules acting downstream of calcium at synapses. What controls the diffusion of molecules in and out of dendritic spines? A simple prediction is that molecular size, steric hindrance, and intermolecular tethering within the confines of dendritic spines may serve a primary role. For example, calcium/calmodulin-dependent kinase II (CaMKII) is a relatively large molecule comprised of twelve subunits that binds to many proteins in dendritic spines (Lisman and McIntyre, 2001; Lisman et al., 2002; Rellos et al., 2010), and so its free diffusion is expected to be relatively limited in contrast to smaller molecules such as Rho-A and Cdc42, which exhibit significantly greater mobility (Patterson and Yasuda, 2011). Interestingly, even these similarly-sized small molecules exhibit different diffusion behaviors at spines, likely reflecting different propensities for intermolecular

interaction which may be under complex control by synaptic activation (Murakoshi et al., 2011). Nevertheless, the available data demonstrate that simple spine morphology (*i.e.,* the presence of a spine neck) can have significant bearing on molecular diffusion at synapses such that stubby spines (with no spine neck) are less effective than mushroom spines at compartmentalizing biochemical signals. As such, regulated changes in spine morphology likely enable control over the biochemical environment of the spine by modulating the propensity for individual synapses to communicate with machinery present in the parent dendrite and neighboring dendritic spines. One intriguing emerging notion is that diffusible molecules may mediate local crosstalk between neighbouring synapses, allowing for the concerted regulation of clusters of dendritic spines (Govindarajan et al., 2006; Harvey and Svoboda, 2007; Harvey et al., 2008; Larkum and Nevian, 2008; Govindarajan et al., 2011). This idea will be explored in more detail in latter sections of this thesis.

Electrical signaling is another major process that is thought to be controlled by spine morphology, although this notion is considerably more controversial than that of biochemical compartmentalization. It has been suggested for many decades that spines may behave as distinct electrical compartments from their parent dendrites (Coss and Perkel, 1985; Shepherd, 1996). However, this possibility was at first largely overlooked due to early estimates of electrical resistance given by spine necks (Harris and Stevens, 1989; Koch and Zador, 1993; Harris and Kater, 1994; Svoboda et al., 1996). Interestingly, however, calcium imaging studies have shown significant activation of both NMDARs and voltage-dependent calcium channels (VGCCs) at spine heads in response to subthreshold synaptic stimulation (Petrozzino et al., 1995; Yuste and Denk, 1995; Mainen et al., 1999; Grunditz et al., 2008; Bloodgood et al., 2009). Given the voltage-dependent conductance of these channels, it was argued that electrical potentials in the

spine head must reach tens of millivolts, and to yield such high amplitude synaptic potentials, the AMPA receptor-mediated currents into the spine head must encounter significant electrical resistance at the spine neck. This has been more carefully revisited in a recent study which yielded strong evidence that at least a subset of mushroom-type spines act as electrical compartments. Using a combination of electrophysiological recordings at dendrites and 2P glutamate uncaging and calcium imaging, Harnett and colleagues found that synaptic depolarization at mushroom spine heads could be upwards of 25 mV, corresponding to an estimated spine neck resistance of ~500 MΩ (Harnett et al., 2012). Although estimates of the absolute magnitude of electrical resistance may vary due to methodological differences, studies using electrophysiology, FRAP, super-resolution techniques and modeling have provided spine neck resistance values in the range of ~100 MΩ to >1 GΩ (Grunditz et al., 2008; Tonnesen et al., 2014), which are sufficient to amplify synaptic potentials and account for observed calcium accumulations via NMDAR and VGCCs at spines. Moreover, spine necks act to linearize the local summation of synaptic potentials (Araya et al., 2006a), which was shown by comparing the summation of excitatory potentials evoked by multi-site glutamate uncaging at spines and dendritic shafts. While coincident uncaging stimuli delivered to two spines generated potentials that summed in a linear manner (*i.e.,* the amplitude of depolarization equaled the expected sum from EPSPs evoked individually at each spines), depolarizing potentials by paired uncaging stimuli delivered to the dendritic shaft regions summed sub-linearly. This sub-linear summation of uncaging-evoked potentials at dendritic shaft regions was argued to be due to a drop in local input resistance, which would act to shunt depolarizing potentials. Moreover, spine neck length is inversely proportional to the amplitude of somatically-recorded synaptic potentials (Araya et al., 2006b; Araya et al., 2014) and exhibit plasticity-induced changes in length that correlate with

changes in synaptic potential amplitude (Araya et al., 2014; Tonnesen et al., 2014). Despite growing consensus, some authors contend that the spine neck offers negligible effects on electrical signals at spines (Popovic et al., 2014), but the experimental data supporting this contention are limited by the low signal-to-noise recordings of voltage-sensitive dyes, and appear to be based on a sample of morphologically different dendritic spines present in dissociated neuronal cultures. It is likely that future work will further solidify the importance of spine neck geometry and plasticity in dictating the electrical function of synapses.

So far, I have introduced the dendritic spine as an important structural component of excitatory synapses. Dendritic spines are structurally heterogeneous and are subject to rapid and sustained changes in morphology and geometry, and these changes have consequences for both electrical and biochemical functions at synapses. Under normal conditions, it is evident that synapse function is closely correlated with spine morphology, suggesting common mechanisms regulate dendritic spine stsructure and function. However, a number of examples in the literature highlight clear departures between the form and function of dendritic spines. These studies therefore suggest that common upstream mechanisms may control the induction of structural and functional plasticity at spines, while their expression is controlled by divergent mechanisms. We are only beginning to understand the different mechanisms that regulate various aspects of spine structure and function, but ongoing and future work will undoubtedly disentangle these intricate details which are crucial for understanding of the role of synapses in information storage and processing. In a review paper that was published in 2012 (Manuscript I: (Lee et al., 2012)), I summarized the current state of knowledge on form and function of dendritic spines.

Hebbian synaptic plasticity

As mentioned above, neurons are plastic entities. In the most general sense, neural plasticity refers to activity-dependent changes in neural function, and such changes are now best known to take place at the synapse (*i.e,* synaptic plasticity). While at McGill University, Donald Hebb published these infamous words in *The Organization of Behavior* (1949): "When the axon of cell A is near enough to excite cell B and repeatedly or persistently takes part in firing it, some growth process or metabolic change takes place in one or both cells such that A's efficiency, as one of the cells firing B, is increased" (Hebb, 1949). With this statement, Hebb exhibited remarkable prescience in suggesting that the strength of synaptic connections between neurons could be persistently altered by specific patterns of synaptic activity. In the subsequent decades, experiments performed on the reflex arc in the spinal cord and at the NMJ offered the first evidence for such synaptic plasticity. These studies described a phenomenon called "post-tetanic potentiation", whereby brief bouts of intense (tetanic) stimuli caused transient elevations in evoked synaptic response amplitudes that lasted several minutes (Lloyd, 1949; Eccles and Rall, 1950; Martin and Pilar, 1964; Shapovalov, 1969). The short-lived duration of these synaptic changes proved to be relatively disappointing, however, because synaptic modifications were hypothesized to serve long-term memory function. Considerable excitement was therefore generated when long-lasting activity-dependent changes in synapse function were described in a brain circuit in 1973, when Bliss and Lomo first documented the phenomenon now known as long-term potentiation (LTP) using extracellular recordings in the dentate gyrus of rabbits (Bliss and Lomo, 1973). In essence, it was found that synaptic responses were persistently (for several hours) increased in amplitude following brief (seconds to minutes) intense trains of synaptic stimulation that were similar to the tetanic stimuli delivered in spinal and neuromuscular circuits

for post-tetanic potentiation. Shortly thereafter, it was found in brain slice preparations that synaptic responses could be persistently depressed by bouts of lower frequency stimuli, and this was termed long-term depression (LTD) (Dunwiddie and Lynch, 1978). These early studies seeded the notion that central synapses carried the capacity to bi-directionally regulate the strength of transmission in an activity dependent manner, paving the way for intense research efforts that have shown no signs of waning up to the present day.

Over four decades of research on synaptic plasticity confirms Hebb's hypothesis and, as such, LTP and LTD are now referred to as Hebbian forms of synaptic plasticity. Hebbian synaptic plasticity is undoubtedly the most intensely studied topic in neuroscience to date, and provides a foundation for our current understanding of the cellular basis for information storage in the brain. Over the years, a number of key determinants have been identified for the induction and expression of Hebbian plasticity at glutamatergic synapses, and innumerable molecular players are thought to be involved in these processes (Malinow and Malenka, 2002; Malenka and Bear, 2004; Caporale and Dan, 2008).

In general, LTP and LTD are induced by calcium influx through synaptic NMDARs (Collingridge et al., 1983; Lynch et al., 1983) and expressed by dynamic changes in postsynaptic AMPAR content at dendritic spines mediating changes in synaptic strength (reviewed in (Malinow and Malenka, 2002; Shepherd and Huganir, 2007)). The postsynaptic control of AMPAR recruitment and stabilization is complex and appears to be influenced by a myriad of molecular players (Malenka and Bear, 2004; Shepherd and Huganir, 2007). What is relatively certain is the requirement for the calcium-dependent activation of CaMKII (Malinow et al., 1988; Malinow et al., 1989). Downstream of CaMKII, synaptic strengthening may be carried out by phosphorylation of AMPARs (Lee et al., 2000; Lee et al., 2003), and stabilization of

AMPARs with scaffolding proteins at the synapse (Hayashi et al., 2000; Shi et al., 2001). Interestingly, the synthesis of new proteins is required to sustain late phases of plasticity (Sutton and Schuman, 2006). The primary model system for studying LTP and LTD has been the synapses in the CA3 to CA1 Schaffer-collateral pathway in rodent hippocampal slice preparations, but this canonical NMDAR-dependent synaptic plasticity is also operant at thalamocortical and cortico-cortical synapses in various cortical regions (Malinow and Malenka, 2002; Malenka and Bear, 2004; Caporale and Dan, 2008) , as well as glutamatergic synapses in subcortical structures such as the amygdala and nucleus accumbens (Blair et al., 2001; Russo et al., 2010). Despite the remarkable progress to date, the mechanisms underlying LTP and LTD are far from solved and the map of molecular players involved in regulating synaptic function appears to grow more complex each year. Nevertheless, a useful core theoretical framework has emerged, positioning dynamic activity-dependent changes in the strength of synaptic transmission as a central component to shaping the functional connectivity of neural circuits, thus dictating information flow and storage in the brain, as it relates to learning and memory.

One pivotal discovery is that the induction of LTP and LTD can be differentially controlled by the relative timing of pre- and postsynaptic spikes – a phenomenon called spike timing dependent plasticity (STDP). STDP revolutionized the thinking in the field of Hebbian plasticity by providing a physiological framework for understanding the rules of LTP and LTD induction in the context of a neuron that integrates synaptic inputs to generate spikes. In essence, it was found that synaptic efficacy can be persistently potentiated if synaptic input is immediately followed by postsynaptic spiking (pre-post pairing), while synaptic depression can be induced when postsynaptic spikes precede synaptic input (post-pre pairing) (Markram et al., 1997). STDP follows strict temporal rules, only occurring if pre- and postsynaptic activity is

paired within less than about thirty milliseconds (Bi and Poo, 1998; Feldman, 2000; Sjostrom et al., 2001); reviewed in (Caporale and Dan, 2008). This timing dependence is attributed to the voltage-dependent activation of synaptic NMDARs by coincident glutamate binding and action potential backpropagation (conduction of action potential depolarization by voltage-gated conductances on the dendritic membrane) into the dendritic arbor. The sign of plasticity (synaptic potentiation versus depression) is thought to be determined by the different synaptic calcium amplitudes elicited by pre-post and post-pre pairing (Koester and Sakmann, 1998; Nevian and Sakmann, 2004, 2006). This simple calcium-dependent mechanism operates well in basic models of STDP (Shouval et al., 2002), although more complex calcium dynamics (Wang et al., 2005; Kampa et al., 2007), spatial extent of action potential backpropagation into dendrites (Froemke et al., 2005; Sjostrom and Hausser, 2006) and the actions of neuromodulators (Bender et al., 2006; Couey et al., 2007; Seol et al., 2007; Edelmann and Lessmann, 2013) are likely also involved in controlling the extent of synaptic alterations. Nevertheless, from a general standpoint, STDP embodies key features of Hebb's original postulate, since synapses that contribute to action potential discharge (as in pre-post pairing) are potentiated, while synapses that are asynchronous relative to spiking activity (as in post-pre pairing) become depressed. These tangible physiological foundations for the induction of synaptic plasticity suggest that Hebbian plasticity follows such STDP rules *in vivo*.

Arguably the most dynamic period for Hebbian synaptic plasticity is during early postnatal development (Lohmann and Kessels, 2014). At birth, pyramidal neurons in the rodent brain are not yet fully developed and must undergo robust dendritic growth and synapse formation, marking a critical period for establishing neural circuits. As aforementioned, nascent synapses at cortical and hippocampal pyramidal neurons during this time are functionally

'silent', that is, they contain NMDARs but not AMPARs (Isaac et al., 1995; Liao et al., 1995; Durand and Konnerth, 1996; Kerchner and Nicoll, 2008; Hanse et al., 2013). Developing synapses become functionally stabilized and acquire AMPARs in a process known as synapse 'unsilencing' via Hebbian LTP mechanisms that are thought to be driven by experience. Interestingly, concurrent with the developmental strengthening of synapses, the molecular machinery involved in regulating synapse function also appears to undergo distinct developmental transitions. A classic example of this is that LTP exhibits a greater dependence on protein kinase-A (PKA) activity during early development, and gradually shifts toward dependence on CaMKII activity with maturity (reviewed in (Lohmann and Kessels, 2014). This transition in kinase-dependence is not well understood, and is only one example of the many developmental changes that take place in the molecular environment of synapses. As will become apparent in later chapters below, developmental changes in synapse function will be a central theme of this thesis since I have discovered a novel switch in the nature of NMDAR-mediated calcium signaling during synapse development and distinct spatial patterns of synaptic maturation in the developing dendritic arbor of pyramidal cells.

Homeostatic synaptic plasticity

LTP and LTD are considered to be the principle cellular mechanisms underlying information storage in the brain because they provide an intuitive strategy to sculpt the trajectory of information transmission between neurons in complex circuits in an experience-dependent manner. However, theoretical studies have noted that neural circuit function tends to be unstable when Hebbian plasticity is implemented in an unrestrained manner (*i.e.,* the 'instability problem') (Miller and MacKay, 1994; Turrigiano and Nelson, 2004; Lazar et al., 2009), leading to a narrowed dynamic range of neural computations and limited information storage capacity.

Specifically, the positive-feedback nature of LTP and LTD renders synapses susceptible to reaching ceiling and floor effects such that potentiated synapses come to dominate the firing of neurons, while depressed synapses become functionally negligible. Consistent with this notion, synaptic competition in model neurons operating with purely Hebbian plasticity mechanisms result in bimodal distributions of synaptic weight, whereby synapses are either extremely weak or extremely strong, with relatively few synapses exhibiting intermediate weights (Song et al., 2000; Morrison et al., 2007; Toyoizumi et al., 2007). This theoretical result is inconsistent with experimentally-measured amplitude distributions of miniature excitatory postsynaptic currents (mEPSCs, 'minis'), whereby mEPSC amplitudes typically follow a unimodal heavy-tailed distribution around a mean of 10-15 pA (Bekkers and Stevens, 1996; Turrigiano et al., 1998; Beique et al., 2006; Goel and Lee, 2007). These experimental synaptic weight distributions therefore suggest that neurons employ some mechanism for normalizing synaptic weights. The discovery of homeostatic synaptic plasticity in 1998 by Turrigiano and colleagues has generated significant inroads toward understanding how synaptic weights can be stabilized to enable optimal neural circuit function. It is important to note, however, that some authors have suggested that STDP mechanisms may sufficiently solve the potential problem of runaway excitation (Abbott and Nelson, 2000), although it is likely that STDP and homeostatic plasticity mechanisms operate in parallel to control synapse function.

Homeostatic synaptic plasticity refers to the ability for neurons to tune their excitability, and therefore spiking behavior, toward a given set point by adjusting synaptic weights in response to prolonged changes in activity (Turrigiano and Nelson, 2004; Turrigiano, 2008). As the name implies, this form of synaptic plasticity operates in a homeostatic manner whereby sustained suppression of neuronal activity results in an increase in synaptic weights such that

excitability is enhanced. Conversely, sustained elevations in neuronal activity lead to an overall reduction in synaptic weights such that neuronal excitability is reduced. In the original study by Turrigiano and colleagues, this phenomenon was demonstrated by pharmacologically suppressing the spiking activity of dissociated neurons in culture using the sodium channel antagonist tetrodotoxin (TTX) to block action potentials, or by elevating activity by blocking inhibition with the GABAergic antagonist bicuculline for 24-48 hours (Turrigiano et al., 1998). Whole-cell recordings of mEPSCs showed that TTX treatment caused a significant increase, while bicuculline caused a reduction, in the strength of synaptic AMPAR transmission. Intriguingly, these homeostatic synaptic changes were not additive or subtractive in nature, but instead multiplicative, which was interpreted to indicate that the weight of each synapse was multiplied (or 'scaled') by a single common factor independently of initial synaptic weight. Such multiplicative scaling was argued to be an advantageous feature of homeostatic synaptic plasticity since it preserves information (or 'memory') stored or encoded in the relative weights distributions between all synapses that were presumably formed by Hebbian plasticity mechanisms. Recently, we provided additional molecular details to expand on these insights by demonstrating that AMPA and NMDARs are under distinct subunit-selective regulatory control during the homeostatic synaptic response to prolonged TTX treatment (Manuscript II: (Soares et al., 2013)).

As we (Manuscript II: (Soares et al., 2013)) and others (Sutton et al., 2006; Soden and Chen, 2010; Groth et al., 2011; Lindskog et al., 2011) have shown, global pharmacological suppression of neuronal activity by prolonged incubation with TTX induces cell-wide homeostatic synaptic scaling. The trigger for this global (cell-wide) homeostatic response has been suggested to be disruption in somatic calcium signaling via VGCCs during periods of

inactivity, leading to changes in downstream calcium-dependent regulation of gene expression by CaMKIV (Ibata et al., 2008; Goold and Nicoll, 2010). Intriguingly, however, homeostatic synaptic plasticity has been shown to also operate locally in a synapse-specific manner under conditions where somatic spiking activity was not altered. These local homeostatic plasticity mechanisms raise the possibility that several loci of homeostatic regulation exist in neurons at different subcellular levels. In a review paper published in 2014, I led a discussion on the evidence for local and global forms of homeostatic synaptic plasticity (Manuscript III: (Lee et al., 2014)). Here, I will briefly introduce key points raised in the review.

A number of recent studies have shown that homeostatic synaptic plasticity can operate at functionally-distinct subsets of synapses, and have offered interesting insight into the potential physiological role of synapse-specific homeostatic regulation. Kim and colleagues showed that feed-forward and recurrent synapses onto hippocampal CA3 neurons differentially respond to prolonged inactivity in slice culture, and found that this synapse-specific tuning reduced the propensity for pathological epileptic bursting activity (Kim and Tsien, 2008). Using a different model system, Deeg and Aizenman showed that synapse-specific homeostatic scaling enabled modality-specific tuning of synaptic transmission in tectal neurons of Xenopus laevis tadpoles, *in vivo* (Deeg and Aizenman, 2011). Taking a step further, two different groups used clever molecular strategies to silence/suppress individual synaptic terminals and demonstrated that individual dendritic spines have the capacity to detect and respond to prolonged activity deprivation (Lee et al., 2010; Beique et al., 2011). At first, these results were argued to be paradoxical, given that such synapse-autonomous forms of homeostatic tuning would, in essence, 'erase' information encoded by Hebbian plasticity (Turrigiano, 2012). However, as we wrote in Manuscript III (Lee et al., 2014), this view of Hebbian plasticity hinges on an overly simplistic

model regarding the role of synaptic plasticity in information storage – especially in light of recent advances in our understanding of dendritic computation neuronal input-output operations. In the paper, I expanded on a notion initially proposed by Goldberg and colleagues (Goldberg et al., 2002), speculating that locally-acting – synapse-specific – homeostatic synaptic plasticity mechanisms may help preserve information processing strategies that involve nonlinear dendritic mechanisms of synaptic integration, such as dendritic spikes and NMDA spikes (London and Hausser, 2005). In this view, local forms of homeostatic plasticity are relieved of any particular paradox and are instead well-positioned to serve an important role in the basic neuronal functions. It is in my opinion that neurons are likely endowed with mechanisms to adapt in a homeostatic manner to both global and local changes in synaptic activity, and that these fundamental stabilizing mechanisms enable neurons to support optimal functional dynamics in the face of perpetual activity-dependent changes in the environment of the brain.

Dendrites exhibit cable properties and passively filter synaptic potentials

For information to flow from one neuron to the next, excitatory synaptic inputs must sufficiently depolarize the postsynaptic neuron to reach action potential threshold. Thus, the most basic neuronal computation is making the 'decision' to spike via the summation of synaptic potentials. This basic operation is deceivingly complex given the expansive dendritic arbors of pyramidal neurons and the tens of thousands of synapses that decorate them. The physical challenges surrounding the integration of synaptic potentials along dendrites was first formalized using cable theory by Wilfred Rall (Rall, 1962). These so-called cable properties of dendrites are neatly summarized in a textbook by Stuart, Spruston and Hausser (Stuart et al., 2007) and in excellent review papers (Magee, 2000; London and Hausser, 2005; Sjostrom et al., 2008; Major et al., 2013). In brief, dendrites pose a major obstacle to synaptic integration because electrical

potentials are attenuated as they passively propagate along the length of a dendrite. Moreover, axial resistivity is inversely proportional to dendrite diameter, making the propagation of synaptic potentials along thin dendrites less reliable compared to large dendrites. Together, the cable properties of dendrites impose important challenges to the integration of synaptic inputs in the large dendritic arbors of pyramidal neurons, since distal synapses on thin dendrites hundreds of micrometers from the soma are significantly disadvantaged in their ability to drive postsynaptic spikes compared to more proximal synapses. Perhaps not surprisingly, pyramidal neurons have evolved diverse strategies to overcome the cable properties of their expansive dendritic arbors in order to optimize synaptic information processing.

One apparently simple strategy to counteract the filtering effect of dendrites was found in pyramidal neurons in region CA1 of the hippocampus: AMPAR content was shown to be increased in a distance dependent manner such that synaptic weights were greater at distal synapses compared to proximal synapses (Magee and Cook, 2000; Andrasfalvy and Magee, 2001; Smith et al., 2003; Nicholson et al., 2006; Shipman et al., 2013). In this way, the cable filtering of distal EPSPs was compensated such that EPSP amplitudes experienced at the soma were relatively uniform along the proximal-distal axis of the dendritic arbor, thus normalizing the synaptic influence over action potential output with respect to distance from soma. Interestingly, it was noted that dendritic filtering of EPSPs should not only reduce the amplitude of EPSPs but also prolong EPSP kinetics, according to cable theory predictions (Magee and Cook, 2000). The passive broadening of EPSP waveforms along dendrites would therefore result in broadened temporal windows for summation for distal synaptic inputs, and thus impose a spatial bias on the kinetics of synaptic integration. Although there is no *a priori* reason to suggest that this arrangement is unfavorable, it seems that CA1 pyramidal neurons have also evolved a

mechanism to counter this effect of dendritic filtering on temporal summation. In particular, it was shown that hyperpolarization-activated cation channels (Ih) followed a gradient in subcellular distribution, with increased channel density in distal dendritic regions (Magee, 1999). It was argued that the net outward current generated by Ih inactivation during depolarization at distal synaptic locations served to sharpen the EPSP time course and therefore minimize the effects of cable filtering of EPSPs on the temporal window for summation. As such, the integration of synaptic potentials from proximal and distal synapses can be kept within similar temporal bounds. Taken together, the distance-dependent tuning of synaptic AMPAR content and membrane channel conductance demonstrate two mechanisms that enable neurons to overcome the effects of dendritic cable filtering on the passive propagation of synaptic potentials. These mechanisms are generally thought to level the 'playing field' such that distal and proximal synapses have relatively equal influence over postsynaptic depolarization, in effect establishing uniform spatial and temporal rules to govern the passive summation of synaptic inputs over the large dendritic arbors of pyramidal neurons.

Active dendrites and neuronal information processing

What factors determine the salience of synaptic input? In other words, what makes some barrages of synaptic input more likely to drive action potential spiking, than others? In a system where synaptic potentials are summed passively in the dendritic arbor, it is well established that temporal coincidence is one defining factor (Rall, 1962): synaptic inputs grouped together within a narrow time window generate larger depolarizations, and are therefore more likely to drive postsynaptic action potentials, than less synchronous synaptic inputs. Interestingly, it has long been known that dendrites have the capacity to generate action potential-like events (Wong et al., 1979; Benardo et al., 1982). These events were found to be driven by the activation of voltage-

dependent sodium channels (VGSCs) and voltage-gated calcium channels (VGCCs) present in the dendritic membrane, and raised the possibility that synaptic inputs can be amplified if sufficient depolarization is achieved in the dendritic arbor. It is now well established that synaptic integration can indeed enter a nonlinear regime, where dendritic action potentials ('dendritic spikes') drive membrane depolarization with amplitudes that are greater than the simple sum of individual synaptic inputs (London and Hausser, 2005; Major et al., 2013). As such, dendritic spikes can dramatically increase the signal-to-noise ratio, and thus salience, of synchronous synaptic inputs. More recently, considerable attention has been directed toward dendritic events called 'NMDA spikes', which are nonlinear dendritic depolarizations arising due to regenerative activation of NMDARs. In contrast to dendritic spikes, which depend on VGSC and/or VGCC activation and respond specifically to membrane depolarization by temporally-coincident synaptic input, NMDA spike initiation is additionally contingent on the precise spatial pattern of synaptic activation.

The role of NMDARs in synaptic integration was first explored in theoretical work by Bartlett Mel in the early 1990's (Mel, 1993), who showed that the simple presence of NMDARs at synapses could enhance the impact of synaptic activity that is spatially clustered along dendrites. This so-called 'cluster-sensitivity' was attributed to the ability for local AMPAR-mediated depolarization at neighboring synapses to generate a voltage-dependent enhancement in synaptic conductance by alleviating the block on NMDARs by magnesium. For some years thereafter, the 'cluster sensitivity' of dendrites remained only a theoretical curio, but in the early 2000's, Schiller and colleagues provided empirical evidence of this NMDAR-dependent form of nonlinear dendritic integration in the basal dendrites of layer 5 pyramidal neurons *in vitro* (Schiller et al., 2000; Polsky et al., 2004). They showed that supra-linear events could be evoked

using by gradually increasing the intensity of glutamate uncaging power or local electrical stimulation at individual dendritic segments. These events exhibited a clear voltage threshold for activation and were dependent on NMDAR activation. In subsequent years, it became clear that NMDAR-dependent dendritic nonlinearities were features of thin dendrites of pyramidal cells in both the cortex and hippocampus (Losonczy and Magee, 2006; Tsay et al., 2007; Larkum et al., 2009; Polsky et al., 2009; Branco et al., 2010; Chalifoux and Carter, 2011). More recently, studies using 2P calcium imaging and electrophysiology have demonstrated these nonlinear dendritic events occurring both spontaneously and in response to sensory stimuli *in vivo* (Lavzin et al., 2012; Smith et al., 2013; Gambino et al., 2014; Grienberger et al., 2014; Palmer et al., 2014). Collectively, these *in vitro* and *in vivo* experiments, combined with theoretical work outlining significant computational advantages of nonlinear dendritic computation neurons, strongly suggest that dendritic nonlinearities are critical for decoding synaptic inputs and govern the forward propagation of information from one neuron to the next (London and Hausser, 2005; Major et al., 2013).

So far, I have introduced two primary classes of nonlinear dendritic events: 1) dendritic spikes, which depend on VGSC and/or VGCC activation; and 2) NMDA spikes, which rely on activation of NMDARs. What are the key differences between dendritic spikes and NMDA spikes, and how do they relate in the broad context of dendritic computation? As I alluded to above, dendritic spikes and NMDA spikes exhibit different contingencies for activation. While dendritic spikes respond exclusively to membrane depolarization driven by synchronous synaptic activation, NMDA spikes are more localized events that report spatial clustering of synaptic input occurring at individual dendritic branches. Further underscoring the spatially restricted locus of NMDA spike activation at the individual dendritic branch, it has also been suggested

that NMDA spike initiation involves local glutamate spillover (Chalifoux and Carter, 2011) (although one theoretical study suggests that activation of synaptic NMDARs is sufficient for NMDA spike initiation (Rhodes, 2006)). I have extended a discussion on the potential role of glutamate spillover in NMDA spike initiation in a paper published in 2012 (Manuscript IV: (Lee, 2012b)). A contemporary view has been put forth by Larkum and colleagues in attempt to consolidate the roles of dendritic spikes and NMDA spikes in dendritic information processing (Larkum et al., 2009). In this model, NMDA spikes are positioned to operate at the earliest stage of synaptic integration, at individual dendritic branches, serving as spatiotemporal coincidence detectors that amplify the synchronous activity of clusters of synapses. Dendritic spikes are then positioned at the next level of integration, with a trigger zone analogous to the axon initial segment along large-calibre dendrites such as primary apical dendrites. Using this step-wise framework for integration, it was proposed that linear/sub-linear summation of distributed synaptic inputs, combined with the initiation of NMDA spikes at individual dendrites, generate excitatory potentials that converge at the primary apical dendrite to trigger dendritic spikes, which in turn further amplify salient events to generate high amplitude depolarizations to drive action potential discharge in the postsynaptic neuron.

The sensitivity of dendritic nonlinearities to spatial features of synaptic input (*i.e.,* cluster sensitivity) suggests that synaptic connectivity along individual dendrites likely adopts some degree of functional organization. Indeed, evidence from calcium imaging experiments both *in vitro* and *in vivo* indicate that synchronous synaptic activity is locally clustered onto short regions of dendrites (Kleindienst et al., 2011; Lavzin et al., 2012; Takahashi et al., 2012; Palmer et al., 2014), and that development of this functional synaptic clustering requires NMDAR activity (Kleindienst et al., 2011; Takahashi et al., 2012). Thus, NMDAR-dependent mechanisms

appear to somehow shape the spatial patterning of synaptic connectivity in a manner suited to optimize neural circuits for nonlinear dendritic computations. From a broader perspective, it is intriguing to consider that while genetic programs may provide axons and dendrites with general cues for growth and elongation (Whitford et al., 2002; O'Donnell et al., 2009), the detailed inscriptions on the so-called tabula rasa of developing neural circuits, given by fine-scale patterns of connectivity along dendrites, are likely not random, but instead conform to general rules such that future 'readings' and potential 'amendments' may be made intelligible according to specific dendritic information processing strategies – a neuronal 'alphabet' and 'language', of sorts. The physics of synaptic integration in dendrites outline specific contingencies underscoring the intimate relationship between the structure and function neural circuits at the subcellular level. As I will attempt to describe in the following section, this is not a new theme in neuroscience, as structure and function appear to resonate in a common chorus at multiple spatial scales in the orchestral symphonies of the brain.

Neural connectivity: structure relates to function at multiple spatial scales

In biology, the relationship between structure and function is ubiquitous. For instance, a protein's function is directly related to its structure, trees and lungs exhibit branching patterns reflecting convergent strategies to optimize function (*i.e.,* gas/nutrient exchange), and opposable thumbs have enabled a number of animals, including humans, to grasp and manipulate objects with great dexterity. Not surprisingly, the relationship between structure and function has long been recognized in the brain. At perhaps the most superficial level, this can be seen in the apparent functional specializations of different brain structures, wherein the hippocampus is required for spatial and declarative memory, the amygdala plays an important role in emotion-related behaviors, and various regions of cortex process different sensory stimuli. At another

level, major white matter tracts organize long-range connectivity between different brain regions, representing general routes of information flow in the brain. The sensory systems further demonstrate that synaptic connectivity adopts a remarkable level of functional organization at yet finer scales. For example, the rodent vibrissae system is organized such that sensory input from individual whiskers is mapped onto specific columns (barrels) of somatosensory cortex (barrel cortex) (Buonomano and Merzenich, 1998), the processing of sound in the auditory cortex is spatially organized according auditory frequencies (Schreiner et al., 2000); and, in the visual system, retinal projections to the lateral geniculate nucleus (LGN) of thalamus are organized to preserve the relative spatial relationships between retinal receptive fields (Chklovskii and Koulakov, 2004). Moreover, the hippocampal tri-synaptic circuit provides perhaps the most famous example of stereotyped microcircuit connectivity responsible for complex operations (Buzsaki and Moser, 2013). These examples highlight the close links between form and function at many spatial scales in the brain.

Interestingly, increasingly higher-order stimulus features seem to be encoded as information is successively transmitted through deeper layers of processing in the brain. Unlike the mapping of simple receptive field information described above for the primary sensory cortices, higher levels of neural information cannot be easily traced to the simple organization of synaptic connectivity. To illustrate this, consider the transformation of receptive field properties in the visual system. As mentioned, early on in the visual stream, spatial relationships in visual information are preserved in the topographic ('retinotopic') mapping from retinal receptive fields onto areas of LGN. As LGN neurons project this information to visual cortex V1, the topographic map of visual space is ceded by receptive fields that are tuned to the orientation of contrast bars. This transformation of receptive field properties requires that neurons

blend/integrate visual information converging from different retinal receptive fields (Kandel et al., 2000). Interestingly, recent work combining *in vivo* 2P calcium imaging and simultaneous multiple whole-cell recordings *in vitro* convincingly demonstrates the functional organization of recurrent microcircuit connectivity between L2/3 pyramidal cells in visual cortex. Specifically, it was found that L2/3 pyramidal cells in V1 sharing receptive field properties tend to connect to one another, and the emergence of this recurrent microcircuit organization was argued to arise from structured feed-forward excitation (Hofer et al., 2011; Ko et al., 2011; Ko et al., 2013; Ko et al., 2014; Cossell et al., 2015). Given the influence of nonlinear dendritic computations on the input-out functions of neurons, the notion that complex tuning properties of individual neurons arise by sorting multiple streams of afferent information suggests an important role for the functional organization of synaptic connectivity along dendrites [1].

As described in the previous section, we have learned a great deal from theoretical modeling (Mel, 1993; Poirazi and Mel, 2001; Gasparini and Magee, 2006; Gomez Gonzalez et al., 2011) and experimental studies *in vitro* (Schiller et al., 2000; Polsky et al., 2004; Losonczy and Magee, 2006; Tsay et al., 2007; Larkum et al., 2009; Polsky et al., 2009; Branco et al., 2010; Chalifoux and Carter, 2011), identifying spatial clustering and temporal coincidence as two important features determining the salience of synaptic input by accessing nonlinear dendritic integration mechanisms. One major hypothesis emerging from these studies is that functionally-

[1] Although it will take a considerable amount of work to directly test these ideas, I believe there are important insights to be gleaned from such conjecture. In principle, the step-wise transformation of receptive field properties at each stage of processing (at each synapse) would provide multimodal streams of higher-order information to be integrated in higher-order regions such as association cortex and hippocampus to enable complex aspects of the environment to be represented. The visual system was used to illustrate these ideas here, but this principle could potentially apply to any neuron faced with the task of integrating multiple sources of synaptic information.

related ensembles of synapses, to be maximally effective at propagating specific information through the neural network, should cluster onto individual dendrites. The recent demonstrations of dendritic spikes *in vivo* offer compelling evidence to support this hypothesis. As expected, not all neurons exhibit clustering of synaptic input and dendritic nonlinearities may not occur in all neurons (Jia et al., 2010; Chen et al., 2011; Varga et al., 2011). The organization of clustered synaptic connectivity and the implementation of nonlinear dendritic integration are likely features of neurons faced with distinct tasks and challenges when integrating synaptic inputs (*i.e,* processing information).

The field is thus beginning to realize a novel interplay where structure and function are once again intimately coupled, now at the fine-scale functional organization of synaptic connectivity along dendrites. This has been a central focus of my studies, and in my primary work (Manuscript V, in revision), I report the results of a series of experiments highlighting a candidate NMDAR-dependent mechanism which may guide the functional patterning of synaptic connectivity along the dendrites of developing CA1 pyramidal cells. This final section of the General Introduction will include a brief tour of the major insights from the experimental results in the context of the concepts described.

Postnatal development and the functional organization of synaptic connectivity

During early postnatal development, pyramidal cells in the cortex and hippocampus undergo robust dendritic growth and exhibit massive increases in synapse number and function. Initially, neurons exhibit short, twiggy dendritic morphologies which transform into large, branching dendritic arbors with development (Pokorny and Yamamoto, 1981b; Petit et al., 1988; Bianchi et al., 2013). During this time, dendritic spines begin to emerge and acquire form and

function, as evidenced by an increase in dendritic spine density (Pokorny and Yamamoto, 1981a; Harris et al., 1992), increases in the frequency and amplitude of mEPSCs and an increase in synaptic AMPAR content (Durand and Konnerth, 1996; Hsia et al., 1998; Beique et al., 2006; Brill and Huguenard, 2008; Busetto et al., 2008). This period of circuit assembly presents a key opportunity to shape the fine-scale functional organization of synaptic connectivity along dendrites.

As mentioned above, NMDAR-dependent synaptic calcium signals are critical for the induction of synaptic plasticity (Collingridge et al., 1983; Lynch et al., 1983; Malenka and Bear, 2004), and play a well-established role in synaptic strengthening and stabilization. Recent observations indicate that NMDAR activity is critical for stabilizing clustered synaptic activity (Kleindienst et al., 2011; Takahashi et al., 2012). Despite the important role of NMDAR-mediated calcium signals in synapse regulation, surprisingly little is known about intracellular calcium dynamics during synapse development. At mature synapses, NMDAR-mediated calcium signals are spatially confined at the activated spine head (Muller and Connor, 1991; Mainen et al., 1999; Majewska et al., 2000b; Majewska et al., 2000a; Sabatini et al., 2002; Noguchi et al., 2005; Grunditz et al., 2008; Araya, 2014). I discovered a dramatic departure from this canonical NMDAR-dependent calcium behavior during early postnatal synapse development by applying a combination of whole-cell electrophysiology, 2P imaging and glutamate uncaging in developing CA1 pyramidal cells from acute brain slices. Specifically, I found that synaptic NMDAR activation in young animals (postnatal days 8-17) generated calcium signals that readily exited the activated spine, propagated locally in the parent dendrite, and routinely invaded neighboring spines. Moreover, these locally propagating calcium signals were due to activation of ryanodine-sensitive calcium-induced calcium release (CICR) and lasted two times longer than isolated

NMDAR calcium signals. By the end of the third postnatal week, NMDAR function appeared to dissociate from CICR mechanisms, enabling synaptic calcium signals to adopt the characteristic spatially compartmentalized profiles of mature dendritic spines.

Spine calcium compartmentalization is thought to afford the synapse with a degree of autonomy, enabling them to regulate their function independently from their neighbours. Along a similar line of reasoning, NMDAR-dependent calcium signals that spread locally in the dendrite by CICR could potentially bind the development of synchronously active neighboring synapses along dendrites (Kleindienst et al., 2011; Takahashi et al., 2012). Consistent with this idea, I found that spatially-clustered synaptic inputs were very effective at triggering NMDAR-dependent CICR, demonstrating that local calcium signals exhibit 'cluster sensitivity'. By biochemically encoding clustered patterns of synaptic activation in a spontaneously active developing network, I hypothesize that NMDAR-mediated CICR may guide the clustered stabilization of synaptic ensembles along developing dendrites, and therefore impact the fine-scale functional organization of neural circuits.

Since it is technically challenging to test this hypothesis directly, I instead tested one immediate prediction: I reasoned that if synapse maturation takes place in a spatially clustered manner along dendrites, AMPA receptor content should be more similar between neighboring synapses than expected by chance (*i.e.,* spatially-random synapse development). To explore this idea experimentally, I used 2P glutamate uncaging to map AMPA/NMDA ratios at spines and analyzed the synaptic weight relationships between neighboring spines, and compared to random synapse development simulated by Monte Carlo shuffling methods. I detected in the experimental data local non-random clustering of synaptic weights between neighboring spines – spines less than 20 μm from each other exhibited the greatest similarity. This is consistent with

the local cooperative mechanisms in dendritic branches that favor the functional clustering of synapses in the dendritic arbor (Govindarajan et al., 2006; Harvey and Svoboda, 2007; Larkum and Nevian, 2008; Govindarajan et al., 2011; Legenstein and Maass, 2011; Winnubst and Lohmann, 2012; DeBello et al., 2014; Kastellakis et al., 2015). The available data provides a fascinating indication that the transitory developmental expression of NMDAR-dependent CICR instructs the early formation of synaptic connectivity motifs that enable neurons to exploit nonlinear regimes of dendritic computation and information processing. It is therefore tempting to speculate that dysregulation of these mechanisms may be involved the genesis of subtle microcircuit disturbances underlying deficits in multisensory integration seen in neurodevelopmental disorders (Geschwind and Levitt, 2007; van Atteveldt et al., 2014; Kastellakis et al., 2015)

Preface to Manuscripts

The manuscripts presented below were prepared during the course of my doctoral studies at the University of Ottawa. Each manuscript was formatted according to the standards of the journals they were submitted to, and therefore exhibit subtle organizational differences (*i.e.,* title page arrangement, order of sections).

As per University of Ottawa guidelines for thesis preparation and organization, figures and figure legends are positioned together in appropriate locations in the body of each manuscript, and all references have been condensed into a single section.

Manuscripts I-IV are published and are presented here in their final submitted form.
Manuscript V was peer-reviewed for the journal Neuron in January 2015, and is undergoing revisions for re-submission at the time of this writing (and is therefore subject to change). For each manuscript, I have included a 'Statement of Contributions' to describe my contributions and those of each author.

MANUSCRIPT I

Examining form and function of dendritic spines

Kevin F.H. Lee, Cary Soares and Jean-Claude Béïque*

*Corresponding author

This manuscript was published in *Neural Plasticity* in 2012:
Lee KF, Soares C, Béïque JC. Examining form and function of dendritic spines. Neural Plast. 2012; 2012:704103. doi: 10.1155/2012/704103. Epub 2012 Apr 17. PMID: 22577585

Statement of Contributions:

For this work, I led the survey of literature, conceived the topics of discussion, and wrote all drafts leading to submission. Cary Soares helped to formulate and develop the ideas and topics of the paper, constructed the figures, and helped edit the drafts. Dr. Jean-Claude Béïque guided the selection of discussion topics, provided detailed comments on the manuscript and edited the final draft prior to submission.

Introduction

Ever since the first description of *espinas* on Purkinje cells by Cajal more than 100 years ago (Cajal, 1888; Yuste, 2010), these tiny, femtolitre-sized, structures have been found on dendrites of a wide variety of neuronal cell types and the role of these minute structures in neuronal function has been the subject of considerable attention, speculation and debate. These discrete dendritic protrusions form a rich structural scaffold for the majority of excitatory synapses in the brain, harbouring a complement of biochemical signalling machinery as well as a proteinaceous postsynaptic density (PSDs) containing, amongst others, ionotropic glutamate receptors of the AMPA and NMDA subtypes (Traynelis et al., 2010). These receptors mediate the bulk of fast excitatory neurotransmission in the brain. During postnatal development, dendritic spines acquire AMPARs and undergo structural enlargement, resulting in a positive correlation between spine size and AMPAR function. Interestingly, the high degree of heterogeneity in dendritic spine structure and function at maturity suggests that spine growth is regulated in a synapse-specific manner and not simply a consequence of *en masse* spine development.

In the past decade or so, a number of technological developments in fluorescence microscopy and molecular techniques have greatly accelerated our understanding of the relationship between structure and function at dendritic spines. For one, the induction of synaptic plasticity at single synapses was found to result in changes in spine structure, providing a plausible mechanism to explain the concurrent developmental changes in spine size and function (Matsuzaki et al., 2004). Furthermore, recent studies have elaborated a mechanistic and molecular framework to suggest that spines function as discrete compartments, offering a basis for computationally-relevant synaptic autonomy. Based on the robust concordance between

structural and functional plasticity, and on the similarities in the molecular underpinnings that drive these two processes, there is a growing trend in synaptic physiology to infer synaptic strength based on characteristics of spine morphology. However, the dissociation of spine structure and function under some experimental conditions suggests an important mechanistic divergence in the regulation of spine form and function. In this review, we will provide an outline of the dendritic spine as a discrete functional compartment, discuss new developments in structural and functional plasticity at single spines and highlight key aspects of our understanding of the relationship between spine structure and function.

Two-photon Microscopy and the Investigation of Individual Dendritic Spines

Despite unsheathing fundamental properties of various forms of synaptic plasticity (Malenka and Bear, 2004), investigations based solely upon electrically evoked synaptic events left a number of open questions. Although minimum-stimulation methods allow the functional study of single synapses in isolation (Allen and Stevens, 1994; Stevens and Wang, 1995; Isaac et al., 1996; Dobrunz and Stevens, 1997), the inherent technical challenges of these experiments hinder the ability to efficiently amass data and resolve spatial parameters such as the morphology and location of the activated synapses (relative to each other and to the soma). The advent of two-photon (2P) laser scanning microscopy circumvented a number of these experimental limitations and has contributed considerable depth to our understanding of spine function and plasticity.

The longer-wavelengths and lower excitation energy used in 2P imaging increases imaging depth in scattering tissue (such as brain) while also reducing photo-damage/toxicity compared to 1P imaging (Denk et al., 1994; Helmchen and Denk, 2005; Svoboda and Yasuda,

2006). Furthermore, the 2P excitation event is highly restricted in physical space with an excitation volume that roughly approximates the diffraction limits of the optical system (Svoboda and Yasuda, 2006). This small excitation volume thus confers the ability to photoactivate molecules with high spatial precision, thereby providing novel opportunities for the study of synaptic physiology. For instance, 2P "uncaging" of caged forms of neurotransmitters (for eg., MNI-Glutamate) provides the ability to selectively activate spatially discrete glutamate receptors in a number of experimental preparations *in vitro* (Matsuzaki et al., 2001; Matsuzaki et al., 2004; Araya et al., 2006a; Beique et al., 2006; Losonczy and Magee, 2006; Harvey and Svoboda, 2007; Busetto et al., 2008; Harvey et al., 2008; Tanaka et al., 2008; Bloodgood et al., 2009; Ashby and Isaac, 2011; Beique et al., 2011; Matsuzaki et al., 2011), and *in vivo* (Noguchi et al.). Pioneering work by Kasai and colleagues used 2P imaging and glutamate uncaging to probe AMPAR content and induce LTP at individual dendritic spines on hippocampal CA1 pyramidal neurons, generating key insight into single synapse plasticity (Matsuzaki et al., 2001; Matsuzaki et al., 2004). For instance, the induction of LTP at single dendritic spines via 2P glutamate uncaging circumvented the presynaptic component of synaptic transmission and provided unequivocal support to the notion that, at least under certain conditions, synaptic plasticity can be mediated by solely postsynaptic mechanisms (Matsuzaki et al., 2004; Kerchner and Nicoll, 2008).

In addition to providing important information regarding plasticity at single synapses, advances in 2P imaging and related optical techniques have been instrumental in generating novel understanding of other neuronal mechanisms and properties such as the spatial distribution of synaptic weights, the autonomy of the spine as a functional compartment, the integrative

behaviour of dendritic branches and the recurrent connectivity of cortical circuits (Smith et al., 2003; Losonczy and Magee, 2006; Ashby and Isaac, 2011; Beique et al., 2011).

A Compartmental Model of Dendritic Spines

Dendritic spines are specialized structures exhibiting a high degree of molecular organization and exist in a wide range of morphologies. Although a number of nomenclatures have been proposed to describe the breadth of morphologies that individual spines can adopt, they can be broadly summarized as follows: "Mushroom-like", identified by a round dendritic spine head connected to the parent dendrite by a spine neck; "Stubby" spines, which are short, stout protrusions or bumps with no definitive spine neck; and filipodial/long spines, which appear as thin, finger-like protrusions (Harris et al., 1992; Arellano et al., 2007). There has been considerable speculation on the specific role imparted by these varying morphologies on aspects of spine function. For one, substantial attention has been given to the role of the spine neck and accumulating experimental evidence suggests that it serves to compartmentalize the dendritic spine head. This compartmental model is particularly attractive in light of the synapse-specificity of the structural and functional changes that take place over development and during plasticity. The compartmentalization of dendritic spines can be broadly divided into two functional domains: i) the biochemical compartment, which describes the spatial confinement of biochemical signalling due to diffusional restriction and physical segregation of proteins and signalling molecules; and ii) the electrical compartment, where spine neck morphology can impact the kinetics and propagation of synaptic potentials in a spine-specific manner. Here, we will sequentially review these two functional domains.

<u>The Biochemical Compartment</u>

Postsynaptic induction and expression of several forms of synaptic plasticity requires calcium influx through NMDARs and the initiation of calcium-dependent biochemical signalling in the dendritic spine. The development of calcium-sensitive fluorescent indicators and imaging techniques has greatly facilitated the study of calcium dynamics during synaptic activity. Specifically, calcium imaging experiments demonstrate that NMDAR-mediated calcium influx elicited during synaptic transmission is tightly restricted to the spine head, with minimal calcium diffusion into the parent dendrite (Muller and Connor, 1992; Connor et al., 1994; Oertner et al., 2002; Noguchi et al., 2005; Busetto et al., 2008). Given the key role of calcium as a second messenger in the regulation of synaptic plasticity, highly compartmentalized calcium signalling at dendritic spines is likely critical for providing the synapse-specificity of synaptic plasticity. As a result, it has been proposed that the primary function of the dendritic spine structure is to compartmentalize signalling molecules such as calcium (Yuste et al., 2000; Noguchi et al., 2005). Many factors can influence the intracellular diffusion of calcium. For instance, the presence of a spine neck has been suggested to restrict calcium diffusion and also appears to limit the diffusion of other molecules such as GFP and fluorescein dextran (Muller and Connor, 1992; Svoboda et al., 1996; Bloodgood and Sabatini, 2005; Noguchi et al., 2005; Zito et al., 2009). In addition, calcium pumps such as PMCAs and SERCA, calcium-binding molecules such as calmodulin (CaM) or calbindin, and differential cytosolic viscocities at individual spines can all contribute to regulate free-calcium concentrations (and its dynamics) and influence intracellular diffusion (Majewska et al., 2000a; Smith et al., 2007; Kenyon et al., 2010). Together, these diverse mechanisms indicate that dendritic spines utilize multiple strategies to compartmentalize biochemical signals and promote autonomous synaptic function (See **Figure 1**).

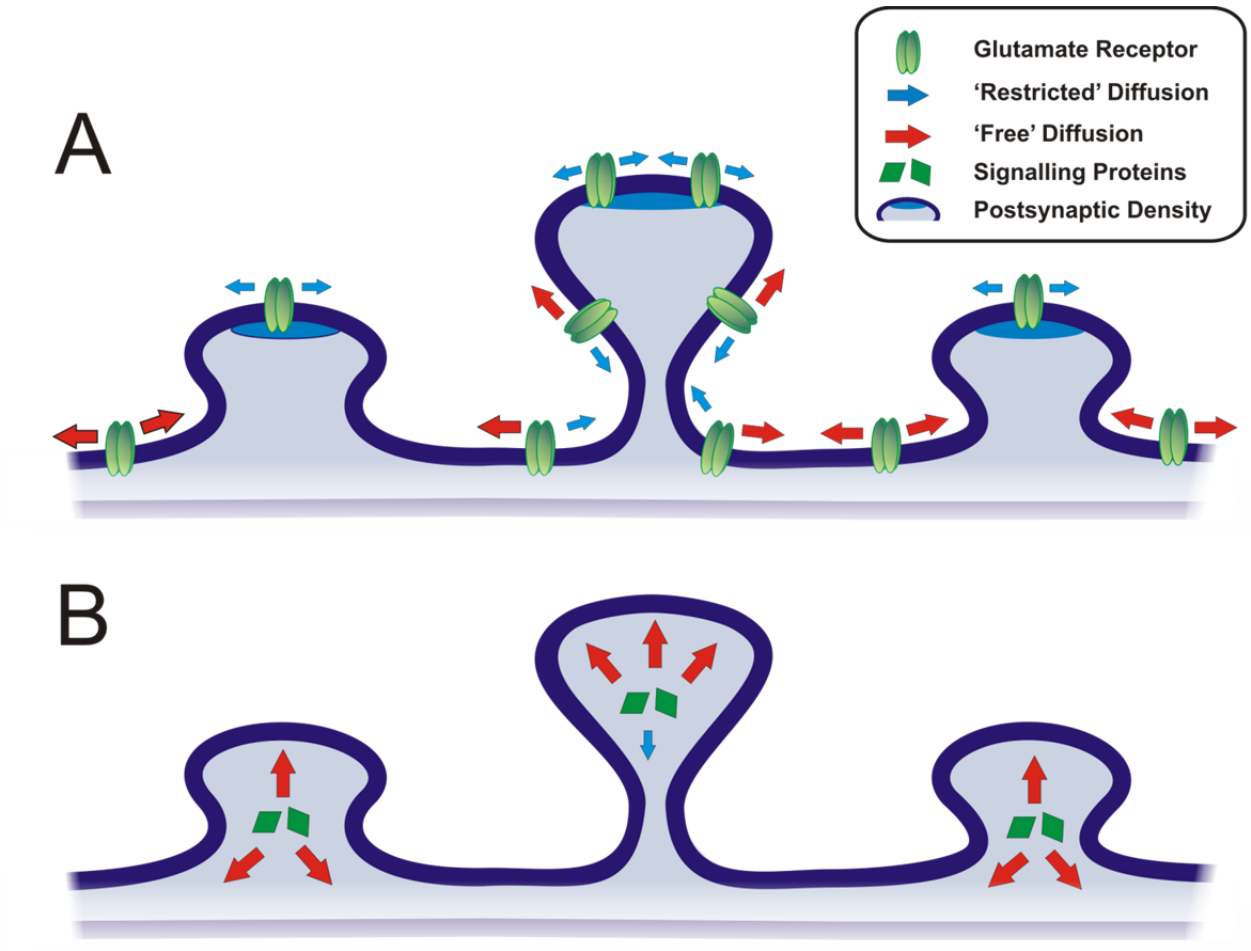

Figure 1: Biochemical compartmentalization in dendritic spines.
The spine neck may offer enhanced compartmentalization of biochemical signalling at synapses. In **A**, the lateral mobility of surface glutamate receptors is attenuated across longer spine necks and at the postsynaptic density. In **B**, the spine neck imposes diffusional constraints on cytosolic signalling proteins. These mobility restraints imposed by the spine neck create spine-specific compartmentalization of cytosolic signalling and surface receptor dynamics.

Dendritic spines must also communicate with protein synthesis machinery located in the parent dendrite to sustain late phases of LTP (Abraham and Williams, 2008; Tanaka et al., 2008; Govindarajan et al., 2011; Redondo and Morris, 2011). Thus, the movement of signalling molecules to-and-from the dendritic spine must not be fully compartmentalized but conforms to

some degree of regulation. An illustration of such regulation is provided by recent experiments showing that calcium/calmodulin-activated kinase II (CaMKII) and Ras, two important molecules for synaptic plasticity, exhibit differential displacements from activated spines into the parent dendrites during synaptic plasticity (Harvey et al., 2008; Lee et al., 2009). Recent work by Murakoshi, Wang and Yasuda (2011) extended these findings using a FRET based approach (Murakoshi et al., 2011). The authors assessed the spatial spread of two synaptically-activated Rho-GTPases, RhoA and Cdc42. Whereas single-spine LTP induced by 2P glutamate uncaging lead to sustained activation (up to 30 min) of both RhoA and Cdc42, only activated RhoA readily traversed the spine neck into the parent dendrite, with activated Cdc42 restricted to the stimulated spine (Murakoshi et al., 2011). Since the measured diffusional properties of these proteins were similar, it was proposed that mechanisms localized to the spine head were likely required to spatially restrict Cdc42 activation, thereby enforcing the notion that spines are highly regulated biochemical compartments. Taken together, the spatial compartmentalization of key regulatory molecules (*eg.,* protein kinases) may also offer powerful constraints that impact the spread of intracellular signals from the spine to the parent dendrite.

Surface (plasma membrane-bound) AMPARs and NMDARs exist at both synaptic and extrasynaptic locations. These surface receptor populations are not rigidly fixed, but in perpetual diffusional flux laterally through the membrane (Borgdorff and Choquet, 2002; Groc et al., 2004; Heine et al., 2008). Similar to intracellular diffusion, the lateral mobility of proteins in the plasma membrane can also be influenced by morphological parameters of spines (Ashby et al., 2006; Holcman and Triller, 2006; Choquet, 2010). For instance, FRAP analysis demonstrated that spine necks restrict the lateral diffusion of surface AMPARs. Specifically, AMPARs at spines connected to the parent dendrite by a spine neck exhibit a two-fold slower rate of lateral

mobility compared to those at spines without a distinguishable spine neck (**Figure 1**). Similar results were obtained using membrane-bound GFP, indicating that the impedance of lateral mobility was dictated by morphological parameters of the spine, and not by intrinsic properties of AMPAR trafficking *per se* (Ashby et al., 2006). Furthermore, AMPARs also undergo constitutive vesicular cycling via endo- and exocytosis. Evidence from both electron microscopy and fluorescence imaging indicates the presence of endocytic and exocytic zones within dendritic spines (Blanpied et al., 2002; Racz et al., 2004; Gerges et al., 2006; Lu et al., 2007). Interestingly, the dynamic balance of endo- and exocytosis modulates synaptic strength and underlie certain forms of plasticity. Indeed, LTP induction results in an enhancement of AMPAR exocytosis (Luscher et al., 1999; Park et al., 2004; Yudowski et al., 2007; Lin et al., 2009; Petrini et al., 2009). Taken together, the strategic clustering of signalling proteins, the development of narrow spine necks and the organization of vesicular cycling machinery can all contribute to biochemical compartmentalization of spines. This compartmentalization provides individual spines with the autonomous capacity to dynamically regulate the surface expression of distinct pools of AMPARs to promote the synapse-specificity of synaptic plasticity.

The Electrical Compartment

In addition to providing the morphological substrate for bestowing features of biochemical compartmentalization, spines may also function as electrical compartments capable of modulating the amplitude, kinetics and integration of synaptic potentials. Early estimations based on Rallian cable theory and measurements of molecular diffusion indicated that only modest ohmic resistances would be provided by spine necks, and therefore largely dismissed the notion that spines behave as electrical compartments (Koch and Zador, 1993; Svoboda et al., 1996). However, recent experimental evidence suggests that electrical compartmentalization can

take place in at least a subset of dendritic spines (Tsay and Yuste, 2004; Araya et al., 2006b; Bloodgood et al., 2009). A combination of current-clamp recordings, 2P uncaging and second harmonic membrane potential measurements provided evidence that long spine necks attenuate synaptic potentials between spine head and the parent dendrite (Araya et al., 2006b). In this line, it is interesting to note that calcium transients induced by activation of NMDARs can be readily detected by 2P calcium imaging in physiological extracellular magnesium concentrations (~1.0mM) in slices (Kovalchuk et al., 2002; Grunditz et al., 2008; Chalifoux and Carter, 2011) and in vivo (Chen et al., 2011; Jia et al., 2011; Varga et al., 2011), despite the presence of the voltage-dependent magnesium block of NMDARs near resting membrane potentials. Furthermore, calcium transients mediated by voltage-sensitive calcium channels (VSCCs) can also be visualized upon synaptic activation, indicating unexpectedly large depolarizations at the spine head (Bloodgood et al., 2009). Together, these data suggest that spine necks may impart an appreciable degree of electrical resistance – and charge accumulation in spine heads – and thus electrically compartmentalize dendritic spines (Tsay and Yuste, 2004). An intriguing and functionally powerful idea is that the degree of both electrical and biochemical compartmentalization might be dictated by active modifications in spine morphology. This possibility is becoming increasingly prominent given the dynamic structural changes which accompany the expression of synaptic plasticity (see below).

Structural and Functional Plasticity at Spines

The development of 2P glutamate uncaging to stimulate and induce LTP at single dendritic spines has been instrumental in providing key insights on the structural and functional changes that take place during plasticity. In 2004, Kasai and colleagues induced LTP at

individual dendritic spines by 2P glutamate uncaging and showed that the expression of LTP is associated with spine enlargement (Matsuzaki et al., 2004). Furthermore, smaller spines carried an inherently higher propensity for LTP expression compared to larger spines, which were functionally and structurally more stable. Interestingly, some of the molecular mechanisms underlying structural plasticity have been found to closely parallel those for synaptic plasticity. For instance, LTP-induction stimuli involving strong synaptic input and large postsynaptic rises in calcium facilitates actin branching and polymerization, providing a protrusive force to mediate spine enlargement (Fukazawa et al., 2003; Matsuzaki et al., 2004; Okamoto et al., 2004; Kasai et al., 2010; Patterson and Yasuda, 2011). Conversely, LTD-inducing stimuli leads to actin depolymerization, spine shrinkage and retraction (Okamoto et al., 2004). Moreover, similar to the expression of long-lasting phases of LTP, the temporal stability of structural plasticity requires the synthesis of new proteins (Tanaka et al., 2008; Govindarajan et al., 2011). These fundamental similarities in the induction of both structural and functional plasticity indicate an intimate relationship between these two processes.

One critical molecular link is CaMKII, a highly abundant protein in spines with an established role in synaptic plasticity (Malinow et al., 1989; Barria et al., 1997; Lisman et al., 2002; Matsuzaki et al., 2004; Lee et al., 2009). At rest, CaMKII directly bundles and stabilizes actin filaments and is involved in the structural stability of spines (Okamoto et al., 2007). CaMKII is activated by LTP-inducing stimuli, remaining persistently active and spatially compartmentalized to the stimulated spine – properties that correlate well with the spatiotemporal characteristics of structural and functional plasticity (Lee et al., 2009). Moreover, active CaMKII dissociates from the actin cytoskeleton causing structural destabilization, thus permitting structural modifications of the spine to take place (Okamoto et al., 2007).

Downstream, CaMKII activates a number of signalling molecules such as members of the Rho-GTPase family (RhoA, Cdc42, Rac1 and Rnd1) to mediate changes in spine structure (Cingolani et al., 2008; Murakoshi et al., 2011; Patterson and Yasuda, 2011). For instance, Cdc42 becomes activated during LTP induction and interacts with p21-activated kinase (PAK) proteins to stabilize structural modifications (Murakoshi et al., 2011). Mice expressing a dominant-negative PAK (dnPAK) transgene in the forebrain show abnormal dendritic spine morphology, defects in both LTP and LTD, and impairments in the consolidation of spatial and fear memory (Hayashi et al., 2004). Whereas it is difficult to attribute the behavioural deficits exhibited by dnPAK mice to synaptic impairments alone, these experimental strategies help to elucidate the interplay between structural and functional plasticity.

Although structural and functional changes rely on common signalling molecules, is it possible for these changes to occur independently of one another? Some evidence suggests that structural and functional plasticity are mutually stabilizing processes. For instance, in CA1 pyramidal neurons, the temporal stability of LTP expression is dependent on actin polymerization (Krucker et al., 2000). Subsequent investigations have expanded on these findings, underscoring a critical role for cytoskeletal actin dynamics in the directed trafficking of AMPARs (Fukazawa et al., 2003; Hayashi and Huganir, 2004; Okamoto et al., 2004; Chen et al., 2007; Ramachandran and Frey, 2009). Conversely, the insertion of AMPARs during LTP not only acts to increase synaptic strength, but has also been suggested to stabilize structural changes of the spine (Kopec et al., 2007). These data suggest that the molecular components that drive structural changes in dendritic spines during plasticity also act to stabilize AMPAR insertion and vice versa. This dynamic interplay thus provides a basis for the tight association between changes in spine volume and AMPAR content during LTP.

Structure versus Function

Dendritic spines on pyramidal cell dendrites number in the thousands and exhibit a high degree of morphological heterogeneity. High resolution electron microscopy studies provided the first indication that spine form and function were related by demonstrating that the size of the PSD and number of AMPARs positively correlates with the size of spines (Baude et al., 1995; Kharazia and Weinberg, 1999; Takumi et al., 1999; Katz et al., 2009). A number of recent studies provided functional support to these ultrastructural findings by showing a strong positive correlation between dendritic spine size and AMPAR function (i.e., size of AMPAR-mediated current), as determined by 2P glutamate uncaging (Matsuzaki et al., 2001; Beique et al., 2006; Zito et al., 2009; Ashby and Isaac, 2011; Noguchi et al., 2011). Considering the parallel changes observed in both structure (*i.e.,* spine volume) and function (*i.e.,* AMPAR content) during activity-dependent plasticity, it is perhaps not at all surprising that such a correlation exists. However, a more detailed and in depth look at the literature, as outlined below, reveals that spines, at least in certain conditions, have the ability to significantly depart from such a tight structure/function coupling.

One of the first indications pointing to a divergence of spine form and function was provided by Smith et al. (2003) while describing the distance-dependent scaling of synaptic AMPARs in hippocampal CA1 pyramidal neurons (Smith et al., 2003). Using a combination of whole-cell and dendritic recordings with 2P glutamate uncaging, they showed the synaptic weights of spines were progressively larger with increasing distances from the soma. However, this apparent increase in spine function was not accompanied with measurable changes in spine volume. Non-stationary fluctuation analysis on 2P glutamate uncaging currents further revealed that this increase in function with dendritic distance reflected a higher density of spine AMPARs,

and not an enhanced single-channel conductance. Together, these data provide a convincing illustration that spines of similar size can express a strikingly wide range of AMPAR density.

A disconnect between dendritic spine structure and function is further evidenced in studies of 'silent' synapses. Silent synapses contain detectable NMDARs but are devoid of AMPARs and are therefore largely 'silent' at rest (ought to the magnesium-dependent blockade NMDARs at resting membrane potential). They are thought to represent immature glutamateric synapses in part because their expression drastically diminishes during postnatal development (Isaac et al., 1997; Zhu and Malinow, 2002; Kerchner and Nicoll, 2008). Not surprisingly, early 2P-glutamate uncaging investigations described the presence of silent synapses on thin, filipodial-like spines in developing CA1 pyramidal neurons (Beique et al., 2006). Interestingly, however, subsequent investigations in the rodent somatosensory cortex reported that silent synapses can be detected at spines spanning a broad range of morphologies (Busetto et al., 2008; Ashby and Isaac, 2011). Although providing indirect support to this notion, work in PSD-95 KO mice also documented the presence of a structure/function uncoupling for spines. At an age where silent synapses were no longer detected in WT mice, PSD-95 KO mice displayed a high proportion of silent synapses onto large spines that otherwise appeared mature (Beique et al., 2006). Collectively, these data indicate that although there is a clear correlation between spine size and function, there is also room for a significant departure from this tight structure/function coupling.

Studies on the dynamical nature of spine structure during LTD also indicate a divergence in the signalling pathways that regulate spine size and function. For instance, Zhou et al (2004) reported that LTD and spine shrinkage at hippocampal synapses show differential requirements for protein phosphatase signalling via PP1 and calcineurin, despite sharing a similar requirement

for NMDAR activation (Zhou et al., 2004). Furthermore, while the actin-binding protein cofilin was involved in spine shrinkage, it seemed to play no role in the expression of LTD. More recent investigations have also indicated that clathrin-mediated endocytosis is not required for spine shrinkage, despite being essential for LTD expression (Wang et al., 2007). Finally, LTD studies in cerebellar Purkinje cells also reported dissociation between spine structure and function. Indeed, Sdrulla and Linden reported that LTD at cerebellar parallel fiber-Purkinje cell synapses was not associated with changes in either spine number or volume. In an interesting twist, the authors further identified a manipulation that lead to a dramatic and global retraction of spines on Purkinje neurons that, surprisingly, was not associated with significant changes in synaptic strength (Sdrulla and Linden, 2007). Thus, evidence obtained from LTD experiments in two distinct brain regions underscores a mechanistic divergence of spine structure and function.

Lastly, this divergence is further exemplified in a model of single-synapse homeostatic plasticity in dissociated cortical neuronal cultures. Homeostatic plasticity refers to the ability of a neuron to bi-directionally tune synaptic AMPAR content in response to changes in overall network activity (Turrigiano, 2011). Recent experiments have expanded these findings by showing that homeostatic regulation of synaptic strength can be achieved at the level of individual dendritic spines (Lee et al., 2010; Beique et al., 2011). In one experimental paradigm, chronic suppression of presynaptic glutamatergic input onto single spines lead to an enhancement of postsynaptic AMPAR function, as determined by 2P glutamate uncaging (Beique et al., 2011). Interestingly, despite a marked increase in AMPAR currents, there were no discernable changes in spine volume (see **Figure 2**). By comparing the current-voltage (I-V) relationship of AMPARs at these two populations of dendritic spines, activity-deprived synapses were found to express AMPARs with a distinct subunit composition (AMPARs lacking the GluA2 subunit). Because this

AMPAR subtype has an inherently higher conductance, this switch in subunit composition provides a mechanistically plausible model to account for the increased synaptic strength onto spines of similar volume.

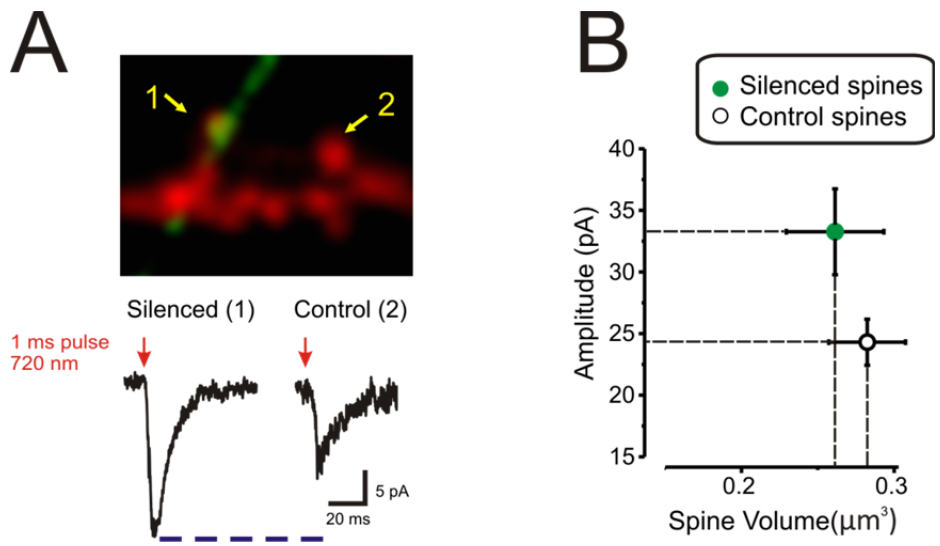

Figure 2: Dissociation of spine size and synaptic strength. In **A,** the release of glutamate was reduced for 48 hours specifically on the spine marked (1). This lead to a homeostatic enhancement of synaptic strength, as assessed by 2P-uncaging of MNI-Glutamate. The size of the synaptic currents induced by 2P-uncaging are shown in the bottom panel. In **B**, the significant enhancement of the amplitude of synaptic currents onto 'silenced' spines was not accompanied by any measurable changes in spine volume. Adapted from (Beique et al., 2011)

Conclusion

As a major component of excitatory synapses, spines are strategically poised to support important modulatory roles in synaptic transmission and neuronal function. Although still subject to debate, an emerging notion posits that spines provide a structural scaffold to act as biochemical and electrical compartments. Interestingly, discrete differences in dendritic spine morphology may directly influence the degree of functional compartmentalization (Figure 1).

In addition, the dynamic nature of spine structure (Blanpied et al.; Blanpied et al., 2008) may generate parallel changes in the compartmentalization features of individual spines. One can speculate that these morphologically-dependent degrees of compartmentalization lead to distinct states of metaplasticity at individual synapses. This notion aligns well with emerging theoretical models of synaptic learning that demonstrate that synapses exhibiting a gradation of states, each bridged by distinct metaplastic transitions, bestow neural networks with enhanced information storage capacity (Fusi et al., 2005; Fusi and Abbott, 2007). Altogether, these considerations highlight the rich computational potential afforded by the yet to be completely understood relationship between form and function of dendritic spines.

MANUSCRIPT II

Title: Differential subcellular targeting of glutamate receptor subtypes during homeostatic synaptic plasticity

Abbreviated Title: AMPA and NMDAR changes in homeostatic plasticity

Authors: Cary Soares [a,b,1], Kevin F.H. Lee [a,b,1], Wissam Nassrallah [b], Jean-Claude Béïque [a,b,c,d]

Author Affiliation:

[a] Neuroscience Graduate Program, [b] Department of Cellular and Molecular Medicine, [c] Centre for Stroke Recovery, [d] Centre for Neural Dynamics, Faculty of Medicine, University of Ottawa, Ottawa, ON K1H 8M5, Canada

[1] C.S and K.L contributed equally to this work.

Corresponding author:

Jean-Claude Béïque

Acknowledgements

The authors would like to thank Nina Ahlskog for her valuable contribution in setting up the surface biotinylation assay, Riadh Haj-Dahmen for his assistance in the early phases of the project, and members of the Béïque and Bergeron laboratories for helpful discussions. This research was funded by the Heart and Stroke Foundation Center for Stroke Recovery, the Canadian Institute of Health Research, the Natural Sciences and Engineering Research Council of Canada and the Canadian Foundation for Innovation (to JCB).

The authors declare no competing financial interests.

This manuscript was published in *The Journal of Neuroscience* in 2013:
Soares C, Lee KF, Nassrallah W, Béïque JC. Differential subcellular targeting of glutamate receptor subtypes during homeostatic synaptic plasticity. J Neurosci. 2013 Aug 14; 33(33):13547-59. doi: 10.1523/JNEUROSCI.1873-13.2013. PMID: 23946413

Statement of Contributions:

I initiated the experiments for this paper in 2009-2010 as the first graduate student in the laboratory. The core observations described in Figures 1-3 and 6 were found during these early stages of the project. However, toward the end of 2010 and during early 2011, we encountered problems maintaining healthy slice cultures and the project was thus put on hiatus. Soon thereafter, Cary Soares became a graduate student in the lab and worked to troubleshoot the slice culture methods. By optimizing the slice cultures, Cary was instrumental in reviving this project. The optimized slice culture methods presently used in the lab were recently published in a textbook chapter:

> Cary Soares, Kevin F.H. Lee, Denise Cook, Jean-Claude Béïque. (2013) *A cost effective method for preparing, maintaining and transfecting neurons in organotypic slices*. Methods in Molecular Biology: Patch Clamp Methods and Protocols. 2nd edition. Humana Press 2014

In the meantime, I took the lead on a separate research project (leading to Manuscript V), and Cary adopted this project as his primary research focus. Cary led the project to its completion, acquiring and analyzing the majority of the data contained in this paper. I assisted in the experimental design, and aided in collecting electrophysiological and morphological data shown in Figures 1-6, and contributed novel computational tools (in MATLAB) for the iterative multiplicative scaling analysis in Figure 1. Wissam Nassrallah, an undergraduate student at the time, performed and analyzed the Western Blot experiments shown in Figures 3 and 5.

In the preparation of the manuscript, Cary Soares analyzed the data and constructed the figures. Cary and I wrote the paper, contributing equal efforts in the interpretation of the data, formulation of the concepts for developing the narrative and discussion topics. We drafted and edited the paper together.

Dr. Jean-Claude Béïque oversaw the entire process (experimental design, data analysis/interpretation, construction of figures) and provided major guidance for the writing/editing of the drafts leading to the publication of the paper.

Abstract

Homeostatic processes are believed to contribute to the stability of neuronal networks that are perpetually influenced by Hebbian forms of synaptic plasticity. Whereas the rules governing the targeting and trafficking of AMPA and NMDA subtypes of glutamate receptors during rapid Hebbian LTP have been extensively studied, those that are operant during homeostatic forms of synaptic strengthening are less well understood. Here, we used biochemical, biophysical and pharmacological approaches to investigate glutamate receptor regulation during homeostatic synaptic plasticity. We show in rat organotypic hippocampal slices that prolonged network silencing induced a robust surface upregulation of GluA2-lacking AMPARs, not only at synapses, but also at extrasynaptic dendritic and somatic regions of CA1 pyramidal neurons. We also detected a shift in NMDAR subunit composition that, in contrast to the cell-wide surface delivery of GluA2-lacking AMPARs, occurred exclusively at synapses. The subunit composition and subcellular distribution of AMPA and NMDARs are therefore distinctly regulated during homeostatic synaptic plasticity. Thus, because subunit composition dictates key channel properties such agonist affinity, gating kinetics and calcium permeability, the homeostatic synaptic process transcends the simple modulation of synaptic strength by also regulating the signaling and integrative properties of central synapses.

Introduction

Hebbian forms of synaptic plasticity *i.e.,* long-term potentiation and long-term depression (LTP and LTD), exhibit features that are consistent with a synaptic encoding of information and, as such, have come to dominate our understanding of how memories are stored in the brain (Kessels and Malinow, 2009). However, neural network models that implement solely Hebbian plasticity are inherently unstable due to the positive feedback nature of LTP and LTD (Turrigiano, 2008; Lee et al., 2014). The discovery of homeostatic plasticity has been received with great interest in part because it provides a biologically plausible means to stabilize perpetually active and plastic neural networks (Turrigiano, 2008; Lazar et al., 2009; Lee et al., 2014). Homeostatic synaptic plasticity (HSP) enables neurons to adapt to sustained alterations in overall cellular activity by bidirectionally regulating the strength of excitatory and inhibitory synaptic transmission. For example, neurons respond to prolonged inactivity by a cell-wide enhancement of excitatory synaptic strength, and adapt to sustained hyperactivity by a global synaptic depression of excitatory synapses (Turrigiano et al., 1998).

Despite enacting fundamentally different roles in neuronal function, Hebbian and homeostatic synaptic plasticity share common synaptic loci of expression. Indeed, both forms of plasticity can manifest through the regulation of postsynaptic glutamate receptor number and/or function. Some, but not all, studies have reported that synaptic strengthening during HSP is mediated by the insertion of GluA2-lacking AMPARs (Ju et al., 2004; Thiagarajan et al., 2005; Sutton et al., 2006; Aoto et al., 2008; Groth et al., 2011), a calcium-permeable subtype of AMPAR expressed at very low levels under baseline conditions in pyramidal neurons (Beique and Huganir, 2009; Lu et al., 2009). Interestingly, this AMPAR subtype has also been implicated in LTP expression (Plant et al., 2006; Guire et al., 2008), although this remains controversial

(Adesnik and Nicoll, 2007; Gray et al., 2007). Furthermore, the subunit composition of synaptic NMDARs is also dynamically regulated. Recent work indicates that synaptic NMDAR subunit composition is highly regulated during LTP, with subunit switching occurring as rapidly as synaptic potentiation *per se* (Bellone and Nicoll, 2007). It remains unclear, however, whether such mechanisms also operate during homeostatic synaptic strengthening.

Here, we show that prolonged network inactivity in organotypic hippocampal slices leads to a cell-wide surface delivery of calcium-permeable GluA2-lacking AMPARs that populate both synaptic and extrasynaptic sites. Synaptic NMDARs, but not their extrasynaptic counterparts, undergo a switch from predominantly GluN2B-containing to GluN2A-containing NMDARs in response to prolonged inactivity. These results therefore expand the known repertoire of the cellular processes involved in the homeostatic regulation of excitability of CA1 pyramidal neurons. The synaptic homeostatic response is thus not merely limited to the regulation of synaptic strength as a means to control excitability, but encompasses broader alterations that fundamentally influence key features of excitatory synaptic transmission.

Materials & Methods:

Organotypic Slice Culture

Organotypic slice cultures were prepared using a modified method of the original interface technique (Stoppini et al., 1991). Male and female Sprague-Dawley rats (Charles River Laboratories; 6-8 days old) were anaesthetized by isofluorane (Baxter Corporation, Canada) inhalation and decapitated according to procedures approved by the University of Ottawa Animal Care Committee. Individual hippocampi were removed in ice-cold cutting solution containing

the following (in mM): 119 choline chloride, 2.5 KCl, 4.3 $MgSO_4$, 1.0 $CaCl_2$, 1.0 NaH_2PO_4–H_2O, 1.3 Na-ascorbate, 11 glucose, 1 kynurenic acid, 26.2 $NaHCO_3$, saturated with 95% O_2 and 5% CO_2 (pH = 7.3; 295-310 mOsm/L) and hippocampal slices (400μm) were obtained using a MX-TS Tissue Slicer (Siskyou). Individual hippocampal slices were transferred to membrane inserts (Millipore, #PICM03050) and maintained in six-well plates at 34°C in 95% O2 and 5% CO2 containing a Neurobasal-A based culture media. Slice culture media was exchanged at 1 day in vitro (DIV) and then every 2-3 days thereafter. After 6-8 DIV, tetrodotoxin (1μM; TTX, Tocris Bioscience) was added to the treatment group.

Whole-Cell Electrophysiology

Whole-cell recordings were performed on CA1 pyramidal neurons from control slices or slices incubated for 3-4 days with TTX. For recording, one slice was removed from a culture insert, placed in a recording chamber and cells in stratum pyramidale of the CA1 subfield were visualized under differential-interference contrast (DIC) using a BX61WI upright microscope (with a 40x/0.8NA or 60x/1.0NA objective; Olympus, Melville, NY) or a Zeiss Axio Examiner D1 upright microscope (40x/0.75NA objective). All experiments were performed at room temperature in Ringer containing (in mM): 119 NaCl, 2.5 KCl, 1.3 $MgSO_4$, 2.5 $CaCl_2$, 1.0 NaH_2PO_4, 11 glucose, and 26.2 $NaHCO_3$ (or low Mg^{2+} Ringer containing 0.1 $MgSO_4$, 3.0 $CaCl_2$) saturated with 95% O_2 and 5% CO_2 (pH = 7.3; 295-310 mOsm/L). Additional drugs were added to the Ringer as follows (in mM), as indicated in the text: 0.001 TTX, 0.1 picrotoxin, 0.01 NBQX, 0.05-0.1 DL-APV, 0.003 ifenprodil; 0.02 1-Naphthyl acetyl sperminetrihydrochloride (NASPM), all purchased from Tocris Bioscience. Whole-cell recordings were carried out using an Axon Multiclamp 700B amplifier, filtered at 2 kHz, sampled at 10 kHz and digitized with an Axon Digidata 1440A digitizer. Borosilicate glass recording electrodes (World Precision

Instruments, Florida or Sutter, California) were pulled using a Narashige PC-10 vertical puller (Narishige, Japan) and had resistances ranging from 3-5 MΩ. For voltage-clamp recordings, electrodes were filled with an internal solution containing (in mM): 115 cesium methane-sulfonate, 0.4 EGTA, 5 tetraethylammonium-chloride, 2.8 NaCl, 20 HEPES, 3 ATP-Mg, 0.5 GTP, 10 Na-phosphocreatine, 5 QX-314 (pH = 7.2-7.3; 280-290 mOsm/L) all purchased from Life Technologies. For all voltage clamp recordings, access resistance was continuously monitored during the experiment by delivering a 5 mV hyperpolarizing step at the onset of every electrophysiological sweep. All recordings were analyzed using Clampfit 10.2 (Molecular Devices) and Origin 8 analysis software (OriginLab). All voltages were left uncompensated. All error bars represent SEM.

For AMPAR I-V curves, 0.1 mM spermine (Tocris) was included in the internal solution. To calculate a rectification index for AMPAR I-V relationships, the slope was calculated for both the inward (-70mV to 0mV) and outward (0mV to +40 mV) portions of the curve, and the ratio of the outward slope over the inward slope was computed (Beique et al., 2011; Granger et al., 2013). The amplitudes of AMPA and NMDA currents for AMPA/NMDA ratios were estimated using the EPSC recorded at +40 mV, based on their respective time-courses, as previously described (Beique et al., 2006). For decay analysis of NMDAR-mediated EPSCs (both evoked EPSCs at +40mV and uncaging EPSCs at -60mV), a bi-exponential fit was used to calculate a weighted tau value (τ_w) (Vicini et al., 1998). To ensure that all evoked currents were monosynaptic, extreme care has been taken to minimize polysynaptic activity. A glass patch electrode was used to electrically stimulate glutamate release from axons and was positioned close to the proximal apical dendritic arbour of the recorded neurons. Stimulation intensity was

kept low, eliciting eEPSCs of small amplitude (<100 pA, typically around 50 pA). In some cases, 10-30 nM TTX was included in the Ringer solution to dampen polysynaptic activity.

Peak Scaled Non-Stationary Noise Analysis of AMPAR-mEPSCs

For estimates of mean AMPAR channel conductance (□) and the number of channels exposed to glutamate (N), peak scaled noise analysis of AMPAR-mEPSCs was performed using Mini Analysis software (Synaptosoft). All recordings with less than 50 events were discarded from the analysis. An average mEPSC waveform from each recording was scaled to the peak of each mEPSC in the recording and the variance of current fluctuations around the mean for each point in time was calculated. The average current variance relationship was then binned into 30 time points (independent of the amplitude of the average mEPSC) and the data was fit with the parabolic equation:

(1) $\sigma^2 = iI - I^2/N + b$

where σ^2 = variance, I = Mean Current, i = single channel current, N =Number of open channels at peak current, and b = background variance. From this equation, □ was calculated by dividing i by the driving force (-80mV). Recordings were discarded if the parabolic fits of the current variance plots had $R^2 < 0.5$. Since R^2 values of the parabolic fits were generally greater than 0.75, our estimate of N (*i.e.,* number of channels) was not affected by a skewed variance versus mean relationship (Traynelis et al., 1993; Hartveit and Veruki, 2007)

Two-Photon Imaging and Uncaging

Simultaneous two-photon imaging and glutamate uncaging was performed using two Ti:Sapphire pulsed lasers (MaiTai-DeepSee, Spectra Physics, USA) coupled to an Olympus MPE-1000 galvanometer scanning system. Prior to uncaging experiments, lasers were aligned to

one another using fluorescent beads. One Ti:Sapphire laser was tuned to 810 nm to visualize morphology (Alexa Fluor 594) and the second laser was tuned to 720 nm for MNI-Glutamate uncaging. Synchronization of electrophysiological and optical equipment was accomplished using a Master-8 pulse generator (A.M.P.I, Israel).

Glutamate uncaging experiments were performed with 2.5 mM MNI-glutamate trifluoroacetate (Femtonics, Hungary) and tetrodotoxin supplemented to the Ringer, while 0.03 mM Alexa Fluor 594 hydrazide (Na-salt; Invitrogen) was included in the internal recording solution. Whole-cell electrophysiological recordings were carried out as described above. Neurons were allowed to fill with the dye for a minimum of 10 minutes before onset of uncaging experiments. All two-photon uncaging EPSCs were generated from proximal secondary and tertiary apical dendrites to minimize issues of space clamp. Intensity of each laser was independently controlled using two independent acousto-optic modulators (AOMs). The intensity of the uncaging laser was tuned to generate a 10-20 pA AMPAR-mediated 2P-EPSC at a holding potential of -70 mV for AMPAR-IV curves. For NMDAR uncaging experiments, laser intensity was set to generate a NMDAR-mediated 2P-EPSCs smaller than 25pA when recorded in low magnesium Ringer (0.1mM Mg^{2+}, 3 mM Ca^{2+}) at -60mV in the presence of 0.01 mM NBQX (Tocris) and 0.01 mM glycine. Because no particular care was taken to assure constant uncaging laser power between experiments in different neurons or slices (by normalizing for uneven light scattering at different tissue depth), we have not directly compared absolute amplitudes of 2P-EPSCs between experiments. Rather, we have compared metrics that are largely independent of laser power (*i.e.,* rectification properties and decay kinetics: see results section). Uncaging laser power was however kept constant when uncaging was performed on neighbouring spines and shaft regions of the same dendritic segment.

Image Analysis

For spine density and spine volume measurements, two photon image stacks of proximal apical dendrites were obtained after a minimum of 30 minutes of dye filling following whole-cell access. Image stacks were gathered in optical sections of 0.5-0.7 μm, with an X-Y resolution between 0.05 and 0.1 μm/pixel. Spine density was calculated after manually sectioning apical dendritic reconstructions into 10 μm segments. Spine volume measurements were calculated using an intensity-based method, as previously described (Matsuzaki et al., 2001; Beique et al., 2006). In cases where spine diameter (*i.e.,* FWHM) are shown (Figure 7-8), the intensity based method of determining spine volume was not applicable to do to limitations in the images gathered (*i.e.,* images of spines from uncaging experiments were not gathered for volume analysis, which necessitates a high resolution image containing many large and resolvable spines for calibrating the intensity-based methods). All measurements for spine volume and spine density were generated from unprocessed images.

Analysis of dendritic complexity was achieved using Neuron Studio analysis software (Computational Neurobiology and Imaging Center, Mount Sinai School of Medicine, New York). Dendritic arbors of CA1 pyramidal neurons were modeled in Neuron Studio software and dendritic complexity measurements were extracted. The dendritic complexity metric reported is an underestimate of the total dendritic complexity, as only apical regions were included in the analysis. Complexity of Alexa-594 filled CA1 pyramidal neurons from control and TTX treated slices (postnatal day 7-8 + 9-10 days *in vitro*) were compared to age matched neurons from acute slices (post natal day 16-18).

Surface biotinylation Assay.

Organotypic slices were removed from the incubator and rapidly placed in ice cold TBS+ (in mM; 20 Tris, 0.5 KCl, 13.7 NaCl, 20 MgCl2, 20 CaCl2, pH 7.4) containing 0.5 mg/ml Sulfo-NHS-SS-Biotin (Pierce/Thermo Scientific, Rockford, IL, USA) for 20 min. Unbound biotin was removed by washing slices with ice-cold TBS+. Slices were lysed in lysis buffer (in mM; 150 NaCl, 20 HEPES, 2 EDTA and, in %; 0.1 SDS, 1 Triton X-100) using a Dounce homogenizer, and sonicated (2 × 10 s, 25% on a Vibra-Cell, VCX130, Sonics, Newtown, CT, USA). The cleared supernatant was incubated with equilibrated NeutrAvidin beads (Pierce/Thermo Scientific, Rockford, IL, USA) at 4°C for 1.5 h. Beads were washed six times in a TBS solution with 0.05% SDS, and bound protein was eluted with elution buffer (in mM; 50 Tris-HCl, 1 DTT, in %; 2 SDS) and boiled at 100°C for 10 min.

Equal concentrations of internal and surface proteins were loaded on SDS-PAGE and Western blot was performed with the following antibodies: anti-GluN1 (1:3000, mouse monoclonal) and anti-GlyR (1:1000, mouse monoclonal) from Synaptic Systems (Goettingen, Germany); anti-GluN2A (1:1500, rabbit polyclonal), anti-GluN2B (1:1500, rabbit polyclonal), anti-GluA1 (1:1000 rabbit monoclonal) from Millipore (Billerica, MA, USA); anti-GluA2 (1:2000, Rabbit polyclonal) from Pierce Antibodies (Rockford, IL, USA) and anti-β-actin (1:6000, mouse monoclonal) from Genscript (Piscataway, NJ, USA). The chemiluminescent intensities were recorded using an Odyssey Fc Imaging System (Li-COR, Lincoln, NE, USA). Quantitative analyses were performed by determining the intensity of each band with Image Studio software (Li-COR, Lincoln, NE, USA).

Results

Enhanced AMPAR conductance during multiplicative homeostatic synaptic strengthening in CA1 pyramidal neurons

We first sought to recapitulate key features of homeostatic synaptic plasticity (HSP) in an organotypic hippocampal slice preparation. Consistent with previous studies, CA1 pyramidal neurons from hippocampal slices incubated for 3-4 days with tetrodotoxin (TTX, 1μM) exhibited a robust increase in the amplitude (CTL: 16.51 ± 0.98 pA, n=35 cells; TTX: 22.50 ± 0.74 pA, n= 33 cells; p<0.01; Figure 1B) (Tyler and Pozzo-Miller, 2003; Kim and Tsien, 2008; Arendt et al., 2013) and frequency of AMPAR mediated miniature excitatory postsynaptic currents (mEPSCs) (CTL: 0.20 ± 0.03 Hz; TTX: 0.36 ± 0.06 Hz; p<0.01; Figure 1C) as determined by whole-cell electrophysiological recordings. A key feature of homeostatic synaptic strengthening is that the amplitude distribution of AMPAR-mEPSCs is scaled by a single common factor, likely reflecting cell-wide synaptic changes whereby each synapse scales proportionally to its original weight (Turrigiano et al., 1998; Lee et al., 2014). To establish whether such multiplicative scaling occurs in our experimental paradigm, we derived a scaling factor using two independent analytical methods (Turrigiano et al., 1998; Kim et al., 2012). First, we plotted the rank-order relationship of 3380 randomly selected AMPAR-mediated mEPSC amplitudes from both control and TTX-treated neurons (Figure 1D). As true multiplicativity necessitates the exclusion of additive components (Kim et al., 2012), the scaling factor was obtained from the slope of the linear relationship through the origin of the rank ordered plot. Consistent with multiplicative HSP, the distribution of mEPSC amplitudes from TTX-treated neurons overlapped well with the control distribution when divided (or "scaled") by this scaling factor (scaling factor = 1.169; p=0.34, Kolmogorov-Smirnov [K-S] test; Figure 1E). Using a separate approach, we iteratively

tested 1000 scaling factors ranging from 0.5 to 1.5 (Figure 1D; see Materials & Methods) (Kim et al., 2012). We found perfect agreement in the scaling factors obtained from these different tests, indicating that prolonged TTX-treatment induced multiplicative scaling of synaptic AMPAR function in our experimental paradigm.

We then performed a peak-scaled non-stationary noise analysis of AMPAR-mediated mEPSCs to determine whether prolonged network silencing alters unitary properties of AMPAR-mediated synaptic transmission (Figure 2A) (Hartveit and Veruki, 2007). Whereas the average number of synaptic AMPARs was unchanged (CTL: 12.44 ± 1.31, n=17 cells; TTX: 12.72 ± 0.72, n=18 cells; p=0.33; Figure 2C), we found that the mean AMPAR channel conductance was enhanced in TTX-treated neurons (CTL: 12.01 ± 1.12 pS; TTX: 17.65 ± 1.05 pS; p<0.01; Figure 2B). These changes in postsynaptic AMPAR function were not accompanied by alterations in the volume (CTL: 0.24 ± 0.01 μm^3, n=227 spines, 8 cells; TTX: 0.26 ± 0.01 μm^3, n=271 spines, 8 cells; p=0.07, K-S test; Figure 2E) or density of dendritic spines (CTL: 6.41 ± 0.27 spines/10 μm; TTX: 6.18 ± 0.24 spines/10 μm; p=0.98, K-S test; Figure 2F), as determined by two-photon imaging of neurons filled with Alexa-594. In principle, this increased AMPAR conductance could be mediated by post-translational modifications to AMPARs, or by changes in the pore-forming subunit composition of AMPARs. Although there is support for the latter possibility in dissociated neuronal cultures (Thiagarajan et al., 2005; Sutton et al., 2006; Groth et al., 2011), it is unclear whether the subunit composition of AMPARs is homeostatically regulated in CA1 pyramidal neurons from organotypic slices. We therefore sought to determine whether the subunit composition of synaptic AMPARs at CA1 synapses is altered following prolonged TTX-treatment.

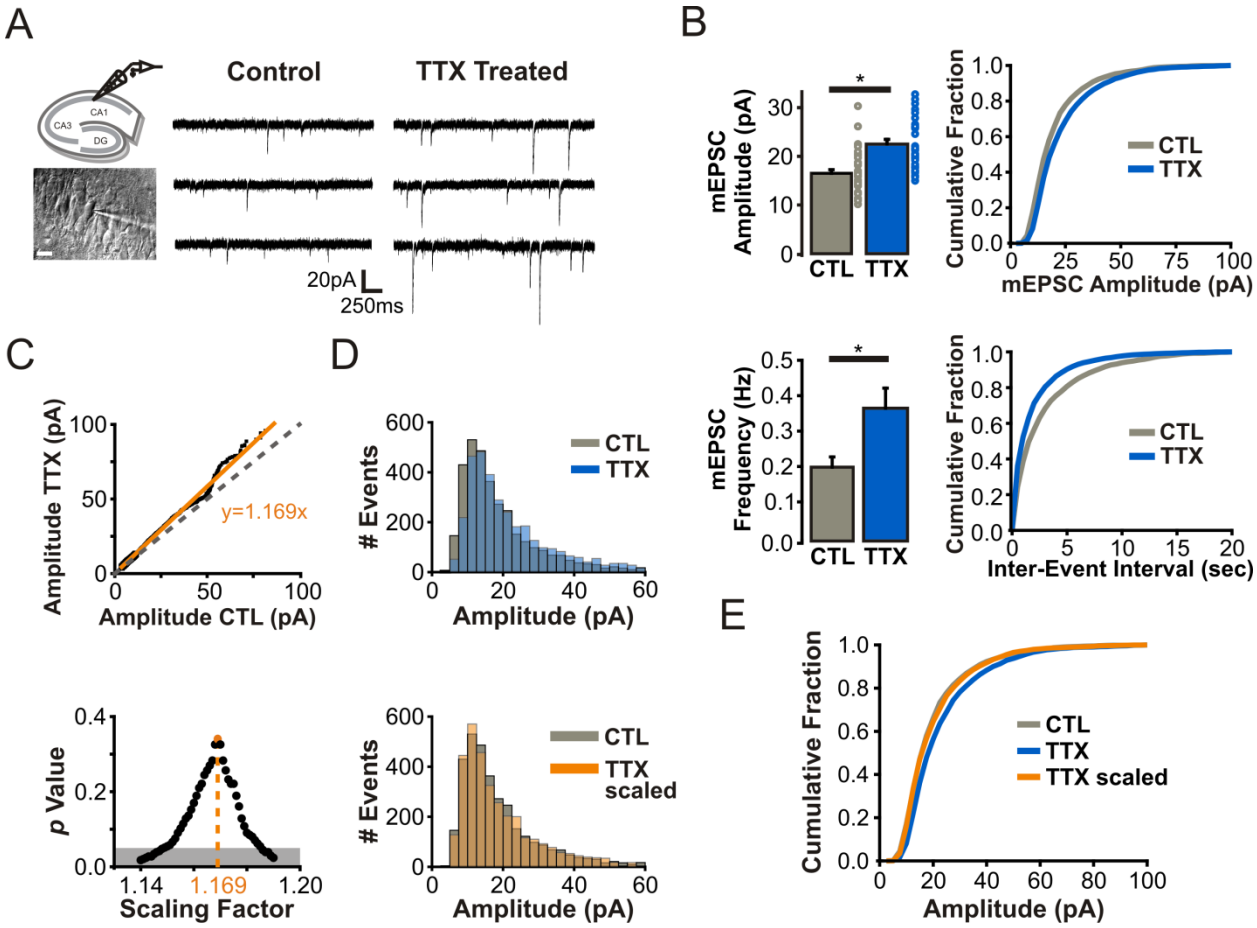

Figure 1: Multiplicative scaling of CA1 pyramidal neurons in response to prolonged TTX treatment. (*A*) Current traces (Vm = -70mV) of AMPAR-mediated mEPSCs (AMPAR-mEPSCs) from CA1 pyramidal neurons in control and TTX-treated hippocampal slices. (*B*) *Top,* Average AMPAR-mEPSC amplitudes (for each cell) and a cumulative distribution of all AMPAR-mEPSC amplitudes (cells pooled) from control and TTX-treated neurons. *Bottom,* Average frequency of AMPAR-mEPSCs (for each cell) and a cumulative distribution of all AMPAR-mEPSC inter-event-intervals (cells pooled) from control and TTX-treated neurons. (*C*) *Top,* Rank ordered plot of pooled AMPAR-mEPSC amplitudes (n = 3380 each, random subset of TTX event amplitudes) was fit through the origin with a linear function (orange line) where the slope (1.169) represents the scaling factor. *Bottom,* the distribution of AMPAR-mEPSC amplitudes of TTX-treated neurons was scaled iteratively by increasing scaling factors from 0.5 to 1.5 (shown in bins of 0.01; only p values flanking the highest p value are shown; K-S test was used to calculate p-values). (D) *Top,* Amplitude distributions of AMPAR-mEPSCs recorded in control neurons (grey) and TTX-treated neurons (blue) (p<0.01, K-S test). *Bottom,* Amplitude distributions of AMPAR-mEPSCs recorded in control neurons (grey) and a 'scaled' TTX-treated distribution (orange) using the scaling factor derived in panel C (p = 0.34, K-S test). (*E*) Cumulative distribution of AMPAR-mEPSC amplitudes (as in panel B) with an additional 'TTX-scaled' distribution (*i.e.,* TTX-treated AMPAR-mEPSC amplitudes divided by the scaling factor).

Homeostatic upregulation of synaptic GluA2-lacking AMPARs

Western blot analyses of organotypic hippocampal slice lysates were performed to first determine whether changes in AMPAR subunit expression occurred in response to prolonged inactivity. TTX-induced inactivity caused an increase in the expression of GluA1, but not GluA2, AMPAR subunits (TTX/CTL ratio; GluA1: of 2.62 ± 0.30, *n*= 3; GluA2: 0.96 ± 0.07, *n*=4; Figure 3A). Moreover, surface biotinylation experiments from these slices revealed a robust homeostatic enhancement of surface GluA1 with no change in the amount of surface GluA2 or glycine receptor subunits (TTX/CTL ratio; GluA1: 2.22 ± 0.26, *n*=9; GluA2: 1.03 ± 0.07, *n*=10; GlyR: 1.01 ± 0.10, *n*=7; Figure 3B). These biochemical findings, combined with the increased AMPAR conductance detected by non-stationary noise analysis (Figure 2B), raise the possibility that prolonged inactivity triggers a specific upregulation of GluA2-lacking AMPARs. Since this hypothesis is consistent with some (Ju et al., 2004; Thiagarajan et al., 2005; Sutton et al., 2006; Aoto et al., 2008; Groth et al., 2011) but not all previously reported evidence (O'Brien et al., 1998; Gainey et al., 2009; Anggono et al., 2011) using broadly analogous manipulations in dissociated neuronal cultures, we further investigated this possibility in our hippocampal slice paradigm using biophysical and pharmacological methods.

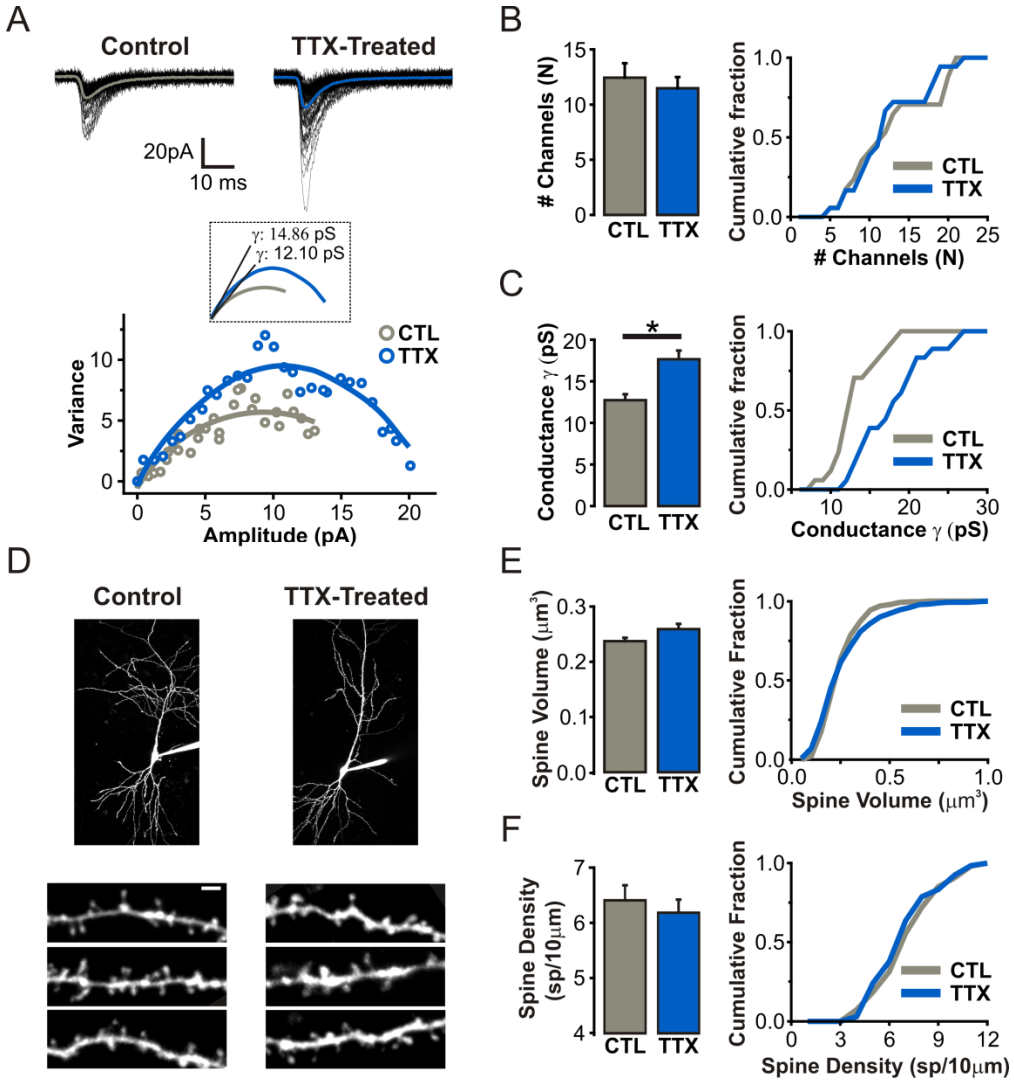

Figure 2: Recruitment of higher conductance synaptic AMPARs following prolonged TTX-treatment (*A*) *Top,* Traces of AMPAR-mEPSC from a single voltage clamp recording (Vm = -70mV) of a control and TTX-treated CA1 pyramidal neuron. *Bottom,* Current-variance plots from peak-scaled non-stationary noise analysis of AMPAR-mEPSCs (see Methods). *Inset,* Initial slope of the parabolic fit was used to calculate the mean AMPAR channel conductance (γ). (*B*) Number of channels 'N' open at the peak of cell-averaged AMPAR-mEPSC. Cumulative distribution of N is plotted for each condition. (*C*) Mean AMPAR channel conductance (γ) for AMPAR-mEPSCs recorded from CTL and TTX-treated neurons. Cumulative distribution of γ is plotted for each condition. (D) Two-photon (2P) images of CA1 pyramidal neurons filled with Alexa 594 (30 μM). All images were taken > 20 minutes after gaining whole-cell access to allow adequate intracellular dye loading. Scale bar = 2 μm. (*E*) Volumes of dendritic spines on apical dendrites of control and TTX-treated neurons calculated using an intensity based method (see Methods). Cumulative distribution of spine volumes for each condition is plotted. (*F*) Average density of dendritic spines on apical dendrites of filled CA1 pyramidal neurons. Cumulative distribution of spine densities sampled in 10 μm dendritic segments.

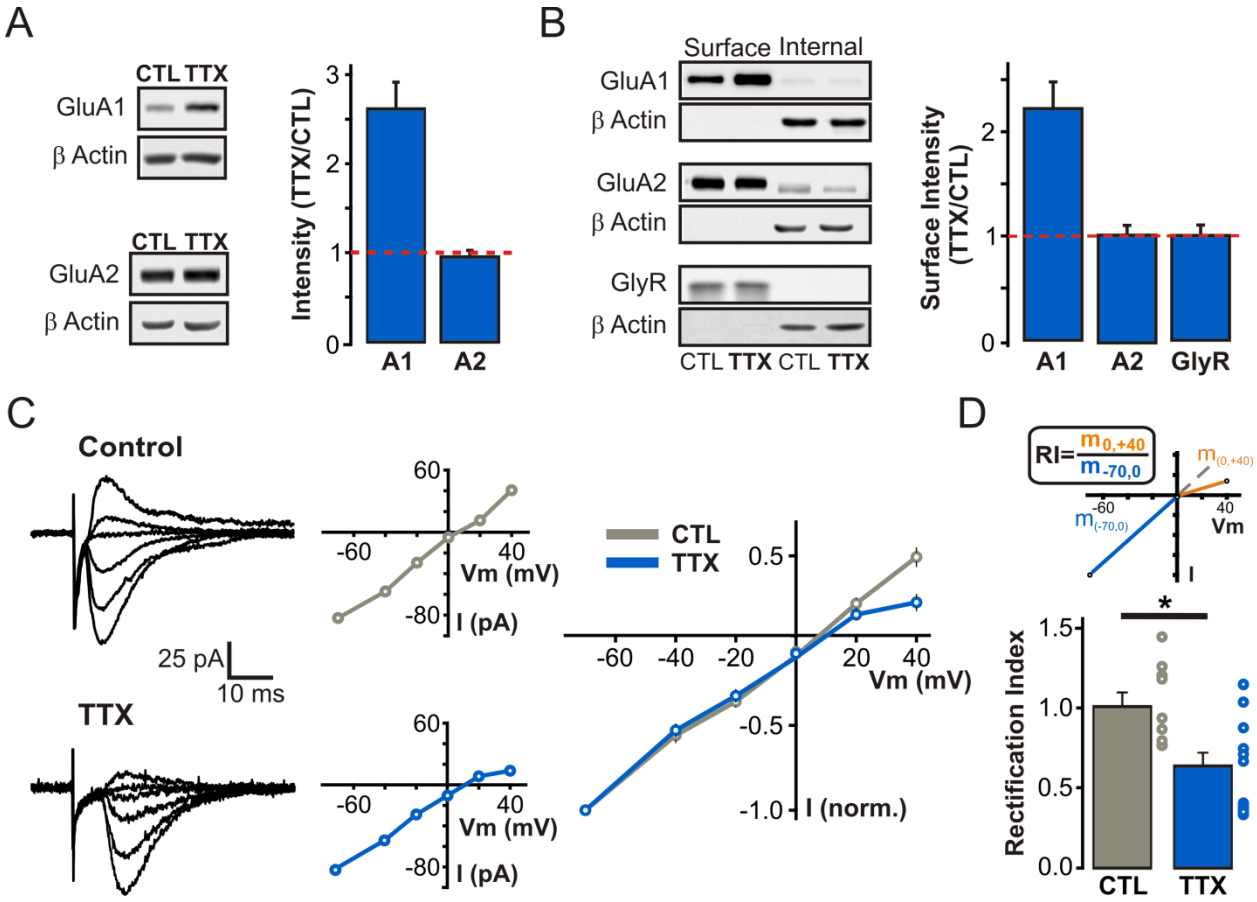

Figure 3: Increased surface expression of GluA1 and the emergence of inwardly rectifying AMPARs at SC-synapses following prolonged TTX-treatment. (*A*) Representative western blots and quantification for the change in AMPA receptor subunit expression, plotted as a TTX/CTL ratio of band intensity, in hippocampal lysates from control and TTX-treated slices. All bands were normalized to β-actin before calculating the TTX/CTL ratio. (*B*) Representative western blots of biotinylated (surface) and non-biotinylated (internal) fractions from control and TTX-treated hippocampal slices. Relative surface expression of AMPA and glycine receptor (GlyR) subunits from control and TTX treated slices, plotted as a TTX/CTL ratio of band intensity. (*C*) Current-voltage (I-V) relationship of evoked AMPAR-EPSCs. *Left,* Current traces at different holding potentials (-70 mV to +40 mV; with 100 μM intracellular spermine) and *Middle,* corresponding I-V curves from individual control and TTX treated neurons. *Right,* Average I-V relationship of evoked AMPAR-EPSCs from control and TTX-treated neurons. (*D*) Rectification indices for control and TTX-treated neurons in panel B, computed as the ratio of the slope (m) of the outward portion of the I-V curve over that of the inward portion ($p<0.01$, unpaired Student's t-test).

AMPARs containing GluA2 subunits exhibit linear current-voltage (I-V) relationships, while those lacking GluA2 display inward rectification due to a pore block by intracellular polyamines at depolarized potentials (Bowie and Mayer, 1995). We thus used this biophysical signature to test the hypothesis that HSP involves an upregulation of GluA2-lacking AMPARs. We calculated rectification indices for I-V curves constructed from pharmacologically-isolated AMPAR-mediated evoked excitatory postsynaptic currents (eEPSCs) at Schaffer-collateral (SC) synapses in the presence of intracellular spermine (100 μM). As expected, control AMPAR-eEPSCs displayed linear I-V relationships (Rectification Index; 1.01 ± 0.09, *n*=13 cells; Figure 3C-D), consistent with the presence of predominantly GluA2-containing AMPARs at these synapses (Beique and Huganir, 2009; Lu et al., 2009). In contrast, we detected a strong voltage-dependent block of AMPAR-eEPSCs in TTX-treated neurons (Rectification Index; TTX: 0.64 ± 0.11, *n*=8 cells; Figure 3C-D), supporting the presence of synaptic GluA2-lacking AMPARs in response to inactivity.

We then measured the sensitivity of AMPAR-eEPSCs to the selective antagonist of GluA2-lacking AMPARs, 1-naphthyl acetyl spermine trihydrochloride (NASPM, 20μM). Bath administration of NASPM robustly reduced the amplitude of AMPAR-eEPSCs recorded from TTX-treated neurons whereas AMPAR-eEPSCs from control slices were unaffected (NASPM inhibition; CTL: -6.15 ± 7.95%, *n*=7 cells, *p*=0.47; TTX: 69% ± 9.48%, *n*=8 cells, *p*<0.01; Figure 4A). To sample a larger population of synapses, we also measured the NASPM sensitivity of pharmacologically isolated spontaneous and miniature AMPAR-EPSCs (sEPSCs and mEPSCs). In agreement with the results outlined above, NASPM did not affect the amplitude of control sEPSCs (from 14.85 ± 1.50 pA to 13.98 ± 1.59 pA in NASPM; *p*=0.12; *n*=8 cells) or mEPSCs (from 13.41 ± 0.59 pA to 13.53 ± 0.86 pA in NASPM; *p*=0.82; *n*=8 cells), but

significantly reduced the amplitude of these events recorded from TTX-treated neurons (sEPSCs: from 26.53 ± 2.26 pA to 19.85 ± 2.13 pA in NASPM, $p<0.01$; mEPSCs: from 18.71 ± 0.79 pA to 15.62 ± 0.64 pA in NASPM, $p<0.01$; Figure 4B-E). Together, these data are consistent with the expression of synaptic GluA2-lacking AMPARs during HSP.

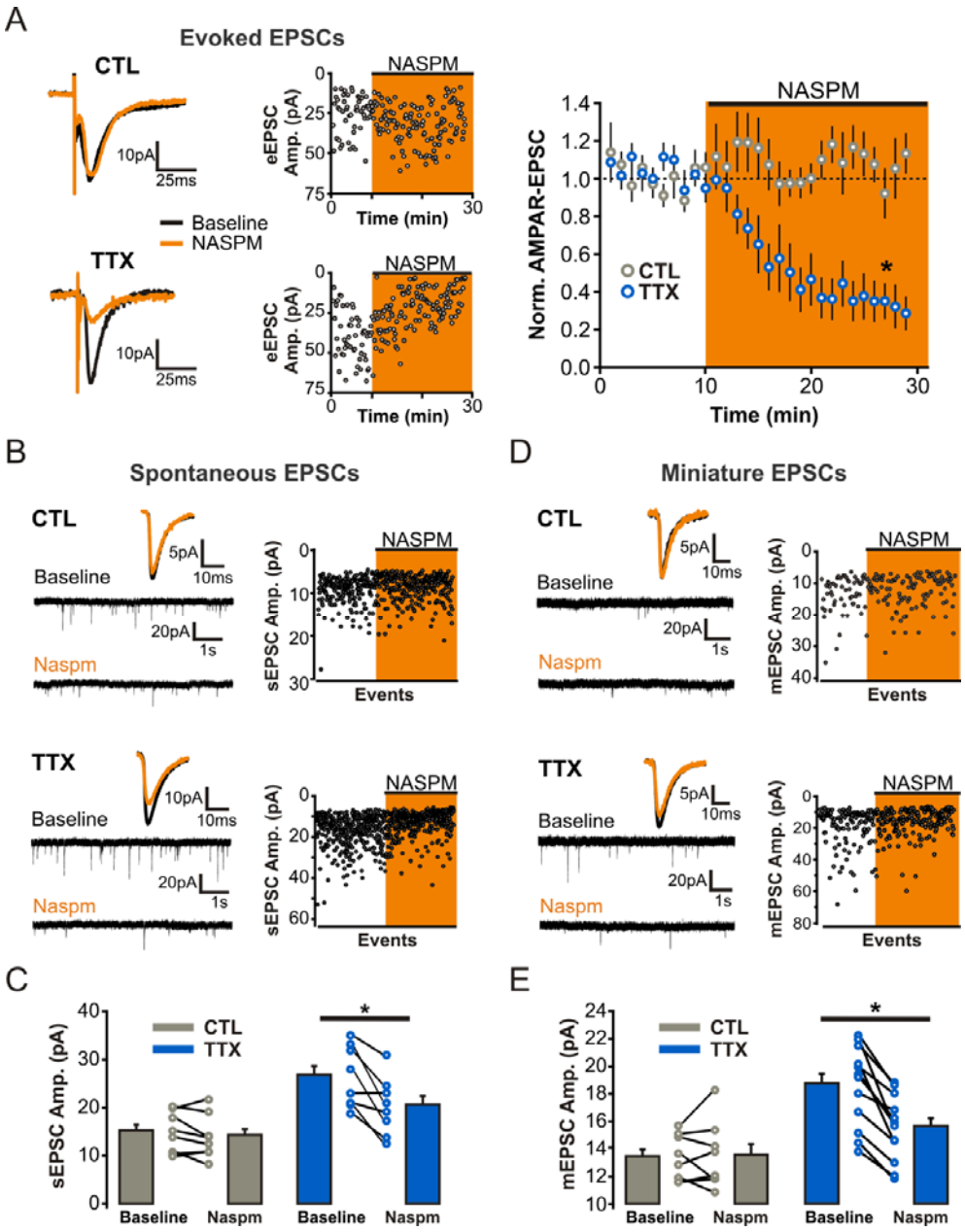

Figure 4: Synaptic incorporation of GluA2-lacking AMPARs in CA1 pyramidal neurons following prolonged TTX-treatment (A) *Left,* Representative traces and event amplitude scatter plots of evoked AMPAR-EPSCs before and after NASPM administration (20 μM). *Right,* Normalized average amplitude of evoked AMPAR-EPSCs. (*B*) Current traces and event amplitude scatter plots of spontaneous AMPAR-EPSCs (*i.e.,* no TTX during recording; AMPAR-sEPSC) before (baseline) and 15-20 minutes after onset of NASPM (20 μM) administration. (*C*) Average AMPAR-sEPSC amplitudes before (baseline) and 15-20 minutes after NASPM administration. (*D*) Current traces and event amplitude scatter plots of AMPAR-mEPSCs (*i.e.,* recorded in TTX) before and 15-20 minutes after onset NASPM administration. (*E)* Average AMPAR-mEPSC amplitudes before (baseline) and 15-20 minutes after NASPM administration.

Previous studies have demonstrated that synaptic strengthening during LTP is mediated by an increase in synaptic AMPAR number and is accompanied by robust dendritic spine enlargement (Matsuzaki et al., 2004; Harvey and Svoboda, 2007). Remarkably, we found that the synaptic strengthening during HSP was not accompanied by changes in the number of AMPARs at synapses (Figure 2C), nor in the volume of dendritic spines (Figure 2E). Rather, our biochemical, biophysical and pharmacological data strongly suggest that the postsynaptic manifestation of HSP is expressed in part through the direct replacement of synaptic GluA2-containing AMPARs with higher conductance GluA2-lacking AMPARs.

Homeostatic switch in synaptic NMDAR subunit composition

The dynamic nature of NMDAR trafficking and targeting behaviour at rest, during postnatal development and during Hebbian plasticity has gained considerable appreciation over the past two decades (Lau and Zukin, 2007). In part because HSP has overwhelmingly been studied in dissociated neuronal cultures, a preparation that does not lend itself with ease to the study of NMDAR function, the homeostatic regulation of NMDARs has been far less extensively studied than that of AMPARs (Perez-Otano and Ehlers, 2005). To determine whether alterations in NMDAR function accompanied the homeostatic enhancement in AMPAR function outlined above, we evoked EPSCs while holding neurons at -70 mV and +40 mV to compute the ratio of AMPAR and NMDAR contributions to SC synapse function (see Methods). We found that the ratio of AMPA to NMDA receptor components of eEPSCs was not altered by prolonged inactivity (CTL: 0.87 ± 0.13, n=13 cells; TTX: 0.87 ± 0.12, n=12 cells; p=0.98; Figure 5A), consistent with previous findings in both neuronal cultures and organotypic slices younger than those used here (Watt et al., 2000; Arendt et al., 2013). Since AMPAR function was significantly enhanced during HSP in our experimental conditions (Figure 1B), this finding suggests a

concomitant upregulation of both synaptic NMDA and AMPAR function during HSP. In line with this notion, Western blot analysis of hippocampal slice lysates (Figure 5B) and surface biotinylation experiments (Figure 5C) revealed an increase in the expression and surface delivery of all three major NMDAR subunits found in the hippocampus in TTX-treated slices (TTX/CTL ratio for hippocampal lysates; GluN1: 1.43 ± 0.09, *n*=4; GluN2A: 1.52 ± 0.16, *n*=6; GluN2B: 1.85 ± 0.13, *n*=3; Figure 5B; TTX/CTL ratio for biotinylated samples; GluN1: 1.31 ± 0.10, *n*=10; GluN2A: 1.86 ± 0.35, *n*=8; GluN2B: 1.69 ± 0.24, *n*=15; Figure 5B).

To further establish whether NMDAR function is homeostatically regulated in CA1 pyramidal neurons, we gathered two complementary electrophysiological readouts of NMDAR function. First, we reasoned that an upregulation of surface NMDARs could be revealed by examining the degree of tonic activation of these receptors by ambient levels of extracellular glutamate (Sah et al., 1989). To this end, we monitored changes in whole-cell current of CA1 pyramidal neurons induced by bath administration of the NMDAR antagonist DL-APV (50μM; see Materials & Methods). NMDAR blockade in control neurons induced a small but highly reproducible change in holding current (15.48 ± 10.86 pA, *n*=5 cells), thus revealing the presence of an ambient glutamate tone in organotypic hippocampal slices (Figure 5D). Interestingly, the magnitude of this tonic current was more than three times greater in TTX treated slices (56.15 ± 9.51 pA, *n*=7 cells) compared to that seen in controls. In principle, this difference could reflect an upregulation of surface NMDARs, an alteration in the regulation of ambient extracellular glutamate concentration, or a combination of both. To directly measure NMDAR function, we next monitored the whole-cell response to bath administration of NMDA (5 μM for 3 minutes) and found that NMDA induced significantly larger whole-cell currents in TTX-treated neurons compared to control (CTL: 128.69 ± 15.44 pA, *n*=16 cells; TTX: 198.98 ± 21.42 pA, *n*=16 cells;

$p<0.05$; Figure 5E). This enhancement was likely not due to an overall greater membrane surface area in TTX-treated neurons, since the dendritic arborisation between control and TTX-treated neurons was not different (CTL: 732.36 ± 86.43 µm, $n=10$ cells; TTX: 787.48 ± 48.56 µm, $n=12$ cells; $p=0.56$; Figure 5F). These functional and morphological measurements aligned well with our biochemical data (Figure 5B-C) and together demonstrate that prolonged inactivity induced a robust upregulation of surface NMDAR expression in CA1 pyramidal neurons.

During Hebbian LTP, synaptic NMDARs undergo a rapid switch in subunit composition, from predominantly NR2B-containing towards NR2A-containing NMDARs (Bellone and Nicoll, 2007). We therefore next wondered on the degree of mechanistic commonality between Hebbian and homeostatic synaptic strengthening and asked whether the subunit composition of synaptic NMDARs is likewise regulated during homeostatic synaptic plasticity. To this end, we probed the subunit composition of synaptic NMDARs by first analyzing the kinetics of pharmacologically isolated NMDAR-eEPSCs from SC synapses and found that TTX-treated neurons exhibited NMDAR-eEPSCs with faster decay kinetics compared to control (weighted tau; CTL: 366.03 ± 19.72 ms, $n=15$ cells; TTX: 315.44 ± 15.16 ms, $n=18$ cells; $p<0.05$; Figure 6A). Based on the well characterized subunit dependence of NMDAR kinetics (Vicini et al., 1998), these results suggest that prolonged inactivity led to synaptic enrichment of GluN2A-containing NMDARs. We further tested this possibility pharmacologically by measuring the sensitivity of NMDAR-eEPSCs to the GluN2B-containing NMDAR antagonist ifenprodil (3 µM) and found that NMDAR-eEPSCs recorded from TTX-treated neurons were significantly less sensitive to ifenprodil than interleaved controls (ifenprodil inhibition; CTL: 56.67 ± 4.80 %, $n=12$ cells; TTX: 37.95 ± 3.65 %, $n=16$ cells; $p<0.01$; Figure 6B). Thus, despite a robust

upregulation of all three major NMDAR subunits at the plasma membrane, we found that GluN2A-containing NMDARs are preferentially stabilized at synapses during HSP.

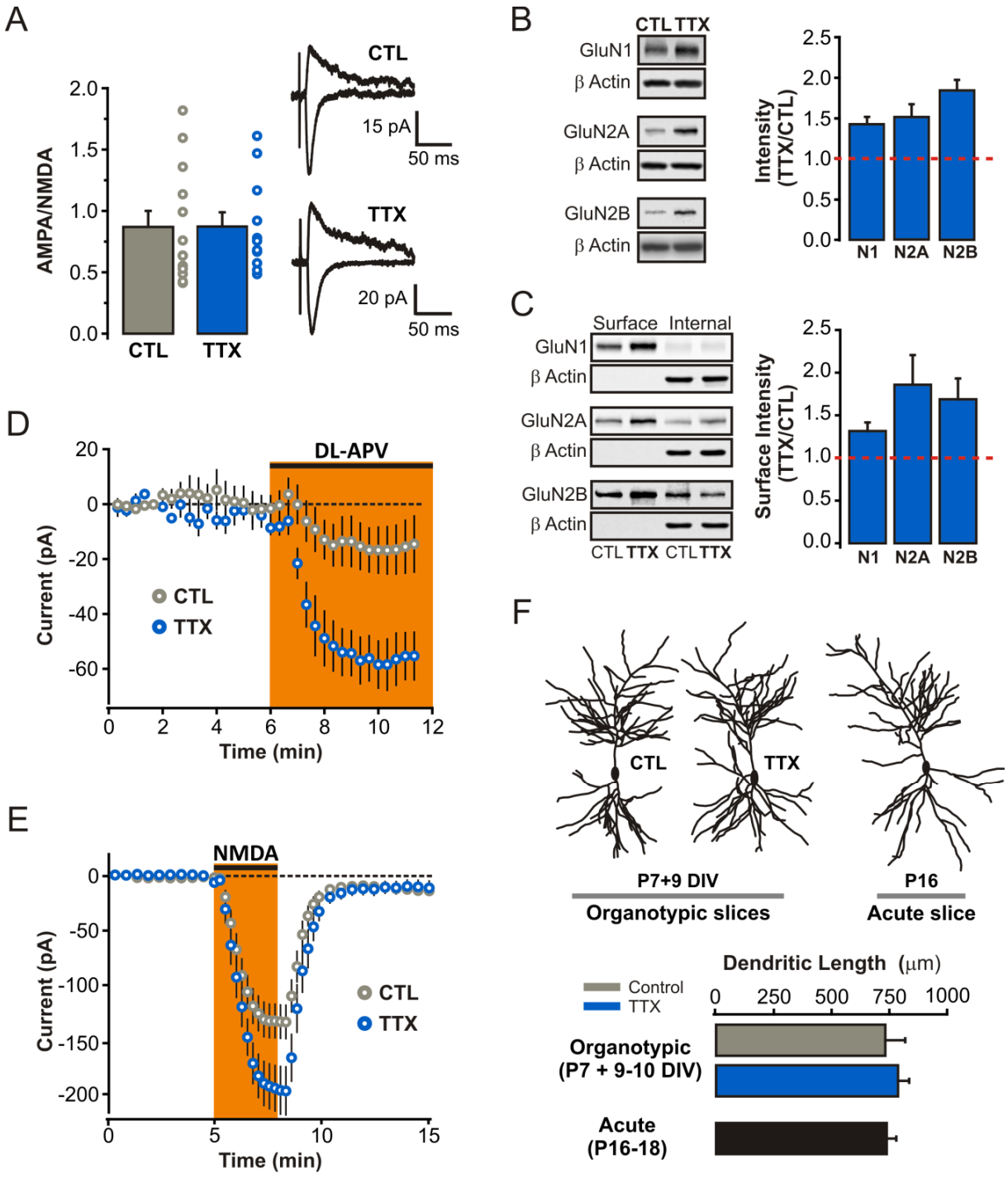

Figure 5: Homeostatic upregulation of surface NMDARs in CA1 pyramidal neurons in response to prolonged TTX-treatment. (*A*) AMPA to NMDA ratio of evoked EPSCs (see Methods). (*B*) Representative western blots and quantification of changes in NMDAR subunit expression, plotted as a TTX/CTL ratio of band intensity, in hippocampal lysates of control and TTX-treated slices. All bands were normalized to β-actin before calculating the TTX/CTL ratio. (*C*) Representative western blots of biotinylated (surface) and non-biotinylated (internal) fractions from control and TTX-treated slices. Relative surface expression of NMDA receptor

subunits between control and TTX treated slices plotted as a TTX/CTL ratio of band intensity. (*D*) Change in holding current induced by bath administration of 50μM DL-APV while holding the neurons at +40mV ($p<0.05$, unpaired Student's t-test). These experiments were performed with NBQX, picrotoxin and TTX in the Ringer solution. (E) Amplitude of the inward current induced by bath administration of NMDA (5 μM; Vm = -60mV in 0.1 mM Mg^{2+}). All NMDA bath administration experiments were performed with NBQX, picrotoxin, and TTX in the Ringer solution. (*F*) 2P images of filled CA1 pyramidal neurons were reconstructed using Neuron Studio software (see Methods). Dendritic length (μm) is plotted for CA1 pyramidal neurons from TTX-treated or control organotypic slices (P7 + 9-10 DIV) and from age-matched neurons from acute slices (P16-17 animals; $n = 10$, 12, and 9 neurons for control, TTX-treated and acute slices, respectively).

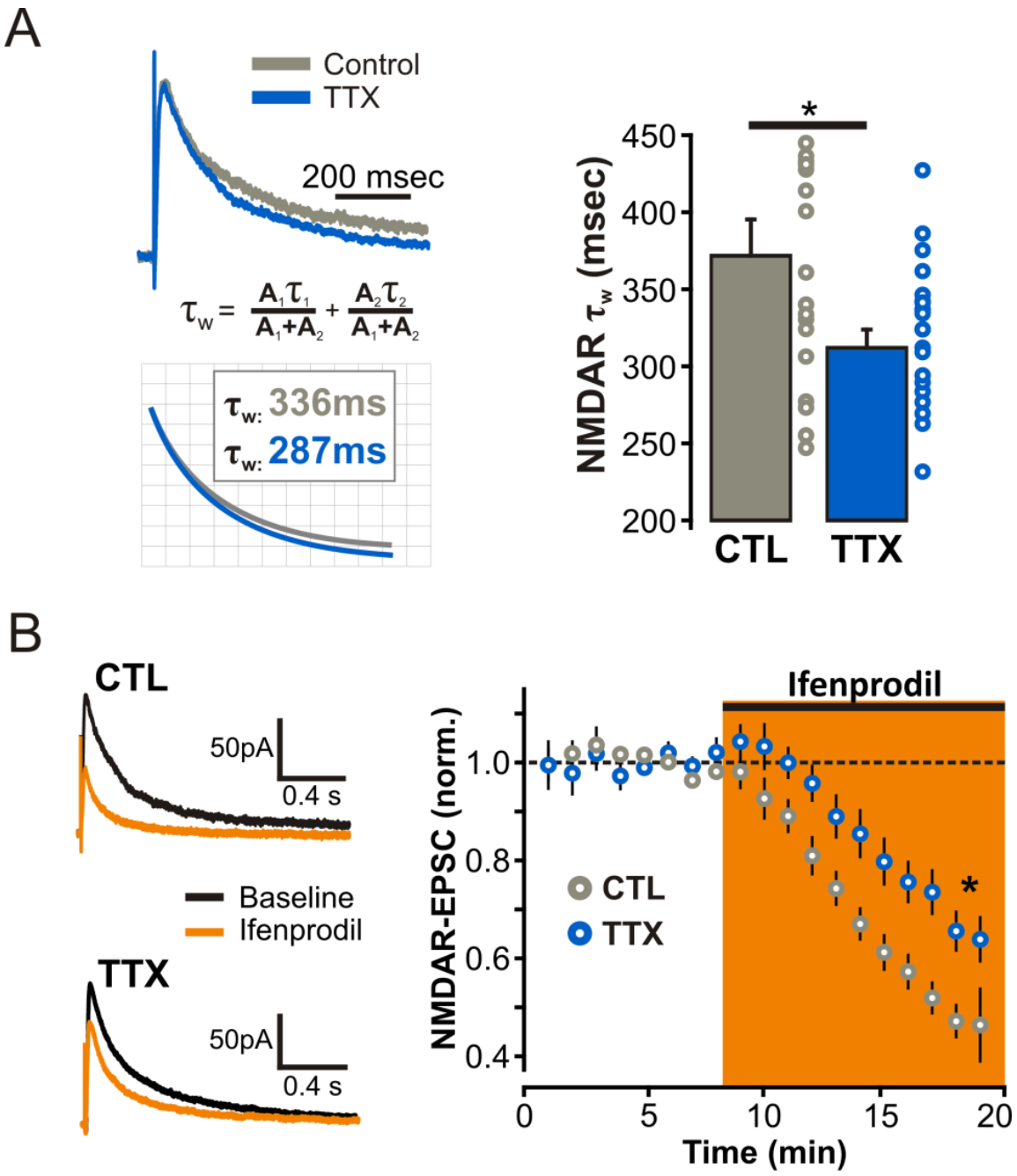

Figure 6: Homeostatic shift in synaptic NMDAR subunit composition in response to prolonged TTX-treatment. (*A*) Weighted tau values from bi-exponential fits of evoked NMDAR-EPSCs recorded at +40mV from control and TTX-treated neurons. (*B*) Amplitude of evoked NMDAR-EPSCs (Vm = +40mV) before (baseline) and after 10-12 minutes administration of the selective GluN2B-containing NMDARs antagonist ifenprodil (3 µM).

Subcellular distribution of AMPA and NMDAR subtypes following network silencing

The trafficking, targeting and stabilization of glutamate receptors at synapses occurs through a number of highly regulated intracellular and extracellular interactions (Shepherd and Huganir, 2007). An emerging model of synaptic AMPAR recruitment involves the trapping of freely diffusing extrasynaptic surface receptors as they enter the synaptic compartment (Opazo and Choquet, 2011), and an analogous diffusional trapping mechanism has also been described for NMDARs (Groc et al., 2006; Bard et al., 2010). Moreover, the functional enhancement of AMPAR transmission during LTP is highly dependent on this reserve pool of non-synaptic receptors (Makino and Malinow, 2009; Granger et al., 2013). Although our electrophysiological data outlined above clearly demonstrate that the subunit composition of synaptic AMPARs (Figures 3 & 4) and NMDARs (Figure 6) are altered during HSP, it is unclear whether these changes reflect synapse-specific regulation or rather diffuse, cell-wide, changes in surface glutamate receptor expression. To specifically address this issue, we took advantage of subunit-specific biophysical signatures of AMPAR and NMDAR subtypes in combination with the ability afforded by 2P-uncaging of MNI-Glutamate (MNI-Glu) to activate glutamate receptors at defined subcellular compartments (Figure 7A-C).

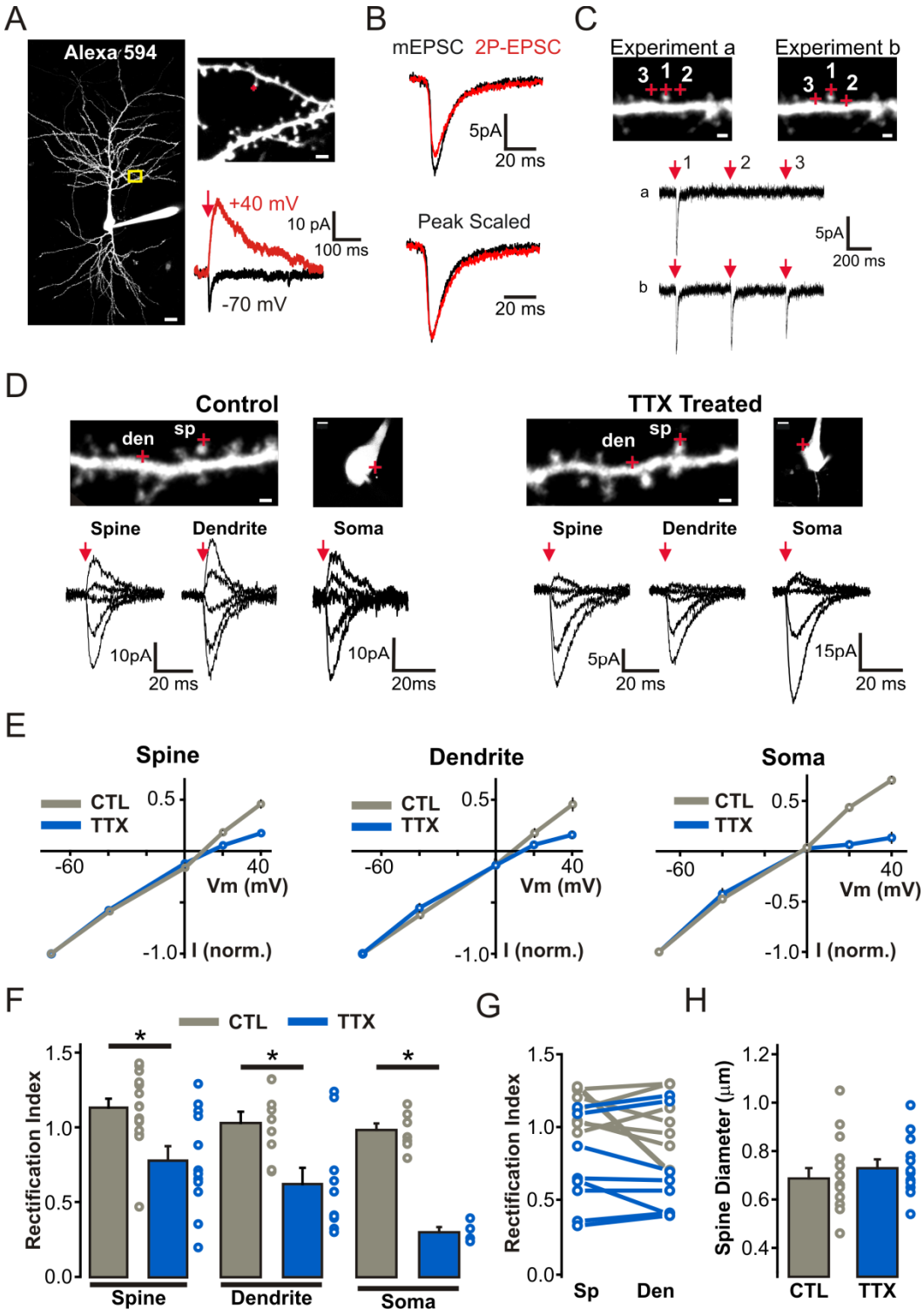

Figure 7: Cell-wide homeostatic upregulation of GluA2-lacking AMPARs in response to prolonged TTX treatment. (*A*) *Left*, 2P image of a control CA1 pyramidal neuron filled with Alexa-594 to visualize dendritic morphology. Scale bar = 15μm. *Right*, Enlarged view of an apical dendritic segment with red crosshairs illustrating the site of 2P glutamate uncaging (1ms at

720nm); scale bar: 2 μM. At -70mV, glutamate uncaging elicits a postsynaptic AMPAR-mediated response whereas at +40mV, uncaging of glutamate also activates longer decaying NMDAR EPSCs. (*B*) *Top*, AMPAR-2P-EPSCs can be generated to match the amplitude of AMPAR-mEPSCs from the same recording. *Bottom*, Peak scaling the average traces of AMPAR-2P-EPSCs and AMPAR-mEPSCs reveals a similar rise and decay time course. (*C*) A set of control experiments whereby three uncaging pulses (separated by 500ms) were elicited at each of the three points illustrated with red crosshairs. In experiment b, the uncaging positions of sites 2 and 3 were brought closer to the dendrite to elicit a response mediated by extrasynaptic receptors. Scale bars = 1 μm. (*D*) I-V relationship of AMPAR-2P-EPSCs generated at distinct subcellular locations. *Top,* 2P images of secondary apical dendritic segment show sites of glutamate uncaging (red crosshairs); Scale bars: 1 μm and 5 μm for images of dendrite and soma, respectively. *Bottom*, AMPAR-2P-EPSCs at different holding potentials (-70 mV to +40 mV; with 100 μM intracellular spermine) with red arrow depicts the timing of the 1ms uncaging pulse. (*E*) Average I-V curves of 2P-EPSCs from each subcellular location in both control and TTX conditions (*F*) Rectification indices for all spine, dendritic, and somatic IV curves presented in panel E ($p<0.01$; unpaired Student's t-test) (*G*) Rectification indices of 2P-EPSCs generated from pairs of spine and neighbouring (<5μm) extrasynaptic shaft regions. (*H*) Diameters (FWHM) of all dendritic spines probed for AMPAR-2P-EPSC I-V relationships.

To determine the spatial extent of GluA2-lacking AMPAR surface expression, we analyzed the I-V relationship of 2P glutamate uncaging-evoked AMPAR-mediated EPSCs (AMPAR-2P-EPSCs) at dendritic spines and nearby (<5μm) extrasynaptic shaft regions of secondary and tertiary proximal apical dendrites. In agreement with a previous study in neuronal cultures (Beique et al., 2011), uncaging of MNI-glutamate onto spines and onto extrasynaptic shaft and somatic regions of control neurons yielded AMPAR-2P-EPSCs exhibiting linear I-V relationships, although rectifying currents were occasionally encountered (Rectification Index; spine: 1.10 ± 0.06, *n*=16; dendrite: 1.01 ± 0.08, *n*=9; soma: 0.98 ± 0.04, *n*=6; Figure 7D-F). Thus, GluA2-containing AMPARs appear to dominate both synaptic and extrasynaptic regions of control CA1 neurons. Consistent with the upregulation of synaptic GluA2-lacking AMPARs (*i.e.,* synaptically evoked-EPSCs; Figures 3-4) in response to prolonged inactivity, we observed strong inwardly-rectifying AMPAR-2P-EPSCs when uncaging pulses were directed onto the tips of dendritic spines in TTX-treated neurons (Rectification Index; 0.76 ± 0.09, *n*=12 spines; Figure 7D-F). The changes in the rectifying properties of 2P-EPSCs from spines between control and TTX-treated neurons could not be accounted for by an experimental bias towards morphologically dissimilar spines in the treatment groups (*p*=0.47; Figure 7H). Interestingly, inwardly-rectifying AMPAR-2P-EPSCs were also detected when glutamate was uncaged onto dendritic shafts and somatic regions of TTX-treated neurons (Rectification Index; dendrite: 0.61 ± 0.11, *n*=10; soma: 0.30 ± 0.04, *n*=4; Figure 7D-F). Together, our data suggest that prolonged inactivity drives a robust cell-wide expression of GluA2-lacking AMPARs at both synaptic and extrasynaptic regions of CA1 pyramidal neurons.

We last investigated the subcellular distribution of GluN2A- and GluN2B-containing NMDARs during HSP by analyzing the decay kinetics of NMDAR-2P-EPSCs elicited at either

dendritic spines or nearby extrasynaptic shaft regions. Consistent with the inactivity induced enrichment of synaptic GluN2A-containing NMDARs (*i.e.,* synaptically evoked EPSCs; Figure 6), we found that NMDAR-2P-EPSCs from dendritic spines of TTX-treated neurons exhibited faster decay kinetics than from morphologically similar control spines (CTL: 191.71 ± 4.73 ms, n=18; TTX: 145.07 ± 16.44 ms, n=26; p<0.01; Figure 8A-D). Strikingly, however, the decay kinetics of NMDAR-2P-EPSCs elicited from shaft regions of TTX-treated neurons were comparable to those elicited from shaft regions of control neurons (CTL: 209.72 ± 10.80 ms, n=13; TTX: 195.54 ± 11.83 ms, n=19; p=0.32) and significantly longer than those from nearby spines (Figure 8A-C). Whereas uncaging onto spines can in principle activate a mixture of synaptic and extrasynaptic of receptors, uncaging onto shaft regions overwhelmingly activates extrasynaptic receptor populations. Thus, in stark contrast to the cell-wide homeostatic upregulation of surface GluA2-lacking AMPARs at both synaptic and extrasynaptic membrane regions, the TTX-induced enrichment of GluN2A-containing NMDARs occurs selectively at synapses. Collectively, by discriminating between synaptic and extrasynaptic glutamate receptor populations, our results expose intriguing differences in the regulatory mechanisms that dictate the synaptic targeting of AMPA and NMDARs of defined subunit composition during homeostatic plasticity (Figure 9A-B).

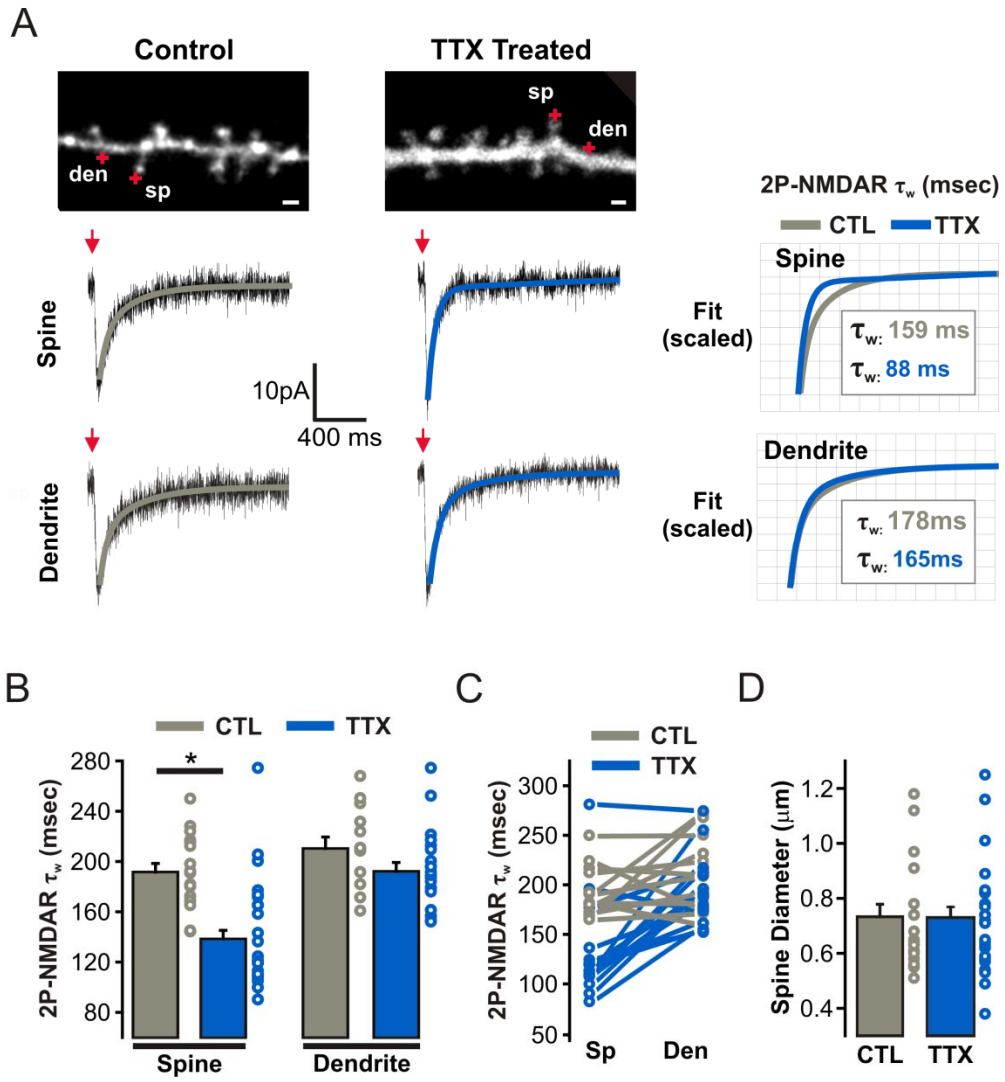

Figure 8: GluN2A-NMDARs are specifically targeted to synapses in response to prolonged TTX-treatment (*A*) *Left*, NMDAR-2P-EPSCs (Vm = -60mV; 0.1 mM Mg^{2+}) elicited by uncaging glutamate onto the tips of dendritic spines and nearby isolated dendritic shaft segments. Bi-exponential fits of NMDAR-2P-EPSC decay are overlaid on the current traces for spine and dendrite uncaging events; Scale bars = 1 μm. *Right*, Scaled bi-exponential fits of NMDAR-2P-EPSC decay from spines and dendrites are overlaid for clarity and the corresponding weighted tau values are indicated. (*B*) Weighted tau values of NMDAR-2P-EPSCs. (*C*) Weighted tau values of NMDAR-2P-EPSCs from 'pairs' of spine and nearby (<5μm) dendritic regions. (*D*) Diameters (FWHM) of all dendritic spines probed for NMDAR-2P-EPSCs (p=0.97, unpaired Student's t-test).

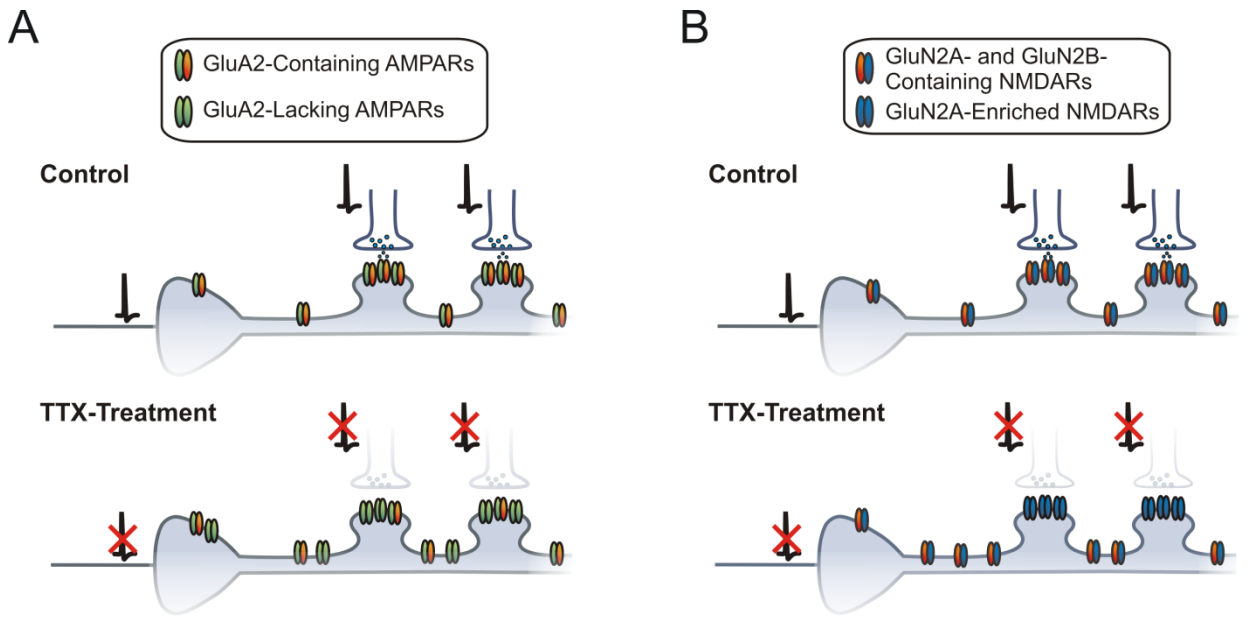

Figure 9: Differential subcellular targeting of glutamate receptor subtypes during HSP

(*A*) *Top*, AMPARs containing the GluA2 subunit predominate at both synaptic and extrasynaptic regions of CA1 pyramidal neurons. *Bottom*, When network activity is silenced by prolonged TTX-treatment, there is a homeostatic upregulation of GluA2-lacking AMPARs in both synaptic and extrasynaptic compartments of the neuronal membrane. (*B*) *Top*, CA1 pyramidal neurons display a mixed population of NMDARs containing both GluN2A and GluN2B subunits. *Bottom*, When network activity is silenced by prolonged TTX-treatment, there is an indiscriminate increase surface NMDARs subunits, however, GluN2A-containing NMDARs are preferentially localized/stabilized at synapses.

Discussion

Here, using a combination of biochemical, biophysical and pharmacological approaches, we found that prolonged TTX treatment altered the subunit composition of both synaptic AMPA and NMDARs in CA1 pyramidal neurons from organotypic hippocampal slices. Notably, we show that prolonged inactivity induced a robust upregulation of the AMPAR subunit GluA1 that resulted in a widespread, cell-wide, surface expression of GluA2-lacking AMPARs. Remarkably, despite inducing a robust and generalized upregulation of the three major hippocampal NMDAR subunits, network silencing triggered a switch in the subunit composition of solely the synaptic population of NMDARs, leaving unaltered the composition of their extrasynaptic counterparts. Altogether, these findings highlight the notion that the homeostatic mechanisms used by neurons to adjust their excitability levels regulate synapse function in ways beyond solely modifying synaptic strength *per se*.

A number of previous studies have reported conflicting evidence regarding the subunit composition of AMPARs involved in homeostatic synaptic potentiation. A recent review (Lee et al., 2014) attempted to reconcile these discrepancies by documenting differences in the pharmacological paradigms used to induce HSP. Specifically, it was highlighted that the selective regulation of GluA1 occurred after prolonged blockade of both network activity (*i.e.*, TTX) and NMDARs (Ju et al., 2004; Sutton et al., 2006; Aoto et al., 2008), whereas both GluA1 and GluA2 expression was affected when neurons were treated with TTX alone (O'Brien et al., 1998; Gainey et al., 2009; Anggono et al., 2011). In contrast to this unifying picture, we provide here a number of complementary and converging lines of evidence indicating that a TTX treatment alone led to a robust and selective upregulation of GluA1 expression and formation of GluA2-lacking AMPARs in CA1 pyramidal neurons in an organotypic slice preparation. The

direct replacement of GluA2-containing AMPARs with higher conductance GluA2-lacking AMPARs during homeostatic plasticity offers an effective means to enhance synaptic strength without the need to increase receptor number or to increase spine volume. This scenario is consistent with homeostatic plasticity occurring at single synapses (Beique et al., 2011) and is in line with manifestations of homeostatic synaptic plasticity *in vivo* (He et al., 2012).

It is pertinent to compare and contrast the mechanistic underpinnings of Hebbian and homeostatic synaptic strengthening, including those involving subunit composition of glutamate receptors. While a transient insertion of GluA2-lacking AMPARs has been observed following LTP induction (Plant et al., 2006; Guire et al., 2008), the role of this particular subtype of AMPARs in LTP is controversial (Adesnik and Nicoll, 2007; Gray et al., 2007). Likewise, the implication of GluA2-lacking AMPARs in homeostatic synaptic strengthening is also debated, as outlined above. These divergences may reflect the presence of distinct synaptic plasticity mechanisms that are heavily dependent on subtleties in experimental conditions and paradigms. Nevertheless, the homeostatic switch in NMDAR subunit composition we report here is highly analogous to that previously shown to occur during Hebbian LTP (Bellone and Nicoll, 2007). Indeed, LTP was shown to be accompanied by a GluN2B-containing towards GluN2A-containing NMDAR subunit switch that exhibited a time course highly similar to that of the synaptic delivery of AMPARs. Although our results provide limited insights into the precise time course of the inactivity induced subunit switches for both AMPA and NMDARs, these homeostatic adaptive mechanisms might be occurring simultaneously. It is thus tempting to speculate that both Hebbian and homeostatic synaptic strengthening utilize common mechanisms involving the concerted upregulation of AMPARs and GluN2A-containing NMDARs. Future

studies will be required to substantiate this possibility and further establish the extent of the molecular commonalities between Hebbian and homeostatic synaptic plasticity.

The homeostatic adjustments reported here for both AMPA and NMDAR subunit composition likely influence Hebbian plasticity rules. Indeed, *in vivo* visual deprivation paradigms that lead to homeostatic upregulation of synapse function in visual cortex (Goel and Lee, 2007; Gao et al., 2010), impart a metaplastic influence that modifies the stimulus threshold for inducing LTP and LTD (Philpot et al., 2001; Philpot et al., 2003), and spike-timing dependent synaptic plasticity (Guo et al., 2012). These changes appear to be caused by an increased proportion of GluN2B-containing NMDARs at synapses, in an apparent contrast to what we report here. Whereas the various *in vivo* visual deprivation paradigms reduce thalamic synaptic input into visual cortex, it is unclear to what extent they reduce overall network excitability in the visual cortex. Thus, it is possible that the GluN2A enrichment we report here following prolonged TTX treatment represents a homeostatic response to a prolonged postsynaptic neuronal silencing, whereas the GluN2B-enrichment observed following visual deprivation reflects a homeostatic response to a reduction in presynaptic activity. In support of this idea, selective presynaptic silencing of individual synapses has recently been shown to cause postsynaptic GluN2B enrichment (Lee et al., 2010). Conversely, the presence of calcium-permeable GluA2-lacking AMPARs following prolonged inactivity may also convey metaplastic influences to synapses, either by lowering the threshold for Hebbian synaptic potentiation, or even by imparting anti-Hebbian features (Lamsa et al., 2007). Future studies are required to better understand the influence of glutamate receptor composition on synaptic plasticity rules.

AMPAR and NMDARs of different subunit composition are differentially localized to synaptic and extrasynaptic membrane compartments. For instance, AMPARs containing

GluA2/GluA3 subunits are found almost exclusively at synapses whereas GluA1/GluA2-AMPARs occupy both synaptic and extrasynaptic membrane regions (Beique and Huganir, 2009; Lu et al., 2009). Moreover, GluN2A-containing NMDARs are believed to be preferentially stabilized at synapses over GluN2B-containing NMDARs (Groc et al., 2006). These subcellular distribution profiles are thought to arise through preferential interactions of specific AMPAR and NMDAR subunits, and/or auxiliary subunits, with PSD scaffolding proteins at synapses (Lau and Zukin, 2007; Shepherd and Huganir, 2007; Jackson and Nicoll, 2011). The differential subcellular distribution of AMPA and NMDAR expression during HSP we have described can be traced, at least in part, to the changes in subunit protein expression. Specifically, the selective upregulation of GluA1 protein expression (over GluA2) was accompanied by a widespread enhancement of surface GluA2-lacking AMPARs, evident at both dendritic spines and extrasynaptic membrane regions. Such a cell-wide upregulation of AMPARs offers an effective means to account for the remarkable multiplicativity of homeostatic synaptic strengthening triggered by a somatic homeostatic sensing mechanism (Lee et al., 2014). Interestingly, the TTX-induced increase in NMDAR protein expression (both total and surface expression) was not subunit selective, as we detected an upregulation of GluN1, GluN2A and GluN2B. Despite this generalized increase in NMDAR surface expression, synapses were specifically enriched with GluN2A-containing NMDARs during HSP, likely reflecting the preferential synaptic stabilization of this subunit compared to GluN2B-containing NMDARs. Thus, whereas the synaptic incorporation of GluA2-lacking AMPARs likely results from the bulk loading of these receptors onto the plasma membrane, the selective synaptic stabilization of GluN2A-containing NMDARs during HSP emphasizes the competitive interactions of GluN2A subunits for synaptic anchoring/scaffolding proteins.

The functional importance of extrasynaptic receptors is increasingly being recognized. For instance, extrasynaptic AMPARs and NMDARs can be recruited to and/or exchanged with synaptic receptor populations in a dynamic and highly regulated manner. Recent studies have shown that extrasynaptic AMPARs can shape synaptic transmission (Heine et al., 2008) and are required for LTP (Makino and Malinow, 2009; Granger et al., 2013). Moreover, extrasynaptic NMDARs can powerfully influence synaptic integration (Chalifoux and Carter, 2011; Lee, 2012b) and differentially regulate neuronal survival and death signaling pathways (Hardingham and Bading, 2003). The homeostatic regulation of the number and subunit composition of extrasynaptic glutamate receptors described here will, in principle, influence all of the functions ascribed to this population of receptors, thus broadening the functional implications of the homeostatic process.

Both *in vitro* and *in vivo* manifestations of homeostatic synaptic plasticity have been documented using several experimental paradigms. Homeostatic synapse regulation operates continuously 'online' to enable tuning of cellular excitability in the face of perpetual alterations in neuronal firing activity. We have demonstrated that, in addition to triggering robust synaptic strengthening, the homeostatic process also involves changes in the subunit composition and subcellular distribution of both AMPA and NMDARs. Thus, the homeostatic adjustment of synapse function is not limited to the regulation of synaptic strength, but likely impacts synaptic properties such as temporal integration of synaptic input and calcium-dependent biochemical signaling. Future studies will be required to fully grasp the functional implications of these homeostatic regulations.

MANUSCRIPT III

Tuning into diversity of homeostatic synaptic plasticity

Kevin F.H. Lee [a,d], Cary Soares [a,d], Jean-Claude Béïque [b,c,d]

[a]Neuroscience Graduate Program, [b]Centre for Stroke Recovery, [c]Centre for Neural Dynamics, [d]Department of Cellular and Molecular Medicine, Faculty of Medicine, University of Ottawa, Ottawa, ON K1H 8M5, Canada

Corresponding author:

Jean-Claude Béïque

This manuscript was published in *Neuropharmacology* in 2014 (2013, ahead of print):
Lee KF, Soares C, Béïque JC. Tuning into diversity of homeostatic synaptic plasticity. Neuropharmacology. 2014 Mar;78:31-7. doi: 10.1016/j.neuropharm.2013.03.016. Epub 2013 Mar 27. PMID: 23541721

Statement of Contributions:

I led the survey of the literature and wrote all drafts leading to submission.

Cary Soares provided important conceptual input to help formulate and develop the major ideas and topics and edited all drafts.

Dr. Béïque helped guide the overarching narrative, provided detailed comments on the manuscript and edited the final draft prior to submission.

Abstract

Neurons are endowed with the remarkable ability to integrate activity levels over time and tune their excitability such that action potential firing is maintained within a computationally optimal range. These feedback mechanisms, collectively referred to as "homeostatic plasticity", enable neurons to respond and adapt to prolonged alterations in neuronal activity by regulating several determinants of cellular excitability. Perhaps the best-characterized of these homeostatic responses involves the regulation of excitatory glutamatergic transmission. This homeostatic synaptic plasticity (HSP) operates bidirectionally, thus providing a means for neurons to tune cellular excitability in response to either elevations or reductions in net activity. The last decade has seen rapid growth in interest and efforts to understand the mechanistic underpinnings of HSP in part because of the theoretical stabilization that HSP confers to neural network function. Since the initial reports describing HSP in central neurons, innovations in experimental approaches have permitted the mechanistic dissection of this cellular adaptive response and, as a result, key advances have been made in our understanding of the cellular and molecular basis of HSP. Here, we review recent evidence that outline the presence of distinct forms of HSP at excitatory glutamatergic synapses which operate at different sub-cellular levels. We further present theoretical considerations on the potential computational roles afforded by local, synapse-specific homeostatic regulation.

Keywords: homeostatic plasticity; synaptic scaling; multiplicative; synapse-specific; local; glutamate; AMPA receptors; synaptic plasticity

Introduction

Defined patterns of pre- and postsynaptic activity can induce input-specific changes in synaptic strength. The two most studied of these activity-dependent synaptic plasticity processes are long-term potentiation (LTP) and long-term depression (LTD). These processes exhibit many of the features described in a model postulated by Donald Hebb more than 50 years ago to account for the ability of a neuronal network to store information (Hebb, 1949). As a result, tremendous efforts have been devoted to define the cellular and molecular mechanisms of LTP and LTD, and to understand their role as substrates of learning and memory (Malenka and Nicoll, 1999; Malinow and Malenka, 2002; Lisman and Raghavachari, 2006; Whitlock et al., 2006; Kerchner and Nicoll, 2008; Kessels and Malinow, 2009; Lisman, 2009). However, the simple implementation of Hebbian-type LTP and LTD processes in different neuronal network models soon revealed an inherent stability problem for network function (Miller and MacKay, 1994; Turrigiano and Nelson, 2004; Lazar et al., 2009).

Destructive instabilities of both synapse and network function are readily apparent in exclusively Hebbian neural network models (Miller and MacKay, 1994; Shouval et al., 2002; Turrigiano and Nelson, 2004; Lazar et al., 2009). Specifically, these models demonstrate that the positive-feedback nature of Hebbian plasticity favors unconstrained synaptic potentiation and depression, thus leading to synapses which hit their functional 'ceiling' (for instance, by reaching maximum AMPA receptor number and density), or synapses that are driven toward functional demise by depressive mechanisms. An important consequence of such positive-feedback behavior in neural circuits is runaway excitation and epileptogenic neural activity (Turrigiano and Nelson, 2004; Lazar et al., 2009). During early childhood, the brain experiences intense growth and development and these normal processes have been linked to enhanced susceptibility

to seizure in young children (Wong, 2005). However, the overall risk of pediatric seizure remains relatively low considering the breadth of developmental changes at play, prompting some to hypothesize that homeostatic mechanisms exist to stabilize neural networks during development (Turrigiano and Nelson, 2004; Davis, 2006) and during mature brain function (Yeung et al., 2004; Toyoizumi et al., 2005; Sullivan and de Sa, 2006, 2008; Turrigiano, 2008; Lazar et al., 2009; Watt and Desai, 2010; Turrigiano, 2012), but see (Houweling et al., 2005; de Vries and van Slochteren, 2008; Thivierge and Cisek, 2008; Gilson and Fukai, 2011).

Several distinct homeostatic plasticity mechanisms have been described, each in principle providing neurons the means to tune and maintain overall levels of spiking activity within biologically-determined set points. Neurons accomplish this by actively regulating several determinants of cellular excitability, including intrinsic excitability (Grubb and Burrone, 2010; Turrigiano, 2011) and synaptic strength (Turrigiano et al., 1998; Turrigiano and Nelson, 2004; Turrigiano, 2012). In particular, the discovery of homeostatic synaptic plasticity (HSP) has received considerable interest because it provides a theoretically plausible solution to the instability problem of Hebbian networks described above. With features that closely resemble the well described denervation supersensitivity at the neuromuscular junction (Cannon, 1949), homeostatic synaptic plasticity (HSP) is characterized by the bidirectional regulation of synaptic strength in response to prolonged alterations in network activity (O'Brien et al., 1998; Turrigiano et al., 1998; Turrigiano, 2008).

Borrowing from the widely-used distinction between the induction and expression of Hebbian forms of synaptic plasticity (LTP/LTD), one can conceptualize a loosely analogous distinction between the *induction* and *expression* of HSP. Determining key mechanistic features of both these processes, in addition of determining how they interact with classic Hebbian

synaptic plasticity, is necessary for developing a thorough understanding of the role played by HSP in neuronal computation. Here, we review recent studies that reveal fundamental mechanistic insights in the *induction* (eg., cell-autonomous vs. non-cell-autonomous) and *expression* (cell-wide vs. local) of HSP and consider conceptual refinements for the role of local forms of HSP in stabilizing neuronal information storage and processing at excitatory glutamatergic synapses.

The Locus of Homeostasis

Whereas Hebbian LTP and LTD occurs within seconds to minutes in response to relatively short bouts of synaptic stimulation, the presence of HSP is experimentally revealed when neuronal activity is altered over longer periods of time (*i.e.,* hours to days). For instance, in perhaps its simplest and most intuitively tractable form, HSP is revealed when neuronal network activity is globally suppressed for a prolonged period of time (*eg.,* by applying tetrodotoxin to the culture media for many hours; see Figure 1B). In response, neurons exhibit a compensatory increase in cellular excitability, in part through a cell-wide up-regulation of synaptic AMPAR function (Turrigiano et al., 1998). This slow-acting regulation of excitability is also bidirectional: when neuronal activity is enhanced for many days (eg., by pharmacological network disinhibition), neurons adapt by a cell-wide down-regulation of synaptic AMPAR function.

These core features of homeostatic plasticity entail a number of conceptual postulates: 1) Neurons are endowed with mechanisms that monitor, and integrate over time, some parameters of neuronal activity; 2) These 'sensing' mechanisms are coupled to cellular 'effectors' that operate within a feedback loop to tune neuronal excitability in a direction that is homeostatic in nature (*eg.,* upregulation of excitatory glutamate receptors following prolonged suppression of

neuronal activity); 3) whereas HSP's activity sensing and integrating mechanisms are likely continuously operating 'on line', the feedback loop acts over a relatively long time course (*i.e.,* usually requiring several hours for expression). This conceptual framework has helped to guide the mechanistic dissection and understanding of HSP in the last several years (Turrigiano, 2008; Turrigiano, 2011; Lee, 2012a).

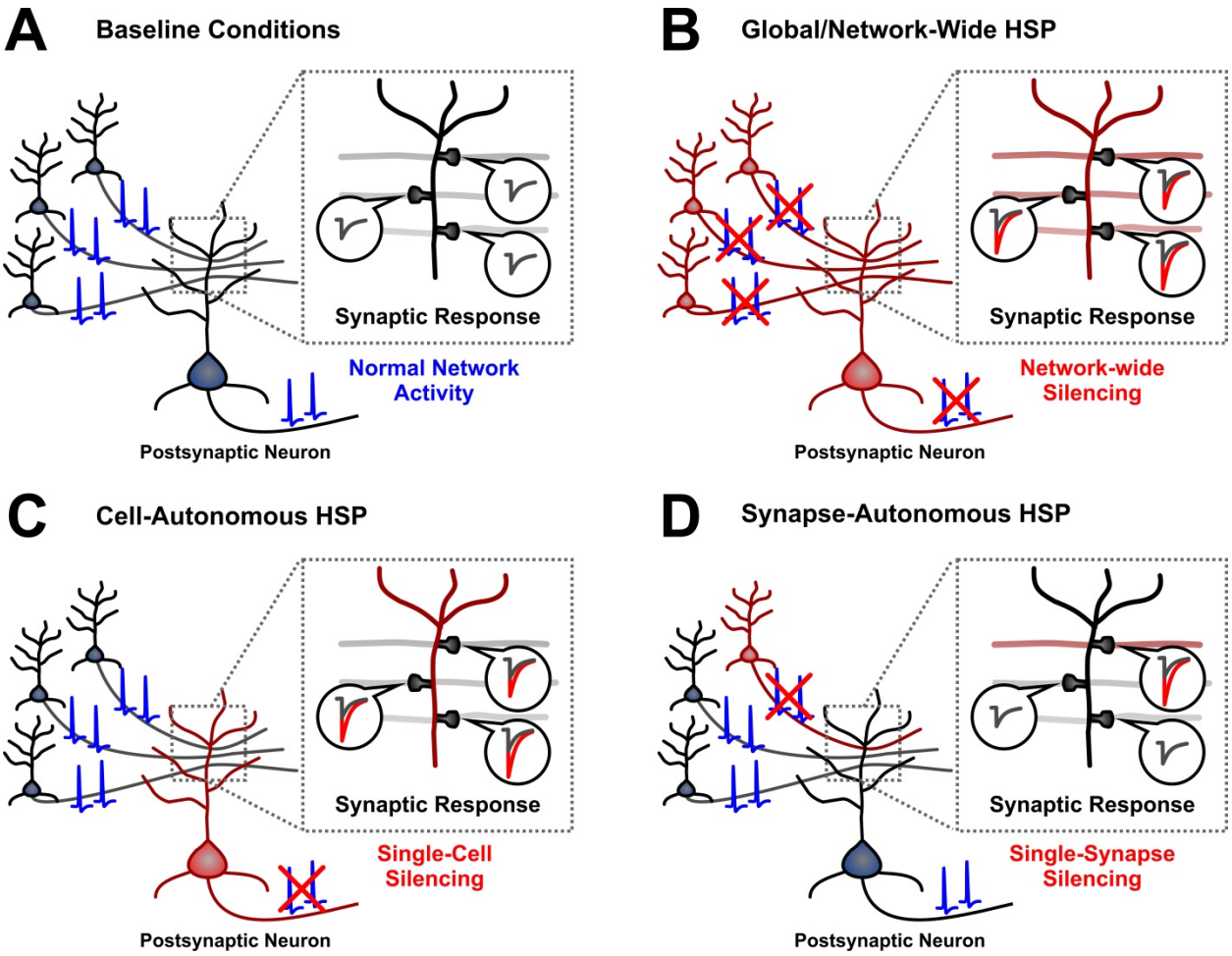

Figure 1: Diversity of Homeostatic Synaptic Plasticity (HSP)

A) A postsynaptic neuron receives excitatory synaptic input from presynaptic neurons in a neuronal network. *Inset:* The amplitude of the excitatory postsynaptic current (EPSC) schematizes the strength of each synapse. B) HSP is revealed when network activity is altered for a prolonged period of time. In this example, action potential firing is abolished in all neurons by prolonged exposure to TTX. In response to the global reduction in activity, HSP mechanisms enhance synapse function in a cell-wide manner by increasing synaptic AMPA receptor content at all synapses (depicted by an increase in synaptic EPSC amplitude). Despite revealing HSP in its most intuitively-tractable form, the roles of pre- and post-synaptic activity cannot be distinguished with this global/network-wide experimental paradigm. C) Cell-Autonomous HSP. Single-cell strategies that alter the activity of individual neurons (eg. via somatic TTX-perfusion) have revealed the cell-autonomous nature of HSP induction in glutamatergic pyramidal cells. Here, reducing the firing activity of a single neuron in an otherwise normal neural network results in cell-wide expression of HSP. D) Synapse-Autonomous HSP. Suppression of firing activity in a single neuron reveals synapse-autonomous HSP at its postsynaptic target neuron. Here, the 'silenced' synapse is selectively strengthened over its nearby unperturbed neighbors. This demonstrates the ability of individual synapses to actively monitor and homeostatically respond to prolonged changes in activity.

One feature of HSP that has received particular attention is its "multiplicative" nature. This refers to the observation that during some forms of HSP, the entire amplitude distribution of synaptic strength scales up (or down) by a single common factor, hence the term 'scaling', often used to denominate HSP (Turrigiano et al., 1998; Turrigiano, 1999, 2008; Kim et al., 2012). A common interpretation of the multiplicativity of HSP is that the relative strengths between synapses are maintained during the cell-wide homeostatic scaling process. As such, multiplicative HSP provides a means to tune neuronal excitability without disrupting the previously encoded catalogue of Hebbian synaptic engrams. A parsimonious cellular model to account for multiplicativity in HSP posits that a cell-wide mechanism drives the upregulation of AMPAR content across all synapses, with each synapse capturing (or stabilizing) AMPARs in a manner that is proportional to its original strength. However, since global/network-wide pharmacological manipulations (*eg.,* TTX treatment) alter the activity of each neuron within the network, a number of mechanistic details of HSP are left largely intractable. For instance, it is impossible to determine the trigger for HSP induction since two broadly distinct changes take place. First, all neurons in the network are deprived of their ability to generate action potentials. Second, all synapses are deprived of presynaptic input. As such, where is the locus of homeostasis? Do neurons monitor and integrate activity over time by counting action potentials? Or rather, do individual synapses monitor and integrate activity over time by tallying presynaptic inputs? Recent studies have provided interesting insight into this important facet of HSP.

Cell-Autonomous HSP

In a first-step to distinguish between these possibilities, a key series of studies examined the ability of individual neurons to autonomously exhibit HSP (cell-autonomous HSP) by specifically modulating the firing activity of a single neuron embedded within an otherwise

normal neural network (i.e., receiving normal ongoing synaptic input; see Figure 1C) (Burrone et al., 2002; Ibata et al., 2008; Goold and Nicoll, 2010). Borrowing from a previous study at the neuromuscular junction (Paradis et al., 2001), Burrone et al. (2002) developed a single-cell silencing strategy by overexpressing an inwardly rectifying potassium channel, Kir2.1, in a small subset of dissociated hippocampal neurons in culture. Single-cell silencing induced a homeostatic upregulation of glutamatergic transmission as evidenced by a robust enhancement of the frequency of AMPAR-mediated miniature excitatory postsynaptic currents (mEPSCs) in transfected neurons. It was concluded that the reduction of action potential firing by Kir2.1 overexpression induced a homeostatic increase in synaptic function, and thus demonstrated that individual neurons can autonomously express HSP. However, it was later argued that because the Kir2.1-mediated silencing strategy used by Burrone et al. (2002) caused cell-wide hyperpolarization, it was not possible to discriminate the involvement of local dendritic excitability from that of somatic action potentials in triggering HSP. Thus, to specifically ascertain the role of somatic spiking activity in HSP induction, Ibata et al. (2008) used prolonged local perfusion of TTX over the soma of individual neurons. The authors found that suppression of action potential firing for 4 hours was sufficient to induce a significant increase in mEPSC amplitude and accumulation of synaptic EYFP-tagged GluA2-containing AMPARs, and that these changes were likely due to an alteration of somatic calcium-dependent signaling by the reduction in action potential firing. Together, these results support the notion that individual cells can autonomously respond to a reduction in action potential firing by expressing HSP.

HSP has been widely shown to operate bidirectionally and, as such, Goold & Nicoll later asked whether prolonged periods of enhanced activity in a single neuron could drive a homeostatic depression of glutamatergic transmission. To this end, the authors developed an

elegant optogenetic approach whereby CA1 pyramidal neurons in organotypic hippocampal slice culture were biolistically transfected to express the light-activated cation channel Channelrhodopsin-2 (ChR2). This strategy allowed the authors to predictably and chronically enhance action potential firing of individual neurons by flashing blue light while the slices were incubated. After prolonged photostimulation (>24 hours), ChR2-expressing neurons exhibited a dramatic reduction in both synaptic AMPAR and NMDAR function – an effect which, similar to the findings of Ibata et al. (2008), was also suggested to be mediated by somatic calcium-dependent signaling.

Altogether, by modulating the firing activity of single-cells in otherwise unperturbed networks, these studies reveal a fundamental conceptual advancement for HSP: at least one parameter of neuronal activity that is homeostatically regulated is action potential firing rate *per se*, which neurons monitor over time by calcium-dependent signaling at the soma. Interestingly, these findings contrast with HSP at inhibitory GABAergic synapses, which rely not on cell-autonomous signals, but upon network-wide activity levels (Hartman et al., 2006). Therefore, cell-autonomous functions likely act in concert with additional network-level mechanisms to regulate neural circuit function and stability (Maffei and Fontanini, 2009).

Synapse-Specificity of HSP

As outlined above, multiplicative HSP is generally interpreted to reflect that all synapses onto a neuron undergo homeostatic scaling by a single common factor. Although it has been well documented and observed by several groups in a number of experimental preparations, multiplicative HSP has not been universally observed (Thiagarajan et al., 2005; Echegoyen et al., 2007; Goel and Lee, 2007; Thiagarajan et al., 2007), suggesting some degree of synapse-

specificity in HSP expression under certain conditions. This was perhaps best illustrated by a series of experiments studying HSP in TTX-treated organotypic hippocampal slice cultures (Kim and Tsien, 2008; Deeg, 2009). In response to prolonged suppression of activity by TTX treatment, CA1 neurons exhibit uniform, cell-wide multiplicative scaling (Kim and Tsien, 2008; Kim et al., 2012). However, the expression of HSP on CA3 neurons was not uniform, but rather synapse-specific. Despite being located on the same CA3 neuron, only throughput, feed-forward synapses exhibited HSP, while recurrent CA3-to-CA3 synapses became functionally depressed. Thus, HSP expression was dependent on the precise role of the synapse in information flow through the hippocampal network. Due to the feed-forward/feedback architecture of the hippocampal circuit, such synapse-specificity was found to impart network stability during HSP by preventing reverberating epileptogenic activity (Kim and Tsien, 2008). These results raise the intriguing possibility that local mechanisms exist to govern, or gate, the expression of HSP at individual synapses in response to cell-wide homeostatic signals. This idea is further illustrated by findings from *in vivo* HSP studies in rodents. Whereas visual sensory deprivation by dark rearing of young animals resulted in the expression of multiplicative HSP in layer II/III visual cortical neurons, non-multiplicative HSP was observed following dark rearing of older animals (Goel and Lee, 2007). These results may therefore reflect an age-related divergence in the potential for HSP expression in a subset of synapses. Future investigations, likely requiring methodological and technological developments, will be necessary to thoroughly define the factors that impact HSP expression at individual synapses during prolonged changes in global network activity.

Local Synapse-Autonomous HSP

A corollary, but distinct, line of questioning relates to whether individual synapses, like neurons, can monitor and integrate their own activity over time and autonomously perform homeostatic adjustments. In other words, are individual synapses autonomous homeostatic units? One way to experimentally address this question is to determine the consequences of reducing (or blocking) neurotransmitter release onto a very small number of synapses - ideally as few as one - such that the overall excitability of the postsynaptic neuron is left unaltered. To this end, studies have used site-directed perfusion of drugs over discrete regions of dendritic segments to locally suppress activity (Sutton et al., 2006; Ibata et al., 2008). Ibata et al. (2008) micro-perfused TTX or CNQX+APV onto defined dendritic regions of cultured neurons for up to 5 hours, but did not observe any measurable changes in the accumulation of EYFP-tagged GluA2 subunits within the 'silenced' dendritic region. These results however do not preclude the possible accumulation of GluA2-lacking AMPARs, as occurs in cell-wide HSP (Sutton et al., 2006; Soden and Chen, 2010; Groth et al., 2011; Lindskog et al., 2011; Lee, 2012a), but see (Gainey et al., 2009; Anggono et al., 2011). In this respect, Sutton et al. (2006) previously found that the expression of HSP (induced by global TTX application) could be locally accelerated by site-directed perfusion of APV over defined dendritic regions, leading to an increase in GluA1-containing AMPARs within the site of APV perfusion. These latter results therefore suggest that mechanisms can 'sense' local synaptic activity and engage local machinery to homeostatically regulate synapse function. However, since local perfusion strategies indiscriminately disrupt presynaptic activity, glutamate receptor function and/or dendritic excitability over broad dendritic segments, it is difficult to substantiate, or refute, the homeostatic autonomy of individual synapses with these methods alone.

To circumvent this problem, molecular-based experimental strategies were developed to modulate the activity of a small number of synaptic inputs onto an otherwise unaltered postsynaptic neuron such that the AMPAR content of 'silenced' synapses can be compared to their neighbors (see Figure 1D). One such strategy involved the overexpression of Kir2.1 in single neurons along with the synaptic marker Synapsin-YFP (Syn-YFP), to label and suppress the activity of a small number of presynaptic terminals onto neurons in culture. Immunocytochemical detection revealed that postsynaptic AMPAR content was enhanced specifically at synapses that were presynaptically suppressed by Kir2.1 overexpression (Hou et al., 2008; Beique et al., 2011). Moreover, electrophysiological recordings showed that the amplitude of AMPAR-mediated postsynaptic currents were larger on 'silenced' synapses, as determined by two-photon glutamate uncaging onto Kir2.1/Syn-YFP-apposed synapses compared to closely neighboring control spines (Beique et al., 2011). This synapse-autonomous form of HSP was mediated by the insertion of inwardly-rectifying calcium-permeable GluA2-lacking AMPARs and, furthermore, was shown to be dependent on the immediate early gene Arc. Altogether, these studies support the notion that individual synapses are endowed with the ability to autonomously sense, and integrate over time, their own level of activity and adapt to it (likely bidirectionally (Hou et al., 2011)) in a homeostatic fashion. Interestingly, because GluA2-lacking AMPARs (Sutton et al., 2006; Soden and Chen, 2010; Groth et al., 2011; Lindskog et al., 2011; Lee, 2012a) (but see (Gainey et al., 2009; Anggono et al., 2011)) and Arc (Shepherd et al., 2006) have previously been shown to be involved in cell-wide HSP, these results reveal at least some degree of mechanistic convergence in the expression mechanisms of local and cell-wide forms of HSP.

Membrane hyperpolarization induced by Kir2.1 overexpression reduces, but does not abolish, action potential firing in the presynaptic neuron - especially in conditions similar to those during incubation of neuronal cultures (Beique et al., 2011). As such, the results outlined above indicate that individual synapses are homeostatically sensitive to relatively small changes in incoming activity and can autonomously undergo HSP. Interestingly, the complete blockade of glutamate release at single synapses by presynaptic overexpression of tetanus toxin light chain (TeTx) does not induce a compensatory homeostatic upregulation of postsynaptic AMPAR content. Indeed, several studies using this approach have either reported no change (Lee et al., 2010) or decreases (Harms et al., 2005; Ehlers et al., 2007; Okuno et al., 2012) in AMPAR function and/or content at TeTx-silenced synapses. Because TetTx blocks both spontaneous and action potential-dependent forms of vesicle release (Harms et al., 2005; Ehlers et al., 2007), these results collectively suggest that spontaneous glutamate release is required for synapse-autonomous HSP. This notion is fully consistent with the well documented role of spontaneous synaptic events in maintaining several aspects of synapse integrity and function, including glutamate receptor stability and clustering at synapses (Craig et al., 1994; McKinney et al., 1999; Saitoe et al., 2001; Verstreken and Bellen, 2001, 2002; Bouwman et al., 2004; Harms et al., 2005; Ehlers et al., 2007; Mateos et al., 2007), thus revealing an interesting subtlety in activity-detection for HSP at single synapses.

Dating back to the late 1970's, several investigations have demonstrated that prolonged *in vivo* blockade of spinal cord motoneuron activity results in enhanced synaptic transmission (Gallego et al., 1979; Manabe et al., 1989; Webb and Cope, 1992), with some suggesting that these homeostatic adaptations are synapse-specific (Webb and Cope, 1992). More recently, by manipulating sensory stimuli to Xenopus tadpoles, Deeg & Aizenman (2011) provided evidence

supporting the presence of such synapse-specific forms of HSP *in vivo* (Deeg and Aizenman, 2011). Neurons of the optic tectum in Xenopus tadpoles receive distinct synaptic inputs from both visual and mechanosensory pathways. By dark-rearing tadpoles, the authors observed a compensatory homeostatic increase in synaptic strength specifically at synapses of the visual pathway. In a complementary manner, prolonged mechanosensory hyperstimulation by persistent ambient vibration caused homeostatic synaptic depression specifically at mechanosensory synapses. These important findings thus demonstrate *in vivo* manifestations of synapse-autonomous HSP.

A Computational Paradox?

One immediate computational appeal of the multiplicative (uniform) nature of cell-wide HSP is that neurons can tune spiking activity to an optimal range without imposing an informational cost since the relative strength between synapses (presumably encoded by prior synaptic activity) would be left unaltered. As a result, it has been argued that local forms of HSP, such as those described above, are computationally costly and paradoxical as they would in essence erase information stored by Hebbian-forms of plasticity (Ibata et al., 2008; Turrigiano, 2012). We provide in this final section some alternative interpretations and speculate on the functional role of local HSP for stabilizing information storage and processing.

First, the informational cost intuitively associated with local HSP exists only within a model whereby information (or memory) is encoded by stable modifications solely of synaptic *strength*. Despite its historical popularity, this model is now believed to be unsatisfactory and too simplistic, as it necessitates unrealistic assumptions and fails to account for many complexities of synapse function (Fusi et al., 2005; Fusi and Abbott, 2007). While imposing realistic bounds on

synaptic strength, one recent theoretical model rather suggested that Hebbian changes in synaptic strength are accompanied by biochemical alterations which permit transitions between cascades of metaplastic 'states' (Fusi et al., 2005). Thus, information can be encoded not solely through changes in synaptic strength, but in a more complex synaptic engram involving subtle biochemical alterations that can span various time scales (enzymatic activity, phosphorylation states, calcium dynamics etc.) (Shouval et al., 2010; Shouval and Gavornik, 2011). This progressive view of Hebbian plasticity is particularly attractive because it enriches the capacity of realistically bounded synapses to store information and ascribes richer computational roles to the known diverse biochemical environments of synapses. Due to the powerful actions of calcium in biochemical signaling, the insertion of calcium-permeable GluA2-lacking AMPARs during cell-wide and synapse-autonomous forms of HSP (Thiagarajan et al., 2005; Beique et al., 2011; Lindskog et al., 2011; Lee, 2012a) may directly enact one such metaplastic state-transition and, in effect, efficaciously encode recent synaptic history (here, prolonged inactivity). In addition, the insertion of this particular AMPAR subtype in HSP of hippocampal neuron cultures has recently been shown to trigger the release of a retrograde messenger to modulate presynaptic release probability (Lindskog et al., 2011), in principle providing further computational potential to local HSP. Future studies will be required to define key features of synapse autonomous HSP such as its long-term stability, functional and temporal upper/lower bounds and effects on Hebbian plasticity rules.

Additional conceptual insight into the possible functions of local HSP can be established in the broader context of dendritic information processing. For instance, it is well established that spatiotemporal integration of synaptic inputs can evoke dendritic non-linearities such as NMDA spikes and dendritic spikes (London and Hausser, 2005; Larkum and Nevian, 2008). Of note,

NMDA spikes in dendrites are well positioned to control the throughput of synaptic information by amplifying spatially-clustered and temporally-succinct inputs, while ignoring uncorrelated synaptic noise (Schiller et al., 2000; Larkum et al., 2009; Polsky et al., 2009; Chalifoux and Carter, 2011; Lee, 2012b). In a prescient commentary published a decade ago, it was suggested that the interplay between such dendritic non-linearities and Hebbian plasticity could lead to functional instability, as subsets of dendrites containing strong synapses would dominate neuronal firing at the expense of dendrites containing weaker synapses (Goldberg et al., 2002). This idea has gained considerable traction in light of recent evidence revealing local dendritic mechanisms that spatially influence Hebbian plasticity (Golding et al., 2002; Holthoff, 2004; Govindarajan et al., 2006; Harvey and Svoboda, 2007; Kampa et al., 2007; Remy and Spruston, 2007; Larkum and Nevian, 2008; Govindarajan et al., 2011). In principle, these mechanisms would favor the emergence of spatially clustered engrams encoded by groups of neighboring synapses, rather than spatially-distributed engrams encoded throughout the dendritic arbor (Larkum and Nevian, 2008; Kleindienst et al., 2011; Makino and Malinow, 2011; Winnubst and Lohmann, 2012). As such, the destructive instabilities inherent to Hebbian networks may also be applicable at the single-cell level by the destabilization of dendritic computation. It was thus suggested that a powerful solution may be offered by HSP mechanisms operating locally to regulate synaptic weight and dendritic excitability (Goldberg et al., 2002). Local HSP mechanisms may therefore function to homeostatically normalize information throughput across all dendrites, providing a level playing field to ensure no single dendrite is too "loud" or too "quiet" during synaptic communications. The plausibility of such mechanism was supported *in silico* using a CA1 pyramidal neuron model, adding that homeostatic adjustments induced by prolonged local changes in activity could be shared between (likely a subset of) neighboring

synapses without informational cost (Rabinowitch and Segev, 2008). Extending this concept even further, one can thus conceptualize multiplicative scaling of a group of synapses located on a dendritic segment. In essence, the compartmentalized nature of dendritic computation imparts a spatial attribute to neuronal information processing and storage that, in turn, shifts the theoretical problem of instability found in Hebbian circuits from a cell-wide level, to a local, dendritic level. Thus, in the context of a compartmentalized neuron model with active dendrites and a synaptic environment that is perpetually influenced by Hebbian plasticity mechanisms, this reformulation of the original instability problem suggests that local HSP could serve a fundamental role in stable information storage and processing by neurons.

Concluding Remarks

A predominant view of HSP posits that the chief parameter of activity that is subjected to homeostatic regulation is action potential firing *per se*. As such, prolonged alteration of neuronal firing would drive uniform cell-wide homeostatic adaptation across all synapses of a neuron. However, in light of recent studies demonstrating that HSP can also operate at a synapse-specific level, it is conceivable that multiple and distinct homeostatic mechanisms exist, each operating with their specific feedback gain and dynamic range, as well as within their own contingencies for induction and expression. Borrowing from the concept that potentially every major electrical neural process will, in time, be shown to exhibit some form of plasticity (Kim and Linden, 2007), it is perhaps equally likely that many other neuronal processes are also governed by homeostatic regulatory mechanisms. The current understanding of these homeostatic mechanisms is still rudimentary and, as such, one overarching challenge is to not only uncover the cellular and molecular details of these processes, but to also account for the diversity of such mechanisms

within the broader framework of neuronal function. This undertaking will ultimately require the synergistic implementation of *in vitro* and *in vivo* investigations in tandem with theoretical mathematical modeling *in silico*. The construction of such a framework will lead to a better appreciation of how information processing and storage occurs in the brain, in both health and disease.

Acknowledgements: This work is supported by grants from the Canadian Institutes of Health Research, the Heart and Stroke Foundation, the Natural Science and Engineering Research Council of Canada. We are grateful to Dr. Denise Cook and Sean Geddes for comments on the manuscript.

The authors declare no conflicts of interest.

MANUSCRIPT IV

Title: A unique mechanism of NMDA spike initiation supports a distinct role in synaptic input integration

Journal Club on: Chalifoux, JR & Carter, AG (2011) Glutamate spillover promotes the generation of NMDA spikes. J Neurosci 31(45):16435-16446.

Author:
Kevin FH Lee*

Author Affiliations:
Neuroscience Graduate Program
Department of Cellular and Molecular Medicine
Faculty of Medicine
University of Ottawa
451 Smyth Rd
Ottawa, Ontario
Canada K1H 8M5

*Corresponding Author

Abbreviated Title: On the mechanism of NMDA spike initiation

Keywords: glutamate, spillover, dendritic spine, NMDA receptor, NMDA spike, dendritic spike, two-photon calcium imaging

Acknowledgements:
The host lab is supported by the Natural Sciences and Engineering Research Council of Canada (NSERC) and the Canadian Institutes of Health Research (CIHR).

This manuscript was published in *The Journal of Neuroscience* in 2012
Lee KF. A unique mechanism of NMDA spike initiation supports a distinct role in synaptic input integration. J Neurosci. 2012 Feb 29;32(9):2913-14. doi: 10.1523/JNEUROSCI.6318-11.2012. PMID: 22378866

Statement of Contributions:

This was a solo effort that began as a writing assignment for a graduate-level neuroscience course taken at the University of Ottawa in Fall 2011 (NSC7100 – *Neurotransmission and Neuromodulation*). This was my first publication.

Dr. Teresa Esch, the Features Editor at the Journal of Neuroscience, handled this manuscript and provided editorial comments before this paper was accepted and published.

To maintain the fidelity of information flow in the brain, neurons must integrate and transform complex patterns of synaptic input into distinct patterns of action potential output. These computations are fundamental to neuronal function and depend upon the spatial and temporal characteristics of the incoming synaptic activity. Because the dendritic arbors of cortical pyramidal cells can reach hundreds of micrometers, passive dendritic cable properties can strongly attenuate throughput of distal synaptic information to the soma. However, neurons have adopted strategies for boosting the transmission of distal synaptic information. Temporally concerted and spatially clustered synaptic inputs can generate high-amplitude regenerative events in individual dendrites called "dendritic spikes" and "NMDA spikes" (London and Hausser, 2005; Larkum and Nevian, 2008). Dendritic spikes occur in apical dendrites of cortical pyramidal neurons and cerebellar Purkinje cells and require the activation of voltage-gated Na^+ and Ca^{2+} channels (VGSCs, VGCCs, respectively). NMDA spikes take place in the thin, basal, oblique and apical tuft dendrites of pyramidal neurons and require the activation of the NMDA subtype of glutamate receptor (NMDARs), but not VGSCs or VGCCs. Dendritic spikes and NMDA spikes provide robust supralinear synaptic integration, and thus have an important role in neuronal information processing (London and Hausser, 2005; Larkum and Nevian, 2008).

The initiation of dendritic spikes can be ascribed to the simple summation of EPSPs, which provides the depolarization necessary to engage VGSCs and VGCCs. But, how brief bursts of synaptic input result in the regenerative activation of NMDARs to initiate NMDA spikes is largely unknown. In principle, the prolonged depolarizations resulting from the slow kinetics of NMDAR deactivation/inactivation may facilitate the activation of additional NMDARs upon subsequent synaptic activation by providing sustained relief of the voltage-dependent magnesium block (Polsky et al., 2009). However, long-decaying depolarization is

believed to be incapable of providing the high conductance required to elicit NMDA spikes (Rhodes, 2006). Furthermore, membrane depolarization alone is insufficient for NMDA spike generation (Polsky et al., 2009). An intriguing alternative is that glutamate released during high-frequency synaptic activation might result in glutamate spillover and the subsequent activation of additional, non-synaptic populations of NMDARs. In a recent issue of *The Journal of Neuroscience*, Chalifoux and Carter (2011) investigated this possibility by visualizing NMDAR spike-mediated calcium transients via two-photon (2P) calcium imaging in the basal dendrites of Layer V pyramidal neurons from mouse prefrontal cortex.

Using low stimulus intensities, Chalifoux and Carter evoked archetypal NMDA spikes by paired-pulse stimulation at 50 Hz. As expected, generation of NMDA spikes required activation of both AMPARs and NMDARs and resulted in large calcium transients that invaded adjacent dendrites and spines. Blocking T- and L-type VGCCs and depleting internal Ca^{2+} stores did not affect NMDA spike calcium dynamics, ruling out the contribution of these calcium sources. Together, the data convincingly identify NMDARs as the primary source of calcium influx during NMDA spikes.

Interestingly, increasing the number of stimuli produced monotonically larger Ca^{2+} transients in neighbouring spine and dendrite compartments, an effect that was enhanced by blocking glutamate transporters with a low concentration of TBOA. This finding suggested that the generation of NMDA spikes involved glutamate spillover and activation of surrounding non-synaptic NMDAR populations. As a mechanism for NMDA spike initiation, glutamate spillover accentuates the highly local nature of this dendritic supralinearity and undescores the different roles of dendritic spikes and NMDA spikes in synaptic integration.

Brief trains of high-frequency stimuli can evoke both dendritic spikes and NMDA spikes (Golding and Spruston, 1998; Schiller et al., 2000). However, the differences in subcellular location and mechanism of initiation (dependence on VGCCs/VGSCs versus NMDARs) indicates an important distinction in the spatial rules that govern the generation of these events, and also hint at the fundamentally distinct roles they might play in neuronal information processing. Dendritic spikes can be generated by spatially-disparate synaptic inputs due to the pure voltage-dependence of initiation – a behaviour that is highly analogous to the threshold-based discharge of action potentials at the axon initial segment. In contrast, the necessity for glutamate spillover and NMDAR activation imparts a spatial limitation on NMDA spike generation, restricting these events to the individual dendritic branch receiving the burst of synaptic input. Recently, dendritic spikes and NMDA spikes were proposed to perform distinct roles in a multi-layered model of dendritic integration (Larkum et al., 2009). In this model, spatially clustered bursts of synaptic inputs in thin distal dendrites initiate NMDA spikes, which propagate toward increasingly larger-calibre dendrites *en route* to the soma. At these larger dendrites, converging depolarizations (perhaps multiple NMDA spikes from different dendrites) can temporally summate to initiate dendritic spikes, which ultimately amplify these events to influence action potential firing at the soma. This multilayered integration process provides a conceptual framework that encompasses the relative roles of dendritic and NMDA spikes in boosting the throughput of temporally synchronous synaptic events. Together, these distinct events provide neurons with the ability to robustly enhance the signal-to-noise ratio of coherent synaptic information while ignoring uncoordinated synaptic noise.

Cortical neurons often communicate via bursts of action potentials, and as few as 2-3 afferent action potentials can be sufficient for driving postsynaptic NMDA spikes (Polsky et al.,

2009). NMDA spikes can thus provide an online readout of local burst input, offering clear theoretical advantages to synaptic integration and information throughput. However, the novel role of glutamate spillover in the generation of NMDA spikes raises an important question: does glutamate spillover occur at all synapses in the brain? Synapses are conventionally regarded as isolated functional units that relay discrete point-to-point synaptic information. This functional isolation is well appreciated in light of the apparent synapse-specificity of synaptic plasticity and the functional autonomy of synapses in theoretical models of information storage and learning. The occurrence of glutamate spillover suggests that the mechanisms that regulate extracellular glutamate concentrations (notably, neuronal and glial glutamate transporters) become saturated during bursts of synaptic activity, introducing a degree of synaptic promiscuity that challenges the point-to-point specificity of synaptic transmission. Because NMDA spikes have been identified primarily in thin dendrites of cortical and hippocampal pyramidal neurons, it is possible that the expression of glutamate transport mechanisms are differentially regulated in a dendrite-specific manner. In principle, this would provide a novel role for glutamate clearance mechanisms in the regulation of dendritic excitability. Speculation aside, it is important to consider that standard electrophysiological methods involving high-frequency stimuli (paired-pulse stimulation, LTP-induction) may be confounded by glutamate spillover and the activation of non-synaptic glutamate receptors. Thus, it will be important for future studies to resolve the spatiotemporal characteristics and the pervasiveness of glutamate spillover at cortical and hippocampal synapses.

Neurophysiologists have developed a growing appreciation for the spatially compartmentalized nature of synaptic integration, dendritic excitability and synaptic plasticity. The data provided by Chalifoux and Carter (2011) further champions these ideas. The novel role

of glutamate spillover in NMDA spike initiation accentuates the highly local nature of these events and further distinguishes them from dendritic spikes. The apparent subcellular segregation of dendritic and NMDA spikes supports a recently proposed multilayer model of dendritic integration, providing a conceptual framework for the relative roles of these regenerative events in neuronal information processing (Larkum et al., 2009). At the same time, the data provided by Chalifoux and Carter have important implications for synaptic physiology in general. It will be interesting to see how future studies of glutamate spillover impact our understanding of synaptic and dendritic function, and the broader implications they impress upon neuronal communications and information processing.

MANUSCRIPT V

Title:
Spatiotemporal transformations of local calcium dynamics during clustered synapse development

Authors: Kevin F.H. Lee [a,b], Cary Soares [a,b], Jean-Philippe Thivierge [d,e] & Jean-Claude Béïque [b,c,d]

Affiliations:
[a] Neuroscience Graduate Program, [b] Department of Cellular and Molecular Medicine, [c] Canadian Partnership for Stroke Recovery, [d] Centre for Neural Dynamics, [e] School of Psychology, University of Ottawa , Ottawa, Canada K1H 8M5

Contact information:
Jean-Claude Béïque

Running title:
Calcium dynamics during synapse formation

This manuscript was submitted to *Neuron* in December 2014 and was peer-reviewed (NEURON-S-14-02618). At the time of this final thesis revision (June 2015), we are working on revisions and intend to resubmit the manuscript by August 2015.

Supplemental Data can be found in the Appendices.

Statement of Contributions:

The work in this manuscript began in February 2011, and was primarily spurred by technical problems faced during the early stages of another research project (Manuscript II).

The research described in this paper involves a combination of whole-cell electrophysiology, 2P glutamate uncaging and 2P calcium imaging. I established the tools for these experiments and was the first in the lab to apply this combination of techniques.

During the course of this work, I developed fluency in technical computing using MATLAB, and generated custom software to process calcium imaging data. I have also used MATLAB to develop rudimentary computational models of synapse development, which are not included in the paper (but see Appendices). I am indebted to a fellow doctoral student in the Dept. of Cellular and Molecular Medicine, Hilary Phenix, who is not an author on the paper, but personally guided me through the initial stages of learning to use MATLAB. Dr. Jean-Philippe Thivierge supervised me through the process of software development and optimization.

I conceived the major ideas driving the research questions, designed all experiments, performed all experiments, analyzed the data and constructed the figures in this paper. I formed the narrative and wrote all major drafts of the manuscript leading to submission.

Cary Soares advised on experimental design, and offered important conceptual insights for analyzing and interpreting the data. He also provided constructive critique on the presentation of data and aided in the organization and construction of figures (specifically, figures 1b, 2a-b, S2f, S4b-c), and helped edit and format the manuscript text for submission. At the time of this writing, Cary has engaged in experimental work to aid in addressing reviewer comments.

Dr. Jean-Claude Béïque provided significant mentorship and supervised the project from start to finish. He guided the conceptual discourse underlying the design and execution of the experiments, and consulted on the presentation of the data. During the writing process, Dr. Béïque provided invaluable editorial comments/criticisms, and provided key conceptual contributions to structure the narrative of the paper.

Summary

Neurons undergo robust dendritic growth and synapse formation during early postnatal development, marking a key period in neural circuit assembly. Despite the eminent role of calcium in synapse regulation, remarkably little is known about calcium dynamics during synaptogenesis. Using whole-cell electrophysiology, two-photon calcium imaging and glutamate uncaging in acute hippocampal slices, we found that synaptic NMDA receptor activation during a narrow developmental epoch triggered intracellular calcium release at CA1 pyramidal cell dendrites, driving calcium propagation to nearby spines. Moreover, this functional coupling of NMDARs to calcium release machinery enabled dendrites to biochemically encode spatiotemporal features of synaptic input, and could thus serve to spatially regulate the activity-dependent development of ensembles of neighboring synapses. Consistent with this hypothesis, we provide evidence for locally clustered synapse maturation. These results reveal novel developmental features of NMDAR-dependent calcium dynamics that are suited to instruct the assembly of synaptic microcircuit motifs for non-linear dendritic computation.

Introduction

Neural circuit function is intimately tied to the organization of synaptic connectivity between constituent neurons. Whereas the targeted macroscopic projections between major brain regions pave general routes for information flow in the brain, stereotyped patterns of connectivity also exist within local circuits, such as in the hippocampus, to support specialized roles in information processing (Buzsaki and Moser, 2013). At a finer level, recent studies further indicate a significant degree of organization of synaptic contacts at the level of individual dendritic segments (Kleindienst et al., 2011; Makino and Malinow, 2011; Druckmann et al., 2014). This evidence for patterned synaptic connectivity at the micro-scale merges with a growing literature describing nonlinear mechanisms of dendritic information processing that depend on the organization of synaptic input in the dendritic arbor. Indeed, dendritic boosting mechanisms favor throughput of spatially-clustered synaptic activity (Mel, 1993; Polsky et al., 2004; Losonczy and Magee, 2006) and are thought to enhance the computational power of individual neurons (Poirazi and Mel, 2001; Poirazi et al., 2003). Remarkably, recent studies have shown such processes operating at pyramidal cell dendrites *in vivo* (Lavzin et al., 2012; Takahashi et al., 2012; Smith et al., 2013; Palmer et al., 2014; Sheffield and Dombeck, 2014), providing strong support for non-linear models of dendritic integration and information processing at individual neurons. Together, these results highlight a fundamental role for fine-scale organization of synaptic connectivity in neural circuit function, and raise the question of how microcircuit motifs for non-linear dendritic computation are assembled in the dendritic field.

During the first postnatal weeks in rodent hippocampus, pyramidal neurons extend elaborate dendritic arbors and rapidly establish synapses at thousands of dendritic spines (Lohmann and Kessels, 2014). This critical stage in neural circuit ontogeny offers a prime opportunity to shape synaptic connectivity through activity-dependent plasticity mechanisms. Despite the well-established role of calcium in regulating synapse function and plasticity (Lynch et al., 1983; Malenka et al., 1988), surprisingly little is known about the intracellular dynamics of activity-dependent calcium signals at developing synapses. We therefore performed whole-cell electrophysiological recordings combined with 2-photon calcium imaging and glutamate uncaging at CA1 pyramidal neurons to study NMDA receptor-mediated calcium signaling during postnatal synapse development. In sharp contrast with canonical models of spatially compartmentalized NMDAR-dependent calcium signaling at mature spine synapses (Yuste and Denk, 1995; Koester and Sakmann, 1998; Mainen et al., 1999; Oertner et al., 2002; Sabatini et al., 2002; Nevian and Sakmann, 2004), we found that NMDAR activation at individual spines during early development triggered robust calcium-induced calcium release (CICR) from intracellular stores that resulted in spreading dendritic calcium signals that invaded neighboring spines. This NMDAR-dependent CICR mechanism was activated by distinct spatiotemporal patterns of excitatory inputs, showing marked sensitivity to clustered synaptic inputs. These properties align well with a mechanism that would provide a spatial bias in the activity-dependent regulation of synapse development along dendrites. To test this prediction, we analyzed the synaptic weights of neighboring spines and found strong support for spatially-clustered synapse development. These results outline a significant departure from calcium dynamics observed at mature spines and demonstrate that NMDAR-dependent calcium signals at developing synapses are powerfully amplified in space and time by calcium release from

intracellular stores. We hypothesize that NMDAR-dependent CICR operates with local plasticity mechanisms (Harvey and Svoboda, 2007; Govindarajan et al., 2011) to shape the fine-scale functional organization of synaptic connectivity in emerging neural circuits.

Results

We obtained whole-cell electrophysiological recordings from postnatal CA1 pyramidal neurons in acute hippocampal slices from rats 7 to 26 days old (P7-P26), spanning a period of hippocampal circuit assembly involving the formation and stabilization of synapses on dendritic spines (Lohmann and Kessels, 2014) (**Figures S1A and S1B**). The Ca^{2+} indicator Fluo-4FF (200 μM) and Alexa Fluor 594 (30 μM) were included in the recording electrode for two-photon (2P) imaging of postsynaptic calcium signals in visually identified spines and dendrites (**Figures 1 and 2** and **Figure S2**) (Yasuda et al., 2004; Higley and Sabatini, 2008). To probe NMDAR-dependent synaptic calcium transients, neurons were voltage-clamped at a steady-state membrane potential (V_m = 0 mV) to inactivate voltage-gated calcium channels (VGCCs), relieve the voltage-dependent magnesium block on NMDARs and maximize calcium conductance through these receptors (Alford et al., 1993; Garaschuk et al., 1996; Mainen et al., 1999). Schaffer-collateral axons were stimulated at low frequency (>0.05 Hz) with a patch electrode placed in stratum radiatum near an apical oblique dendrite of the recorded neuron (Mainen et al., 1999; Oertner et al., 2002) (**Figures 1A-C and 1F**). We observed striking differences in the behavior of postsynaptic calcium signals evoked during early and late phases of postnatal development (P8-11 and P20-26, respectively). While late postnatal neurons exhibited synaptic calcium transients that were spatially-compartmentalized to spine heads as widely described (Yuste and Denk, 1995; Koester and Sakmann, 1998; Mainen et al., 1999; Oertner et al., 2002;

Sabatini et al., 2002; Nevian and Sakmann, 2004) (**Figure 1B**), similar stimuli at early postnatal synapses triggered spreading calcium signals that spanned several micrometers along the dendrite (**Figure 1C**). These synaptically-evoked calcium signals emanated from single spine-like protrusions and propagated with clear temporal delay in rise-time along the dendritic segment (**Figures 1C-E**). These events were likely the result of neurotransmitter release activating NMDARs, rather than direct dendritic depolarization by the stimulating electrode, since spine calcium signals exhibited failures (**Figure 1B**), and were not observed at V_m = -70 mV (n = 8 dendrites), even in response to paired-pulse stimuli (**Figures 1F and 1G**). Given the limited spatial and temporal control of synapse activation by electrical stimulation, we next turned to 2P glutamate uncaging to activate glutamate receptors at single spines and dissect the mechanisms underlying this developmental change in synaptic calcium behavior.

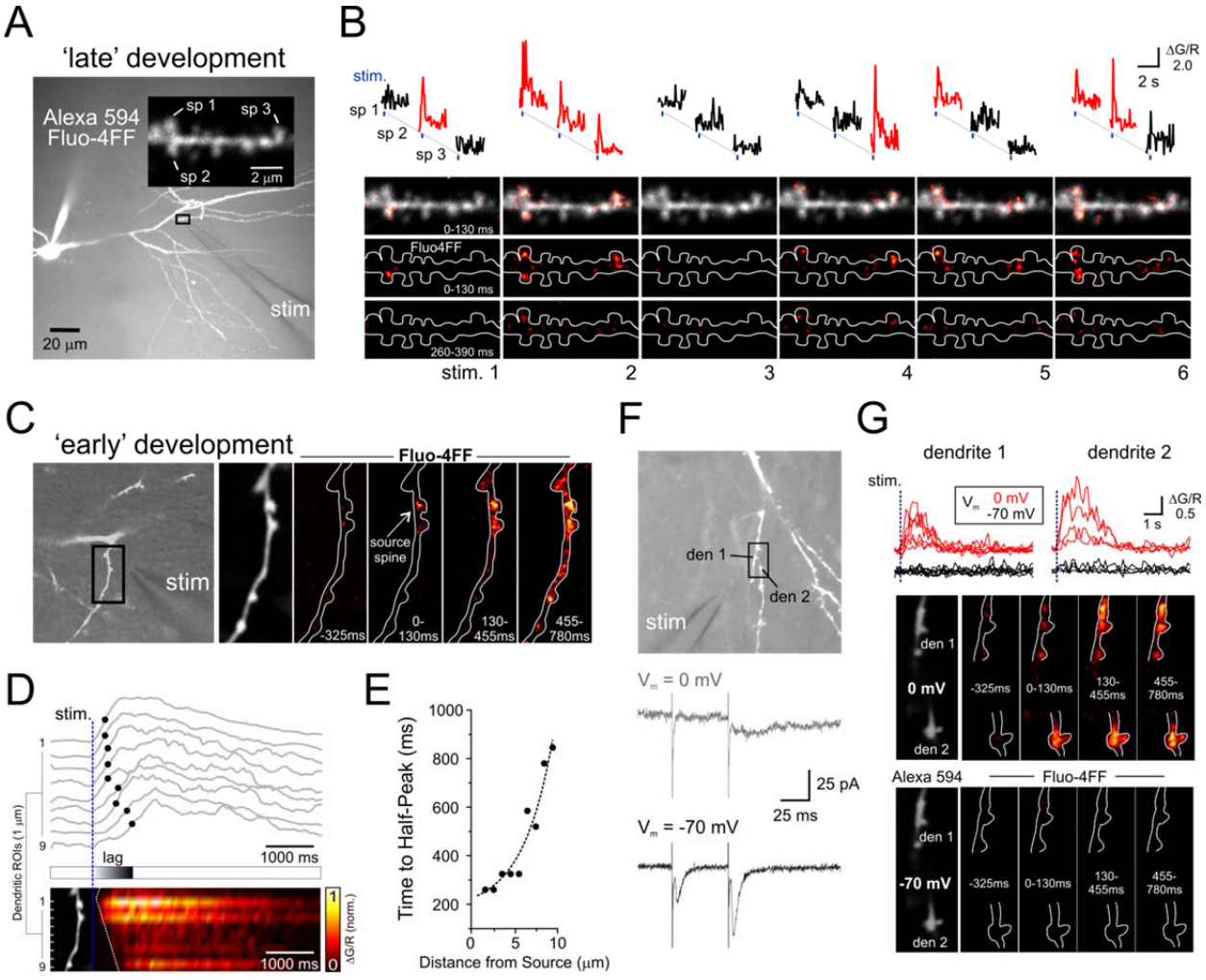

Figure 1. 2P imaging of synaptic calcium signals during postnatal development. (A) A DIC image overlaid with a 2P z-stack reconstruction of a P22 CA1 pyramidal neuron filled with 30 µM Alexa 594 and 200µM Fluo-4FF. Synaptic stimulation was delivered through a patch electrode (stim) positioned near an identified dendrite (*inset*). Three spines of interest are indicated (sp1-3). (B) Six consecutive synaptic stimuli (> 0.05 Hz) were delivered at a holding potential of V_m = 0 mV. Synaptic calcium transients were spatially limited to dendritic spine heads (shown in summed calcium fluorescence composites) and showed successes (red) and failures (black). (C) At P10 (V_m = 0 mV), similar synaptic stimuli triggered dendritic calcium signals that locally propagate. (D) *Upper panel:* Peak-normalized calcium fluorescence signals from ROIs (1 µm) along the dendrite shown in panel C. Blue circles mark the time to half-peak. *Lower panel:* Calcium fluorescence amplitude map along the length of the dendrite through time. (E) Time to half-peak from panel D plotted against distance from source spine. (F) *Upper,* Dendritic segments at P9 (den 1 & 2) imaged on a single optical plane and targeted for paired-pulse stimulation at V_m = 0 mV and -70 mV. *Lower,* Example EPSCs shown with simultaneously recorded calcium fluorescence signals in (G), where calcium fluorescence signals from 1 µm ROIs along each segment are shown with corresponding fluorescence images. See also **Figures S1-S2**.

Calcium signal propagation from single spines during early postnatal development

With 2.5mM caged glutamate in the extracellular solution, 1 ms laser pulses (720 nm) directed at individual dendritic spines (**Figure S2B**) triggered excitatory postsynaptic currents that closely matched the kinetics of AMPAR-mediated EPSCs (V_m = -70mV) (**Figure S2C**). At V_m = +40 mV, glutamate uncaging evoked EPSCs with a long-decaying component (**Figure S2E**). The glutamate receptor antagonists NBQX (10μM) and DL-APV (100μM) abolished uncaging-evoked EPSCs at V_m = -70 and +40 mV, respectively (**Figure S2E)**, confirming the activation of AMPA and NMDA type glutamate receptors by 2P glutamate uncaging (Matsuzaki et al., 2001; Beique et al., 2006; Busetto et al., 2008; Ashby and Isaac, 2011; Soares et al., 2013).

Consistent with the electrical synaptic stimulation experiments described above (**Figure 1**), 2P glutamate uncaging (V_m = 0 mV) at individual spines during early postnatal development triggered propagating dendritic calcium signals that invaded neighboring dendritic protrusions (**Figure 2A**) (median speed = 35.3 μm/s; mean speed = 71.5 ± 5.2 μm/s, see **Figure S3** and Supplemental Experimental Procedures), while the same uncaging stimulus triggered compartmentalized calcium transients at dendritic spines from more mature animals (P20-26) (**Figures 2B** and **S2F**). The histogram distribution of calcium propagation distances (P8-17 pooled) (**Figure 2C**) showed that propagating events ($prop^+$, 7.97 ± 3.68 μm; mean ± S.D, *n* = 191) and failures ($prop^-$) were well separated by a spatial threshold of 2 μm, suggesting the presence of an underlying regenerative mechanism. We observed a sharp increase in the frequency of calcium signal propagation failure with development (**Figure 2D**) that was accompanied by an age-dependent reduction in mean calcium propagation distance (**Figure 2E**).

Although the presence of a mobile buffer such as Fluo-4FF could in principle facilitate calcium diffusion and thus the spatial spread of calcium signals (Higley and Sabatini, 2008), this cannot fully account for the calcium signal propagation we observed since the peak calcium fluorescence amplitudes along the dendrite were often larger than those measured at the source spine (**Figures 2F-2H**). In several instances (8 dendrites from 8 cells), traveling calcium signals were clearly amplified at 'hot spots' along the dendrite (**Figures 2F-2G**). The magnitude of this calcium amplification in dendrites, measured by the peak fluorescence amplitude ratio between dendritic and source spine compartments, was significantly reduced with age (**Figure 2H**). Given the heterogeneity of the spine calcium responses (compartmentalized vs propagating) (**Figures 2A & 2B**), the spatial profile of the propagating calcium signal (**Figures 2F-2H**) and the spatial resolution of a single 2P glutamate point-source uncaging pulse (Matsuzaki et al., 2001; Beique et al., 2006; Soares et al., 2013), it is also unlikely that dendritic activation of NMDARs located several microns away from the source spine contributed to the calcium signals observed. Moreover, voltage-sensitive calcium channels are inactivated in our depolarized steady-state voltage-clamped recording conditions, therefore minimizing this potential source of calcium influx. Together, these results show a marked developmental transformation of synaptic calcium signaling in CA1 pyramidal neurons: whereas single-synapse activation early in development triggers calcium signals that propagate into the parent dendrite and invade closely neighboring spines, the same synaptic stimuli trigger calcium signals that are confined to activated spines in more mature neurons.

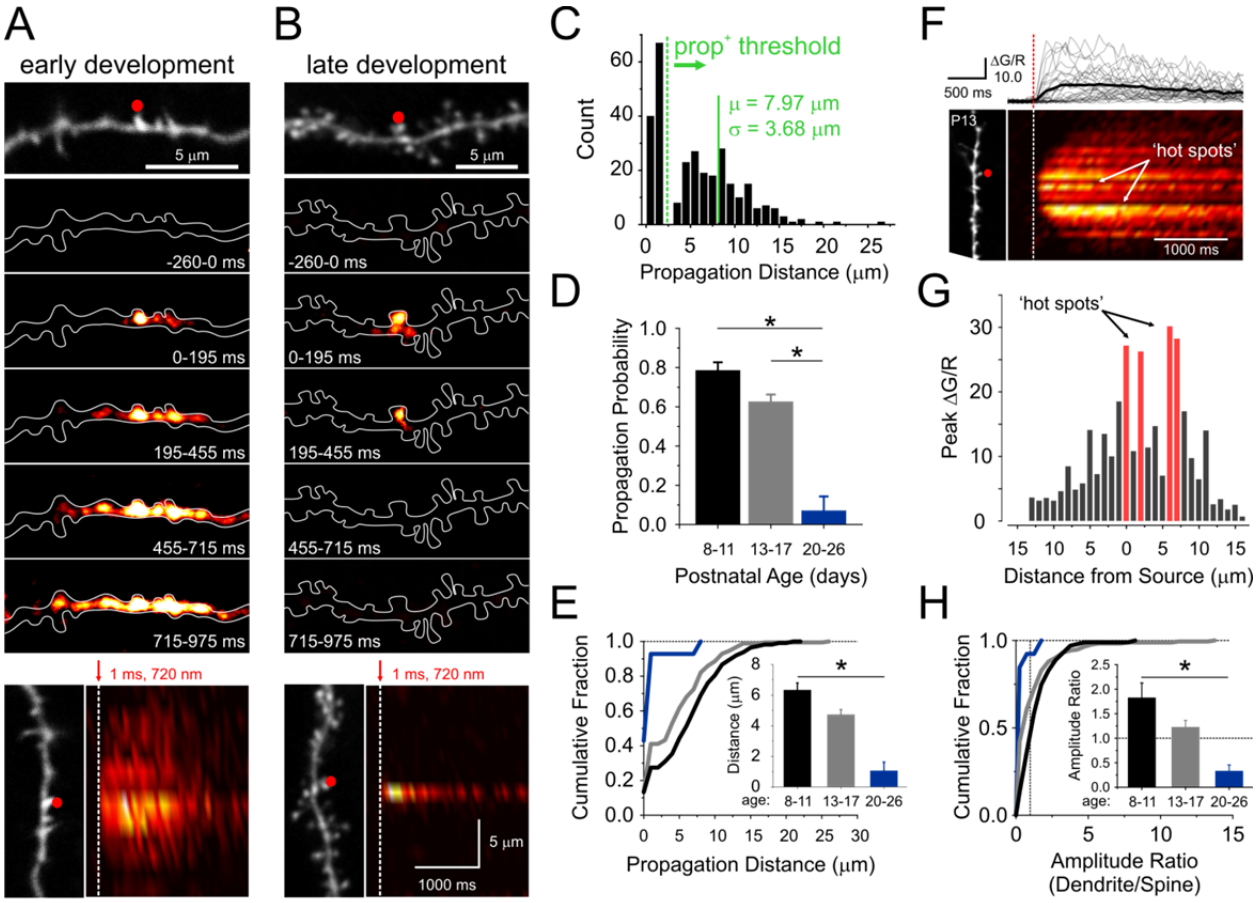

Figure 2. 2P glutamate uncaging at individual dendritic spines triggers regenerative dendritic calcium signals during early postnatal development. (A, B) Summed fluorescence image series showing calcium propagating along a dendrite at P10 (panel A), and a spatially-compartmentalized calcium signal at P26 (panel B); Lower panels are pseudo-colored dendritic calcium fluorescence maps through time. The red dots indicate the site of uncaging (at V_m = 0 mV). (C) Histogram count of propagation distances for calcium signals evoked by single spine uncaging (P8-17). A 2 µm threshold separated propagating calcium signals ($prop^+$) from non-propagating events ($prop^-$). (D) Probability of triggering propagating calcium signals by glutamate uncaging at spines (P8-11, n = 103 spines from 32 cells; P13-17: 185 spines from 15 cells, p = 0.0054; P20-26, n = 14 spines from 5 cells, p < 0.0001; Wilcoxon test). (E) Cumulative distribution and bar graph (*inset*) of calcium propagation distances with postnatal age. (P8-11 vs P20-26, p < 0.0001; Wilcoxon test). (F) *Top,* Dendritic calcium signals from dendritic ROIs (mean in bold) is shown above the corresponding dendritic calcium fluorescence map. Local calcium 'hot spots' are evident >5 µm from the source. (G) Peak calcium fluorescence amplitudes at each ROI along the dendrite shown in panel F. (H) Summary data of peak fluorescence amplitude ratios (dendrite/spine) with age (P8-11 vs P20-26, p = 0.0023; Wilcoxon test). Data shown as mean ± SEM. See also **Figures S2-S3**.

NMDAR activation triggers ryanodine receptor-dependent intracellular calcium release

The basic characteristics of the propagating calcium signals described above collectively point to the involvement of a regenerative mechanism for intracellular calcium amplification. We therefore next applied pharmacological tools to probe the relationship between glutamate receptor activation and intracellular calcium release (**Figure 3**). Blockade of Group I metabotropic glutamate receptors (mGluRs) with MCPG (500 μM) did not alter uncaging-evoked calcium signals (**Figures 3A and 3D-3F**), arguing against IP_3-mediated calcium release (Ross, 2012). In contrast, uncaging-evoked calcium signals were completely blocked by the NMDAR antagonist DL-APV (100 μM) (**Figures 3B and 3D-3F**). We next included ryanodine in the recording electrode (100-200 μM) to block ryanodine receptors (**Figure 3C**) (Isokawa and Alger, 2006) and found that ryanodine significantly reduced calcium signal detection at a large fraction of spines (**Figure 3D**). Moreover, the calcium signals detected in the presence of ryanodine were largely confined to spines and did not propagate along the dendrite (**Figures 3C and 3E-3F**). Depletion of intracellular calcium stores by blocking the endoplasmic reticulum (ER) Ca^{2+}-ATPase with cyclopiazonic acid (CPA, 30 μM) (Treiman et al., 1998; Qin et al., 2012) resulted in changes to spine and dendrite calcium behavior in young neurons (P8-11) that were consistent with the effects of intracellular ryanodine (**Figures 3D-3F and S4A-S4B**). CPA did not alter spine calcium behavior in older neurons (P20-26) (**Figures S4C-S4D**). Altogether, these results show that dendritic calcium propagation in developing dendrites is mediated by the functional coupling between NMDARs and ryanodine receptor-dependent intracellular calcium release mechanisms, and that this coupling becomes disengaged with age, enabling spines to adopt spatially-compartmentalized synaptic calcium profiles that are commonly observed at maturity (Mainen et al., 1999; Kovalchuk et al., 2000; Oertner et al., 2002; Sabatini et al., 2002)

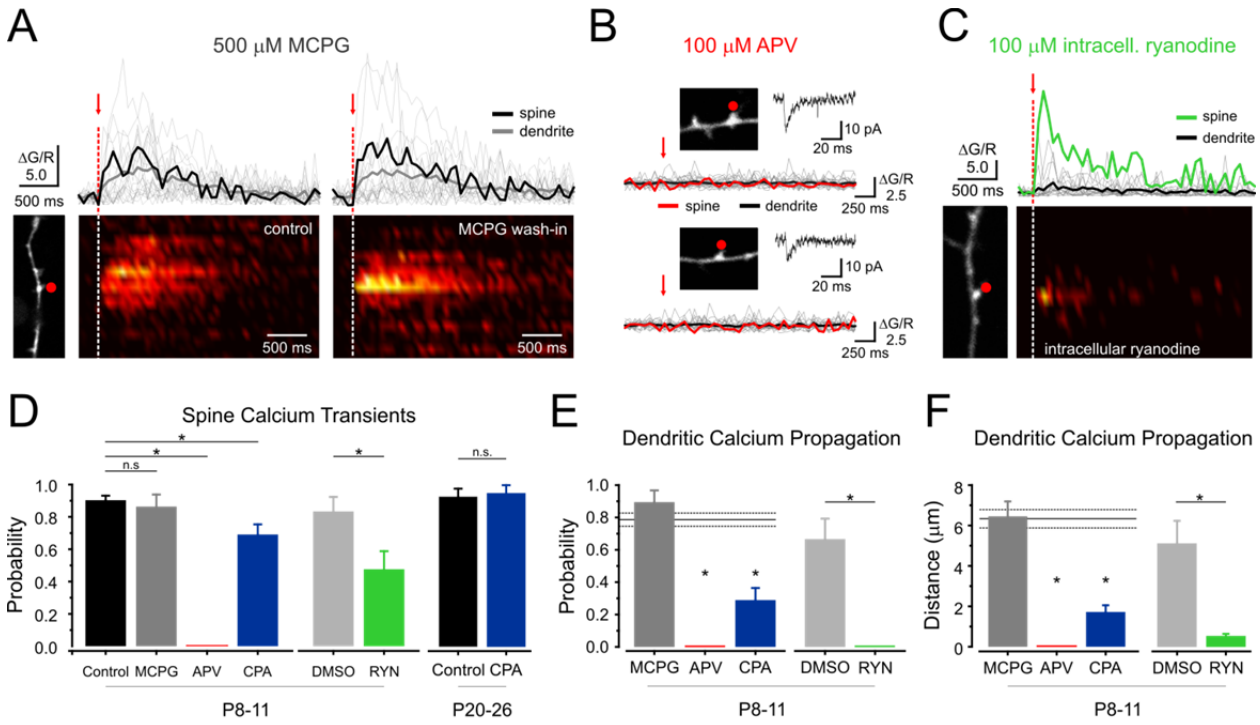

Figure 3. Pharmacological dissection of synaptic calcium signal propagation. (A) Bath application of the Group I mGluR antagonist MCPG (500 μM, >5 min) did not alter glutamate uncaging-evoked dendritic calcium propagation at P8. Calcium fluorescence traces from spine (black) and dendrite (gray, mean in bold) are shown above corresponding pseudo-colored dendritic calcium maps. (B) Two example spines at P9 showing that the competitive NMDAR antagonist DL-APV (100 μM) abolished uncaging-evoked calcium signals (n = 9 spines from 4 cells) while fast AMPAR-mediated EPSCs were unaffected (*inset*, V_m = -70 mV). Spine (red) and dendrite (gray, mean in black) calcium fluorescence traces and dendritic calcium maps are shown. (C) A dendrite at P9 infused with ryanodine (100 μM) via the recording electrode (> 15 mins after break-in) showed reduced dendritic calcium invasion. Calcium signals from the stimulated spine (green) and dendrites (gray; mean in black) and corresponding dendritic calcium map are shown. (D) Bar graph showing the probability of triggering spine calcium signals by glutamate uncaging under various pharmacological conditions (MCPG, p = 0.5784, n = 22 spines from 4 cells; CPA, p = 0.0097, n = 55 spines from 7 cells; DMSO, p = 0.3881, n = 18 spines from 3 cells; RYN, p = 0.0231, *n* = 21 spines from 10 cells; Wilcoxon test). (E, F) Summary of pharmacological experiments on dendritic calcium propagation probability (≥ 2 μm; MCPG, p = 0.2793; CPA, p < 0.0001; DMSO, p = 0.0958; RYN, p = 0.0012; Wilcoxon test) and (F) propagation distance (MCPG, p = 0.8225; CPA, p < 0.0001; DMSO, p = 0.9905; RYN, p = 0.0008; Wilcoxon test). Effects of MCPG, CPA and DMSO were compared to pooled drug-free control data (shown in **Figure 2**; re-plotted here with solid/dashed lines representing mean ± SEM, respectively), which includes data from control experiments interleaved with pharmacological experiments. Ryanodine experiments were compared to DMSO (vehicle) treated controls. Data shown as mean ± SEM. See also **Figure S4**.

Intracellular calcium release is a major determinant of calcium kinetics at developing spines

The developmental down-regulation of NMDAR-dependent CICR was accompanied by a robust acceleration of spine calcium kinetics (**Figures 4A and 4B**, see also **Figures 3E** and **S2G-S2H**). To directly assess the role of CICR mechanisms in shaping calcium kinetics at developing spines, we sorted uncaging-evoked spine calcium transients (pooled in **Figure 2C**) based on whether or not they triggered a propagating dendritic calcium signal (**Figures 4C-4E**, $prop^+$ vs $prop^-$). The spine calcium signals at $prop^+$ spines lasted more than twice as long as those recorded from $prop^-$ spines (**Figure 4F**). Although the switch towards faster-decaying GluN2A-containing NMDARs during synapse development (**Figures S1C-S1E**) would also be expected to accelerate spine calcium kinetics, we could not resolve differences between $prop^-$ spines across development (**Figure 4G**; **'**$prop^-$', $p > 0.4$). Further confirming the role of intracellular calcium release in prolonging calcium signal duration in spines, spine calcium signals recorded in the presence of intracellular ryanodine were significantly faster decaying than those recorded under control conditions (**Figure 4G**). Thus, although calcium extrusion mechanisms likely contribute to calcium dynamics to some extent (**Figure S4B**) (Pozzo-Miller et al., 1997; Majewska et al., 2000b; Scheuss et al., 2006), our results demonstrate that NMDAR-dependent CICR is the major determinant of calcium kinetics at developing spine synapses.

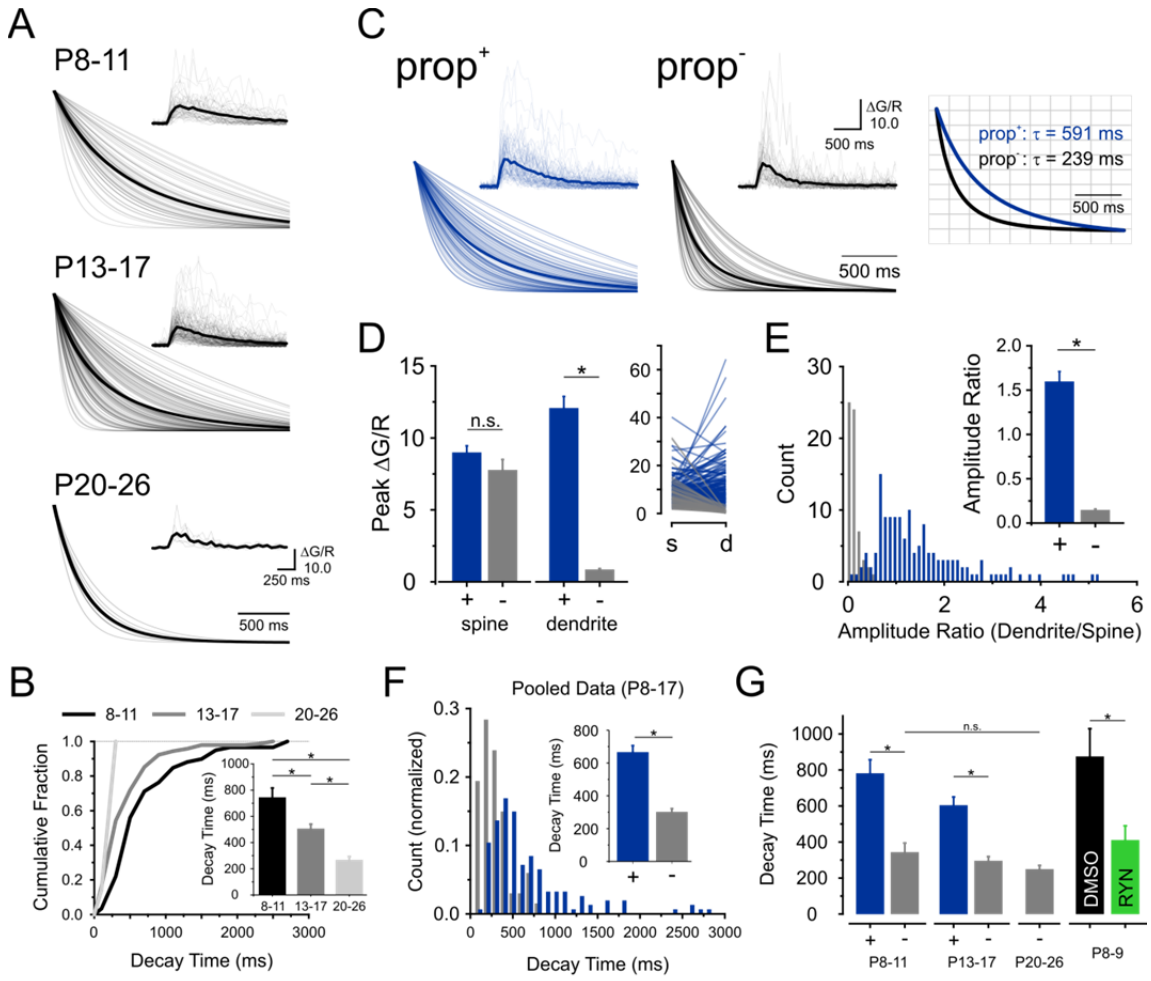

Figure 4. Calcium release from intracellular stores is a major determinant of NMDAR-dependent calcium kinetics at developing dendritic spines. (A) Monoexponential fits of uncaging-evoked spine calcium transients (~15 Hz frame scan imaging) throughout development. *Insets* show fitted spine calcium signals at each age bin. Signals that were poorly fit ($R^2 < 0.5$) were excluded from the analysis and are not shown (see Methods). (B) Cumulative distribution and bar graph (*inset*) of spine calcium decay times (P8-11 as control; P13-17, $p = 0.0007$; P20-26, $p = 0.0019$; Wilcoxon test) (C) Monoexponential fits and corresponding spine calcium transients from P8-17 animals, pooled and sorted based on whether they induced or not a propagating dendritic calcium signal (*i.e.*, $prop^+$ or $prop^-$). *Right*, mean fits overlaid, with decay times indicated. (D) Peak calcium fluorescence amplitudes at spine and dendrite compartments for $prop^+$ and $prop^-$ signals (peak ΔG/R: spine, $p = 0.7374$; dendrite, $p < 0.0001$). *Inset*, Peak ΔG/R at spine (s) and dendrite (d) compartments from individual experiments. (E) Histogram count and bar graph (*inset*) of fluorescence amplitude ratios (dendrite/spine) for $prop^+$ and $prop^-$ events (amplitude ratios, $p < 0.0001$). (F) Histogram count and bar graph of spine calcium decay kinetics for $prop^+$ and $prop^-$ events ($p < 0.0001$). (G) Bar graph showing spine calcium decay kinetics for $prop^+$ and $prop^-$ events during early postnatal development ($prop^+$ vs $prop^-$: P8-11, $p < 0.0001$; P13-17, $p = 0.0003$; Wilcoxon test) and the effect of intracellular ryanodine ($P8\text{-}9_{DMSO}$ vs RYN, $p = 0.0155$, Wilcoxon test). Data shown as mean ± SEM.

Individual dendritic spines control the expression of NMDAR-dependent CICR

We noticed considerable heterogeneity in the propensity of individual spines to trigger propagating dendritic calcium signals, even along the same parent dendrite, thus raising the possibility that the functional coupling of NMDAR-activation to CICR machinery is regulated at individual spines during development. To explore this further, we examined the relationship between calcium behavior and spine morphology since spines undergo distinct structural changes during plasticity and development (Harris et al., 1992; Yuste and Bonhoeffer, 2001; Matsuzaki et al., 2004; Harvey and Svoboda, 2007; Govindarajan et al., 2011; Tonnesen et al., 2014). Specifically, we wondered whether the behavior of NMDAR-mediated calcium signaling (that is, a change from $prop^+$ to $prop^-$) could be predicted by the apparent maturity of a spine given its morphology. Due to our limited ability to adequately resolve fine structural features of spines with 2P imaging, we restricted our analysis to a conservative comparison of only two spine morphologies: stubby spines and mushroom spines (**Figure S5A**). Consistent with ultrastructural observations (Harris et al., 1992), we found that young dendrites were sparsely studded with short stubby protrusions and progressively acquired mushroom-shaped spines with increasing age (**Figure S1A**). On average, dendritic calcium signal propagation was more frequently evoked by uncaging at stubby spines compared to mushroom spines (**Figures 5A and 5B**), with stubby spines displaying longer calcium kinetics than mushroom spines on average (**Figures 5C and 5D**). Peak calcium fluorescence amplitudes were not different between spine morphologies (**Figure 5E**, $p = 0.60$). Interestingly, we observed in a few cases a peculiar calcium behavior: whereas uncaging onto mushroom spines triggered a highly compartmentalized calcium signals, the same mushroom spines were readily invaded by dendritic calcium propagating from activation of a neighboring spine (**Figure 5A**). Indeed, calcium signals appeared to invade

stubby and mushroom spines equally, as shown by calcium fluorescence amplitude ratios (spine/base) computed at neighboring 'recipient' spines (**Figures S5B-S5D**). Although stubby spines appeared to exhibit a higher propensity for NMDAR-dependent CICR than mushroom spines, it is important to note that calcium signal propagation was still observed from a relatively large fraction (~60%) of mushroom spines (**Figure 5B**). These data collectively suggest that the spatial and temporal profile of NMDAR-dependent calcium signaling observed at mature spines may not be solely attributable to spine morphology (*i.e.*, the presence of a spine neck), but also requires the functional disengagement of NMDARs from intracellular calcium release machinery during postnatal development.

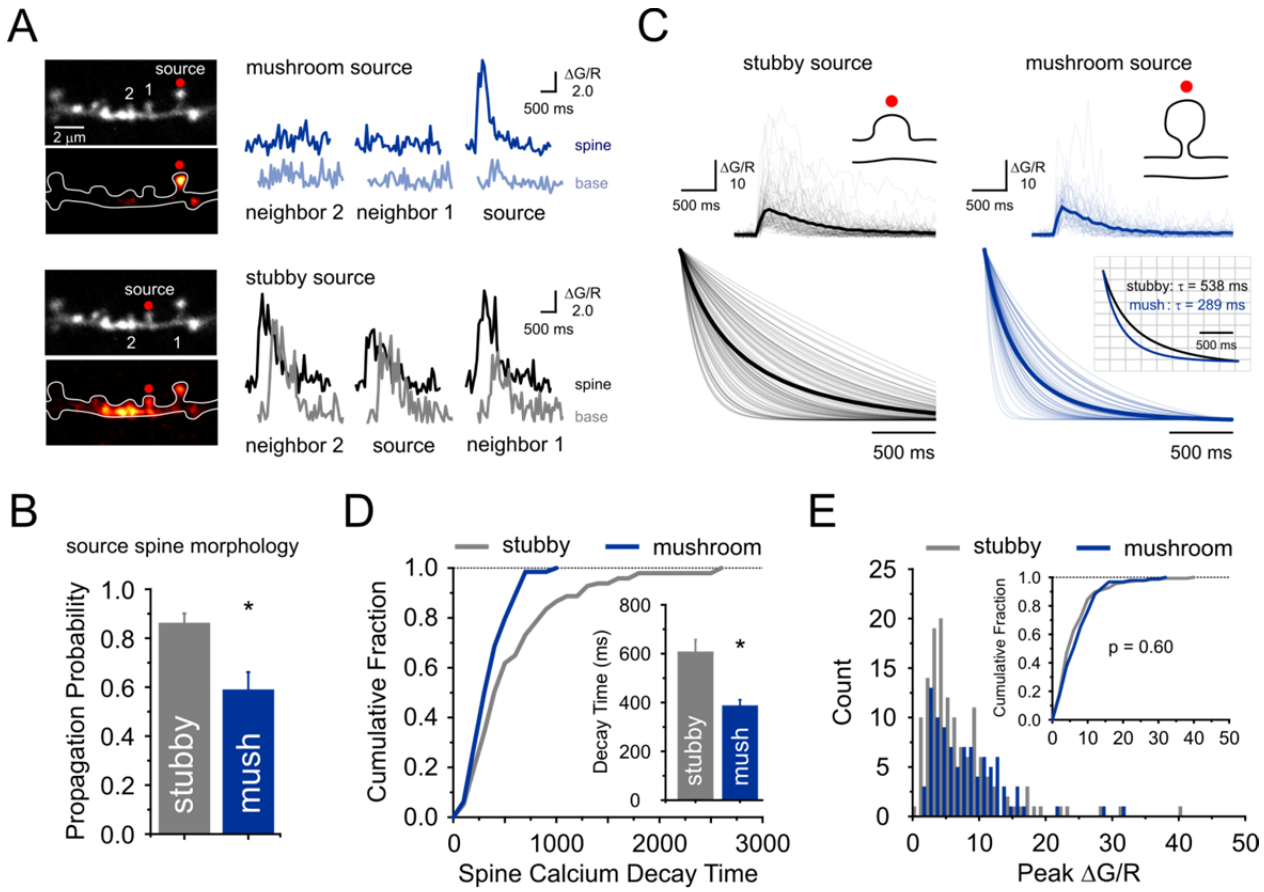

Figure 5. Effect of spine morphology on calcium propagation. (A) Dendritic segment at P13 with neighboring stubby and mushroom spines in a single focal plane. 2P glutamate uncaging was directed at either the mushroom spine *(upper*, 'mushroom source') or stubby spine (*lower*, 'stubby source'). Calcium fluorescence traces from the spine head and base are shown for the stimulated spine ('source') and two neighboring spines. (B) Probability of triggering dendritic calcium propagation by glutamate uncaging from visually identified stubby (n = 97 spines from 37 cells) and mushroom (n = 64 spines from 24 cells) spines (p = 0.0187, Wilcoxon test). (C) Uncaging-evoked spine calcium transients (*upper*) and corresponding mono-exponential fits (*lower*) from stubby and mushroom spines. *Insets,* schematized spine morphologies and glutamate uncaging position. (D) Cumulative distribution and bar graph (*inset*) of calcium decay kinetics at stubby and mushroom spines (p = 0.0007, Wilcoxon test). (E) Peak calcium fluorescence amplitudes of stubby and mushroom spines were not different. Data shown as mean ± SEM. See also **Figure S5**.

NMDAR-dependent CICR encodes spatiotemporal features of synaptic inputs

The experiments outlined above were all carried out using voltage-clamp recordings in order to maximize NMDAR conductance in response to glutamate uncaging. We next carried out a series of current-clamp recordings to examine the contingencies for triggering NMDAR-dependent CICR under more physiological conditions. Since the rules for NMDAR activation, namely coincident presynaptic input and postsynaptic depolarization (Markram et al., 1997; Nevian and Sakmann, 2004), likely also govern NMDAR-dependent CICR during development, we visualized calcium signals in response to EPSPs evoked at single spines by glutamate uncaging, and tested the effects of pairing these EPSPs with back-propagating action potentials (bAPs) driven by somatic current injection (**Figures 6A and 6B**). Under our recording conditions, spine calcium signals were rarely detected in response to glutamate uncaging alone (n = 3/21 spines, EPSP amplitude: 1.09 ± 0.21 mV) and were also rarely triggered by bAPs alone (n = 1/20 dendrites from 8 cells) (Sabatini et al., 2002). Preceding the uncaging pulse with bAPs (*i.e.,* post-pre) only marginally increased the probability of spine calcium detection (**Figures 6C and 6D**). However, spine calcium detection was significantly enhanced when the single-spine uncaging was followed by bAPs (*i.e.,* pre-post) (**Figure 6B**, $p = 0.0028$), which corresponded with an increase in dendritic calcium invasion (**Figure 6D**, $p = 0.004$). Together, these results show that the functional coupling between NMDAR-activation and CICR can be observed in response to more naturalistic patterns of synaptic input, broadly following the rules for activation expected for an NMDAR-dependent mechanism.

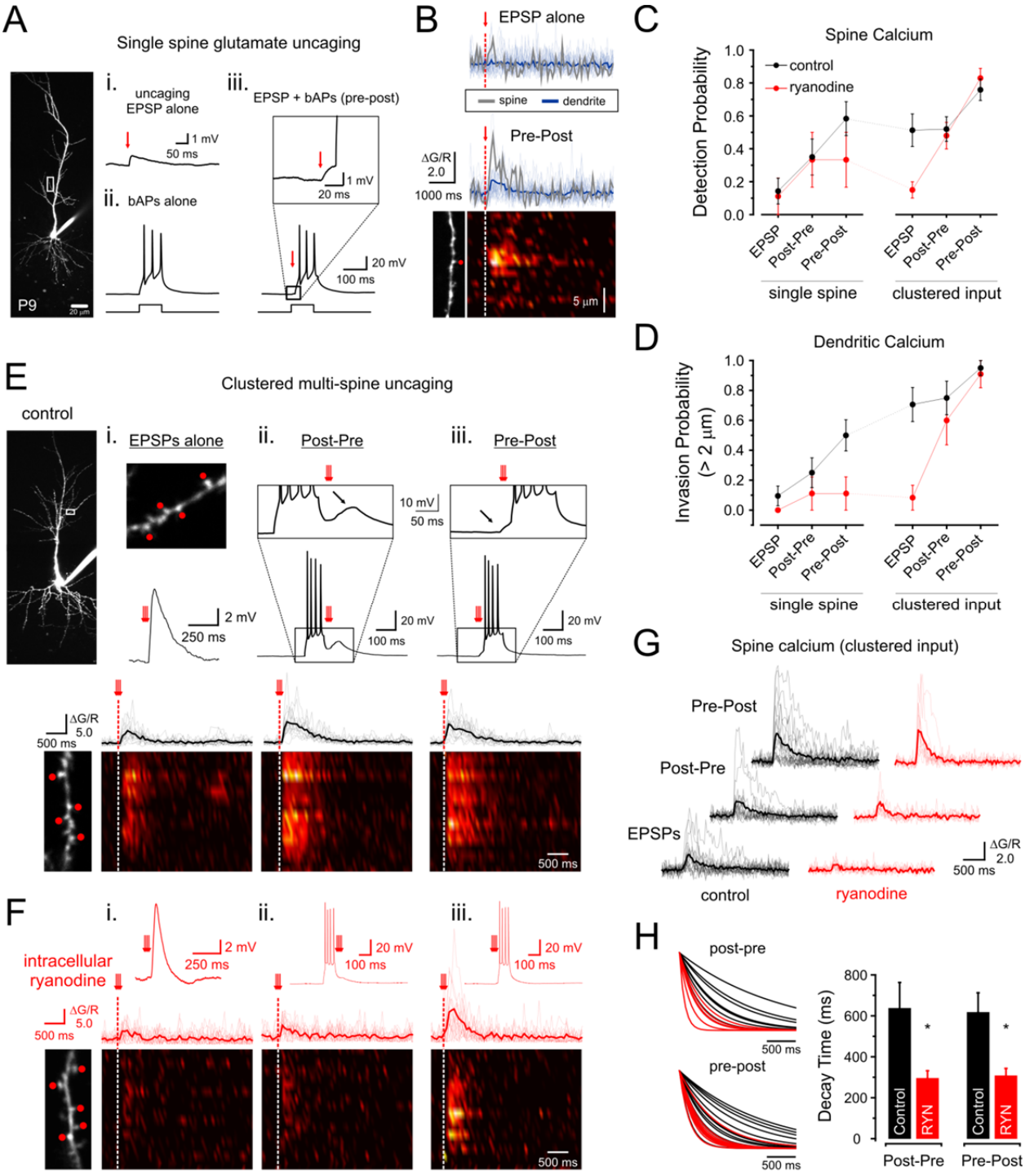

Figure 6. NMDAR-dependent CICR encodes spatiotemporal features of synaptic inputs (A) Example current-clamp experiment at a P9 CA1 pyramidal cell showing the voltage responses to: (i) EPSP evoked by 2P glutamate uncaging at a single dendritic spine (shown in panel B); (ii) Backpropagating action-potentials (bAPs) evoked by somatic current injection (100 pA, 100 ms; 3-5 spikes; first spike amplitude: 108.35 ± 3.16 mV); (iii) Pre-post spike pairing: glutamate

uncaging was delivered ~ 20 ms before bAPs. (B) Calcium signals from the dendrite (blue; mean in bold) and stimulated spine (gray) recorded during stimuli shown in panel A (i and iii): glutamate uncaging alone (*upper,* EPSP alone), and pre-post stimulation (*lower,* Pre-Post) aligned to corresponding dendritic calcium map. (C) Spine calcium detection probability and (D) dendritic calcium invasion probability in response to spike-paired uncaging at single spines and spine clusters (clustered input) for control (black) and ryanodine-treated (red) neurons (see Supplemental Experimental Procedures). (E) Clustered glutamate uncaging onto four neighboring spines at P9. Current-clamp recordings are shown for i) EPSP, ii) Post-Pre, and iii) Pre-Post stimulation and simultaneously recorded calcium traces from dendritic ROIs (mean, bold) aligned to corresponding dendritic calcium maps for each stimulus configuration (*lower panel*). (F) A P10 CA1 pyramidal cell dialyzed with 100 μM ryanodine and subjected to clustered spike-paired uncaging stimuli, as in panel E. (G) Average spine calcium signals shown for all clustered uncaging experiments in control (black) and ryanodine (red) (population mean shown in bold). (H) *Left,* Mono-exponential fits ($R^2 > 0.5$) for averaged spine calcium signals during spike-paired clustered glutamate uncaging in control (black) and ryanodine (red). *Right,* Bar graph of spine calcium decay kinetics (post-pre, $p = 0.0101$; pre-post, $p = 0.0339$) (See also Supplementary **Figure 6B** for dendritic calcium decay analysis). Data shown as mean ± SEM. See also **Figure S6**.

Although the propagating dendritic calcium signals triggered by spike-paired glutamate uncaging at single spines closely resembled those observed in voltage-clamp (**Figures 1 and 2**), they were triggered with much lower reliability, leaving open the possibility that the full recruitment of NMDAR-mediated CICR may occur in other conditions. A growing body of theoretical and experimental work indicates that NMDAR activation is particularly sensitive to multiple, spatially-clustered, synaptic inputs (Mel, 1993; Schiller et al., 2000; Polsky et al., 2004; Losonczy and Magee, 2006; Branco et al., 2010). To evaluate whether this 'cluster sensitivity' (Mel, 1993) relates to NMDAR-dependent CICR, we delivered spatially-clustered glutamate uncaging to neighboring spines (P8-11, mean 4.12 ± 0.38 spines; range, 3-10 spines; 5 ms inter-stimulus interval) (**Figure 6E**). Remarkably, clustered glutamate uncaging alone (no bAPs) was significantly more effective than single-spine uncaging at triggering spine calcium signals (**Figure 6C,** $p = 0.0012$) and dendritic calcium invasion (**Figure 6D,** $p = 0.0001$). Moreover, clustered uncaging-evoked calcium signals were facilitated most effectively by pre-post spike-

pairing sequences (**Figures 6C**, post-pre, p = 0.9121; pre-post, p = 0.0130; and **Figure 6D,** post-pre, p = 0.7974; pre-post, p = 0.0504) such that local dendritic calcium elevations served as nearly perfect reporters of coincident clustered synaptic input and postsynaptic spiking. Therefore, developing dendrites exhibit the ability to encode with high discriminability spatiotemporal features of synaptic inputs in the form of local NMDAR-dependent calcium signals.

We next applied intracellular ryanodine (100-200 μM) to examine the role of intracellular calcium release in the local calcium read-out of spike-paired excitatory input at single spines and spine clusters. Ryanodine reduced the probability of dendritic calcium signal invasion during pre-post uncaging at single-spines (**Figure 6D**, p = 0.0476) and virtually abolished calcium signals triggered by clustered glutamate uncaging input (**Figure 6D**, p = 0.0012). Consistent with the voltage-dependent activation of NMDARs, spine calcium signals recorded in ryanodine showed clear spike-dependent facilitation (**Figures 6C-D and S6A**). Closer inspection of the calcium signals triggered by spike-paired post-pre and pre-post clustered input (**Figure 6G**) revealed significantly faster decaying calcium signals in the presence of ryanodine compared to control (**Figures 6H and S6B**), confirming the powerful effects of CICR on intracellular calcium kinetics in these conditions (**Figure 4G**).

To examine more closely the role of CICR mechanisms in local dendritic calcium elevations driven by clustered synaptic inputs, we examined the extent of dendritic calcium invasion (μm) evoked by clustered glutamate uncaging compared to the baseline expectation that dendritic calcium invasion will correspond to the number of uncaging points in a 1:1 manner, assuming spatially-restricted NMDAR-dependent calcium influx (*i.e.,* 4 uncaging spots = 4 μm of calcium invasion; see Supplemental Experimental Methods). Under control conditions, we

detected on average a net gain of dendritic calcium in response to clustered glutamate uncaging input (**Figure S6C**). Interestingly, this analysis further revealed an apparent loss of calcium in response to clustered input in the presence of ryanodine (**Figure S6C**), which is consistent with the reduction of spine calcium detection by ryanodine in our voltage-clamp experiments (**Figure 3D**), further outlining a critical role for intracellular calcium release in synaptic calcium signaling at developing neurons. Uncaging-evoked EPSP amplitudes measured in the presence of ryanodine were not different from control (**Figure S6D**, $p > 0.2$). Similarly, there was no difference in action potential amplitude, number of spines stimulated, distance between uncaging points, or length of the spine cluster between ryanodine-treated and control neurons (**Figure S6E**). Taken together, the functional coupling between NMDARs and CICR machinery provides an efficient mechanism to transform spatially- and temporally-clustered synaptic inputs into local biochemical traces through salient, long-decaying calcium signals, during CA1 spine synapse development.

Clustered synapse maturation along developing dendrites

The properties of the NMDAR-mediated CICR process outlined above align well with a mechanism that would spatially bias the development and stabilization of ensembles of co-active neighboring synapses in the dendritic arbor, and thus govern the initial patterning of synaptic connectivity in developing circuits. Since synapse maturation involves the recruitment and stabilization of AMPARs through NMDAR- and calcium-dependent synaptic plasticity mechanisms (Durand et al., 1996; Zhu and Malinow, 2002; Kerchner and Nicoll, 2008), we hypothesized that a locally-acting associative signal such as NMDAR-dependent CICR operating *in vivo* should give rise to a non-random spatial distribution of weak (immature) and strong (mature) synapses along dendrites (*i.e.,* spatial clustering of synaptic weights). To directly

address this possibility, we used 2P glutamate uncaging and mapped AMPA/NMDA ratios (**Figure S7A**) (Beique et al., 2006) at cohorts of neighboring spines along segments of young dendrites (**Figures 7A-7C;** P7-11; mean dendritic segment length 16.96 ± 1.61 μm; inter-spine distance: 3.02 ± 0.12 μm; see Supplemental Experimental Procedures). In order to normalize the uncaging laser power across neighbor spines, we targeted segments of dendrite that were parallel with the imaging plane. The uncaging laser was first tuned to generate a resolvable outward EPSC at a holding potential of V_m = +40 mV (mean EPSC amplitude, 17.1 ± 0.65 pA; median, 13.8 pA, n = 472 spines, P7-22); we then probed AMPAR content at the spine using the same uncaging laser power at V_m = -70 mV (mean EPSC amplitude, 11.8 ± 0.72 pA; median, 8.1 pA). We detected a robust developmental increase in AMPA/NMDA ratio at spines (**Figure S7B**), indicative of strengthening of glutamatergic synaptic transmission with age (Durand et al., 1996; Zhu and Malinow, 2002; Beique et al., 2006). We also detected silent (weak) synapses by glutamate uncaging (Beique et al., 2006; Busetto et al., 2008; Ashby and Isaac, 2011) at ~20% of spines probed before P12 (**Figures 7D-E**) and, in agreement with recent studies, silent synapses were found at morphologically diverse dendritic protrusions (**Figures 7A-B**) (Busetto et al., 2008; Ashby and Isaac, 2011). As expected, AMPA/NMDA ratios were well-correlated with the amplitude of EPSCs recorded at V_m = -70 mV (**Figure S7C**) but not with EPSCs recorded at V_m = +40 mV (**Figure S7D**). We found no bias in the spatial distribution of silent spines along the proximal-distal axis of the apical dendritic arbor, indicating no obvious spatial regulation of synapse development at the cell-wide level (inside-out or outside-in), at least within the proximal apical arbor, < 180 μm from soma (**Figures 7D and 7E**).

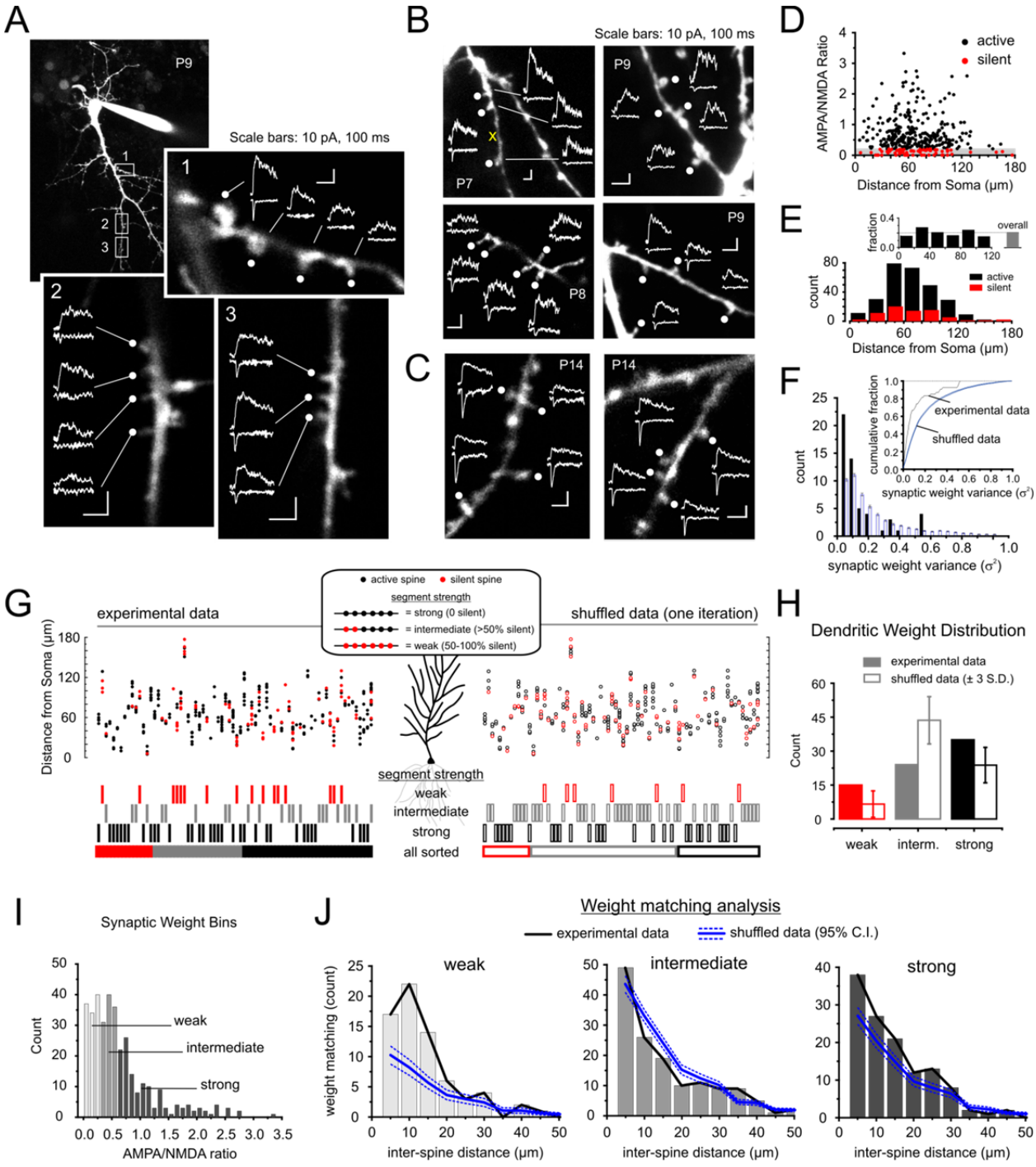

Figure 7. Clustered synaptic weights during synapse development. (A) Example P9 neuron with three dendritic segments probed by glutamate uncaging; inward AMPAR-mediated currents (V_m = -70 mV) and outward NMDA-mediated currents (V_m = +40 mV) evoked by 2P glutamate uncaging are shown next to each stimulated spine (see Supplemental Experimental Procedures). (B, C) Additional examples from different neurons at indicated postnatal ages; glutamate uncaging at an aspiny region of dendrite at P7 (yellow *x* in panel B, *upper left*). (C) At P14, AMPAR-mediated EPSCs were readily evoked by glutamate uncaging. Scale bars (panels A-C):

100 ms, 10 pA. (D) Distribution of AMPA/NMDA ratios from 336 dendritic spines used for clustering analysis. Silent spines are shown in red and were defined by AMPA/NMDA ratios < 0.25. (E) Histogram count of AMPA/NMDA ratios along the proximal-distal axis (20 μm bins). *Inset*, fraction of silent synapses plotted against distance from soma. (F) Histogram count and cumulative distribution (*inset*) showing variance of AMPA/NMDA ratios at experimentally-probed dendritic segments (black) compared to shuffled data (blue) (mean ± SEM from 100 shuffle iterations; p = 0.004, Wilcoxon test corrected for multiple comparisons). (G) *Upper panel:* two-dimensional rendering of the experimental dataset (*left*) and one iteration of shuffled data (*right*); Active (black) and silent (red) spines are positioned along individual dendritic segments in the vertical axis (distance from soma). *Lower panel:* Individual segments were assigned to one of three dendritic segment strengths according to silent synapse fraction: strong, intermediate, and weak (see Supplemental Experimental Methods). Raster plots are aligned to corresponding dendritic segments, and sorted (*bottom*) to show relative dendritic segment strength distributions. (H) Summary counts of segment strengths for experimental data (solid bars) and 100 iterations of shuffling (open bars; mean ± 3 S.D.). (I) The distribution of synaptic weights was divided into three synaptic weight classes: weak, intermediate, strong. (J) Tally of synaptic weight-matching as a function of inter-spine distance from experimental (black) and shuffled data (blue; mean ± 95% C.I., 100 iterations). See also **Figure S7**.

We next analyzed the synaptic weights of neighboring spines at the level of individual dendritic segments for evidence of clustered synapse development. We compared our experimental data to simulations of spatially-random synapse development using Monte Carlo shuffling methods. In brief, experimentally-measured AMPA/NMDA ratios were randomly sorted onto an array of model dendrites matched to experimental data for segment length and spine number (see Supplemental Experimental Procedures). In principle, AMPA/NMDA ratios of closely neighboring synapses should exhibit lower variability if synapse development is spatially-regulated rather than spatially-random along dendrites. We therefore examined the variance of AMPA/NMDA ratios between spines along each dendritic segment and found that AMPA/NMDA ratios were significantly less variable between neighboring spines than expected by chance (**Figure 7F**, 100 shuffles; p = 0.004, Wilcoxon test corrected for multiple comparisons; see Supplemental Experimental Procedures). We noted that silent spines were often neighbored by other silent spines (**Figures 7A and 7B**). As a means to further quantify the

spatial distribution of synaptic weights, we calculated the fraction of silent spines for each dendritic segment (*i.e.,* the number of silent spines/total spines probed) to assign a relative strength to each segment: and *i) weak* segments, which exhibited 50-100% silent spines *ii) intermediate* segments, where less than 50% of spines were silent; and *iii) strong* segments, at which we detected zero silent spines. In line with the largely uniform cell-wide distribution of silent synapses (**Figures 7D and 7E**), the fraction of silent synapses on a given dendrite was not correlated with distance from the soma (**Figure S7E**). The shuffled data exhibited a larger fraction of *intermediate* segments than *weak* or *strong* segments (**Figure 7G**), which was expected given the overall 20% fraction of silent synapses in our experimental dataset (**Figure 7E**). The experimental data showed a significantly different distribution of segment strengths compared to shuffled data, showing more *strong* and *weak* segments, and fewer *intermediate* segments (**Figure 7G**). These results suggest that functional synapse maturation is under the influence of local cooperative plasticity mechanisms along developing dendrites.

Last, we estimated the spatial bounds of this local cooperative mechanism by examining how closely the weights of individual spines relate to the weights of their neighbors. To do this, we divided the distribution of synaptic weights of individual synapses (*i.e.,* AMPA/NMDA ratios) into three weight classes of even size (*i.e.,* approximate thirds: weak, intermediate, strong; **Figure 7I**), and tallied the instances when neighboring spines shared the same weight class (‘weight-matching’). Both weak spines and strong spines exhibited significant clustering (*i.e.,* increased weight matching beyond that observed from shuffled data) (**Figures 7J**), but only within a range of ~15 μm which, incidentally, is highly reminiscent of the spatial profile of the CICR-dependent dendritic propagating calcium signals induced by NMDAR activation (**Figure 2C**). Taken together, these results show spatial clustering of synaptic weights in the dendritic

arbor of developing CA1 neurons, and implicate NMDAR-dependent CICR in regulating the stabilization of co-active assemblies of neighboring synapses along dendrites.

Discussion

Using whole-cell electrophysiology combined with 2P calcium imaging and glutamate uncaging in acute hippocampal slices, we found that synaptic NMDAR activation triggered ryanodine-sensitive CICR from intracellular stores during a narrow developmental window when spine synapses first take form and acquire function. This NMDAR-mediated CICR was detected at a large fraction of dendritic protrusions during early postnatal development and generated long-lasting calcium elevations that spread locally along the dendrite and invaded neighboring spines. By the third postnatal week, spine calcium signals did not involve intracellular calcium release, displayed faster kinetics, and were spatially restricted to the spine head. In a series of current-clamp experiments, we further found that NMDAR-mediated CICR was modulated by spike-timing and tuned to report clustered synaptic input. These activation parameters of NMDAR-dependent CICR outline a plausible mechanism for dendrites to detect computationally relevant features of synaptic input (*i.e.,* spatiotemporal correlations) and coordinate the activity-dependent stabilization of coactive neighbor synapses along dendrites. We found evidence supporting the presence of such a mechanism in the non-random clustering of synaptic weights along developing dendrites. Our results reveal novel elements of NMDAR-dependent calcium signaling that are particularly well-suited to regulate the spatial organization of synaptic contacts along the dendrites of CA1 pyramidal neurons during a critical period in the functional establishment and refinement of neural circuits.

Given the integral role of calcium signaling in synapse regulation, considerable efforts have been directed to comprehensively describe synaptic calcium dynamics at mature dendritic spines. Whereas CICR mechanisms have been suggested to be a major contributor to spine calcium signals (Emptage et al., 1999), this has not been universally reported, raising a controversy that has largely been attributed to differences experimental methods (acute vs. organotypic slice; whole-cell vs. sharp electrodes). The transitory developmental coupling of NMDARs to CICR mechanisms described here provides a tangible biological explanation to satisfactorily reconcile this discrepancy. Indeed, aligning well with the present study, CICR was reported to play a dominant role at dendritic spines in experiments using slice cultures from neonatal brain tissue (Emptage et al., 1999), while similar calcium imaging studies in acute slices from animals older than about two weeks of age reported little or no contribution of CICR to spine calcium signals (Mainen et al., 1999; Kovalchuk et al., 2000; Oertner et al., 2002; Sabatini et al., 2002). Our results further demonstrate that CICR is the major determinant of intracellular calcium kinetics, on average prolonging calcium signals by about two-fold. Thus, the coupling between NMDAR activation and CICR-machinery conspicuously extends the integration time window for summating calcium signals during a key period in synapse development.

One of the major functional attributes commonly assigned to spines is their ability to spatially compartmentalize calcium influx by NMDAR activation, which is thought to lead to a degree of synapse-specific biochemical signaling and regulation. Whereas our data in mature neurons is fully consistent with this model of compartmentalized synapse function, we observed a fundamental departure from this synaptic calcium behavior during early postnatal development. During early development, the calcium signals evoked by NMDAR activation at single spines readily exited the spine, traveled short distances along the parent dendrite and reliably invaded

closely neighboring spines, thus providing a mechanism for associative biochemical signaling along dendrites. Interestingly, despite the positive-feedback nature of CICR, calcium signals rarely propagated the entire visualized length of dendrite but rather exhibited clear spatial limits. Although the factors that control the dynamics of intracellular calcium release in dendrites are poorly understood, local variability in dendritic endoplasmic reticulum complexity (Cui-Wang et al., 2012), calcium buffering/extrusion mechanisms (Pozzo-Miller et al., 1997; Majewska et al., 2000b; Scheuss et al., 2006) and ryanodine receptor density (Segal et al., 2010) could in principle shape the spatial profile of these NMDAR-induced propagating calcium signals. With age, the functional coupling between NMDAR activation and CICR was down-regulated, and calcium transients became increasingly restricted to the dendritic spine head. Although mushroom spines were less likely to exhibit NMDAR-dependent CICR compared to stubby spines (**Figure 5**), spine morphology was generally a poor predictor of NMDAR-CICR coupling overall. The mechanisms accounting for the developmental profile of the NMDA-dependent CICR does not appear to reflect a simple down-regulation of ryanodine receptors with age (Mori et al., 2000), nor can it be easily explained by an obvious physical correlate (*eg.,* ER membrane has been reported to extend in *ca.* 50% of mature spines and up to *ca.* 80% of mature mushroom spines) (Spacek and Harris, 1997). Thus, an abrupt switch in synaptic calcium behavior appears to be a key step in synapse development, and involves the functional uncoupling of NMDARs from CICR mechanisms.

Input-output transformations at mature pyramidal neurons are known to be influenced by the spatial organization of synaptic inputs in the dendritic arbor (London and Hausser, 2005; Larkum and Nevian, 2008). The activation parameters governing NMDAR-mediated CICR in developing dendrites outline an effective mechanism to biochemically encode spatiotemporal

features of incoming synaptic inputs. By attributing postsynaptic salience to spatially- and temporally-clustered synaptic activity in developing neural circuits, NMDAR-mediated CICR is well positioned to regulate the cooperative development of co-active ensembles of neighboring synapses, and thus instruct micro-scale patterning of functional synaptic connectivity along developing dendrites. The clustering of synaptic weights we report (**Figure 7**) together with other recently reported manifestations of clustered synaptic plasticity and stabilization (McBride et al., 2008; Makino and Malinow, 2011; Takahashi et al., 2012; Druckmann et al., 2014) attest to the instructed assembly of microcircuit templates that are apt to exploit the non-linear regime of dendritic computation (London and Hausser, 2005; Larkum and Nevian, 2008; DeBello et al., 2014). Future studies will be required to fully understand the relationship between NMDAR-dependent CICR and other local plasticity-related mechanisms operating with different time scales (Harvey and Svoboda, 2007; Harvey et al., 2008; Patterson et al., 2010; Govindarajan et al., 2011; Murakoshi et al., 2011), and how these processes ultimately regulate the fine-scale functional organization of synaptic connectivity in the brain. Disruptions to these mechanisms could potentially underlie subtle yet functionally important changes in neuronal information processing, and may thus contribute to neurodevelopmental disorders such as autism and schizophrenia.

Experimental Procedures

Slice Preparation and whole-cell electrophysiology

Sprague-Dawley rats (Charles River Laboratories; postnatal days 6 to 26) were anaesthetized by isoflurane (Baxter Corporation, Canada) inhalation and decapitated, in accordance with methods approved by the University of Ottawa Animal Care Committee. Coronal hippocampal slices

(300-350 μm) were prepared on a Vibratome sectioning system (Leica Microsystems) in ice-cold cutting solution and transferred to a pre-warmed (37°C) recovery chamber containing a standard Ringer solution. Slices were recovered for >1 hour at room temperature prior to electrophysiology experiments. Composition of cutting and ringer solutions can be found in Supplemental Experimental Procedures. Hippocampal slices were placed in a recording chamber and cells in stratum pyramidale of the CA1 subfield were visualized under differential-interference contrast (DIC) using an Olympus MPE-1000 system (BX61WI upright microscope Olympus, Melville, NY)) using a 40x/0.8NA objective (**Figure 1**) or 60x/1.0NA objective glutamate uncaging (**Figures 2-7**). Whole-cell recordings were performed using an Axon Multiclamp 700B amplifier, and signals were filtered at 2 kHz and digitized with an Axon Digidata 1440A at 10 kHz. Borosilicate glass recording electrodes with resistances ranging from 3-5 MΩ were pulled using a Narashige PC-10 vertical puller (Narishige, Japan). Access resistance was monitored with a 5 mV hyperpolarizing step at the beginning of each sweep and experiments were discarded if this resistance changed by more than 20%. For voltage-clamp recordings, electrodes were filled with a cesium-based intracellular solution, and for current clamp experiments, a potassium gluconate based solution was used. See Supplemental Experimental Procedures for detailed recipes.

Two-Photon Imaging and Uncaging

Glutamate uncaging experiments were performed with 2.5 mM MNI-glutamate-trifluoroacetate (Femtonics, Hungary) added to the extracellular solution and 0.03 mM Alexa Fluor 594 hydrazide (Na-salt; Life Technologies) included in the recording electrode; for calcium imaging experiments, 0.2 mM Fluo-4FF (pentapotassium salt; Life Technologies) was also added to the electrode solution. Neurons were loaded for at least 15 min before imaging. Simultaneous two-

photon imaging and glutamate uncaging was performed using two ultrafast Ti:Sapphire pulsed lasers with pre-chirp compensation (MaiTai DeepSee, Spectra Physics, USA) coupled to an Olympus MPE-1000 twin-galvanometer scanning system. Image acquisition and stimulation patterns were performed through Olympus FV-1000 software (Olympus, Melville, NY) externally-triggered by a Master-8 pulse generator (A.M.P.I, Israel). Imaging and uncaging laser power was controlled using two independent acousto-optic modulators. One Ti:Sapphire laser was tuned to 810 nm to visualize neuronal morphology (Alexa Fluor 594) and intracellular calcium (Fluo-4FF), and the second Ti:Sapphire laser was tuned to 720 nm for glutamate uncaging (1 ms pulse). Calcium fluorescence signals were given by the change in Fluo-4FF fluorescence normalized to the Alexa Fluor 594 signal ($\Delta G/R$). See Supplemental Experimental Procedures for more information.

Data Analysis

All data were plotted in Origin (OriginLab, USA) and figures were assembled in Corel Draw (Corel, Canada). Electrophysiological recordings were analyzed in Clampfit (Molecular Devices, USA). Data are reported as mean ± SEM unless otherwise indicated. Statistical significance was assessed at $p < 0.05$ using the nonparametric Wilcoxon (Mann-Whitney) test, or the unpaired Student's t-test for normally-distributed data. Calcium fluorescence signals were analyzed off-line using custom software in Image J (NIH, Maryland) and MATLAB (MathWorks, USA). Monte Carlo shuffling experiments were performed in MATLAB. See Supplemental Experimental Procedures for more information.

Supplemental Data

Supplemental Data include Supplemental Experimental Procedures and seven figures.

Acknowledgements: We thank Hilary Phenix for help with the initial development of analytical tools in MATLAB and Dr. Leonard Maler for expert advice during the completion of this work and for comments on the manuscript. This work is supported by the Natural Sciences and Engineering Research Council of Canada (NSERC), Canadian Institutes of Health Research (CIHR), and The Heart and Stroke Foundation Partnership for Stroke Recovery to JCB.

The authors declare no competing financial interests.

Author Contributions: KL, CS and JCB designed the experiments. KL performed the experiments. KL, CS, JPT and JCB analyzed and interpreted the data. KL, CS and JCB wrote the manuscript.

General Discussion

In the quest to understand how the brain carries out its remarkable higher-order functions such as learning, memory, perception and cognition, and to comprehend how these processes go awry in diseased states, it is important to elucidate the biological mechanisms that fundamentally govern the flow of information in the brain. How is synapse function regulated, and how do neurons compute and process their synaptic inputs? It was my goal to present Manuscripts I to V as a tour through my exploration of these fundamental questions during my doctoral studies. In this general discussion, I aim to distill the key insights and contributions to the field from this work and highlight major questions arising that, I believe, will be of interest to pursue in future research.

The chemical synapse is the fundamental unit for rapid information transmission in the brain. In the past century, neuroscientists have made enormous strides in determining with great detail the many intricate and intertwined mechanisms that regulate the function of synapses. In Manuscript I (Lee et al., 2012), I reviewed experimental and theoretical evidence outlining how the shape of the dendritic spine affords flexibility and specificity to synapse function. In the past decade, the development and application of 2P imaging and glutamate uncaging has significantly advanced the discourse in the field by enabling detailed structural and functional investigations at the level of individual dendritic spines. Current models now suggest that structural plasticity of dendritic spines enables control of both biochemical and electrical properties of the synapse. An emerging consensus is that changes in dendritic spine morphology can alter the biochemical and electrical behavior of spines. Reflecting on the various abstracts and poster presentations I have seen recently at the annual meetings of the Society for Neuroscience (SfN: San Diego, 2010; San Diego, 2013; Washington D.C., 2014), Federation for European Neuroscience

Societies (FENS: Barcelona, 2012; Milan, 2014) and the Gordon Research Conference on Synaptic Transmission (GRC: New Hampshire, 2014), it is reasonable to predict that the literature will soon include many new details on the mechanisms controlling of dendritic spine structure and function. Current and future research will continue to apply a combination of molecular interventions, single synapse activation, fluorescently-labeled synaptic components, novel fluorescent voltage and calcium sensors, and super-resolution imaging techniques and to enrich our understanding of synapse biology.

Synapses exhibit plasticity on several time scales. Short term plasticity mechanisms, which were not covered in this thesis, can facilitate or depress presynaptic function on the order of milliseconds-seconds in response to transient bursts of activity (Zucker and Regehr, 2002). Hebbian forms of synaptic plasticity (LTP and LTD) can last hours or perhaps weeks, and manifest in response to relatively brief (minutes) changes in activity (Malenka and Bear, 2004). These Hebbian plasticity mechanisms offer a powerful means to persistently 'train' information processing routes in neural circuits. Moreover, an emerging literature is beginning to document homeostatic synaptic responses to more prolonged changes in neural activity (hours-days). These homeostatic synaptic plasticity mechanisms are thought to counterbalance the unstable positive-feedback nature of Hebbian plasticity and thus maintain neurons within a biologically defined range of excitability that is perhaps optimized for computation. On homeostatic synaptic plasticity, I contributed to a paper detailing changes in the expression of glutamate receptor subtypes, AMPA and NMDARs, during homeostatic synaptic plasticity (Manuscript II: (Soares et al., 2013)). We showed that both AMPA and NMDARs exhibit a switch in subunit composition during a cell-wide homeostatic response to network inactivity, and further found

striking differences in the way these receptors are distributed at synaptic and extrasynaptic subcellular compartments.

Notably, we found that prolonged inactivity induced a switch in AMPARs subunit composition from the archetypal calcium-impermeable subtypes (containing the GluA2 subunit) in CA1 pyramidal neurons to an atypical calcium-permeable subtype lacking the GluA2 subunit. This change in AMPAR identity was detected cell-wide, that is, not just at dendritic spines, but also at aspiny regions of dendritic shafts and at the soma. Therefore, neurons appear to gain access to a novel source of calcium influx during a homeostatic response to inactivity, and in this case, a source that is not voltage dependent. This is interesting in light of studies suggesting that alterations in calcium-dependent processes maintained by a calcium signals given by spike-dependent VGCC activation may control homeostatic plasticity mechanisms (Ibata et al., 2008; Goold and Nicoll, 2010). Under conditions where normal calcium influx is lost due to prolonged suppression of spiking activity, the switch towards calcium-permeable AMPARs may reflect a mechanism toward calcium homeostasis. One caveat to this hypothesis is that somatic changes in calcium influx cannot account for more local homeostatic changes (*i.e.,* synapse-specific homeostatic plasticity) (Hou et al., 2008; Lee et al., 2010; Beique et al., 2011; Hou et al., 2011) since the experimental manipulations to reveal these phenomena do not change the overall spiking behavior of the neuron. Current students in the lab are testing the hypothesis that the homeostatic response may not be due to changes in cytosolic calcium *per se*, but instead due to depletion of intracellular calcium stores and activation of the so-called store-operated response. This hypothesis is based on the idea that intracellular calcium stores in the endoplasmic reticulum (ER) are prone to depletion in the absence of neuronal activity, triggering a store-operated response where ER calcium pumps couple to plasma membrane calcium channels to

refill stores (Harraz and Altier, 2014). One intriguing possibility is that the cell-wide delivery of calcium-permeable AMPARs may be a novel manifestation of this response over an extended time scale, and ongoing work in the laboratory is designed to explore this possibility in detail. Taken further, given the presence of ER calcium stores throughout the dendritic arbor, a store-operated mechanism of homeostatic plasticity could act locally and perhaps explain homeostatic at individual single synapses, which also involves a change in AMPAR subunit composition (Beique et al., 2011).

Our measurements of synaptic AMPA/NMDA ratios indicated that synaptic NMDAR were upregulated with AMPARs in response to inactivity, and whole-cell NMDAR currents and Western blots of surface biotinylated NMDAR subunits indicated a cell-wide increase in NMDAR content in the plasma membrane. Interestingly, however, we found that the switch toward fast-decaying GluN2A-containing NMDARs occurred preferentially at synapses compared to dendritic shaft regions, unlike the global switch in AMPAR subunit composition. Presently, the mechanisms responsible for this NMDAR trafficking are not known, although it is highly reminiscent of normal developmental switch in NMDAR subunit composition at synapses (Cull-Candy and Leszkiewicz, 2004), and the insertion of GluN2A-containing NMDARs during LTP (Bellone and Nicoll, 2007). Our results may thus reflect an overlap in the mechanisms underlying synaptic potentiation during homeostatic and Hebbian plasticity. Different NMDAR subtypes are thought to couple to distinct intracellular signaling cascades (Lau and Zukin, 2007; Paoletti et al., 2013), and the distinct decay kinetics of GluN2B- and GluN2A containing (slow versus fast, respectively) shape the temporal profiles of synaptic calcium signals that regulate diverse calcium-dependent processes including synaptic plasticity. As such, the dynamic subunit-specific regulation of NMDARs at synapses may have consequences for the metaplasticity of

synapses. Certainly, future work is necessary to understand the mechanisms and functional consequences of subtype-selective trafficking of AMPA and NMDARs during both Hebbian and homeostatic plasticity.

To what extent do global and local homeostatic plasticity mechanisms overlap? As aforementioned, global inactivity induces a change toward calcium-permeable GluA2-lacking AMPARs, and this is consistent with single synapse manifestations of homeostatic scaling (Beique et al., 2011). However, this does not accurately depict the equivocality of results surrounding the regulation of glutamate receptors during global and local forms of homeostatic plasticity. For example, there is no consensus regarding the direction or magnitude of AMPAR regulation during homeostatic plasticity at single synapses, since increases (Beique et al., 2011), decreases (Harms et al., 2005; Ehlers et al., 2007) and no change (Lee et al., 2010) have been reported with prolonged synaptic inactivity. Moreover, it appears that the subunit switch in NMDARs towards GluN2A-containing receptors found in global scaling (Manuscript II: (Soares et al., 2013)) contrasts the homeostatic response to inactivity at individual synapses, which was reported to involve a switch toward GluN2B-containing receptors (Lee et al., 2010). Not surprisingly, differences in experimental design may be critical for explaining these conflicting data. For example, while overexpression of tetanus toxin light chain (Harms et al., 2005; Ehlers et al., 2007) abolishes spontaneous neurotransmitter release and likely also impairs glutamate receptor trafficking, TTX treatment (Turrigiano et al., 1998; Soares et al., 2013) and overexpression of the potassium channel Kir2.1 (Burrone et al., 2002; Beique et al., 2011) do not disrupt spontaneous vesicle fusion. A discussed in Manuscript III (Lee et al., 2014), it is becoming increasingly clear that spontaneous synaptic transmission may play a critical role in synapse maintenance and, as such, the conflicting results obtained from different experimental

modes of synaptic silencing may indicate deeper mechanistic insights into synapse regulation. Future work will need to compare and contrast global and local forms of synaptic manipulations, and apply novel molecular strategies to elucidate the players involved in detecting and responding to sustained perturbations in activity.

Local forms of homeostatic synaptic plasticity likely serve important roles in neural circuits. For example, synapse-specific scaling in CA3 pyramidal cells suppresses epileptic activity in hippocampal slices (Kim and Tsien, 2008), and a similar phenomenon also enables modality-specific synaptic tuning in sensory processing neurons *in vivo* (Deeg and Aizenman, 2011). These forms of homeostatic scaling therefore seem to act on populations of synapses depending on their functional identity, such as feed-forward versus recurrent feedback synapses (Kim and Tsien, 2008), or visual versus mechano-sensory pathway synapses (Deeg and Aizenman, 2011). This synapse-selective homeostatic plasticity therefore indicates that homeostatic mechanisms can operate more locally than cell-wide scaling mechanisms suggests, perhaps reflecting regulation at individual synapses (Hou et al., 2008; Beique et al., 2011). However, a concern was raised that homeostatic tuning of individual synapses would act to cancel any changes in synaptic strength mediated by Hebbian plasticity mechanisms, and thus 'erase' any information encoded by these changes (Turrigiano, 2012). We made an attempt to address this concern in Manuscript III (Lee et al., 2014) by revisiting the 'instability problem' that homeostatic plasticity was originally proposed to solve, and reframing the problem in the context of dendritic computation and information processing. Given emerging insights into the compartmentalized nonlinear function of dendrites, we reasserted the hypothesis that an instability problem may exist at the level of dendrites whereby, analogous to the instability problem at the neuron level, individual dendrites may tend toward hyper-excitability (or

functional silence) by unconstrained Hebbian plasticity (Goldberg et al., 2002). Thus, within the context of dendritic computation, local forms of homeostatic plasticity may have significant utility – by serving to normalize the strength of individual synapses or subsets of synapses that participate in driving nonlinear dendritic spikes.

One form of dendritic spike that appears to be central to synaptic integration in the thin dendrites of pyramidal neurons is the NMDA spike, which likely serves complementary roles to dendritic spikes carried by VGSCs and/or VGCCs. Here, I will step through a simple thought experiment to illustrate what I believe are the most important functional distinctions between NMDA spikes and dendritic spikes to contextualize the role of these two major dendritic nonlinearities in neuronal information processing. First, imagine the synchronous activity of 10 synapses that are randomly distributed in the dendritic arbor of a neuron, with the amplitude of each synaptic potential ~1 mV. If the dendritic membrane was purely passive, the net depolarization at the soma is expected to be less than 10 mV, and may not be sufficient to drive an action potential (Rall, 1962). In a scenario where dendrites are endowed with VGSCs and VGCCs, the membrane depolarization from the same 10 synapses randomly distributed in the arbor could potentially evoke a dendritic spike, which would amplify the synaptic depolarization and enhance the probability of driving a postsynaptic action potential (Golding and Spruston, 1998). However, it is possible (perhaps likely) that these 10 synapses fail to trigger a dendritic spike, resulting in a subthreshold somatic depolarization as in the first scenario with passive dendrites. Now, suppose the 10 synapses were spatially clustered onto an individual dendritic branch (rather than randomly distributed across many dendrites). This spatially clustered arrangement of synaptic activation would depolarize the neuron more effectively for two reasons: First, the synaptic depolarization is concentrated at the dendritic branch and can thus

drive the local regenerative activation of NMDARs, resulting in an NMDA spike (Schiller et al., 2000; Polsky et al., 2004; Losonczy and Magee, 2006). Although NMDA spikes can be sustained by activation of synaptic NMDARs (Rhodes, 2006), these events may also include the voltage-dependent gating of extrasynaptic NMDARs bound by ambient glutamate molecules present in the extracellular milieu (Wu et al., 2012; Soares et al., 2013) or from spillover from activated synapses (Chalifoux and Carter, 2011). Second, the depolarization generated by spatially clustered synaptic input can directly trigger a local dendritic spike via activation of VGSCs/VGCCs (Losonczy and Magee, 2006; Branco et al., 2010). Thus, local electrogenesis by clustered synaptic activation is expected to increase the overall probability of action potential discharge (Larkum et al., 2009). From these three scenarios, it is clear that the fine-scale spatial organization of synaptic input along active dendrites can have strong influence over the transmission of information from one neuron to the next.

In Manuscript V, I described the results of a series of experiments that reveal novel features of NMDAR-dependent calcium signaling that are apt to impact the fine-scale functional organization of synaptic connectivity in emerging neural circuits. Specifically, I discovered that NMDARs are transiently coupled to ryanodine receptor-dependent intracellular calcium release mechanisms during the second postnatal week, when spine synapses undergo rapid structural and functional maturation. This discovery is important because it helps to resolve a long-standing controversy over the role of intracellular calcium release mechanisms in synaptic calcium signaling at dendritic spines. In 1999, Emptage et al. argued that a significant component of NMDAR-activated synaptic calcium signals at dendritic spines was due to intracellular calcium release (Emptage et al., 1999). Indeed, they found by 2P calcium imaging that fluorescence amplitudes of synaptically-evoked calcium signals at spines were significantly diminished by

pharmacologically suppressing intracellular calcium release with cyclopiazonic acid (CPA), a drug which acts to deplete intracellular calcium stores by blocking calcium uptake into the endoplasmic reticulum. The authors therefore concluded that the primary source of calcium at dendritic spines was not through synaptic NMDARs but from intracellular calcium stores. This conclusion, however, is not consistent with data presented by several other laboratories who found that CPA (or thapsigargin, a drug with similar mechanism of action) had little or no effect on the amplitude of synaptic calcium signal amplitudes at dendritic spines (Mainen et al., 1999; Kovalchuk et al., 2000; Oertner et al., 2002; Sabatini et al., 2002), suggesting intracellular calcium release does not contribute to synaptic calcium signals. To reconcile the conflicting results, some authors have pointed to differences in experimental design, suggesting that nuances in experimental approach may lead to these disparate observations (Svoboda and Mainen, 1999; Sabatini et al., 2001). Specifically, it was argued that intracellular dialysis by whole-cell recording electrodes could significantly disrupt CICR, and thus mask it, compared to sharp-electrode recordings. Moreover, it was further suggested that differences in slice preparation methods and/or culturing environment could also lead to different synaptic calcium signaling behaviors. In my opinion, these explanations are wholly unsatisfactory, simply because they tend to propel a culture of (perhaps unjust) skepticism and general distrust of data, thus offering no scientific insight into the physiological problem at hand. As such, it is deeply satisfying to present experimental results that offer a tangible biological explanation to reconcile the different calcium behaviors observed at dendritic spines – that the mechanisms underlying intracellular calcium dynamics are regulated during postnatal development.

If spatiotemporal coincidence of synaptic input is important for dendritic information processing in mature neurons, there must be mechanisms that ‘pave’ the pathways for optimal

synaptic transmission. As we proposed in Manuscript V, the transitory expression of NMDAR-mediated CICR during synapse development provides an ideal candidate mechanism to detect and stabilize functional ensembles of synapses in the developing dendritic arbor, and thus instruct synaptic connectivity patterns for nonlinear dendritic computation. This is fully consistent with recent observations indicating that the stabilization of spontaneously active synaptic cohorts requires NMDAR activity, since spontaneous clustered synaptic activity was abolished by blocking NMDARs during circuit development (Kleindienst et al., 2011; Takahashi et al., 2012). I contend that the features NMDAR-mediated CICR align well with a mechanism that would enable neurons to carry out this task. Not only does NMDAR-mediated CICR exhibit powerful control over the spatial and temporal profile of postsynaptic calcium elevations consistent with a local cooperative plasticity signal, but the activation parameters for NMDAR-mediated CICR are sensitively tuned to report clustered synapse activity. As such, NMDAR-mediated CICR would enable individual dendrites to detect salient synaptic input (*i.e.,* clustered synaptic activity) amidst spontaneous activity in the developing circuit and thus selectively stabilize the synaptic ensembles responsible for these events. In this way, the transitory developmental expression of NMDAR-CICR coupling could serve to establish elementary associations between ensembles of pre- and postsynaptic neurons during early neural circuit development.

The progressive increase in synaptic AMPAR transmission during early postnatal development provides a unique opportunity to map the relative developmental maturity of sets of synapses in individual neurons. We reasoned that if NMDAR-CICR coupling spatially influences synapse development in the dendritic arbor, synaptic weights should tend to cluster along individual dendritic stretches since neighboring synapses would develop as cohorts

independently of synapses on other dendritic branches. To this end, I spatially mapped AMPA/NMDA ratios as a proxy of synaptic weight of neighboring dendritic spines using 2P glutamate uncaging. I found that the spatial distribution of synaptic weights along dendrites significantly deviated from simulated data of random synapse development using Monte Carlo shuffling methods, therefore supporting the notion of clustered synapse development. Notably, the clustering of synaptic weights showed a distance-dependence that aligned well with the spatial spread of local dendritic calcium signals generated by NMDAR-dependent CICR. These data suggest that NMDAR-dependent CICR may indeed contribute to guiding the clustered development of synapses along dendrites, although future work is required to directly test this possibility. The hallmarks of clustered synapse development appear to persist in the rapidly accumulating evidence of nonlinear dendritic computations *in vivo* (Lavzin et al., 2012; Smith et al., 2013; Gambino et al., 2014; Grienberger et al., 2014; Palmer et al., 2014). At the present time, the field is beginning to close the gaps in our understanding of the link between mechanisms governing clustered plasticity rules and the formation of fine-scale connectivity motifs in neural circuits as they relate to information processing in the pyramidal cell dendrites.

It is prudent to consider additional factors that were not investigated in Manuscript V in order to appraise the available data in the broader context of neural circuit development *per se*. The experiments in Manuscript V were designed to selectively interrogate glutamatergic transmission using flash photolysis of caged glutamate in controlled electrophysiological recordings. Although these experiments revealed novel and important features of glutamatergic synapse function, they did not address the well-known role of GABAergic transmission as the primary excitatory (depolarizing) force during early development (Mueller et al., 1983; Mueller et al., 1984; Leinekugel et al., 1999). This is an important consideration because during the

earliest periods of synapse development, when synapses are predominantly weak or silent (lacking AMPARs), GABAergic activity likely plays a major role in alleviating the voltage-dependent magnesium block on NMDARs (Ben-Ari et al., 1997; Leinekugel et al., 1997; Mohajerani and Cherubini, 2006) by driving spontaneous giant depolarizing potentials (GDPs) (Ben-Ari et al., 1989; Bolea et al., 1999; Leinekugel et al., 2002; Sipila et al., 2005). Thus, an intriguing concert of glutamatergic and GABAergic synchrony appears to takes place during synapse development before these neurotransmitter systems adopt functionally opposing roles. Some outstanding questions that I find interesting are: What are the primary drivers of GABAergic activity (*i.e.,* are they truly 'spontaneous' events or instead a consequence of feed-forward activity)? How do dendrite-targeting interneurons differ from interneurons that target the peri-somatic region (Klausberger and Somogyi, 2008; Muller and Remy, 2014) in the generation of GDPs? Is the change in the sign of GABAergic transmission from excitatory to inhibitory, which is thought to be governed by developmental changes in chloride transporter expression (Kaila et al., 2014), a time-locked cell-wide phenomenon or rather controlled locally along dendrites in an activity-dependent manner? The prominent role of GABA transmission during development requires careful consideration in future studies to understand the dynamics of NMDAR-dependent glutamatergic synapse development.

Concluding Remarks

In the course of my experimental studies, I have aided in documenting details of glutamate receptor regulation during homeostatic plasticity and, notably, I have discovered novel features of NMDAR-mediated calcium dynamics at synapses and dendrites during early postnatal brain development. In stark contrast to the canonical model of synaptic calcium compartmentalization at dendritic spines, synaptically evoked calcium signals engaged intracellular calcium release mechanisms to generate long-lasting and spatially spreading local calcium elevations in developing synapses and dendrites. The rapidly growing literature detailing the various factors that govern the input-output functions of neurons provides an ideal context for framing the interpretation of these data. The theoretical advantages of nonlinear dendritic computations and recent observations of localized dendritic spikes occurring *in vivo* raise interesting questions regarding how neural circuits adopt the synaptic connectivity patterns that are required support these dendritic functions. My observations suggest that such fine-scale synaptic connectivity may emerge due to NMDAR-dependent calcium mechanisms that are transiently expressed in neurons during a critical period in neural circuit assembly. The principal role that non-linear dendritic computations are hypothesized to play in the broader realm of information processing in the brain imply that disruptions to the microscopic functional organization of synaptic connections could culminate into significant changes in the computational capacity of neural circuits. As such, my experimental results may have important implications for neurodevelopmental disorders such as autism spectrums disorders and schizophrenia – diseases that are not readily apparent in macroscopic brain structure but perhaps involve more subtle microcircuit disturbances that lead to compromised brain function.

References

Abbott LF, Nelson SB (2000) Synaptic plasticity: taming the beast. Nat Neurosci 3 Suppl:1178-1183.

Abraham WC, Williams JM (2008) LTP maintenance and its protein synthesis-dependence. Neurobiol Learn Mem 89:260-268.

Adesnik H, Nicoll RA (2007) Conservation of glutamate receptor 2-containing AMPA receptors during long-term potentiation. J Neurosci 27:4598-4602.

Adrian M, Kusters R, Wierenga CJ, Storm C, Hoogenraad CC, Kapitein LC (2014) Barriers in the brain: resolving dendritic spine morphology and compartmentalization. Frontiers in neuroanatomy 8:142.

Alford S, Frenguelli BG, Schofield JG, Collingridge GL (1993) Characterization of Ca2+ signals induced in hippocampal CA1 neurones by the synaptic activation of NMDA receptors. J Physiol 469:693-716.

Allen C, Stevens CF (1994) An evaluation of causes for unreliability of synaptic transmission. Proc Natl Acad Sci U S A 91:10380-10383.

Alvarez VA, Sabatini BL (2007) Anatomical and physiological plasticity of dendritic spines. Annu Rev Neurosci 30:79-97.

Andrasfalvy BK, Magee JC (2001) Distance-dependent increase in AMPA receptor number in the dendrites of adult hippocampal CA1 pyramidal neurons. J Neurosci 21:9151-9159.

Anggono V, Clem RL, Huganir RL (2011) PICK1 Loss of Function Occludes Homeostatic Synaptic Scaling. J Neurosci 31:2188-2196.

Aoto J, Nam CI, Poon MM, Ting P, Chen L (2008) Synaptic signaling by all-trans retinoic acid in homeostatic synaptic plasticity. Neuron 60:308-320.

Araya R (2014) Input transformation by dendritic spines of pyramidal neurons. Frontiers in neuroanatomy 8:141.

Araya R, Eisenthal KB, Yuste R (2006a) Dendritic spines linearize the summation of excitatory potentials. Proc Natl Acad Sci U S A 103:18799-18804.

Araya R, Vogels TP, Yuste R (2014) Activity-dependent dendritic spine neck changes are correlated with synaptic strength. Proc Natl Acad Sci U S A 111:E2895-2904.

Araya R, Jiang J, Eisenthal KB, Yuste R (2006b) The spine neck filters membrane potentials. Proc Natl Acad Sci U S A 103:17961-17966.

Arellano JI, Benavides-Piccione R, Defelipe J, Yuste R (2007) Ultrastructure of dendritic spines: correlation between synaptic and spine morphologies. Frontiers in neuroscience 1:131-143.

Arendt KL, Sarti F, Chen L (2013) Chronic inactivation of a neural circuit enhances LTP by inducing silent synapse formation. J Neurosci 33:2087-2096.

Ashby MC, Isaac JT (2011) Maturation of a recurrent excitatory neocortical circuit by experience-dependent unsilencing of newly formed dendritic spines. Neuron 70:510-521.

Ashby MC, Maier SR, Nishimune A, Henley JM (2006) Lateral diffusion drives constitutive exchange of AMPA receptors at dendritic spines and is regulated by spine morphology. J Neurosci 26:7046-7055.

Bard L, Sainlos M, Bouchet D, Cousins S, Mikasova L, Breillat C, Stephenson FA, Imperiali B, Choquet D, Groc L (2010) Dynamic and specific interaction between synaptic NR2-NMDA receptor and PDZ proteins. Proc Natl Acad Sci U S A 107:19561-19566.

Barria A, Derkach V, Soderling T (1997) Identification of the Ca2+/calmodulin-dependent protein kinase II regulatory phosphorylation site in the alpha-amino-3-hydroxyl-5-methyl-4-isoxazole-propionate-type glutamate receptor. J Biol Chem 272:32727-32730.

Baude A, Nusser Z, Molnar E, McIlhinney RA, Somogyi P (1995) High-resolution immunogold localization of AMPA type glutamate receptor subunits at synaptic and non-synaptic sites in rat hippocampus. Neuroscience 69:1031-1055.

Beique JC, Huganir RL (2009) AMPA receptor subunits get their share of the pie. Neuron 62:165-168.

Beique JC, Na Y, Kuhl D, Worley PF, Huganir RL (2011) Arc-dependent synapse-specific homeostatic plasticity. Proc Natl Acad Sci U S A 108:816-821.

Beique JC, Lin DT, Kang MG, Aizawa H, Takamiya K, Huganir RL (2006) Synapse-specific regulation of AMPA receptor function by PSD-95. Proc Natl Acad Sci U S A 103:19535-19540.

Bekkers JM, Stevens CF (1996) Cable properties of cultured hippocampal neurons determined from sucrose-evoked miniature EPSCs. J Neurophysiol 75:1250-1255.

Bellone C, Nicoll RA (2007) Rapid bidirectional switching of synaptic NMDA receptors. Neuron 55:779-785.

Ben-Ari Y, Cherubini E, Corradetti R, Gaiarsa JL (1989) Giant synaptic potentials in immature rat CA3 hippocampal neurones. J Physiol 416:303-325.

Ben-Ari Y, Khazipov R, Leinekugel X, Caillard O, Gaiarsa JL (1997) GABAA, NMDA and AMPA receptors: a developmentally regulated 'menage a trois'. Trends Neurosci 20:523-529.

Benardo LS, Masukawa LM, Prince DA (1982) Electrophysiology of isolated hippocampal pyramidal dendrites. J Neurosci 2:1614-1622.

Benavides-Piccione R, Ballesteros-Yanez I, DeFelipe J, Yuste R (2002) Cortical area and species differences in dendritic spine morphology. Journal of neurocytology 31:337-346.

Bender VA, Bender KJ, Brasier DJ, Feldman DE (2006) Two coincidence detectors for spike timing-dependent plasticity in somatosensory cortex. J Neurosci 26:4166-4177.

Bhatt DH, Zhang S, Gan WB (2009) Dendritic spine dynamics. Annual review of physiology 71:261-282.

Bi GQ, Poo MM (1998) Synaptic modifications in cultured hippocampal neurons: dependence on spike timing, synaptic strength, and postsynaptic cell type. J Neurosci 18:10464-10472.

Bianchi S, Stimpson CD, Duka T, Larsen MD, Janssen WG, Collins Z, Bauernfeind AL, Schapiro SJ, Baze WB, McArthur MJ, Hopkins WD, Wildman DE, Lipovich L, Kuzawa CW, Jacobs B, Hof PR, Sherwood CC (2013) Synaptogenesis and development of pyramidal neuron dendritic morphology in the chimpanzee neocortex resembles humans. Proc Natl Acad Sci U S A 110 Suppl 2:10395-10401.

Blair HT, Schafe GE, Bauer EP, Rodrigues SM, LeDoux JE (2001) Synaptic plasticity in the lateral amygdala: a cellular hypothesis of fear conditioning. Learn Mem 8:229-242.

Blanpied TA, Scott DB, Ehlers MD (2002) Dynamics and regulation of clathrin coats at specialized endocytic zones of dendrites and spines. Neuron 36:435-449.

Blanpied TA, Kerr JM, Ehlers MD (2008) Structural plasticity with preserved topology in the postsynaptic protein network. Proc Natl Acad Sci U S A 105:12587-12592.

Bliss TV, Lomo T (1973) Long-lasting potentiation of synaptic transmission in the dentate area of the anaesthetized rabbit following stimulation of the perforant path. J Physiol 232:331-356.

Bloedel J, Gage PW, Llinas R, Quastel DM (1966) Transmitter release at the squid giant synapse in the presence of tetrodotoxin. Nature 212:49-50.

Bloodgood BL, Sabatini BL (2005) Neuronal activity regulates diffusion across the neck of dendritic spines. Science 310:866-869.

Bloodgood BL, Giessel AJ, Sabatini BL (2009) Biphasic synaptic Ca influx arising from compartmentalized electrical signals in dendritic spines. PLoS Biol 7:e1000190.

Bolea S, Avignone E, Berretta N, Sanchez-Andres JV, Cherubini E (1999) Glutamate controls the induction of GABA-mediated giant depolarizing potentials through AMPA receptors in neonatal rat hippocampal slices. J Neurophysiol 81:2095-2102.

Borgdorff AJ, Choquet D (2002) Regulation of AMPA receptor lateral movements. Nature 417:649-653.

Bourgeois JP, Rakic P (1993) Changes of synaptic density in the primary visual cortex of the macaque monkey from fetal to adult stage. J Neurosci 13:2801-2820.

Bouwman J, Maia AS, Camoletto PG, Posthuma G, Roubos EW, Oorschot VM, Klumperman J, Verhage M (2004) Quantification of synapse formation and maintenance in vivo in the absence of synaptic release. Neuroscience 126:115-126.

Bowie D, Mayer ML (1995) Inward rectification of both AMPA and kainate subtype glutamate receptors generated by polyamine-mediated ion channel block. Neuron 15:453-462.

Branco T, Clark BA, Hausser M (2010) Dendritic discrimination of temporal input sequences in cortical neurons. Science 329:1671-1675.

Brill J, Huguenard JR (2008) Sequential changes in AMPA receptor targeting in the developing neocortical excitatory circuit. J Neurosci 28:13918-13928.

Brock LG, Coombs JS, Eccles JC (1952) The recording of potentials from motoneurones with an intracellular electrode. J Physiol 117:431-460.

Buonomano DV, Merzenich MM (1998) Cortical plasticity: from synapses to maps. Annu Rev Neurosci 21:149-186.

Burrone J, O'Byrne M, Murthy VN (2002) Multiple forms of synaptic plasticity triggered by selective suppression of activity in individual neurons. Nature 420:414-418.

Busetto G, Higley MJ, Sabatini BL (2008) Developmental presence and disappearance of postsynaptically silent synapses on dendritic spines of rat layer 2/3 pyramidal neurons. J Physiol 586:1519-1527.

Buzsaki G, Wang XJ (2012) Mechanisms of gamma oscillations. Annu Rev Neurosci 35:203-225.

Buzsaki G, Moser EI (2013) Memory, navigation and theta rhythm in the hippocampal-entorhinal system. Nat Neurosci 16:130-138.

Cajal Ry (1888) Estructura de los centros nerviosos de las aves. Rev Trim Histol Norm Pat 1:1.

Cannon WBR, A. (1949) The supersensitivity of denervated structure. New York.

Caporale N, Dan Y (2008) Spike timing-dependent plasticity: a Hebbian learning rule. Annu Rev Neurosci 31:25-46.

Chalifoux JR, Carter AG (2011) Glutamate spillover promotes the generation of NMDA spikes. J Neurosci 31:16435-16446.

Chen X, Leischner U, Rochefort NL, Nelken I, Konnerth A (2011) Functional mapping of single spines in cortical neurons in vivo. Nature 475:501-505.

Chen Z, Kujawa SG, Sewell WF (2007) Auditory sensitivity regulation via rapid changes in expression of surface AMPA receptors. Nat Neurosci 10:1238-1240.

Chklovskii DB, Koulakov AA (2004) Maps in the brain: what can we learn from them? Annu Rev Neurosci 27:369-392.

Choquet D (2010) Fast AMPAR trafficking for a high-frequency synaptic transmission. Eur J Neurosci 32:250-260.

Choquet D, Triller A (2003) The role of receptor diffusion in the organization of the postsynaptic membrane. Nat Rev Neurosci 4:251-265.

Cingolani LA, Thalhammer A, Yu LM, Catalano M, Ramos T, Colicos MA, Goda Y (2008) Activity-dependent regulation of synaptic AMPA receptor composition and abundance by beta3 integrins. Neuron 58:749-762.

Colgan LA, Yasuda R (2014) Plasticity of dendritic spines: subcompartmentalization of signaling. Annual review of physiology 76:365-385.

Collingridge GL, Kehl SJ, McLennan H (1983) The antagonism of amino acid-induced excitations of rat hippocampal CA1 neurones in vitro. J Physiol 334:19-31.

Connor JA, Miller LD, Petrozzino J, Muller W (1994) Calcium signaling in dendritic spines of hippocampal neurons. J Neurobiol 25:234-242.

Connors BW, Long MA (2004) Electrical synapses in the mammalian brain. Annu Rev Neurosci 27:393-418.
Coss RG, Perkel DH (1985) The function of dendritic spines: a review of theoretical issues. Behavioral and neural biology 44:151-185.
Cossell L, Iacaruso MF, Muir DR, Houlton R, Sader EN, Ko H, Hofer SB, Mrsic-Flogel TD (2015) Functional organization of excitatory synaptic strength in primary visual cortex. Nature 518:399-403.
Couey JJ, Meredith RM, Spijker S, Poorthuis RB, Smit AB, Brussaard AB, Mansvelder HD (2007) Distributed network actions by nicotine increase the threshold for spike-timing-dependent plasticity in prefrontal cortex. Neuron 54:73-87.
Craig AM, Blackstone CD, Huganir RL, Banker G (1994) Selective clustering of glutamate and gamma-aminobutyric acid receptors opposite terminals releasing the corresponding neurotransmitters. Proc Natl Acad Sci U S A 91:12373-12377.
Cui-Wang T, Hanus C, Cui T, Helton T, Bourne J, Watson D, Harris KM, Ehlers MD (2012) Local zones of endoplasmic reticulum complexity confine cargo in neuronal dendrites. Cell 148:309-321.
Cull-Candy SG, Leszkiewicz DN (2004) Role of distinct NMDA receptor subtypes at central synapses. Sci STKE 2004:re16.
Davis GW (2006) Homeostatic control of neural activity: from phenomenology to molecular design. Annu Rev Neurosci 29:307-323.
de Vries PH, van Slochteren KR (2008) The nature of the memory trace and its neurocomputational implications. J Comput Neurosci 25:188-202.
DeBello WM, McBride TJ, Nichols GS, Pannoni KE, Sanculi D, Totten DJ (2014) Input clustering and the microscale structure of local circuits. Frontiers in neural circuits 8:112.
Deeg KE (2009) Synapse-specific homeostatic mechanisms in the hippocampus. J Neurophysiol 101:503-506.
Deeg KE, Aizenman CD (2011) Sensory modality-specific homeostatic plasticity in the developing optic tectum. Nat Neurosci 14:548-550.
Delcastillo J, Katz B (1954) Quantal Components of the End-Plate Potential. J Physiol-London 124:560-573.
Denk W, Delaney KR, Gelperin A, Kleinfeld D, Strowbridge BW, Tank DW, Yuste R (1994) Anatomical and functional imaging of neurons using 2-photon laser scanning microscopy. J Neurosci Methods 54:151-162.
Dobrunz LE, Stevens CF (1997) Heterogeneity of release probability, facilitation, and depletion at central synapses. Neuron 18:995-1008.
Druckmann S, Feng L, Lee B, Yook C, Zhao T, Magee JC, Kim J (2014) Structured Synaptic Connectivity between Hippocampal Regions. Neuron 81:629-640.
Dunwiddie T, Lynch G (1978) Long-term potentiation and depression of synaptic responses in the rat hippocampus: localization and frequency dependency. J Physiol 276:353-367.
Durand GM, Konnerth A (1996) Long-term potentiation as a mechanism of functional synapse induction in the developing hippocampus. J Physiol Paris 90:313-315.
Durand GM, Kovalchuk Y, Konnerth A (1996) Long-term potentiation and functional synapse induction in developing hippocampus. Nature 381:71-75.
Eccles JC (1946) An Electrical Hypothesis of Synaptic and Neuro-Muscular Transmission. Ann Ny Acad Sci 47:429-455.
Eccles JC (1949) A Review and Restatement of the Electrical Hypotheses of Synaptic Excitatory and Inhibitory Action. Arch Sci Physiol 3:567-584.
Eccles JC (1982) The Synapse - from Electrical to Chemical Transmission. Annual Review of Neuroscience 5:325-339.

Eccles JC, Kuffler SW (1941) Initiation of muscle impulses at neuro-muscular junction. Journal of Neurophysiology 4:402-417.
Eccles JC, Rall W (1950) Post-tetanic potentiation of responses of motoneurones. Nature 166:465-466.
Eccles JC, Katz B, Kuffler SW (1941) Nature of the "endplate potential" in curarized muscle. Journal of Neurophysiology 4:362-387.
Eccles JC, Fatt P, Koketsu K (1954) Cholinergic and Inhibitory Synapses in a Pathway from Motor-Axon Collaterals to Motoneurones. J Physiol-London 126:524-562.
Echegoyen J, Neu A, Graber KD, Soltesz I (2007) Homeostatic plasticity studied using in vivo hippocampal activity-blockade: synaptic scaling, intrinsic plasticity and age-dependence. PLoS One 2:e700.
Edelmann E, Lessmann V (2013) Dopamine regulates intrinsic excitability thereby gating successful induction of spike timing-dependent plasticity in CA1 of the hippocampus. Frontiers in neuroscience 7:25.
Ehlers MD, Heine M, Groc L, Lee MC, Choquet D (2007) Diffusional trapping of GluR1 AMPA receptors by input-specific synaptic activity. Neuron 54:447-460.
Elston GN (2000) Pyramidal cells of the frontal lobe: all the more spinous to think with. J Neurosci 20:RC95.
Emptage N, Bliss TV, Fine A (1999) Single synaptic events evoke NMDA receptor-mediated release of calcium from internal stores in hippocampal dendritic spines. Neuron 22:115-124.
Fatt P (1949) The Depolarizing Action of Acetylcholine on Muscle. J Physiol-London 109:P10-P11.
Fatt P, Katz B (1952) Spontaneous Subthreshold Activity at Motor Nerve Endings. J Physiol-London 117:109-128.
Feldman DE (2000) Timing-based LTP and LTD at vertical inputs to layer II/III pyramidal cells in rat barrel cortex. Neuron 27:45-56.
Froemke RC, Poo MM, Dan Y (2005) Spike-timing-dependent synaptic plasticity depends on dendritic location. Nature 434:221-225.
Frost NA, Lu HE, Blanpied TA (2012) Optimization of cell morphology measurement via single-molecule tracking PALM. PLoS One 7:e36751.
Fukazawa Y, Saitoh Y, Ozawa F, Ohta Y, Mizuno K, Inokuchi K (2003) Hippocampal LTP is accompanied by enhanced F-actin content within the dendritic spine that is essential for late LTP maintenance in vivo. Neuron 38:447-460.
Fusi S, Abbott LF (2007) Limits on the memory storage capacity of bounded synapses. Nat Neurosci 10:485-493.
Fusi S, Drew PJ, Abbott LF (2005) Cascade models of synaptically stored memories. Neuron 45:599-611.
Gainey MA, Hurvitz-Wolff JR, Lambo ME, Turrigiano GG (2009) Synaptic scaling requires the GluR2 subunit of the AMPA receptor. J Neurosci 29:6479-6489.
Gallego R, Kuno M, Nunez R, Snider WD (1979) Disuse enhances synaptic efficacy in spinal mononeurones. J Physiol 291:191-205.
Gambino F, Pages S, Kehayas V, Baptista D, Tatti R, Carleton A, Holtmaat A (2014) Sensory-evoked LTP driven by dendritic plateau potentials in vivo. Nature 515:116-119.
Gao M, Sossa K, Song L, Errington L, Cummings L, Hwang H, Kuhl D, Worley P, Lee HK (2010) A specific requirement of Arc/Arg3.1 for visual experience-induced homeostatic synaptic plasticity in mouse primary visual cortex. J Neurosci 30:7168-7178.
Garaschuk O, Schneggenburger R, Schirra C, Tempia F, Konnerth A (1996) Fractional Ca2+ currents through somatic and dendritic glutamate receptor channels of rat hippocampal CA1 pyramidal neurones. J Physiol 491 (Pt 3):757-772.
Gasparini S, Magee JC (2006) State-dependent dendritic computation in hippocampal CA1 pyramidal neurons. J Neurosci 26:2088-2100.

Gerges NZ, Backos DS, Rupasinghe CN, Spaller MR, Esteban JA (2006) Dual role of the exocyst in AMPA receptor targeting and insertion into the postsynaptic membrane. The EMBO journal 25:1623-1634.

Geschwind DH, Levitt P (2007) Autism spectrum disorders: developmental disconnection syndromes. Curr Opin Neurobiol 17:103-111.

Gilson M, Fukai T (2011) Stability versus neuronal specialization for STDP: long-tail weight distributions solve the dilemma. PLoS One 6:e25339.

Goel A, Lee HK (2007) Persistence of experience-induced homeostatic synaptic plasticity through adulthood in superficial layers of mouse visual cortex. J Neurosci 27:6692-6700.

Goldberg J, Holthoff K, Yuste R (2002) A problem with Hebb and local spikes. Trends Neurosci 25:433-435.

Golding NL, Spruston N (1998) Dendritic sodium spikes are variable triggers of axonal action potentials in hippocampal CA1 pyramidal neurons. Neuron 21:1189-1200.

Golding NL, Staff NP, Spruston N (2002) Dendritic spikes as a mechanism for cooperative long-term potentiation. Nature 418:326-331.

Gomez Gonzalez JF, Mel BW, Poirazi P (2011) Distinguishing Linear vs. Non-Linear Integration in CA1 Radial Oblique Dendrites: It's about Time. Front Comput Neurosci 5:44.

Goold CP, Nicoll RA (2010) Single-cell optogenetic excitation drives homeostatic synaptic depression. Neuron 68:512-528.

Govindarajan A, Kelleher RJ, Tonegawa S (2006) A clustered plasticity model of long-term memory engrams. Nat Rev Neurosci 7:575-583.

Govindarajan A, Israely I, Huang SY, Tonegawa S (2011) The dendritic branch is the preferred integrative unit for protein synthesis-dependent LTP. Neuron 69:132-146.

Granger AJ, Shi Y, Lu W, Cerpas M, Nicoll RA (2013) LTP requires a reserve pool of glutamate receptors independent of subunit type. Nature 493:495-500.

Gray EE, Fink AE, Sarinana J, Vissel B, O'Dell TJ (2007) Long-term potentiation in the hippocampal CA1 region does not require insertion and activation of GluR2-lacking AMPA receptors. J Neurophysiol 98:2488-2492.

Grienberger C, Chen X, Konnerth A (2014) NMDA receptor-dependent multidendrite Ca(2+) spikes required for hippocampal burst firing in vivo. Neuron 81:1274-1281.

Groc L, Heine M, Cognet L, Brickley K, Stephenson FA, Lounis B, Choquet D (2004) Differential activity-dependent regulation of the lateral mobilities of AMPA and NMDA receptors. Nat Neurosci 7:695-696.

Groc L, Heine M, Cousins SL, Stephenson FA, Lounis B, Cognet L, Choquet D (2006) NMDA receptor surface mobility depends on NR2A-2B subunits. Proc Natl Acad Sci U S A 103:18769-18774.

Groth RD, Lindskog M, Thiagarajan TC, Li L, Tsien RW (2011) Beta Ca2+/CaM-dependent kinase type II triggers upregulation of GluA1 to coordinate adaptation to synaptic inactivity in hippocampal neurons. Proc Natl Acad Sci U S A 108:828-833.

Grubb MS, Burrone J (2010) Activity-dependent relocation of the axon initial segment fine-tunes neuronal excitability. Nature 465:1070-1074.

Grunditz A, Holbro N, Tian L, Zuo Y, Oertner TG (2008) Spine neck plasticity controls postsynaptic calcium signals through electrical compartmentalization. J Neurosci 28:13457-13466.

Guire ES, Oh MC, Soderling TR, Derkach VA (2008) Recruitment of calcium-permeable AMPA receptors during synaptic potentiation is regulated by CaM-kinase I. J Neurosci 28:6000-6009.

Guo Y, Huang S, de Pasquale R, McGehrin K, Lee HK, Zhao K, Kirkwood A (2012) Dark exposure extends the integration window for spike-timing-dependent plasticity. J Neurosci 32:15027-15035.

Hanse E, Seth H, Riebe I (2013) AMPA-silent synapses in brain development and pathology. Nat Rev Neurosci 14:839-850.

Hardingham GE, Bading H (2003) The Yin and Yang of NMDA receptor signalling. Trends Neurosci 26:81-89.
Harms KJ, Tovar KR, Craig AM (2005) Synapse-specific regulation of AMPA receptor subunit composition by activity. J Neurosci 25:6379-6388.
Harnett MT, Makara JK, Spruston N, Kath WL, Magee JC (2012) Synaptic amplification by dendritic spines enhances input cooperativity. Nature 491:599-602.
Harraz OF, Altier C (2014) STIM1-mediated bidirectional regulation of Ca(2+) entry through voltage-gated calcium channels (VGCC) and calcium-release activated channels (CRAC). Frontiers in cellular neuroscience 8:43.
Harris KM, Stevens JK (1989) Dendritic spines of CA 1 pyramidal cells in the rat hippocampus: serial electron microscopy with reference to their biophysical characteristics. J Neurosci 9:2982-2997.
Harris KM, Kater SB (1994) Dendritic spines: cellular specializations imparting both stability and flexibility to synaptic function. Annu Rev Neurosci 17:341-371.
Harris KM, Jensen FE, Tsao B (1992) Three-dimensional structure of dendritic spines and synapses in rat hippocampus (CA1) at postnatal day 15 and adult ages: implications for the maturation of synaptic physiology and long-term potentiation. J Neurosci 12:2685-2705.
Hartman KN, Pal SK, Burrone J, Murthy VN (2006) Activity-dependent regulation of inhibitory synaptic transmission in hippocampal neurons. Nat Neurosci 9:642-649.
Hartveit E, Veruki ML (2007) Studying properties of neurotransmitter receptors by non-stationary noise analysis of spontaneous postsynaptic currents and agonist-evoked responses in outside-out patches. Nat Protoc 2:434-448.
Harvey CD, Svoboda K (2007) Locally dynamic synaptic learning rules in pyramidal neuron dendrites. Nature 450:1195-1200.
Harvey CD, Yasuda R, Zhong H, Svoboda K (2008) The spread of Ras activity triggered by activation of a single dendritic spine. Science 321:136-140.
Hayashi ML, Choi SY, Rao BS, Jung HY, Lee HK, Zhang D, Chattarji S, Kirkwood A, Tonegawa S (2004) Altered cortical synaptic morphology and impaired memory consolidation in forebrain- specific dominant-negative PAK transgenic mice. Neuron 42:773-787.
Hayashi T, Huganir RL (2004) Tyrosine phosphorylation and regulation of the AMPA receptor by SRC family tyrosine kinases. J Neurosci 24:6152-6160.
Hayashi Y, Shi SH, Esteban JA, Piccini A, Poncer JC, Malinow R (2000) Driving AMPA receptors into synapses by LTP and CaMKII: requirement for GluR1 and PDZ domain interaction. Science 287:2262-2267.
He K, Petrus E, Gammon N, Lee HK (2012) Distinct sensory requirements for unimodal and cross-modal homeostatic synaptic plasticity. J Neurosci 32:8469-8474.
Hebb DO (1949) The organization of behavior: a neuropsychological theory. New York: Wiley.
Heine M, Groc L, Frischknecht R, Beique JC, Lounis B, Rumbaugh G, Huganir RL, Cognet L, Choquet D (2008) Surface mobility of postsynaptic AMPARs tunes synaptic transmission. Science 320:201-205.
Helmchen F, Denk W (2005) Deep tissue two-photon microscopy. Nat Methods 2:932-940.
Higley MJ, Sabatini BL (2008) Calcium signaling in dendrites and spines: practical and functional considerations. Neuron 59:902-913.
Hill TC, Zito K (2013) LTP-induced long-term stabilization of individual nascent dendritic spines. J Neurosci 33:678-686.
Hofer SB, Ko H, Pichler B, Vogelstein J, Ros H, Zeng H, Lein E, Lesica NA, Mrsic-Flogel TD (2011) Differential connectivity and response dynamics of excitatory and inhibitory neurons in visual cortex. Nat Neurosci 14:1045-1052.

Holcman D, Triller A (2006) Modeling synaptic dynamics driven by receptor lateral diffusion. Biophys J 91:2405-2415.
Hollmann M, O'Shea-Greenfield A, Rogers SW, Heinemann S (1989) Cloning by functional expression of a member of the glutamate receptor family. Nature 342:643-648.
Holthoff K (2004) Regenerative dendritic spikes and synaptic plasticity. Curr Neurovasc Res 1:381-387.
Hou Q, Gilbert J, Man HY (2011) Homeostatic regulation of AMPA receptor trafficking and degradation by light-controlled single-synaptic activation. Neuron 72:806-818.
Hou Q, Zhang D, Jarzylo L, Huganir RL, Man HY (2008) Homeostatic regulation of AMPA receptor expression at single hippocampal synapses. Proc Natl Acad Sci U S A 105:775-780.
Houweling AR, Bazhenov M, Timofeev I, Steriade M, Sejnowski TJ (2005) Homeostatic synaptic plasticity can explain post-traumatic epileptogenesis in chronically isolated neocortex. Cereb Cortex 15:834-845.
Hsia AY, Malenka RC, Nicoll RA (1998) Development of excitatory circuitry in the hippocampus. J Neurophysiol 79:2013-2024.
Ibata K, Sun Q, Turrigiano GG (2008) Rapid synaptic scaling induced by changes in postsynaptic firing. Neuron 57:819-826.
Isaac JT, Nicoll RA, Malenka RC (1995) Evidence for silent synapses: implications for the expression of LTP. Neuron 15:427-434.
Isaac JT, Hjelmstad GO, Nicoll RA, Malenka RC (1996) Long-term potentiation at single fiber inputs to hippocampal CA1 pyramidal cells. Proc Natl Acad Sci U S A 93:8710-8715.
Isaac JT, Crair MC, Nicoll RA, Malenka RC (1997) Silent synapses during development of thalamocortical inputs. Neuron 18:269-280.
Isokawa M, Alger BE (2006) Ryanodine receptor regulates endogenous cannabinoid mobilization in the hippocampus. J Neurophysiol 95:3001-3011.
Jackson AC, Nicoll RA (2011) The expanding social network of ionotropic glutamate receptors: TARPs and other transmembrane auxiliary subunits. Neuron 70:178-199.
Jia H, Rochefort NL, Chen X, Konnerth A (2010) Dendritic organization of sensory input to cortical neurons in vivo. Nature 464:1307-1312.
Jia H, Rochefort NL, Chen X, Konnerth A (2011) In vivo two-photon imaging of sensory-evoked dendritic calcium signals in cortical neurons. Nat Protoc 6:28-35.
Ju W, Morishita W, Tsui J, Gaietta G, Deerinck TJ, Adams SR, Garner CC, Tsien RY, Ellisman MH, Malenka RC (2004) Activity-dependent regulation of dendritic synthesis and trafficking of AMPA receptors. Nat Neurosci 7:244-253.
Kaila K, Price TJ, Payne JA, Puskarjov M, Voipio J (2014) Cation-chloride cotransporters in neuronal development, plasticity and disease. Nat Rev Neurosci 15:637-654.
Kampa BM, Letzkus JJ, Stuart GJ (2007) Dendritic mechanisms controlling spike-timing-dependent synaptic plasticity. Trends Neurosci 30:456-463.
Kandel ER, Schwartz JH, Jessel TM (2000) Principles of Neural Science, 4th Edition. New York: McGraw-Hill.
Kasai H, Fukuda M, Watanabe S, Hayashi-Takagi A, Noguchi J (2010) Structural dynamics of dendritic spines in memory and cognition. Trends Neurosci 33:121-129.
Kastellakis G, Cai DJ, Mednick SC, Silva AJ, Poirazi P (2015) Synaptic clustering within dendrites: An emerging theory of memory formation. Progress in neurobiology.
Katz B, Miledi R (1965) Release of Acetylcholine from a Nerve Terminal by Electric Pulses of Variable Strength and Duration. Nature 207:1097-&.
Katz B, Miledi R (1967) Ionic Requirements of Synaptic Transmitter Release. Nature 215:651-&.
Katz B, Miledi R (1968) Role of Calcium in Neuromuscular Facilitation. J Physiol-London 195:481-&.

Katz B, Miledi R (1969) Tetrodotoxin-Resistant Electric Activity in Presynaptic Terminals. J Physiol-London 203:459-&.
Katz B, Miledi R (1970) Further Study of Role of Calcium in Synaptic Transmission. J Physiol-London 207:789-&.
Katz Y, Menon V, Nicholson DA, Geinisman Y, Kath WL, Spruston N (2009) Synapse distribution suggests a two-stage model of dendritic integration in CA1 pyramidal neurons. Neuron 63:171-177.
Kenyon KA, Bushong EA, Mauer AS, Strehler EE, Weinberg RJ, Burette AC (2010) Cellular and subcellular localization of the neuron-specific plasma membrane calcium ATPase PMCA1a in the rat brain. J Comp Neurol 518:3169-3183.
Kerchner GA, Nicoll RA (2008) Silent synapses and the emergence of a postsynaptic mechanism for LTP. Nat Rev Neurosci 9:813-825.
Kessels HW, Malinow R (2009) Synaptic AMPA receptor plasticity and behavior. Neuron 61:340-350.
Kharazia VN, Weinberg RJ (1999) Immunogold localization of AMPA and NMDA receptors in somatic sensory cortex of albino rat. J Comp Neurol 412:292-302.
Kim J, Tsien RW (2008) Synapse-specific adaptations to inactivity in hippocampal circuits achieve homeostatic gain control while dampening network reverberation. Neuron 58:925-937.
Kim J, Tsien RW, Alger BE (2012) An improved test for detecting multiplicative homeostatic synaptic scaling. PLoS One 7:e37364.
Kim SJ, Linden DJ (2007) Ubiquitous plasticity and memory storage. Neuron 56:582-592.
Kirov SA, Sorra KE, Harris KM (1999) Slices have more synapses than perfusion-fixed hippocampus from both young and mature rats. J Neurosci 19:2876-2886.
Kirov SA, Goddard CA, Harris KM (2004a) Age-dependence in the homeostatic upregulation of hippocampal dendritic spine number during blocked synaptic transmission. Neuropharmacology 47:640-648.
Kirov SA, Petrak LJ, Fiala JC, Harris KM (2004b) Dendritic spines disappear with chilling but proliferate excessively upon rewarming of mature hippocampus. Neuroscience 127:69-80.
Klausberger T, Somogyi P (2008) Neuronal diversity and temporal dynamics: the unity of hippocampal circuit operations. Science 321:53-57.
Kleindienst T, Winnubst J, Roth-Alpermann C, Bonhoeffer T, Lohmann C (2011) Activity-dependent clustering of functional synaptic inputs on developing hippocampal dendrites. Neuron 72:1012-1024.
Ko H, Mrsic-Flogel TD, Hofer SB (2014) Emergence of feature-specific connectivity in cortical microcircuits in the absence of visual experience. J Neurosci 34:9812-9816.
Ko H, Hofer SB, Pichler B, Buchanan KA, Sjostrom PJ, Mrsic-Flogel TD (2011) Functional specificity of local synaptic connections in neocortical networks. Nature 473:87-91.
Ko H, Cossell L, Baragli C, Antolik J, Clopath C, Hofer SB, Mrsic-Flogel TD (2013) The emergence of functional microcircuits in visual cortex. Nature 496:96-100.
Koch C, Zador A (1993) The function of dendritic spines: devices subserving biochemical rather than electrical compartmentalization. J Neurosci 13:413-422.
Koester HJ, Sakmann B (1998) Calcium dynamics in single spines during coincident pre- and postsynaptic activity depend on relative timing of back-propagating action potentials and subthreshold excitatory postsynaptic potentials. Proc Natl Acad Sci U S A 95:9596-9601.
Koh IY, Lindquist WB, Zito K, Nimchinsky EA, Svoboda K (2002) An image analysis algorithm for dendritic spines. Neural Comput 14:1283-1310.
Kopec CD, Real E, Kessels HW, Malinow R (2007) GluR1 links structural and functional plasticity at excitatory synapses. J Neurosci 27:13706-13718.
Kovalchuk Y, Eilers J, Lisman J, Konnerth A (2000) NMDA receptor-mediated subthreshold Ca(2+) signals in spines of hippocampal neurons. J Neurosci 20:1791-1799.

Kovalchuk Y, Hanse E, Kafitz KW, Konnerth A (2002) Postsynaptic Induction of BDNF-Mediated Long-Term Potentiation. Science 295:1729-1734.
Krnjevic K, Phillis JW (1963) Iontophoretic studies of neurones in the mammalian cerebral cortex. J Physiol 165:274-304.
Krucker T, Siggins GR, Halpain S (2000) Dynamic actin filaments are required for stable long-term potentiation (LTP) in area CA1 of the hippocampus. Proc Natl Acad Sci U S A 97:6856-6861.
Kuffler SW (1942a) Electric potential changes at an isolated nerve-muscle junction. Journal of Neurophysiology 5:18-26.
Kuffler SW (1942b) Further study on transmission in an isolated nerve-muscle fibre preparation. Journal of Neurophysiology 5:309-322.
Kuno M, Miyahara JT (1969a) Analysis of synaptic efficacy in spinal motoneurones from 'quantum' aspects. J Physiol 201:479-493.
Kuno M, Miyahara JT (1969b) Non-linear summation of unit synaptic potentials in spinal motoneurones of the cat. J Physiol 201:465-477.
Lamsa KP, Heeroma JH, Somogyi P, Rusakov DA, Kullmann DM (2007) Anti-Hebbian long-term potentiation in the hippocampal feedback inhibitory circuit. Science 315:1262-1266.
Larkum ME, Nevian T (2008) Synaptic clustering by dendritic signalling mechanisms. Curr Opin Neurobiol 18:321-331.
Larkum ME, Nevian T, Sandler M, Polsky A, Schiller J (2009) Synaptic integration in tuft dendrites of layer 5 pyramidal neurons: a new unifying principle. Science 325:756-760.
Lau CG, Zukin RS (2007) NMDA receptor trafficking in synaptic plasticity and neuropsychiatric disorders. Nat Rev Neurosci 8:413-426.
Lavzin M, Rapoport S, Polsky A, Garion L, Schiller J (2012) Nonlinear dendritic processing determines angular tuning of barrel cortex neurons in vivo. Nature 490:397-401.
Lazar A, Pipa G, Triesch J (2009) SORN: a self-organizing recurrent neural network. Front Comput Neurosci 3:23.
Lee HK (2012a) Ca-permeable AMPA receptors in homeostatic synaptic plasticity. Front Mol Neurosci 5:17.
Lee HK, Barbarosie M, Kameyama K, Bear MF, Huganir RL (2000) Regulation of distinct AMPA receptor phosphorylation sites during bidirectional synaptic plasticity. Nature 405:955-959.
Lee HK, Takamiya K, Han JS, Man H, Kim CH, Rumbaugh G, Yu S, Ding L, He C, Petralia RS, Wenthold RJ, Gallagher M, Huganir RL (2003) Phosphorylation of the AMPA receptor GluR1 subunit is required for synaptic plasticity and retention of spatial memory. Cell 112:631-643.
Lee KF (2012b) A unique mechanism of NMDA spike initiation supports a distinct role in synaptic input integration. J Neurosci 32:2913-2914.
Lee KF, Soares C, Beique JC (2012) Examining form and function of dendritic spines. Neural plasticity 2012:704103.
Lee KF, Soares C, Beique JC (2014) Tuning into diversity of homeostatic synaptic plasticity. Neuropharmacology 78:31-37.
Lee MC, Yasuda R, Ehlers MD (2010) Metaplasticity at single glutamatergic synapses. Neuron 66:859-870.
Lee SJ, Escobedo-Lozoya Y, Szatmari EM, Yasuda R (2009) Activation of CaMKII in single dendritic spines during long-term potentiation. Nature 458:299-304.
Legenstein R, Maass W (2011) Branch-specific plasticity enables self-organization of nonlinear computation in single neurons. J Neurosci 31:10787-10802.
Leinekugel X, Medina I, Khalilov I, Ben-Ari Y, Khazipov R (1997) Ca2+ oscillations mediated by the synergistic excitatory actions of GABA(A) and NMDA receptors in the neonatal hippocampus. Neuron 18:243-255.

Leinekugel X, Khazipov R, Cannon R, Hirase H, Ben-Ari Y, Buzsaki G (2002) Correlated bursts of activity in the neonatal hippocampus in vivo. Science 296:2049-2052.

Leinekugel X, Khalilov I, McLean H, Caillard O, Gaiarsa JL, Ben-Ari Y, Khazipov R (1999) GABA is the principal fast-acting excitatory transmitter in the neonatal brain. Advances in neurology 79:189-201.

Liao D, Hessler NA, Malinow R (1995) Activation of postsynaptically silent synapses during pairing-induced LTP in CA1 region of hippocampal slice. Nature 375:400-404.

Lin DT, Makino Y, Sharma K, Hayashi T, Neve R, Takamiya K, Huganir RL (2009) Regulation of AMPA receptor extrasynaptic insertion by 4.1N, phosphorylation and palmitoylation. Nat Neurosci 12:879-887.

Lindskog M, Li L, Groth RD, Poburko D, Thiagarajan TC, Han X, Tsien RW (2011) Postsynaptic GluA1 enables acute retrograde enhancement of presynaptic function to coordinate adaptation to synaptic inactivity. Proc Natl Acad Sci U S A 107:21806-21811.

Lisman J, Raghavachari S (2006) A unified model of the presynaptic and postsynaptic changes during LTP at CA1 synapses. Sci STKE 2006:re11.

Lisman J, Schulman H, Cline H (2002) The molecular basis of CaMKII function in synaptic and behavioural memory. Nat Rev Neurosci 3:175-190.

Lisman JE (2009) The pre/post LTP debate. Neuron 63:281-284.

Lisman JE, McIntyre CC (2001) Synaptic plasticity: a molecular memory switch. Curr Biol 11:R788-791.

Lloyd DP (1949) Post-tetanic potentiation of response in monosynaptic reflex pathways of the spinal cord. The Journal of general physiology 33:147-170.

Lohmann C, Kessels HW (2014) The developmental stages of synaptic plasticity. J Physiol 592:13-31.

London M, Hausser M (2005) Dendritic computation. Annu Rev Neurosci 28:503-532.

Losonczy A, Magee JC (2006) Integrative properties of radial oblique dendrites in hippocampal CA1 pyramidal neurons. Neuron 50:291-307.

Lu J, Helton TD, Blanpied TA, Racz B, Newpher TM, Weinberg RJ, Ehlers MD (2007) Postsynaptic positioning of endocytic zones and AMPA receptor cycling by physical coupling of dynamin-3 to Homer. Neuron 55:874-889.

Lu W, Shi Y, Jackson AC, Bjorgan K, During MJ, Sprengel R, Seeburg PH, Nicoll RA (2009) Subunit composition of synaptic AMPA receptors revealed by a single-cell genetic approach. Neuron 62:254-268.

Luscher C, Xia H, Beattie EC, Carroll RC, von Zastrow M, Malenka RC, Nicoll RA (1999) Role of AMPA receptor cycling in synaptic transmission and plasticity. Neuron 24:649-658.

Lynch G, Larson J, Kelso S, Barrionuevo G, Schottler F (1983) Intracellular injections of EGTA block induction of hippocampal long-term potentiation. Nature 305:719-721.

MacGillavry HD, Blanpied TA (2013) Single-Molecule Tracking Photoactivated Localization Microscopy to Map Nano-Scale Structure and Dynamics in Living Spines. Current protocols in neuroscience / editorial board, Jacqueline N Crawley [et al] 2:2 20 21-22 20 19.

Maffei A, Fontanini A (2009) Network homeostasis: a matter of coordination. Curr Opin Neurobiol 19:168-173.

Magee JC (1999) Dendritic Ih normalizes temporal summation in hippocampal CA1 neurons. Nat Neurosci 2:848.

Magee JC (2000) Dendritic integration of excitatory synaptic input. Nat Rev Neurosci 1:181-190.

Magee JC, Cook EP (2000) Somatic EPSP amplitude is independent of synapse location in hippocampal pyramidal neurons. Nat Neurosci 3:895-903.

Mainen ZF, Malinow R, Svoboda K (1999) Synaptic calcium transients in single spines indicate that NMDA receptors are not saturated. Nature 399:151-155.

Majewska A, Tashiro A, Yuste R (2000a) Regulation of spine calcium dynamics by rapid spine motility. J Neurosci 20:8262-8268.
Majewska A, Brown E, Ross J, Yuste R (2000b) Mechanisms of calcium decay kinetics in hippocampal spines: role of spine calcium pumps and calcium diffusion through the spine neck in biochemical compartmentalization. J Neurosci 20:1722-1734.
Major G, Larkum ME, Schiller J (2013) Active properties of neocortical pyramidal neuron dendrites. Annu Rev Neurosci 36:1-24.
Makino H, Malinow R (2009) AMPA receptor incorporation into synapses during LTP: the role of lateral movement and exocytosis. Neuron 64:381-390.
Makino H, Malinow R (2011) Compartmentalized versus global synaptic plasticity on dendrites controlled by experience. Neuron 72:1001-1011.
Malenka RC, Nicoll RA (1999) Long-term potentiation--a decade of progress? Science 285:1870-1874.
Malenka RC, Bear MF (2004) LTP and LTD: an embarrassment of riches. Neuron 44:5-21.
Malenka RC, Kauer JA, Zucker RS, Nicoll RA (1988) Postsynaptic calcium is sufficient for potentiation of hippocampal synaptic transmission. Science 242:81-84.
Malinow R, Malenka RC (2002) AMPA receptor trafficking and synaptic plasticity. Annu Rev Neurosci 25:103-126.
Malinow R, Madison DV, Tsien RW (1988) Persistent protein kinase activity underlying long-term potentiation. Nature 335:820-824.
Malinow R, Schulman H, Tsien RW (1989) Inhibition of postsynaptic PKC or CaMKII blocks induction but not expression of LTP. Science 245:862-866.
Manabe T, Kaneko S, Kuno M (1989) Disuse-induced enhancement of Ia synaptic transmission in spinal motoneurons of the rat. J Neurosci 9:2455-2461.
Marder E, O'Leary T, Shruti S (2014) Neuromodulation of circuits with variable parameters: single neurons and small circuits reveal principles of state-dependent and robust neuromodulation. Annu Rev Neurosci 37:329-346.
Markram H, Lubke J, Frotscher M, Sakmann B (1997) Regulation of synaptic efficacy by coincidence of postsynaptic APs and EPSPs. Science 275:213-215.
Martin AR, Pilar G (1964) Presynaptic and Post-Synaptic Events during Post-Tetanic Potentiation and Facilitation in the Avian Ciliary Ganglion. J Physiol 175:17-30.
Mateos JM, Luthi A, Savic N, Stierli B, Streit P, Gahwiler BH, McKinney RA (2007) Synaptic modifications at the CA3-CA1 synapse after chronic AMPA receptor blockade in rat hippocampal slices. J Physiol 581:129-138.
Matsuzaki M, Honkura N, Ellis-Davies GC, Kasai H (2004) Structural basis of long-term potentiation in single dendritic spines. Nature 429:761-766.
Matsuzaki M, Ellis-Davies GC, Kanemoto Y, Kasai H (2011) Simultaneous two-photon activation of presynaptic cells and calcium imaging in postsynaptic dendritic spines. Neural systems & circuits 1:2.
Matsuzaki M, Ellis-Davies GC, Nemoto T, Miyashita Y, Iino M, Kasai H (2001) Dendritic spine geometry is critical for AMPA receptor expression in hippocampal CA1 pyramidal neurons. Nat Neurosci 4:1086-1092.
Mayer ML, Westbrook GL (1987) The physiology of excitatory amino acids in the vertebrate central nervous system. Progress in neurobiology 28:197-276.
Mayer ML, Westbrook GL, Guthrie PB (1984) Voltage-dependent block by Mg2+ of NMDA responses in spinal cord neurones. Nature 309:261-263.
McBride TJ, Rodriguez-Contreras A, Trinh A, Bailey R, Debello WM (2008) Learning drives differential clustering of axodendritic contacts in the barn owl auditory system. J Neurosci 28:6960-6973.

McKinney RA, Capogna M, Durr R, Gahwiler BH, Thompson SM (1999) Miniature synaptic events maintain dendritic spines via AMPA receptor activation. Nat Neurosci 2:44-49.
Mel BW (1993) Synaptic integration in an excitable dendritic tree. J Neurophysiol 70:1086-1101.
Michel AE, Garey LJ (1984) The development of dendritic spines in the human visual cortex. Human neurobiology 3:223-227.
Miller KD, MacKay DJ (1994) The Role of Constraints in Hebbian Learning. Neural Comput 6:100-126.
Mohajerani MH, Cherubini E (2006) Role of giant depolarizing potentials in shaping synaptic currents in the developing hippocampus. Critical reviews in neurobiology 18:13-23.
Molnar E, Pickard L, Duckworth JK (2002) Developmental changes in ionotropic glutamate receptors: lessons from hippocampal synapses. Neuroscientist 8:143-153.
Mori F, Fukaya M, Abe H, Wakabayashi K, Watanabe M (2000) Developmental changes in expression of the three ryanodine receptor mRNAs in the mouse brain. Neurosci Lett 285:57-60.
Morrison A, Aertsen A, Diesmann M (2007) Spike-timing-dependent plasticity in balanced random networks. Neural Comput 19:1437-1467.
Mueller AL, Chesnut RM, Schwartzkroin PA (1983) Actions of GABA in developing rabbit hippocampus: an in vitro study. Neurosci Lett 39:193-198.
Mueller AL, Taube JS, Schwartzkroin PA (1984) Development of hyperpolarizing inhibitory postsynaptic potentials and hyperpolarizing response to gamma-aminobutyric acid in rabbit hippocampus studied in vitro. J Neurosci 4:860-867.
Muller C, Remy S (2014) Dendritic inhibition mediated by O-LM and bistratified interneurons in the hippocampus. Front Synaptic Neurosci 6:23.
Muller W, Connor JA (1991) Dendritic Spines as Individual Neuronal Compartments for Synaptic Ca2+ Responses. Nature 354:73-76.
Muller W, Connor JA (1992) Ca2+ signalling in postsynaptic dendrites and spines of mammalian neurons in brain slice. J Physiol Paris 86:57-66.
Murakoshi H, Wang H, Yasuda R (2011) Local, persistent activation of Rho GTPases during plasticity of single dendritic spines. Nature 472:100-104.
Murphy EH, Magness R (1984) Development of the rabbit visual cortex: a quantitative Golgi analysis. Experimental brain research 53:304-314.
Neher E, Sakmann B (1976) Single-channel currents recorded from membrane of denervated frog muscle fibres. Nature 260:799-802.
Neher E, Sakmann B, Steinbach JH (1978) The extracellular patch clamp: a method for resolving currents through individual open channels in biological membranes. Pflugers Arch 375:219-228.
Nevian T, Sakmann B (2004) Single spine Ca2+ signals evoked by coincident EPSPs and backpropagating action potentials in spiny stellate cells of layer 4 in the juvenile rat somatosensory barrel cortex. J Neurosci 24:1689-1699.
Nevian T, Sakmann B (2006) Spine Ca2+ signaling in spike-timing-dependent plasticity. J Neurosci 26:11001-11013.
Nicholson DA, Trana R, Katz Y, Kath WL, Spruston N, Geinisman Y (2006) Distance-dependent differences in synapse number and AMPA receptor expression in hippocampal CA1 pyramidal neurons. Neuron 50:431-442.
Noguchi J, Matsuzaki M, Ellis-Davies GC, Kasai H (2005) Spine-neck geometry determines NMDA receptor-dependent Ca2+ signaling in dendrites. Neuron 46:609-622.
Noguchi J, Nagaoka A, Watanabe S, Ellis-Davies GC, Kitamura K, Kano M, Matsuzaki M, Kasai H (2011) In vivo two-photon uncaging of glutamate revealing the structure-function relationships of dendritic spines in the neocortex of adult mice. J Physiol 589:2447-2457.
Nowak L, Bregestovski P, Ascher P, Herbet A, Prochiantz A (1984) Magnesium gates glutamate-activated channels in mouse central neurones. Nature 307:462-465.

O'Brien RJ, Kamboj S, Ehlers MD, Rosen KR, Fischbach GD, Huganir RL (1998) Activity-dependent modulation of synaptic AMPA receptor accumulation. Neuron 21:1067-1078.
O'Donnell M, Chance RK, Bashaw GJ (2009) Axon growth and guidance: receptor regulation and signal transduction. Annu Rev Neurosci 32:383-412.
Oertner TG, Sabatini BL, Nimchinsky EA, Svoboda K (2002) Facilitation at single synapses probed with optical quantal analysis. Nat Neurosci 5:657-664.
Oh WC, Hill TC, Zito K (2013) Synapse-specific and size-dependent mechanisms of spine structural plasticity accompanying synaptic weakening. Proc Natl Acad Sci U S A 110:E305-312.
Okamoto K, Nagai T, Miyawaki A, Hayashi Y (2004) Rapid and persistent modulation of actin dynamics regulates postsynaptic reorganization underlying bidirectional plasticity. Nat Neurosci 7:1104-1112.
Okamoto K, Narayanan R, Lee SH, Murata K, Hayashi Y (2007) The role of CaMKII as an F-actin-bundling protein crucial for maintenance of dendritic spine structure. Proc Natl Acad Sci U S A 104:6418-6423.
Okuno H, Akashi K, Ishii Y, Yagishita-Kyo N, Suzuki K, Nonaka M, Kawashima T, Fujii H, Takemoto-Kimura S, Abe M, Natsume R, Chowdhury S, Sakimura K, Worley PF, Bito H (2012) Inverse synaptic tagging of inactive synapses via dynamic interaction of Arc/Arg3.1 with CaMKIIbeta. Cell 149:886-898.
Opazo P, Choquet D (2011) A three-step model for the synaptic recruitment of AMPA receptors. Mol Cell Neurosci 46:1-8.
Palmer LM, Shai AS, Reeve JE, Anderson HL, Paulsen O, Larkum ME (2014) NMDA spikes enhance action potential generation during sensory input. Nat Neurosci 17:383-390.
Paoletti P, Bellone C, Zhou Q (2013) NMDA receptor subunit diversity: impact on receptor properties, synaptic plasticity and disease. Nat Rev Neurosci 14:383-400.
Paradis S, Sweeney ST, Davis GW (2001) Homeostatic control of presynaptic release is triggered by postsynaptic membrane depolarization. Neuron 30:737-749.
Park M, Penick EC, Edwards JG, Kauer JA, Ehlers MD (2004) Recycling endosomes supply AMPA receptors for LTP. Science 305:1972-1975.
Patterson M, Yasuda R (2011) Signalling pathways underlying structural plasticity of dendritic spines. Br J Pharmacol 163:1626-1638.
Patterson MA, Szatmari EM, Yasuda R (2010) AMPA receptors are exocytosed in stimulated spines and adjacent dendrites in a Ras-ERK-dependent manner during long-term potentiation. Proc Natl Acad Sci U S A 107:15951-15956.
Perez-Otano I, Ehlers MD (2005) Homeostatic plasticity and NMDA receptor trafficking. Trends Neurosci 28:229-238.
Petit TL, LeBoutillier JC, Gregorio A, Libstug H (1988) The pattern of dendritic development in the cerebral cortex of the rat. Brain Res 469:209-219.
Petrini EM, Lu J, Cognet L, Lounis B, Ehlers MD, Choquet D (2009) Endocytic trafficking and recycling maintain a pool of mobile surface AMPA receptors required for synaptic potentiation. Neuron 63:92-105.
Petrozzino JJ, Pozzo Miller LD, Connor JA (1995) Micromolar Ca2+ transients in dendritic spines of hippocampal pyramidal neurons in brain slice. Neuron 14:1223-1231.
Philpot BD, Espinosa JS, Bear MF (2003) Evidence for altered NMDA receptor function as a basis for metaplasticity in visual cortex. J Neurosci 23:5583-5588.
Philpot BD, Sekhar AK, Shouval HZ, Bear MF (2001) Visual experience and deprivation bidirectionally modify the composition and function of NMDA receptors in visual cortex. Neuron 29:157-169.

Plant K, Pelkey KA, Bortolotto ZA, Morita D, Terashima A, McBain CJ, Collingridge GL, Isaac JT (2006) Transient incorporation of native GluR2-lacking AMPA receptors during hippocampal long-term potentiation. Nat Neurosci 9:602-604.

Poirazi P, Mel BW (2001) Impact of active dendrites and structural plasticity on the memory capacity of neural tissue. Neuron 29:779-796.

Poirazi P, Brannon T, Mel BW (2003) Pyramidal neuron as two-layer neural network. Neuron 37:989-999.

Pokorny J, Yamamoto T (1981a) Postnatal ontogenesis of hippocampal CA1 area in rats. II. Development of ultrastructure in stratum lacunosum and moleculare. Brain Res Bull 7:121-130.

Pokorny J, Yamamoto T (1981b) Postnatal ontogenesis of hippocampal CA1 area in rats. I. Development of dendritic arborisation in pyramidal neurons. Brain Res Bull 7:113-120.

Polsky A, Mel BW, Schiller J (2004) Computational subunits in thin dendrites of pyramidal cells. Nat Neurosci 7:621-627.

Polsky A, Mel B, Schiller J (2009) Encoding and decoding bursts by NMDA spikes in basal dendrites of layer 5 pyramidal neurons. J Neurosci 29:11891-11903.

Popovic MA, Gao X, Carnevale NT, Zecevic D (2014) Cortical dendritic spine heads are not electrically isolated by the spine neck from membrane potential signals in parent dendrites. Cereb Cortex 24:385-395.

Portera-Cailliau C, Pan DT, Yuste R (2003) Activity-regulated dynamic behavior of early dendritic protrusions: evidence for different types of dendritic filopodia. J Neurosci 23:7129-7142.

Pozzo-Miller LD, Pivovarova NB, Leapman RD, Buchanan RA, Reese TS, Andrews SB (1997) Activity-dependent calcium sequestration in dendrites of hippocampal neurons in brain slices. J Neurosci 17:8729-8738.

Qin Z, Zhou X, Gomez-Smith M, Pandey NR, Lee KF, Lagace DC, Beique JC, Chen HH (2012) LIM domain only 4 (LMO4) regulates calcium-induced calcium release and synaptic plasticity in the hippocampus. J Neurosci 32:4271-4283.

Rabinowitch I, Segev I (2008) Two opposing plasticity mechanisms pulling a single synapse. Trends Neurosci 31:377-383.

Racz B, Blanpied TA, Ehlers MD, Weinberg RJ (2004) Lateral organization of endocytic machinery in dendritic spines. Nat Neurosci 7:917-918.

Rall W (1962) Theory of physiological properties of dendrites. Ann N Y Acad Sci 96:1071-1092.

Ramachandran B, Frey JU (2009) Interfering with the actin network and its effect on long-term potentiation and synaptic tagging in hippocampal CA1 neurons in slices in vitro. J Neurosci 29:12167-12173.

Redondo RL, Morris RG (2011) Making memories last: the synaptic tagging and capture hypothesis. Nat Rev Neurosci 12:17-30.

Rellos P, Pike AC, Niesen FH, Salah E, Lee WH, von Delft F, Knapp S (2010) Structure of the CaMKIIdelta/calmodulin complex reveals the molecular mechanism of CaMKII kinase activation. PLoS Biol 8:e1000426.

Remy S, Spruston N (2007) Dendritic spikes induce single-burst long-term potentiation. Proc Natl Acad Sci U S A 104:17192-17197.

Rhodes P (2006) The properties and implications of NMDA spikes in neocortical pyramidal cells. J Neurosci 26:6704-6715.

Risher WC, Ustunkaya T, Singh Alvarado J, Eroglu C (2014) Rapid Golgi analysis method for efficient and unbiased classification of dendritic spines. PLoS One 9:e107591.

Rodriguez A, Ehlenberger DB, Dickstein DL, Hof PR, Wearne SL (2008) Automated three-dimensional detection and shape classification of dendritic spines from fluorescence microscopy images. PLoS One 3:e1997.

Ross WN (2012) Understanding calcium waves and sparks in central neurons. Nat Rev Neurosci 13:157-168.
Russo SJ, Dietz DM, Dumitriu D, Morrison JH, Malenka RC, Nestler EJ (2010) The addicted synapse: mechanisms of synaptic and structural plasticity in nucleus accumbens. Trends Neurosci 33:267-276.
Sabatini BL, Maravall M, Svoboda K (2001) Ca(2+) signaling in dendritic spines. Curr Opin Neurobiol 11:349-356.
Sabatini BL, Oertner TG, Svoboda K (2002) The life cycle of Ca(2+) ions in dendritic spines. Neuron 33:439-452.
Sah P, Hestrin S, Nicoll RA (1989) Tonic activation of NMDA receptors by ambient glutamate enhances excitability of neurons. Science 246:815-818.
Saitoe M, Schwarz TL, Umbach JA, Gundersen CB, Kidokoro Y (2001) Absence of junctional glutamate receptor clusters in Drosophila mutants lacking spontaneous transmitter release. Science 293:514-517.
Scheuss V, Yasuda R, Sobczyk A, Svoboda K (2006) Nonlinear [Ca2+] signaling in dendrites and spines caused by activity-dependent depression of Ca2+ extrusion. J Neurosci 26:8183-8194.
Schiller J, Major G, Koester HJ, Schiller Y (2000) NMDA spikes in basal dendrites of cortical pyramidal neurons. Nature 404:285-289.
Schreiner CE, Read HL, Sutter ML (2000) Modular organization of frequency integration in primary auditory cortex. Annu Rev Neurosci 23:501-529.
Sdrulla AD, Linden DJ (2007) Double dissociation between long-term depression and dendritic spine morphology in cerebellar Purkinje cells. Nat Neurosci 10:546-548.
Segal M, Vlachos A, Korkotian E (2010) The spine apparatus, synaptopodin, and dendritic spine plasticity. Neuroscientist 16:125-131.
Seol GH, Ziburkus J, Huang S, Song L, Kim IT, Takamiya K, Huganir RL, Lee HK, Kirkwood A (2007) Neuromodulators control the polarity of spike-timing-dependent synaptic plasticity. Neuron 55:919-929.
Shapovalov AI (1969) Posttetanic potentiation of monosynaptic and disynaptic actions from supraspinal structures on lumbar motoneurons. J Neurophysiol 32:948-959.
Sheffield ME, Dombeck DA (2014) Calcium transient prevalence across the dendritic arbour predicts place field properties. Nature.
Shepherd GM (1996) The dendritic spine: a multifunctional integrative unit. J Neurophysiol 75:2197-2210.
Shepherd JD, Huganir RL (2007) The cell biology of synaptic plasticity: AMPA receptor trafficking. Annu Rev Cell Dev Biol 23:613-643.
Shepherd JD, Rumbaugh G, Wu J, Chowdhury S, Plath N, Kuhl D, Huganir RL, Worley PF (2006) Arc/Arg3.1 mediates homeostatic synaptic scaling of AMPA receptors. Neuron 52:475-484.
Shi P, Zhou X, Li Q, Baron M, Teylan MA, Kim Y, Wong ST (2009) Online Three-Dimensional Dendritic Spines Mophological Classification Based on Semi-Supervised Learning. Proceedings / IEEE International Symposium on Biomedical Imaging: from nano to macro IEEE International Symposium on Biomedical Imaging:1019-1022.
Shi S, Hayashi Y, Esteban JA, Malinow R (2001) Subunit-specific rules governing AMPA receptor trafficking to synapses in hippocampal pyramidal neurons. Cell 105:331-343.
Shipman SL, Herring BE, Suh YH, Roche KW, Nicoll RA (2013) Distance-dependent scaling of AMPARs is cell-autonomous and GluA2 dependent. J Neurosci 33:13312-13319.
Shouval HZ, Gavornik JP (2011) A single spiking neuron that can represent interval timing: analysis, plasticity and multi-stability. J Comput Neurosci 30:489-499.

Shouval HZ, Bear MF, Cooper LN (2002) A unified model of NMDA receptor-dependent bidirectional synaptic plasticity. Proc Natl Acad Sci U S A 99:10831-10836.
Shouval HZ, Wang SS, Wittenberg GM (2010) Spike timing dependent plasticity: a consequence of more fundamental learning rules. Front Comput Neurosci 4.
Sipila ST, Huttu K, Soltesz I, Voipio J, Kaila K (2005) Depolarizing GABA acts on intrinsically bursting pyramidal neurons to drive giant depolarizing potentials in the immature hippocampus. J Neurosci 25:5280-5289.
Sjostrom PJ, Hausser M (2006) A cooperative switch determines the sign of synaptic plasticity in distal dendrites of neocortical pyramidal neurons. Neuron 51:227-238.
Sjostrom PJ, Turrigiano GG, Nelson SB (2001) Rate, timing, and cooperativity jointly determine cortical synaptic plasticity. Neuron 32:1149-1164.
Sjostrom PJ, Rancz EA, Roth A, Hausser M (2008) Dendritic excitability and synaptic plasticity. Physiol Rev 88:769-840.
Smith BA, Roy H, De Koninck P, Grutter P, De Koninck Y (2007) Dendritic spine viscoelasticity and soft-glassy nature: balancing dynamic remodeling with structural stability. Biophys J 92:1419-1430.
Smith MA, Ellis-Davies GC, Magee JC (2003) Mechanism of the distance-dependent scaling of Schaffer collateral synapses in rat CA1 pyramidal neurons. J Physiol 548:245-258.
Smith SL, Smith IT, Branco T, Hausser M (2013) Dendritic spikes enhance stimulus selectivity in cortical neurons in vivo. Nature 503:115-120.
Soares C, Lee KF, Nassrallah W, Beique JC (2013) Differential subcellular targeting of glutamate receptor subtypes during homeostatic synaptic plasticity. J Neurosci 33:13547-13559.
Soden ME, Chen L (2010) Fragile X protein FMRP is required for homeostatic plasticity and regulation of synaptic strength by retinoic acid. J Neurosci 30:16910-16921.
Son J, Song S, Lee S, Chang S, Kim M (2011) Morphological change tracking of dendritic spines based on structural features. Journal of microscopy 241:261-272.
Song S, Miller KD, Abbott LF (2000) Competitive Hebbian learning through spike-timing-dependent synaptic plasticity. Nat Neurosci 3:919-926.
Spacek J, Harris KM (1997) Three-dimensional organization of smooth endoplasmic reticulum in hippocampal CA1 dendrites and dendritic spines of the immature and mature rat. J Neurosci 17:190-203.
Spruston N (2008) Pyramidal neurons: dendritic structure and synaptic integration. Nat Rev Neurosci 9:206-221.
Stevens CF, Wang Y (1995) Facilitation and depression at single central synapses. Neuron 14:795-802.
Stoppini L, Buchs PA, Muller D (1991) A simple method for organotypic cultures of nervous tissue. J Neurosci Methods 37:173-182.
Stuart G, Spruston N, Hausser M (2007) Dendrites, 2nd Edition: Oxford University Press.
Sudhof TC (2004) The synaptic vesicle cycle. Annu Rev Neurosci 27:509-547.
Sullivan TJ, de Sa VR (2006) Homeostatic synaptic scaling in self-organizing maps. Neural Netw 19:734-743.
Sullivan TJ, de Sa VR (2008) Sleeping our way to weight normalization and stable learning. Neural Comput 20:3111-3130.
Sutton MA, Schuman EM (2006) Dendritic protein synthesis, synaptic plasticity, and memory. Cell 127:49-58.
Sutton MA, Ito HT, Cressy P, Kempf C, Woo JC, Schuman EM (2006) Miniature neurotransmission stabilizes synaptic function via tonic suppression of local dendritic protein synthesis. Cell 125:785-799.
Svoboda K, Mainen ZF (1999) Synaptic [Ca2+]: intracellular stores spill their guts. Neuron 22:427-430.

Svoboda K, Yasuda R (2006) Principles of two-photon excitation microscopy and its applications to neuroscience. Neuron 50:823-839.
Svoboda K, Tank DW, Denk W (1996) Direct measurement of coupling between dendritic spines and shafts. Science 272:716-719.
Takahashi N, Kitamura K, Matsuo N, Mayford M, Kano M, Matsuki N, Ikegaya Y (2012) Locally synchronized synaptic inputs. Science 335:353-356.
Takasaki K, Sabatini BL (2014) Super-resolution 2-photon microscopy reveals that the morphology of each dendritic spine correlates with diffusive but not synaptic properties. Frontiers in neuroanatomy 8:29.
Takumi Y, Ramirez-Leon V, Laake P, Rinvik E, Ottersen OP (1999) Different modes of expression of AMPA and NMDA receptors in hippocampal synapses. Nat Neurosci 2:618-624.
Tanaka J, Horiike Y, Matsuzaki M, Miyazaki T, Ellis-Davies GC, Kasai H (2008) Protein synthesis and neurotrophin-dependent structural plasticity of single dendritic spines. Science 319:1683-1687.
Thiagarajan TC, Lindskog M, Tsien RW (2005) Adaptation to synaptic inactivity in hippocampal neurons. Neuron 47:725-737.
Thiagarajan TC, Lindskog M, Malgaroli A, Tsien RW (2007) LTP and adaptation to inactivity: overlapping mechanisms and implications for metaplasticity. Neuropharmacology 52:156-175.
Thivierge JP, Cisek P (2008) Nonperiodic synchronization in heterogeneous networks of spiking neurons. J Neurosci 28:7968-7978.
Tonnesen J, Katona G, Rozsa B, Nagerl UV (2014) Spine neck plasticity regulates compartmentalization of synapses. Nat Neurosci.
Toyoizumi T, Pfister JP, Aihara K, Gerstner W (2005) Generalized Bienenstock-Cooper-Munro rule for spiking neurons that maximizes information transmission. Proc Natl Acad Sci U S A 102:5239-5244.
Toyoizumi T, Pfister JP, Aihara K, Gerstner W (2007) Optimality model of unsupervised spike-timing-dependent plasticity: synaptic memory and weight distribution. Neural Comput 19:639-671.
Traynelis SF, Silver RA, Cull-Candy SG (1993) Estimated conductance of glutamate receptor channels activated during EPSCs at the cerebellar mossy fiber-granule cell synapse. Neuron 11:279-289.
Traynelis SF, Wollmuth LP, McBain CJ, Menniti FS, Vance KM, Ogden KK, Hansen KB, Yuan H, Myers SJ, Dingledine R (2010) Glutamate receptor ion channels: structure, regulation, and function. Pharmacol Rev 62:405-496.
Treiman M, Caspersen C, Christensen SB (1998) A tool coming of age: thapsigargin as an inhibitor of sarco-endoplasmic reticulum Ca(2+)-ATPases. Trends Pharmacol Sci 19:131-135.
Triller A, Choquet D (2005) Surface trafficking of receptors between synaptic and extrasynaptic membranes: and yet they do move! Trends Neurosci 28:133-139.
Tsay D, Yuste R (2004) On the electrical function of dendritic spines. Trends Neurosci 27:77-83.
Tsay D, Dudman JT, Siegelbaum SA (2007) HCN1 channels constrain synaptically evoked Ca2+ spikes in distal dendrites of CA1 pyramidal neurons. Neuron 56:1076-1089.
Turrigiano G (2011) Too many cooks? Intrinsic and synaptic homeostatic mechanisms in cortical circuit refinement. Annu Rev Neurosci 34:89-103.
Turrigiano G (2012) Homeostatic synaptic plasticity: local and global mechanisms for stabilizing neuronal function. Cold Spring Harb Perspect Biol 4:a005736.
Turrigiano GG (1999) Homeostatic plasticity in neuronal networks: the more things change, the more they stay the same. Trends Neurosci 22:221-227.
Turrigiano GG (2008) The self-tuning neuron: synaptic scaling of excitatory synapses. Cell 135:422-435.
Turrigiano GG, Nelson SB (2004) Homeostatic plasticity in the developing nervous system. Nat Rev Neurosci 5:97-107.

Turrigiano GG, Leslie KR, Desai NS, Rutherford LC, Nelson SB (1998) Activity-dependent scaling of quantal amplitude in neocortical neurons. Nature 391:892-896.
Tyler WJ, Pozzo-Miller L (2003) Miniature synaptic transmission and BDNF modulate dendritic spine growth and form in rat CA1 neurones. J Physiol 553:497-509.
van Atteveldt N, Murray MM, Thut G, Schroeder CE (2014) Multisensory Integration: Flexible Use of General Operations. Neuron 81:1240-1253.
Varga Z, Jia H, Sakmann B, Konnerth A (2011) Dendritic coding of multiple sensory inputs in single cortical neurons in vivo. Proc Natl Acad Sci U S A 108:15420-15425.
Verkhratsky A, Krishtal OA, Petersen OH (2006) From Galvani to patch clamp: the development of electrophysiology. Pflugers Arch 453:233-247.
Verstreken P, Bellen HJ (2001) Neuroscience. The meaning of a mini. Science 293:443-444.
Verstreken P, Bellen HJ (2002) Meaningless minis? Mechanisms of neurotransmitter-receptor clustering. Trends Neurosci 25:383-385.
Vicini S, Wang JF, Li JH, Zhu WJ, Wang YH, Luo JH, Wolfe BB, Grayson DR (1998) Functional and pharmacological differences between recombinant N-methyl-D-aspartate receptors. J Neurophysiol 79:555-566.
Wang HX, Gerkin RC, Nauen DW, Bi GQ (2005) Coactivation and timing-dependent integration of synaptic potentiation and depression. Nat Neurosci 8:187-193.
Wang XB, Yang Y, Zhou Q (2007) Independent expression of synaptic and morphological plasticity associated with long-term depression. J Neurosci 27:12419-12429.
Watt AJ, Desai NS (2010) Homeostatic Plasticity and STDP: Keeping a Neuron's Cool in a Fluctuating World. Front Synaptic Neurosci 2:5.
Watt AJ, van Rossum MC, MacLeod KM, Nelson SB, Turrigiano GG (2000) Activity coregulates quantal AMPA and NMDA currents at neocortical synapses. Neuron 26:659-670.
Webb CB, Cope TC (1992) Modulation of la EPSP amplitude: the effects of chronic synaptic inactivity. J Neurosci 12:338-344.
Whitford KL, Dijkhuizen P, Polleux F, Ghosh A (2002) Molecular control of cortical dendrite development. Annu Rev Neurosci 25:127-149.
Whitlock JR, Heynen AJ, Shuler MG, Bear MF (2006) Learning induces long-term potentiation in the hippocampus. Science 313:1093-1097.
Wijetunge LS, Angibaud J, Frick A, Kind PC, Nagerl UV (2014) Stimulated emission depletion (STED) microscopy reveals nanoscale defects in the developmental trajectory of dendritic spine morphogenesis in a mouse model of fragile X syndrome. J Neurosci 34:6405-6412.
Winnubst J, Lohmann C (2012) Synaptic clustering during development and learning: the why, when, and how. Front Mol Neurosci 5:70.
Wong M (2005) Advances in the pathophysiology of developmental epilepsies. Semin Pediatr Neurol 12:72-87.
Wong RK, Prince DA, Basbaum AI (1979) Intradendritic recordings from hippocampal neurons. Proc Natl Acad Sci U S A 76:986-990.
Wu YW, Grebenyuk S, McHugh TJ, Rusakov DA, Semyanov A (2012) Backpropagating action potentials enable detection of extrasynaptic glutamate by NMDA receptors. Cell reports 1:495-505.
Yasuda R, Nimchinsky EA, Scheuss V, Pologruto TA, Oertner TG, Sabatini BL, Svoboda K (2004) Imaging calcium concentration dynamics in small neuronal compartments. Sci STKE 2004:pl5.
Yeung LC, Shouval HZ, Blais BS, Cooper LN (2004) Synaptic homeostasis and input selectivity follow from a calcium-dependent plasticity model. Proc Natl Acad Sci U S A 101:14943-14948.
Yudowski GA, Puthenveedu MA, Leonoudakis D, Panicker S, Thorn KS, Beattie EC, von Zastrow M (2007) Real-time imaging of discrete exocytic events mediating surface delivery of AMPA receptors. J Neurosci 27:11112-11121.

Yuste R (2010) Dendritic spines. Cambridge: The MIT Press.
Yuste R, Denk W (1995) Dendritic spines as basic functional units of neuronal integration. Nature 375:682-684.
Yuste R, Bonhoeffer T (2001) Morphological changes in dendritic spines associated with long-term synaptic plasticity. Annu Rev Neurosci 24:1071-1089.
Yuste R, Majewska A, Holthoff K (2000) From form to function: calcium compartmentalization in dendritic spines. Nat Neurosci 3:653-659.
Zecevic N, Bourgeois JP, Rakic P (1989) Changes in synaptic density in motor cortex of rhesus monkey during fetal and postnatal life. Brain research Developmental brain research 50:11-32.
Zhou Q, Homma KJ, Poo MM (2004) Shrinkage of dendritic spines associated with long-term depression of hippocampal synapses. Neuron 44:749-757.
Zhu JJ, Malinow R (2002) Acute versus chronic NMDA receptor blockade and synaptic AMPA receptor delivery. Nat Neurosci 5:513-514.
Zito K, Scheuss V, Knott G, Hill T, Svoboda K (2009) Rapid functional maturation of nascent dendritic spines. Neuron 61:247-258.
Zucker RS, Regehr WG (2002) Short-term synaptic plasticity. Annual review of physiology 64:355-405.

Appendix A

Iterative test for multiplicative scaling in MATLAB used in Manuscript III (Soares, Lee, et al. 2013). Save and run the following code as a '.m' file:

--

```
% This script performs an iterative Kolmogorov-Smirnov Test of mEPSC as
described by Kim, Tsien & Alger (PLoS One, 2012)
% Fill (paste) columns 1 and 2 in dat matrix with mEPSC amplitudes (pooled
distributions) from control and treated neurons

% mEPSC amplitude vectors can be different lengths

% dat = [];
% control data in column 1; treated data in column 2
control = dat(:,1);
treated = dat(:,2)

pvalues=[];
k = 1;

% Define scaling factor range to be tested:
% from
low = 0;
% to
high = 2;
% interval
int = 0.001;

for i = low:int:high
    scaled = treated./i;
    [h p] = kstest2(control,scaled);
    pvalues(k) = p;
    k = k+1;
end

scaling_factors = low:int:high;
plot(scaling_factors,pvalues,'.')
% xlim([1.13 1.21])

pmax = max(pvalues);
loc = find(pvalues == pmax);
best_scaling_factor = low+(loc*int);

summarydata(:,1) = scaling_factors;
summarydata(:,2) = pvalues;
summarydata(1:length(best_scaling_factor),3) = best_scaling_factor;
summarydata(1:length(pmax),4) = pmax;
```

--

Appendix B

Analysis for Frame Scan calcium imaging experiments

1) **Identifying regions of interest (ROIs)**
- Draw circular ROIs using Fluoview software
- *First*, place a large ROI in a background region
- *Then* place 1 µm ROIs along the dendrite of interest
- Save .oib file

2) **Data extraction using ImageJ**
- This macro was developed by Cary Soares
- Saved as a .txt file, this macro can be run in ImageJ

Copy and paste the following text in a notepad and save it as a .txt file.

```
--

for (i=0; i<X; i++)
{
      setSlice(1);
      roiManager("Select", i);
      for (j=0; j<Y; j++)
      {
            run("Measure");
            run("Next Slice [>]");
      }
}

--
```

Change the value of 'X' to the number of ROIs in the experiment.
Change the value of 'Y' to the total number of frames to be analyzed at each ROI.

Run the macro using (Plugins > Macros > Run)
The output will be a string of values of length (X*Y), and this data will be processed in MATLAB.

Note:
- Dendrite data strings should be extracted separate from spine data strings. It is up to the user to maintain organization of the dataset.
- Data from both RED (*i.e.,* Alexa 594 for morphology) and GREEN (*i.e.,* Fluo-4FF calcium indicator) channels should be extracted

3) **Data processing using MATLAB**

Data extracted from each frame scan sweep should be pasted into individual MATLAB matrices and saved as individual variables in a .mat file, as follows:

```
green = []; % dendrite 4FF calcium
red = []; % dendrite alexa
% % %
```

```
spgreen = []; % spine 4FF calcium
spred = []; % spine alexa
% % %
ROIs = []; % number of ROIs
timepts = []; % number of frames
```

Re-shape the linearized dataset back into the spatial relationships between adjacent ROIs with the following code (Key outputs, dendritic calcium matrix (den_dGR) and spine calcium signal (spine_dGR):

--

```
% Process spine data by setting aa = 1, dendrite data with aa = 2

keep spgreen spred green red ROIs timepts

aa = 0;
% close all

if aa == 1
    ROIs = 2;
    g = spgreen;
    r = spred;
else
    ROIs = length(green)/timepts;
    g = green;
    r = red;
end

green_FL = g(:,3); red_FL = r(:,3);
green_area = g(:,2); red_area = r(:,2);
sorted_green = []; sorted_green_area = [];
sorted_red = []; sorted_red_area = [];

for gg = 1:ROIs
    sorted_green(:,gg) = green_FL(((gg-1)*timepts)+1:gg*timepts);
    sorted_red(:,gg) = red_FL(((gg-1)*timepts)+1:gg*timepts);
    sorted_green_area(:,gg) = green_area(((gg-1)*timepts)+1:gg*timepts);
    sorted_red_area(:,gg) = red_area(((gg-1)*timepts)+1:gg*timepts);
end

green_data = sorted_green(:,2:end).*sorted_green_area(:,2:end);
red_data = sorted_red(:,2:end).*sorted_red_area(:,2:end);
red_data_mean = nanmean(red_data);
red_mean = repmat(red_data_mean,[timepts,1,1]);

background_green = nanmean(sorted_green(:,1));
background_green_mat = repmat(background_green,[timepts,ROIs,1]);
G_background = background_green_mat(:,2:end).*sorted_green_area(:,2:end);

% subtract background green and normalize to red
G = green_data - background_green_mat(:,1:ROIs-1,1);
GR = G./red_mean;
GRmin = min(GR);
% subtract minimum to yield positive fluorescence values
```

```
GRmin_mat = repmat(GRmin,[timepts,1,1]);
GRprime = GR - GRmin_mat;

% normalize to baseline
baseline = nanmean(GRprime(1:4,:));
baseline_std = mean(nanstd(GRprime(1:15,:)));
baseline_mat = repmat(baseline,[timepts,1,1]);
dGR = (GRprime - baseline_mat)./baseline_mat;

den_dGR = dGR;

if aa == 0
%     calculate dendrite peaks
    ROI_peaks = max(den_dGR);
    [r,c] = size(ROI_peaks);
    for ii = 1:c
        ptimes = find(den_dGR(:,ii) == ROI_peaks(ii));
        peaktime(ii) = ptimes(1);
        if peaktime(ii) > 1 & peaktime(ii) < 40
            peaks(ii) = mean(den_dGR(peaktime(ii)-1:peaktime(ii)+1,ii));
            peaktimes(ii) = peaktime(ii);
        else
%             peaks(ii) = NaN;
            peaks(ii) = ROI_peaks(ii);
            peaktimes(ii) = peaktime(ii);
        end
    end

    den_peak = max(peaks);

%     calculate calcium spread (fwhm)
    wave_profile = smooth(peaks);
    [r,c] = size(wave_profile);
    dFWHM = fwhm(1:r,wave_profile);

%     calculate dendritic signal mean
    noise_threshold = mean(baseline) + 3*(baseline_std);
    signal_ROIs = find(peaks > mean(baseline) + 3*baseline_std);
    dcat_mean = nanmean(dGR(:,signal_ROIs),2);

    figure;
    pcolor(den_dGR)
    shading interp
    colormap hot
    caxis([noise_threshold max(max(den_dGR))])
%     ylim ([1 timepts])
    ylim([10 70])
    caxis([max(baseline) max(max(den_dGR))])
%     caxis([1+max(baseline) 25])
%     caxis([1 5])
    title('delta G/R')

%     figure;
%     hold off
%     plot(den_dGR,'LineWidth',1);hold on;
%     plot(dcat_mean,'-r','LineWidth',5);
%     ylim([-2 1.1*max(max(den_dGR))]);
```

```
%     xlim([1 timepts]);
%     title('dcat')
end
% % % % % % % % % % % % % % % % % % % %
% % SPINE fluorescence
% % % % % % % % % % % % % % % % % % % %

if isempty(spgreen) == 0
    ROIs = 2;
    g = spgreen;
    r = spred;
    timepts = length(spgreen)/ROIs;

    green_FL = g(:,3); red_FL = r(:,3);
    green_area = g(:,2); red_area = r(:,2);
    sorted_green = []; sorted_green_area = [];
    sorted_red = []; sorted_red_area = [];

    for gg = 1:ROIs
        sorted_green(:,gg) = green_FL(((gg-1)*timepts)+1:gg*timepts);
        sorted_red(:,gg) = red_FL(((gg-1)*timepts)+1:gg*timepts);
        sorted_green_area(:,gg) = green_area(((gg-1)*timepts)+1:gg*timepts);
        sorted_red_area(:,gg) = red_area(((gg-1)*timepts)+1:gg*timepts);
    end

    green_data = sorted_green(:,2:end).*sorted_green_area(:,2:end);
    red_data = sorted_red(:,2:end).*sorted_red_area(:,2:end);
    red_data_mean = nanmean(red_data);
    red_mean = repmat(red_data_mean,[timepts,1,1]);

    background_green = nanmean(sorted_green(:,1));
    background_green_mat = repmat(background_green,[timepts,ROIs,1]);
    G_background = background_green_mat(:,2:end).*sorted_green_area(:,2:end);

    % normalize to red (G/R) and subtract background (G/R min)
    G = green_data - background_green_mat(:,1:ROIs-1,1);
    GR = G./red_mean;
    GRmin = min(GR);
    % subtract minimum to yield positive fluorescence values
    GRmin_mat = repmat(GRmin,[timepts,1,1]);
    GRprime = GR - GRmin_mat;

    % normalize to baseline
    baseline = nanmean(GRprime(1:4,:));
    baseline_std = mean(nanstd(GRprime(1:4,:)));
    baseline_mat = repmat(baseline,[timepts,1,1]);

    dGR = (GRprime - baseline_mat)./baseline_mat;
    spine_dGR = dGR;

    %     calculate spine peak
    spinepeak = max(spine_dGR(2:end-1));
    peaktime = find(spine_dGR == spinepeak);
    spine_peak = mean(spine_dGR(peaktime-1:peaktime+1));
end
```

```
% summary
% dcat = dcat_mean';
% scat = spine_dGR';
% fluo_data = [spine_peak,den_peak,dFWHM];

figure;plot(dGR(:,1:end-2))

return % this stops the script here; comment out to continue below

% tally signal successes and failures
% total number of successes may be used at “propagation distance”
%
x = nonZeroVec(dGR); x = x';
xbaseline = x(1:4,:);
baseline_mean = nanmean(xbaseline);
xstd = nanstd(xbaseline);
noise = baseline_mean + 2*xstd;

[r,c] = size(x);
for i = 1:c
    trace = x(:,i);
    tracepeak = max(trace(2:end-1));
    traceind = find(trace == tracepeak);
    avgpeak(i) = nanmean(trace(traceind-1:traceind+1));
    if avgpeak(i) > noise(i)
        success(i) = 1;
    else
        success(i) = 0;
    end
end

success = success';
avgpeak = avgpeak';
```

--

Comments on the analysis:

The number of pre-stimulus frames (baseline) must be defined according to the experimental design.
Data output from this code can be exported and analyzed in other software programs.
For example, the dendritic calcium map (den_dGR) can be plotted as a pseudo-color heatmap in MATLAB for figures, but can also be compressed into a single mean calcium signal to represent the dendritic calcium behavior. Spine calcium signals (spine_dGR) are single fluorescence time series.
Analysis of decay kinetics can be performed on peak-normalized and peak-aligned calcium signals in Origin.
Spatial calcium spread can be calculated as the user wishes. For Manuscript V, I used the full-width of half-maximum of smoothed dendritic calcium profiles. Total spread may be calculated simply by counting the number of 1μm ROIs that showed a positive calcium signal. Continuity between ROIs is difficult to define and generalize between experiments, but clever code writing may overcome this minor obstacle.

Appendix C

Analysis for Line Scan calcium imaging experiments

1) Use ImageJ to save line scan data as .tiff files
2) Each experiment (sweep) should have individual green and red .tiff files
3) Name the .tiff files with 'green' and 'red' at the end of the file name
   For example, .tiff files for data from cell 1001, sweep 12 might be saved as '100112green' and '100112red'
4) Sort the .tiff files into individual folders according to experimental conditions, the script will analyze an entire folder and output results organized according to the file names.
5) There should be no other files in the folder to be analyzed. (.tiffs *only*)

Outputs:

For line scans where two compartments are detected, calcium signals will be separated into '**spine**' and '**dend**' outputs based on their different rise-times.
For line scans where distinct compartments could not be discerned, calcium signals will be output into 'spOnly'.

I wrote the short script '**find_breaks.m**', which is used in this analysis.

Save and run the following codes:

```
--

% save this script as 'find_breaks.m';

function [breaks] = find_breaks(vector)

i = length(vector);
output = ones(i,1);
for k = 1:i-1
    dif(k,1) = vector(k+1) - vector(k);
    output = dif;
end
breaks = find(output ~= 1);

--

clear all;
% close all;
clc;


% Make sure the folder of interest is in the search path
% lines will populate a vector with file names
addpath('C:\Users\Owner\Desktop');
addpath('C:\Users\Kevin\Desktop\New Folder');
lines = load_dir('C:\Users\Kevin\Desktop\New Folder');

lines_names = lines(4:end);
lines_names = sort(lines_names);
```

```
clear lines

green = [];
red = [];

averaging_factor = 10;
line_time = 0.244; % milliseconds
time_factor = averaging_factor*line_time;

k = 0;
j = 0;
slot = 1;

for i = 1:length(lines_names(1,1:end));
    disp(i)

    line = imread(sprintf('%s', lines_names{i})); %loads all variables into
workspace
    line = imrotate(line,90);
    [numrows numcols] = size(line);
    line = imresize(line, [numrows numcols/averaging_factor], 'bilinear');
    background_avg = mean(mean(line(1:10,:)));
    background_SD = std(mean(line(1:10,:)));
    baseline_avg = mean(mean(line(:,1:100),2));
    baseline_SD = std(mean(line(:,1:100),2));
    signal_range = range(line);
    sig_sorted = sort(mean(line));
    peakavg = mean(sig_sorted(900:1000));

% % Odd numbers in lines_names refers to "green" channel
    oddmat = 1:2:length(lines_names);
    odd = find(oddmat == i);
    even = isempty(odd);

    if even == 0
        green = line - background_avg;
        green = double(green) + 1;
        red=[];
    else
        red = line - background_avg;
        red = double(red) + 1;
    end

    empty = isempty(red);
    if empty == 0
        background_red = red(1:10,:);
        SDred = mean(std(background_red));

        red_signal = mean(red(:,1:100),2);
        signal_ind = find(red_signal > 3*SDred);
        baseline_red = red_signal(signal_ind(1,1):signal_ind(end,1),:);
        baseline_red = mean(baseline_red);
        red = red./baseline_red;

%         SIMPLIFIED COMPARTMENT IDENTIFICATION
```

```
%         average the red channel first, find second derivative, ID indices
%         of negative peaks
%         Output is flagcoords, which identifies the compartments
%         Find local extremum with derivatives of red signal
        [rows columns] = size(red);
        x = 1:columns;
        y = 1:rows;

        redmean = mean(red,2);
        [dredmean_dx] = gradient(redmean);
        [dredmean_dx2] = gradient(dredmean_dx);
        dred_extreme = min(dredmean_dx2(signal_ind(1,1):signal_ind(end,1)));
% % % % SITE FOR MODULATING THE SENSITIVITY OF SECOND COMPARTMENT DETECTION
        dred_extreme_thresh = 0.25*dred_extreme;
        signal_dx2 = dredmean_dx2(signal_ind(1,1):signal_ind(end,1));
        flagcoords = find(signal_dx2 < dred_extreme_thresh);
        flagcoords = flagcoords + signal_ind(1,1);
% % %
        breaks = find_breaks(flagcoords);
        sizebreaks = length(breaks);
        if breaks > 0
            if sizebreaks > 1
                greenpeak1(:,1) = 1:columns;
                greenpeak1(:,2) =
mean(green(flagcoords(1,1):flagcoords(breaks(1)),:));
                greenpeak2(:,1) = 1:columns;
                greenpeak2(:,2) =
mean(green(flagcoords(breaks(1)+1):flagcoords(end),:));
            elseif sizebreaks == 1
                greenpeak1(:,1) = 1:columns;
                greenpeak1(:,2) =
mean(green(flagcoords(1,1):flagcoords(breaks),:));
                greenpeak2(:,1) = 1:columns;
                greenpeak2(:,2) =
mean(green(flagcoords(breaks+1):flagcoords(end),:));
            end

            greenpeak1 = greenpeak1(:,2);
            greenpeak2 = greenpeak2(:,2);

            rough_norm_base1 = mean(greenpeak1(50:130));
            rough_norm_base2 = mean(greenpeak2(50:130));
            greenpeak1 = greenpeak1./rough_norm_base1;
            greenpeak2 = greenpeak2./rough_norm_base2;

            % % % % % % % % % % % % % % % % % % % % % % % % % % % % % % %
            % % % % % % % % % % % % % % % % % % % % % % % % % % % % % % %
            %         BUTTERWORTH FILTER
            acquisitionRate = 500; %your data acquisition rate in Hz (account
for averaging_factor at start)
            filterFreq = 20; %frequency of filtering (Hz); everything above
that gets cut (play around with that value
            [b,a]=butter(2,1/(acquisitionRate/filterFreq),'low'); %2nd order
butterworth low-pass filter with xHz cutoff (500/x)
            filtered_x1 = filter(b,a,greenpeak1); % filtered signal 1
            filtered_x2 = filter(b,a,greenpeak2); % filtered signal 2
```

```
% %          New baseline preceding peak
             peakfiltered_x1 = max(filtered_x1);
             peaktime1 = find(filtered_x1 == peakfiltered_x1);
             on1 = min(filtered_x1(peaktime1-round(peaktime1/2):peaktime1));
             mp1 = find(filtered_x1 == on1);
             new_base1 = mean(filtered_x1(mp1-(mp1-1):mp1));
             filtered_x1 = filtered_x1./new_base1;

             peakfiltered_x2 = max(filtered_x2);
             peaktime2 = find(filtered_x2 == peakfiltered_x2);
             on2 = min(filtered_x2(peaktime2-round(peaktime2/2):peaktime2));
             mp2 = find(filtered_x2 == on2);
             new_base2 = mean(filtered_x2(mp2-(mp2-1):mp2));
             filtered_x2 = filtered_x2./new_base2;

% % %        New normalized maximum
             abs_peak1 = max(filtered_x1(100:500));
             abs_peak2 = max(filtered_x2(100:500));

             max1 = find(filtered_x1 == abs_peak1);
% % %        peak amplitude will be reported as mean around the peak (~10ms)
             meanpeak1 = mean(filtered_x1((max1-2):(max1+2)),1);
             max2 = find(filtered_x2 == abs_peak2);
             meanpeak2 = mean(filtered_x2((max2-2):(max2+2)),1);

% % Find CaT onset time using variability in the length of intervals above
1.0
             onset1 = filtered_x1 < 1;
             onset1 = onset1*1; onset1 = nonZeroVec(onset1);
             onset1(end,1) = 1;
             onset2 = filtered_x2 < 1;
             onset2 = onset2*1; onset2 = nonZeroVec(onset2);
             onset2(end,1) = 1;
             on_intervals1 = find(onset1 == 1);
             on_intervals2 = find(onset2 == 1);
             clear diffs1 diffs2
             for k = 1:length(on_intervals1)-1
                 diffs1(k,1) = on_intervals1(k+1) - on_intervals1(k);
             end
             for k = 1:length(on_intervals2)-1
                 diffs2(k,1) = on_intervals2(k+1) - on_intervals2(k);
             end
             ind1 = find(diffs1 == max(diffs1));
             ind2 = find(diffs2 == max(diffs2));
% % % % % % Calcium transient ONSET TIME
             onset_time1 = on_intervals1(ind1(1));
             onset_time2 = on_intervals2(ind2(1));
             risetime1 = peaktime1 - onset_time1;
             risetime2 = peaktime2 - onset_time2;
% % % % % % Calculate times at 66% rise and decay (tau value)

             sorted_decay1 = sort(filtered_x1(peaktime1:end),'descend');
             sorted_decay2 = sort(filtered_x2(peaktime2:end),'descend');
             TAUdiff1 = (max(sorted_decay1)-min(sorted_decay1))*0.368;
             TAUamp1 = min(sorted_decay1) + TAUdiff1;
```

```
TAUdiff2 = (max(sorted_decay2)-min(sorted_decay2))*0.368;
TAUamp2 = min(sorted_decay2) + TAUdiff2;

for k = 1:length(sorted_decay1)-1
    decdiffs1(k,1) = abs(sorted_decay1(k+1) - TAUamp1);
end
TAUtime1 = find(decdiffs1 == min(decdiffs1));
decayTAU1 = TAUtime1;
for k = 1:length(sorted_decay2)-1
    decdiffs2(k,1) = abs(sorted_decay2(k+1) - TAUamp2);
end
TAUtime2 = find(decdiffs2 == min(decdiffs2));
decayTAU2 = TAUtime2;

if onset_time1 < onset_time2
    spine_cat = filtered_x1;
    dend_cat = filtered_x2;
    spine_peak = meanpeak1;
    spine_cat_onset = onset_time1;
    spine_risetime = risetime1;
    spine_decay = decayTAU1;
    dend_peak = meanpeak2;
    dend_cat_onset = risetime2;
    dend_risetime = risetime2;
    dend_decay = decayTAU2;
else
    spine_cat = filtered_x2;
    dend_cat = filtered_x1;
    spine_peak = meanpeak2;
    spine_cat_onset = onset_time2;
    spine_risetime = risetime2;
    spine_decay = decayTAU2;
    dend_peak = meanpeak1;
    dend_cat_onset = risetime1;
    dend_risetime = risetime1;
    dend_decay = decayTAU1;
end

spine(:,i) = spine_cat;
dend(:,i) = dend_cat;

if slot == 1
    twocomp_data(1,1) = spine_peak;
    twocomp_data(1,2) = spine_cat_onset*time_factor;
    twocomp_data(1,3) = spine_risetime*time_factor;
    twocomp_data(1,4) = spine_decay*time_factor;
    twocomp_data(1,5) = dend_peak;
    twocomp_data(1,6) = dend_cat_onset*time_factor;
    twocomp_data(1,7) = dend_risetime*time_factor;
    twocomp_data(1,8) = dend_decay*time_factor;
else
    twocomp_data(slot,1) = spine_peak;
    twocomp_data(slot,2) = spine_cat_onset*time_factor;
    twocomp_data(slot,3) = spine_risetime*time_factor;
    twocomp_data(slot,4) = spine_decay*time_factor;
    twocomp_data(slot,5) = dend_peak;
```

```
                twocomp_data(slot,6) = dend_cat_onset*time_factor;
                twocomp_data(slot,7) = dend_risetime*time_factor;
                twocomp_data(slot,8) = dend_decay*time_factor;
            end

        else

% % % % % % % % % % % % % % % % % % % % % % % % % % % % % % % % % % % % % % % % % %
%             FOR SPINES NOT DISTINGUISHED FROM PARENT DENDRITE
% % % % % % % % % % % % % % % % % % % % % % % % % % % % % % % % % % % % % % % % % %

            greenpeak = mean(green(signal_ind(1,1):signal_ind(end,1),:));
            rough_norm_base = mean(greenpeak(50:130));
            greenpeak = greenpeak./rough_norm_base;

            filtered_x = filter(b,a,greenpeak); % filtered signal 1

            peakfiltered_x = max(filtered_x);
%
%             New baseline preceding peak
            peaktime = find(filtered_x == peakfiltered_x);
            on = min(filtered_x(peaktime-round(peaktime/2):peaktime));
            mp = find(filtered_x == on);
            new_base = mean(filtered_x(mp-(mp-1):mp));
            filtered_x = filtered_x./new_base;

% % %       New normalized maximum
            abs_peak = max(filtered_x);
            onemax = find(filtered_x == abs_peak);
% % %       peak amplitude will be reported as mean around the peak (~10ms)
%             meanpeak = mean(mean(filtered_x((onemax-2):(onemax+2)),1));
            meanpeak = abs_peak;

% % Find CaT onset time using variability in the length of intervals above
1.0
            onset = filtered_x < 1;
            onset = onset*1; onset = nonZeroVec(onset);
            onset(end,1) = 1;
            on_intervals = find(onset == 1);
            clear diffs
            for k = 1:length(on_intervals)-1
                diffs(k,1) = on_intervals(k+1) - on_intervals(k);
            end
            ind = find(diffs == max(diffs));

% % % % % % Calcium transient ONSET TIME
            onset_time = on_intervals(ind(1));
            risetime = peaktime - onset_time;
% % % % % % Calculate times at 66% rise and decay (tau value)
            sorted_decay = sort(filtered_x(peaktime:end),'descend');
            TAUdiff = (max(sorted_decay)-min(sorted_decay))*0.368;
            TAUamp = min(sorted_decay) + TAUdiff;

            for k = 1:length(sorted_decay)-1
                decdiffs(k,1) = abs(sorted_decay(k+1) - TAUamp);
```

```
            end
            TAUtime = find(decdiffs == min(decdiffs));
            decayTAU = TAUtime;

            one_peak = meanpeak;
            one_cat_onset = onset_time;
            one_risetime = risetime;
            one_decay = decayTAU;

            spOnly(:,i) = filtered_x;

            if slot == 1
                onecomp_data(1,1) = one_peak;
                onecomp_data(1,2) = one_cat_onset*time_factor;
                onecomp_data(1,3) = one_risetime*time_factor;
                onecomp_data(1,4) = one_decay*time_factor;
            else
                onecomp_data(slot,1) = one_peak;
                onecomp_data(slot,2) = one_cat_onset*time_factor;
                onecomp_data(slot,3) = one_risetime*time_factor;
                onecomp_data(slot,4) = one_decay*time_factor;
            end
%             figure(2)
%             hold on
%             plot(filtered_x,'k.')
%             plot(0:1000,1,'g')
%             plot(0:1000,one_peak,'k')
%             plot(0:1000,on_cat_onset,'k')
%             plot(0:1000,decayTAU+peaktime,'k')
        end
        slot = slot + 1;
    end
end

[r c] = size(twocomp_data);
for i = 1:r
    if twocomp_data(i,2) > 500
        twocomp_data(i,2) = NaN;
    end
    if twocomp_data(i,2) < 0
        twocomp_data(i,2) = NaN;
    end
    if twocomp_data(i,6) > 500
        twocomp_data(i,6) = NaN;
    end
    if twocomp_data(i,6) < 0
        twocomp_data(i,6) = NaN;
    end
end
twocomp_data = nonZeroVec(twocomp_data);

spine = nonZeroVec(spine);
dend = nonZeroVec(dend);
N = sum(spine(1,:) > 0);

sp_onset_mean = round(nanmean(twocomp_data(:,2))/time_factor);
```

```
spine_base = nanmean(nanmean(spine(20:sp_onset_mean,:),2));
mean_spine = nanmean(spine,2);
mean_spine = mean_spine/spine_base;
sem_spine = nanstd(spine,0,2)./spine_base;
sem_spine = sem_spine./sqrt(N);

d_onset_mean = round(nanmean(twocomp_data(:,6))/time_factor);
dend_base = nanmean(nanmean(dend(20:d_onset_mean,:),2));
mean_dend = nanmean(dend,2);
mean_dend = mean_dend/dend_base;
sem_dend = nanstd(dend,0,2)./dend_base;
sem_dend = sem_dend./sqrt(N);

figure(4);plot(mean_spine,'r.','LineWidth',5);
hold on;
plot(mean_spine+sem_spine,'r')
plot(mean_spine-sem_spine,'r')
plot(mean_dend,'k','LineWidth',5)
plot(mean_dend+sem_dend,'k')
plot(mean_dend-sem_dend,'k')

--
```

Appendix D

Synaptic weight clustering analysis

These analyses utilize Monte Carlo type shuffling methods to generate synthetic datasets reflecting 'random chance' using experimental data.

There are two important codes that need to be saved in the MATLAB search path:

shuffle.m
fdr_bh.m

1) Shuffling requires the function '**shuffle.m**', which was downloaded online from MATLAB central. Save the following code in the appropriate directory for use in MATLAB.

--

```
function [s,myorder]=shuffle(x,varargin)

%SHUFFLE    Shuffles vectors or matrices.
%   SHUFFLE(X) shuffles the elements of a vector or matrix X.
%   SHUFFLE(X,DIM) shuffles along the dimension DIM.
%   [Y,I] = SHUFFLE(X) also returns an index matrix I. If X is
%   a vector, then Y = X(I). If X is an m-by-n matrix, then
%       for j = 1:n, Y(:,j) = X(I(:,j),j); end
%
%   Input arguments:
%      X - the vector or matrix to shuffle (array)
%      DIM - the dimension along which to shuffle (integer)
%   Output arguments:
%      Y - the vector or matrix with the elements shuffled (array)
%      I - the index matrix with the shuffle order (array)
%
%   Examples:
%      X = [10 25 30 40]
%      [Y,I] = SHUFFLE(X)
%      Y = 30    25    10    40
%      I =  3     2     1     4
%
%      X = [10 25 ; 3.2 4.1 ; 102 600]
%      [Y,I] = SHUFFLE(X)
%      Y =   3.2000  600.0000
%           10.0000   25.0000
%          102.0000    4.1000
%      I =  2     3
%           1     1
%           3     2
%
%      X = [10 25 50 ; 3.2 4.1 5.5 ; 102 600 455 ; 0.03 0.34 0.01]
%      DIM = 1
%      [Y,I] = SHUFFLE(X,DIM)
%      Y =  10.0000   25.0000   50.0000
%            0.0300    0.3400    0.0100
%          102.0000  600.0000  455.0000
%            3.2000    4.1000    5.5000
%      I =  1     4     3     2
```

```
%
%      X = [10 25 50 ; 3.2 4.1 5.5 ; 102 600 455 ; 0.03 0.34 0.01]
%      DIM = 2
%      [Y,I] = SHUFFLE(X,DIM)
%      Y =  10.0000   50.0000   25.0000
%            3.2000    5.5000    4.1000
%          102.0000  455.0000  600.0000
%            0.0300    0.0100    0.3400
%      I =  1     3     2
%
%   See also ORDERBY
%
%   Created: Sara Silva (sara@itqb.unl.pt) - 2002.11.02

switch nargin
case 1
   if size(x,1)==1 | size(x,2)==1
      [ans,myorder]=sort(rand(1,length(x)));
      s=x(myorder);
   else
      [ans,myorder]=sort(rand(size(x,1),size(x,2)));
    for c=1:size(x,2)
        s(:,c)=x(myorder(:,c),c);
      end
   end
case 2
   d=varargin{1};
   switch d
   case 1
      [ans,myorder]=sort(rand(1,size(x,1)));
        s=x(myorder,:);
   case 2
      [ans,myorder]=sort(rand(1,size(x,2)));
      s=x(:,myorder);
   otherwise
      error('SHUFFLE: Unknown command option.')
   end
end
```

--

2) The analysis also utilizes the **Benjamini & Hochberg (1995) method** for controlling for false discovery rate (FDR) of hypothesis tests. This is very similar to the Bonferroni method, but argued to be less conservative and more powerful. This code was downloaded online from MATLAB Central.

Save the following code as '**fdr_bh.m**' in a folder in the MATLAB search path.

--

```
% fdr_bh() - Executes the Benjamini & Hochberg (1995) and the Benjamini &
%            Yekutieli (2001) procedure for controlling the false discovery
%            rate (FDR) of a family of hypothesis tests. FDR is the expected
%            proportion of rejected hypotheses that are mistakenly rejected
%            (i.e., the null hypothesis is actually true for those tests).
```

```
%            FDR is a somewhat less conservative/more powerful method for
%            correcting for multiple comparisons than procedures like
Bonferroni
%            correction that provide strong control of the family-wise
%            error rate (i.e., the probability that one or more null
%            hypotheses are mistakenly rejected).
%
% Usage:
%  >> [h, crit_p, adj_p]=fdr_bh(pvals,q,method,report);
%
% Required Input:
%   pvals - A vector or matrix (two dimensions or more) containing the
%           p-value of each individual test in a family of tests.
%
% Optional Inputs:
%   q       - The desired false discovery rate. {default: 0.05}
%   method  - ['pdep' or 'dep'] If 'pdep,' the original Bejnamini & Hochberg
%             FDR procedure is used, which is guaranteed to be accurate if
%             the individual tests are independent or positively dependent
%             (e.g., Gaussian variables that are positively correlated or
%             independent).  If 'dep,' the FDR procedure
%             described in Benjamini & Yekutieli (2001) that is guaranteed
%             to be accurate for any test dependency structure (e.g.,
%             Gaussian variables with any covariance matrix) is used. 'dep'
%             is always appropriate to use but is less powerful than 'pdep.'
%             {default: 'pdep'}
%   report  - ['yes' or 'no'] If 'yes', a brief summary of FDR results are
%             output to the MATLAB command line {default: 'no'}
%
% Outputs:
%   h       - A binary vector or matrix of the same size as the input
"pvals."
%             If the ith element of h is 1, then the test that produced the
%             ith p-value in pvals is significant (i.e., the null hypothesis
%             of the test is rejected).
%   crit_p  - All uncorrected p-values less than or equal to crit_p are
%             significant (i.e., their null hypotheses are rejected).  If
%             no p-values are significant, crit_p=0.
%   adj_p   - All adjusted p-values less than or equal to q are significant
%             (i.e., their null hypotheses are rejected). Note, adjusted
%             p-values can be greater than 1.
%
% References:
%   Benjamini, Y. & Hochberg, Y. (1995) Controlling the false discovery
%     rate: A practical and powerful approach to multiple testing. Journal
%     of the Royal Statistical Society, Series B (Methodological). 57(1),
%     289-300.
%   Benjamini, Y. & Yekutieli, D. (2001) The control of the false discovery
%     rate in multiple testing under dependency. The Annals of Statistics.
%     29(4), 1165-1188.
%
% Example:
%   [dummy p_null]=ttest(randn(12,15)); %15 tests where the null hypothesis
%                                       %is true
%   [dummy p_effect]=ttest(randn(12,5)+1); %5 tests where the null
%                                          %hypothesis is false
%   [h crit_p adj_p]=fdr_bh([p_null p_effect],.05,'pdep','yes');
```

```
%
% For a review on false discovery rate control and other contemporary
% techniques for correcting for multiple comparisons see:
%   Groppe, D.M., Urbach, T.P., & Kutas, M. (2011) Mass univariate analysis
% of event-related brain potentials/fields I: A critical tutorial review.
% Psychophysiology, 48(12) pp. 1711-1725, DOI: 10.1111/j.1469-
8986.2011.01273.x
% http://www.cogsci.ucsd.edu/~dgroppe/PUBLICATIONS/mass_uni_preprint1.pdf
%
% Author:
% David M. Groppe
% Kutaslab
% Dept. of Cognitive Science
% University of California, San Diego
% March 24, 2010

%%%%%%%%%%%%%%%% REVISION LOG %%%%%%%%%%%%%%%%
%
% 5/7/2010-Added FDR adjusted p-values
% 5/14/2013- D.H.J. Poot, Erasmus MC, improved run-time complexity

function [h crit_p adj_p]=fdr_bh(pvals,q,method,report)

if nargin<1,
    error('You need to provide a vector or matrix of p-values.');
else
    if ~isempty(find(pvals<0,1)),
        error('Some p-values are less than 0.');
    elseif ~isempty(find(pvals>1,1)),
        error('Some p-values are greater than 1.');
    end
end

if nargin<2,
    q=.05;
end

if nargin<3,
    method='pdep';
end

if nargin<4,
    report='no';
end

s=size(pvals);
if (length(s)>2) || s(1)>1,
    [p_sorted, sort_ids]=sort(reshape(pvals,1,prod(s)));
else
    %p-values are already a row vector
    [p_sorted, sort_ids]=sort(pvals);
end
[dummy, unsort_ids]=sort(sort_ids); %indexes to return p_sorted to pvals
order
m=length(p_sorted); %number of tests
```

```
if strcmpi(method,'pdep'),
    %BH procedure for independence or positive dependence
    thresh=(1:m)*q/m;
    wtd_p=m*p_sorted./(1:m);

elseif strcmpi(method,'dep')
    %BH procedure for any dependency structure
    denom=m*sum(1./(1:m));
    thresh=(1:m)*q/denom;
    wtd_p=denom*p_sorted./[1:m];
    %Note, it can produce adjusted p-values greater than 1!
    %compute adjusted p-values
else
    error('Argument ''method'' needs to be ''pdep'' or ''dep''.');
end

if nargout>2,
    %compute adjusted p-values
    adj_p=zeros(1,m)*NaN;
    [wtd_p_sorted, wtd_p_sindex] = sort( wtd_p );
    nextfill = 1;
    for k = 1 : m
        if wtd_p_sindex(k)>=nextfill
            adj_p(nextfill:wtd_p_sindex(k)) = wtd_p_sorted(k);
            nextfill = wtd_p_sindex(k)+1;
            if nextfill>m
                break;
            end;
        end;
    end;
    adj_p=reshape(adj_p(unsort_ids),s);
end

rej=p_sorted<=thresh;
max_id=find(rej,1,'last'); %find greatest significant pvalue
if isempty(max_id),
    crit_p=0;
    h=pvals*0;
else
    crit_p=p_sorted(max_id);
    h=pvals<=crit_p;
end

if strcmpi(report,'yes'),
    n_sig=sum(p_sorted<=crit_p);
    if n_sig==1,
        fprintf('Out of %d tests, %d is significant using a false discovery
rate of %f.\n',m,n_sig,q);
    else
        fprintf('Out of %d tests, %d are significant using a false discovery
rate of %f.\n',m,n_sig,q);
    end
    if strcmpi(method,'pdep'),
        fprintf('FDR procedure used is guaranteed valid for independent or
positively dependent tests.\n');
```

```
    else
        fprintf('FDR procedure used is guaranteed valid for independent or
dependent tests.\n');
    end
end
```

--

Synaptic weight analysis:

1) **Fraction of silent synapse analysis (segment strength)**

This script was initially written by JP Thivierge to analyze synaptic weight clustering.
I have made revisions and optimized the code for the analysis.|
The output variables '**s**', '**d**', '**peakpeak**' and '**silent**' from this analysis are required as input variables for Code 2: Synaptic weight variance analysis, and Code 3: Weight matching analysis.

Input variables:

'method40'
AMPA/NMDA ratios calculated by the '+40 mV method' (Beique et al., PNAS 2006)

'peakpeak'
AMPA/NMDA ratios calculated using the 'Peak to Peak' method: the peak EPSC at -70 mV, peak EPSC at +40 mV at a time point ~3x AMPAR tau from time of -70 mV peak.

'cell'
A vector containing the cell number matched to each AMPA/NMDA ratio in 'method40' and 'peakpeak'.

'dendrite'
A vector containing the dendrite number for each AMPA/NMDA ratio in 'method40' and 'peakpeak'.

'div'
A vector containing the postnatal age matched to each AMPA/NMDA ratio in 'method40' and 'peakpeak'.

'd'
A vector containing the distance-from-soma (in microns) for each AMPA/NMDA ratio value in 'method40' and 'peakpeak' variables.

Save and run the following code as an .m file:

--

```
clear all
warning off all;
dat = [];
method40 = dat(:,1);
```

```
peakpeak = dat(:,2);

f = find(method40>=0 & peakpeak>=0);
method40 = method40(f);
peakpeak = peakpeak(f);
peakpeak = peakpeak + 10^-5; % remove 'zero' values for silent synapses by
adding tiny value (zeros are used to pad matrices, create problems down the
line)

% threshold A/N ratio for silent synapses
SSthresh = 0.25;

% Exclude residuals where AMPA/NMDA ratios from two methods disagree
[b,bint,r] = regress(method40,peakpeak);
% residuals are returned in r
% sort residuals in descending order
% ind is original index of residual in dataset
[sr ind] = sort(r,'descend');

pc = round(size(dat,1)/20);

accepted = ind(1:end-pc);
rejected = ind(end-pc+1:end);

figure(1)
hold on;
plot(method40(accepted),peakpeak(accepted),'k.','markersize',20);
plot(method40(rejected),peakpeak(rejected),'r.','markersize',20);
set(gca,'FontSize',20);
xlabel('40 method');
ylabel('peak peak method');
% return;

accepted = sort(accepted,'ascend');
p = peakpeak(accepted);
load('d'); %load distances of spine from soma
dist = d(accepted);
load('cell'); %load cell number
cell = cell(accepted);
load('dendrite'); %load dendrite number
dendrite = dendrite(accepted);

%load postnatal age data
load('div');
div = div(accepted);

%create a matrix with cells and dendrites
k = 1; % cell
kk = 1; % dendrite
kkk = 1; % spine
s = [];
d = [];
divM = [];
for i = 1:length(p)-1
%  x(cell,dendrite,spine)
```

```
%    s(k,kk,kkk) = p(i);
%    d(k,kk,kkk) = dist(i);
   divM(k,kk,kkk) = div(i);

   if cell(i+1)~=cell(i)
        k = k+1;
        kk = 1;
        kkk = 1;
   elseif cell(i+1)==cell(i) & dendrite(i)~=dendrite(i+1)
       kk = kk+1;
       kkk = 1;
   elseif cell(i+1)==cell(i) & dendrite(i)==dendrite(i+1)
       kkk = kkk+1;
   end
end

s(end,end,end+1) = p(end);
d(end,end,end+1) = dist(end);
divM(end,end,end+1) = div(end);

%calculate the number of spines on ea dendritic segment on ea cell
%rows are dendrites, cols are spines
segLen = [];
minDist = [];
maxDist = [];
meanDist = [];
numSpines = [];
for i = 1:size(s,1) %for ea cell
    seg = nonZeroVec(squeeze(d(i,:,:)));
    for j = 1:size(seg,1)
        f = find(~isnan(seg(j,:)));
        numSpines(i,j) = length(f);
        mind = min(seg(j,:));
        maxd = max(seg(j,:));
        meand = nanmean(seg(j,:));
        m = maxd-mind;
        if ~isnan(m)
        segLen(i,j) = m;
        minDist(i,j) = mind;
        maxDist(i,j) = maxd;
        meanDist(i,j) = meand;
        if m==0
           segLen(i,j) = nan;
           minDist(i,j) = nan;
           maxDist(i,j) = nan;
           meanDist(i,j) = nan;
        end
        end
    end
end

%find silent synapses
s = nonZeroVec(s); %  turns zeros into NaNs
silent = s;
f = find(s<=SSthresh & ~isnan(s)); % finds silent synapses (given threshold)
that are not NaNs
```

```
silent(f) = 100; % sets silent synapses to 100
f = find(silent~=100 & ~isnan(silent)); % finds active synapses that are not
NaNs
silent(f) = 0; % sets active synapses to 0
f = find(silent==100);
silent(f) = 1; % set silent synapses to 1

proportion_silent = (nanmean(nanmean(nanmean(silent))));

%go through ea segment, and calculate the proportion of SILENT synapses on a
segment
% STORE pSilent
for i = 1:size(silent,1) %for ea cell
    seg = squeeze(silent(i,:,:));
    for j = 1:size(seg,1)
        silsynapses = length(find(seg(j,:)==1));
        totspines = length(find(seg(j,:)==1 | seg(j,:)==0));
        pSilent(i,j) = silsynapses/totspines;
    end
end

p1 = pSilent(:,1);
p2 = pSilent(:,2);
p3 = pSilent(:,3);
p4 = pSilent(:,4);
p5 = pSilent(:,5);
p6 = pSilent(:,6);
pSilent_cat = vertcat(p1,p2,p3,p4,p5,p6);
pSilent_count = histc(pSilent_cat,0:0.1:1);
totalsegs = sum(pSilent_count);
pSilent_prob = pSilent_count./totalsegs;



% MONTE CARLO SIMULATION: shuffling experiment
% shuffle and compare to chance estimate

for numShuffle = 1:100

    f1 = find(silent==1);
    c1 = length(f1);
    f0 = find(silent==0);
    c0 = length(f0);
    f = shuffle([f1' f0']);
    sh_silent = zeros(size(silent))+nan;
    sh_silent(f(1:c1)) = 1;
    sh_silent(f(c1+1:end)) = 0;

    for k = 1:10
        for w = k
            count = 0;
            for i = 1:size(silent,1) %for ea cell
                seg = squeeze(sh_silent(i,:,:));
                for j = 1:size(seg,1)
                    silsynapses = length(find(seg(j,:)==1));
```

```
                    totspines = length(find(seg(j,:)==1 | seg(j,:)==0));
                    pSilent_sh = silsynapses/totspines;
                    pSilent_sh_tab(i,j,numShuffle) = pSilent_sh;
                end
            end
        end
    end
end

% Calc MEAN and SEM of simulation for dends and cells
pSilent_sh_mean = nanmean(pSilent_sh_tab,3);
sem = nanstd(pSilent_sh_tab,1,3)/sqrt(100);
% sem = nanmean(nanmean(sem));

pSH1 = pSilent_sh_mean(:,1);
pSH2 = pSilent_sh_mean(:,2);
pSH3 = pSilent_sh_mean(:,3);
pSH4 = pSilent_sh_mean(:,4);
pSH5 = pSilent_sh_mean(:,5);
pSH6 = pSilent_sh_mean(:,6);
pSilent_sh_mean_cat = vertcat(pSH1,pSH2,pSH3,pSH4,pSH5,pSH6);
sem1 = sem(:,1);
sem2 = sem(:,2);
sem3 = sem(:,3);
sem4 = sem(:,4);
sem5 = sem(:,5);
sem6 = sem(:,6);
sem_cat = vertcat(sem1,sem2,sem3,sem4,sem5,sem6);
totalsegs = sum(pSilent_count);
pSilent_sh_count = histc(pSilent_sh_mean_cat,0:0.1:1);
pSilent_sh_prob = pSilent_sh_count./totalsegs;
plusSEM = pSilent_sh_mean_cat+sem_cat;
plusSEM_count = histc(plusSEM,0:0.1:1);
plusSEM_prob = plusSEM_count./totalsegs;
minusSEM = pSilent_sh_mean_cat-sem_cat;
minusSEM_count = histc(minusSEM,0:0.1:1);
minusSEM_prob = minusSEM_count./totalsegs;

X = [0:0.1:1.0];
% hold off
% figure
hold on
plot(X,pSilent_prob, 'k-', 'LineWidth',5)
% plot(X,binomial_estimate, 'b-', 'LineWidth',5);
plot(X,pSilent_sh_prob, 'b-', 'LineWidth',5)
plot(X,plusSEM_prob, 'g-.','MarkerSize',20)
plot(X,minusSEM_prob, 'g-.','MarkerSize',20)
X = [0:Q];
X = X/Q;
plot(X,binomial_estimate, 'b-', 'LineWidth',5);

--
```

2) Synaptic weight variance analysis (weight variability)

This analysis uses the output variables '**s**', '**d**', '**peakpeak**' and '**silent**' from Fraction of Silent Synapse analysis (code 1).
The analysis calculates the variance of AMPA/NMDA ratios between neighboring spines and generates a distribution of variance values from the experimental dataset.
The per-segment variance analysis can be performed on shuffled experimental data.
The user must toggle the "shuffle" on or off, and manually save the output data.

Save and run the following code as a .m file:

```
--

close all;
clear
segvar_store = [];

for rep = 1:100
    % % % % SHUFFLE DATA
    on = 1; off = 0;
    shuff = on;

    if shuff == 1
        f = find(isnan(s) == 0);
        slotshuff = shuffle(f);
        shuf_weights = s(slotshuff);
        s(f) = shuf_weights;
    end
    [r,c,z] = size(s);
    f = find(isnan(s(:,:,:)) == 0);
    match_store = s;
    match_store = nonZeroVec(match_store); match_store(f) = 0;
    ff = find(isnan(s) == 1);
    d(ff) = NaN;
    distmatch_tally = zeros(1,100);
    dist_tally = zeros(1,100);
    [rind,cind,zind] = find(isnan(s(:,:,1)) == 0);
    seg_inds = [rind,cind];

    for i = 1:length(seg_inds)
    %   isolate dendritic segment and spine positions (d)
        seg = squeeze(s(seg_inds(i,1),seg_inds(i,2),:));
        seg_d = squeeze(d(seg_inds(i,1),seg_inds(i,2),:));
        numnum = length(seg)-sum(isnan(seg));
        if numnum > 2
            segmean = nanmean(seg);
            segvar = (nanstd(seg))^2;
            segVMR = segvar/segmean;
            segvar_store(i,1,rep) = segvar;
%             segvar_store(i,1,rep) = segVMR;
        else
            segvar_store(i,1,rep) = NaN;
        end
```

```
    end
end

[r,c,z] = size(segvar_store);
for i = 1:z
    segvar_histc = histc(segvar_store(:,:,i),Xlim);
    segvar_cumsum = cumsum(segvar_histc);
    segvar_cumuldist(:,i) = segvar_cumsum./sum(segvar_histc);
end

cumdist = nanmean(segvar_cumuldist,2);

figure(10);
hold on;
plot(segvar_cumuldist,'k')
plot(cumdist,'r.-')

[r,c,z] = size(segvar_store);
for i = 1:z
    segvar_histc = histc(segvar_store(:,:,i),Xlimhistc);
    segvar_histctally(:,i) = segvar_histc;
end
[r,c,z] = size(segvar_cumuldist);
for i = 1:c
%     [~,p] = kstest2(cumdist_data,segvar_cumuldist(:,i));
    [p,~] = ranksum(cumdist_data,segvar_cumuldist(:,i));
    pstore(i) = p;
end

% Benjamini & Hochberg false-discovery rate correction for multiple
comparisons
[h,crit_p,adj_p] = fdr_bh(pstore,0.05,'pdep','yes');

--
```

3) **Weight matching analysis (spatial bounds)**

This analysis was used to measure the spatial distance of the synaptic weight clustering effect. It is based on a division of the synaptic weight distribution into 'weight classes', and a running tally of 'weight-matching' between neighboring spines. For example, for each spine designated as a 'weak' synapse, a tally is kept of the distance to each neighbor that is also 'weak'.

There are two scripts to this analysis: weightsimilarity_neighborMASTER.m is used to set analysis conditions (provides flexibility in defining synaptic weight classes), and runs weightsimilarity_neighbor.m.

This analysis uses the output variables '**s**', '**d**', '**peakpeak**' and '**silent**' from Fraction of Silent Synapse analysis (code 1).
Save these variables in a single .mat file named '**silent_set.mat**'.

Save and run the following code as 'weightsimilarity_neighborMASTER.m'

```
--

clear all;

% shuffle on/off
%     on = 1; off = 0;

%%%%%%%%%%%%%%%%%%%%%%%%%
% EXPERIMENTAL DATA ANALYSIS (shuffle off)
%%%%%%%%%%%%%%%%%%%%%%%%%
shuff = 0;

% % below threshold focus
% uppopthresh_vec = 0.999;
% lowpopthresh_vec = [0:0.1:0.99];

% % % above threshold focus
% uppopthresh_vec = 0:0.01:0.99;
% lowpopthresh_vec = 0.001;

% % % overall population in thirds
uppopthresh_vec = 0.32:0.33:0.99;
lowpopthresh_vec = uppopthresh_vec-0.33;

% % % % overall population in quarters
% uppopthresh_vec = 0.24:0.25:0.99;
% lowpopthresh_vec = uppopthresh_vec-0.25;

% % overall population in fifths
% uppopthresh_vec = 0:0.2:0.99;
% lowpopthresh_vec = uppopthresh_vec-0.2;

match_dat_count = [];

% for irun = 1:length(uppopthresh_vec)
% for irun = 1:length(lowpopthresh_vec)
for irun = 3
    keep lowpopthresh_vec uppopthresh_vec irun shuff match_dat_count
match_dat_fract spine_tally

    lowpopthresh = lowpopthresh_vec(irun);
%     lowpopthresh = lowpopthresh_vec;
%     uppopthresh = uppopthresh_vec;
    uppopthresh = uppopthresh_vec(irun);

    run weightsimilarity_neighbor.m

    spine_tally(irun,:) = dist_tally;
    match_dat_count(irun,:) = dmatch_avg;
    match_dat_fract(irun,:) = pMATCH_avg;
end
```

```
% mdc = match_dat_count(irun,:)';
mdc_dat = dmatch(:,1);
mdf_dat = pMATCH;
spcnt = nansum(spine_tally);

%%%%%%%%%%%%%%%%%%%%%%%%
% SHUFFLED DATA ANALYSIS
%%%%%%%%%%%%%%%%%%%%%%%%
shuff = 1;
% % % overall population in thirds
uppopthresh_vec = 0.32:0.33:0.99;
lowpopthresh_vec = uppopthresh_vec-0.33;

% % % % overall population in quarters
% uppopthresh_vec = 0.24:0.25:0.99;
% lowpopthresh_vec = uppopthresh_vec-0.25;

% % overall population in fifths
% uppopthresh_vec = 0:0.2:0.99;
% lowpopthresh_vec = uppopthresh_vec-0.2;

match_dat_count = [];

% for irun = 1:length(uppopthresh_vec)
% for irun = 1:length(lowpopthresh_vec)
for irun = 3
%     keep lowpopthresh_vec uppopthresh_vec irun shuff match_dat_count
match_dat_fract spine_tally
    lowpopthresh = lowpopthresh_vec(irun);
%     lowpopthresh = lowpopthresh_vec;
%     uppopthresh = uppopthresh_vec;
    uppopthresh = uppopthresh_vec(irun);
    run weightsimilarity_neighbor.m

    spine_tally(irun,:) = dist_tally;
    match_dat_count(irun,:) = dmatch_avg;
    match_dat_fract(irun,:) = pMATCH_avg;

end
mdc_shuff = dmatch;
mdf_shuff = pMATCH;
% spcnt = nansum(spine_tally);

%%%%%%%%%%%%%%%%%%%%%%%%
% % % % STATISTICS
%%%%%%%%%%%%%%%%%%%%%%%%
% KS or Wilcoxon test of state matching counts, corrected for multiple
comparisons
hist_mdc_dat = cumsum(mdc_dat);
cumul_mdc_dat = hist_mdc_dat/max(hist_mdc_dat);
[r,c] = size(mdc_shuff);
for i = 1:c
    hist_mdc_shuff(:,i) = cumsum(mdc_shuff(:,i));
    cumul_mdc_shuff(:,i) = hist_mdc_shuff(:,i)/max(hist_mdc_shuff(:,i));
end
```

```
[r,c,z] = size(hist_mdc_shuff);
for i = 1:c
%     [~,p] = kstest2(cumul_mdc_dat,cumul_mdc_shuff(:,i));
%     [p,~] = ranksum(cumul_mdc_dat,cumul_mdc_shuff(:,i));
%     [~,p] = kstest2(hist_mdc_dat,hist_mdc_shuff(:,i));
    [p,~] = ranksum(hist_mdc_dat,hist_mdc_shuff(:,i));
    pstore(i) = p;
end
% Benjamini & Hochberg FDR correction
[h,crit_p,adj_p] = fdr_bh(pstore,0.05,'pdep','yes');
```

Save and run the following code as 'weightsimilarity_neighbor.m'

```
load('silent_set.mat')

for rep = 1:100
    if shuff == 1
        f = find(isnan(s) == 0);
        slotshuff = shuffle(f);
        shuf_weights = s(slotshuff);
        s(f) = shuf_weights;
    end
    [r,c,z] = size(s);
    f = find(isnan(s(:,:,:)) == 0);
    match_store = s;
    match_store = nonZeroVec(match_store); match_store(f) = 0;
    ff = find(isnan(s) == 1);
    d(ff) = NaN;
    distmatch_tally = zeros(1,100);
    dist_tally = zeros(1,100);
    [rind,cind,zind] = find(isnan(s(:,:,1)) == 0);
    seg_inds = [rind,cind];

    for i = 1:length(seg_inds)
    %   isolate dendritic segment and spine positions (d)
        seg = squeeze(s(seg_inds(i,1),seg_inds(i,2),:));
        seg_d = squeeze(d(seg_inds(i,1),seg_inds(i,2),:));
        numnum = length(seg)-sum(isnan(seg));
        if numnum > 2
            for n = 1:numnum-1
    %   isolate individual spine/position, examine neighbors
                state = seg(n);
                upper_f = find(ANratio_pop(:,2) > uppopthresh);
                upper_weight_threshold = ANratio_pop(upper_f(1),1);
                lower_f = find(ANratio_pop(:,2) > lowpopthresh);
                lower_weight_threshold = ANratio_pop(lower_f(1),1);
                if state > lower_weight_threshold && state <
upper_weight_threshold
                state_d = seg_d(n);
        %   identify neighbors
                    neighs_states = seg(n+1:numnum);
                    neighs_d = seg_d(n+1:numnum);
        %   tally neighbor spines at all distances, regardless of match
                    ddiff_tot = abs(state_d - neighs_d);
                    dist_tally(ddiff_tot+1) = dist_tally(ddiff_tot+1)+1;
    % %             define similarity boundaries
```

```
%                     state_plus = state+ANratio_std;
%                     state_minus = state-ANratio_std;
                    statematch = zeros(length(neighs_states),1);
        %   find distances of matching neighbors
                    if isempty(statematch) == 0
                        match_d = neighs_d(statematch);
                        ddiff = abs(state_d - match_d);
                %   tally matching neighbors in respective distance bins
                        distmatch_tally(ddiff+1) =
distmatch_tally(ddiff+1)+1;
%                         for nn = 1:length(ddiff)
%                             distmatch_tally(ddiff(nn)+1) =
distmatch_tally(ddiff(nn)+1)+1;
%                         end

                    end
                end
            end
        end
    end
    dmatch(:,rep) = distmatch_tally;
    pMATCH(:,rep) = distmatch_tally./dist_tally;
end

dmatch_avg = nanmean(dmatch,2);
pMATCH_avg = nanmean(pMATCH,2);

--
```

Appendix E

Modeling synapse development

This project was presented to my Thesis Advisory Committee (Drs. Len Maler, Richard Bergeron and Johnny Ngsee) in April 2013.

For better or for worse, I worked on this project and invented these model neurons before taking the course in Computational Neuroscience (NSC8104) in June 2013.

The Motive

Synaptic plasticity is known to be spatially influenced by factors which operate locally at the level of the postsynaptic dendrite. We hypothesized that such mechanisms may also operate during synapse development, perhaps explaining the clustering of synaptic weights that I have found experimentally. I sought to develop a simple model of synapse development to determine whether we could recapitulate clustering features by imposing variable degrees of local spatial influences on random synapse development.

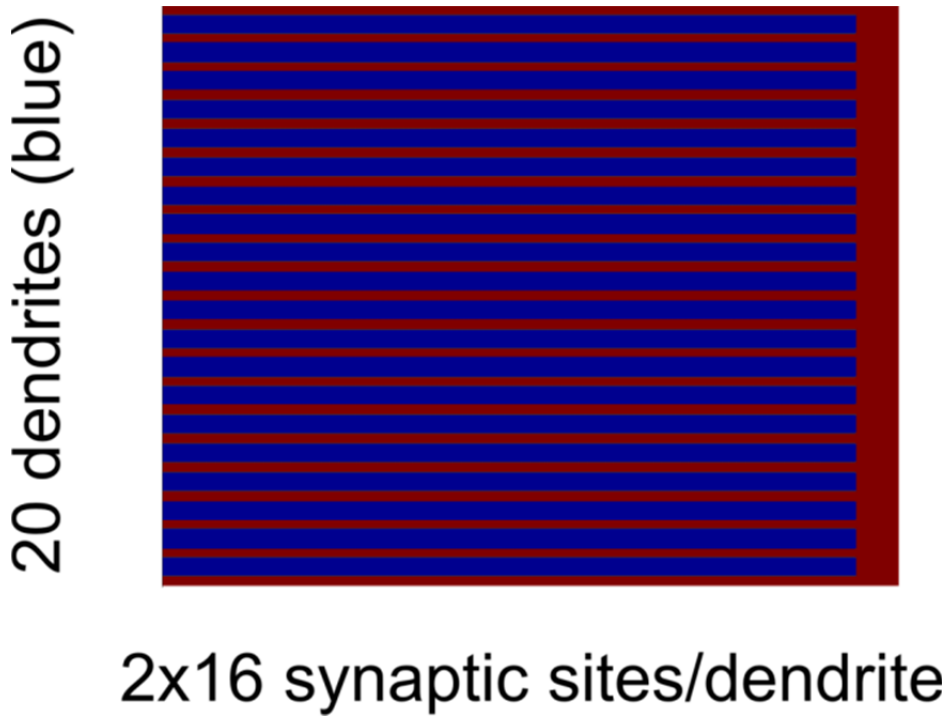

MSD Figure 1 – The dendritic space. Each dendrite (blue) operates as an independent unit and is comprised of 2x16 synaptic sites. With an average spine density of approx 0.3 spines/µm during the peak of postnatal synaptogenesis (from 2P imaging), each dendrite represents roughly 50µm of 'real' dendrite

Part 1: A Markov Chain Model

Modeled after a simple Markov chain, synapse development was represented by probabilistic state transitions (*i.e.,* Immature **State 1** → Mature **State 10**). Two factors were systematically manipulated:

1) Transition probability: the probability that any given synapse will transition to the next state
2) Local spatial influence: a spatially-graded local signal along a dendrite that facilitates the state transition of neighbour synapses (akin to local plasticity mechanisms)

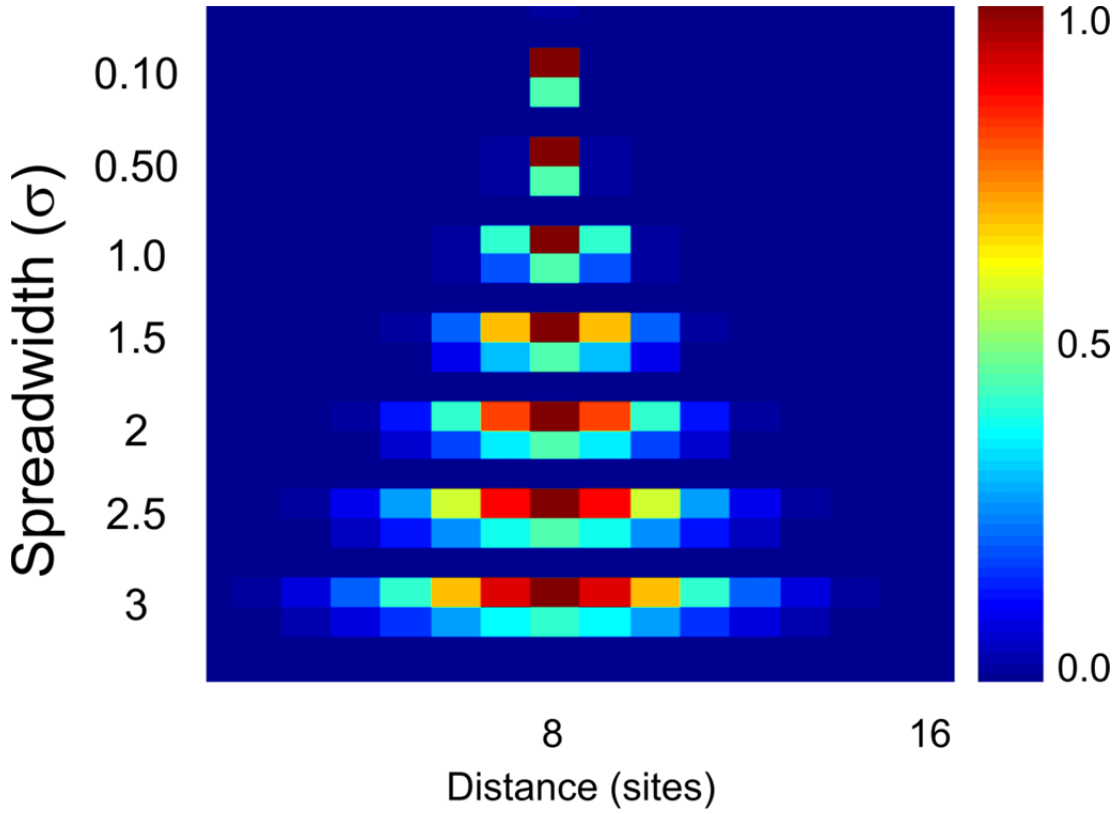

MSD Figure 2 – The local spatial influence. Synaptic sites that successfully transition to the next state (stochastically, based on the transition probability) are allowed to exert a local spatial influence that increases the transition probability of neighbouring synapses. The spatial influences are shaped to "reach" variable lengths along each dendrite via the spreadwidth factor (σ). A range of σ-values were systematically tested against various baseline transition probabilities.

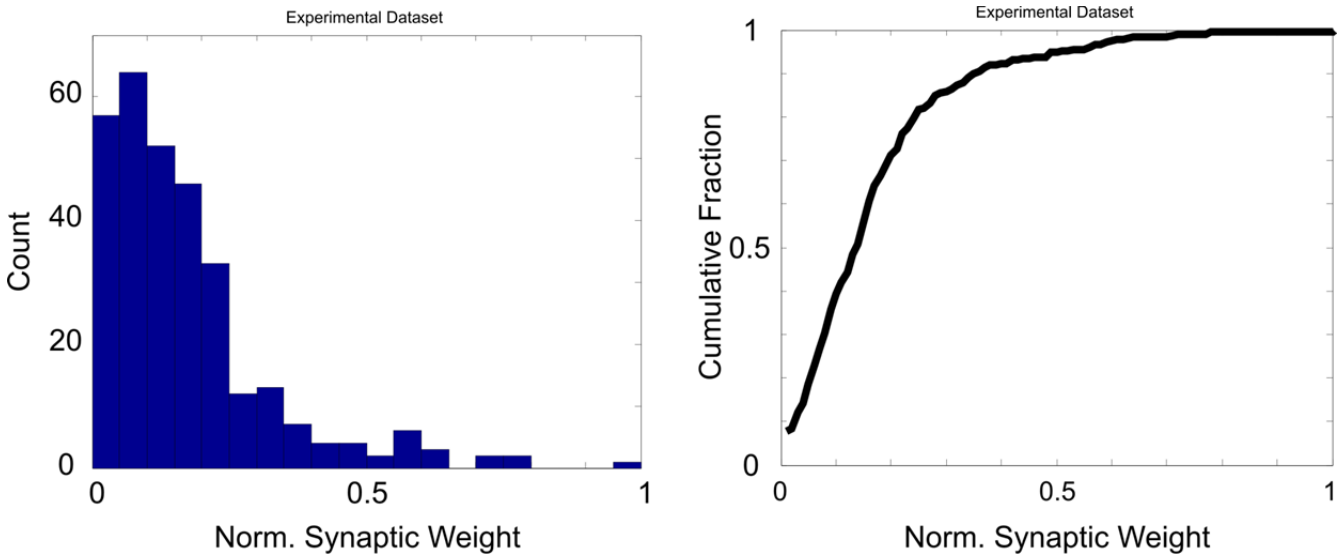

MSD Figure 3 – Validating the developmental trajectory of the model with experimental data.

MSD Figure 3 shows the histogram count (left) and cumulative distribution (right) of the experimental data containing over 300 AMPA/NMDA ratios (reflecting synaptic weight) from individual spines. These distributions represent the overall synaptic weight distribution during an early developmental epoch, when ~20% of synapses are *'silent'* (extremely weak). To determine how closely the synapses in the model develop compared to experimental data, we will stop the simulations when 20% of synapses are *'silent'* (in State 1) and statistically compare the distribution of synaptic weights between experimental and model data.

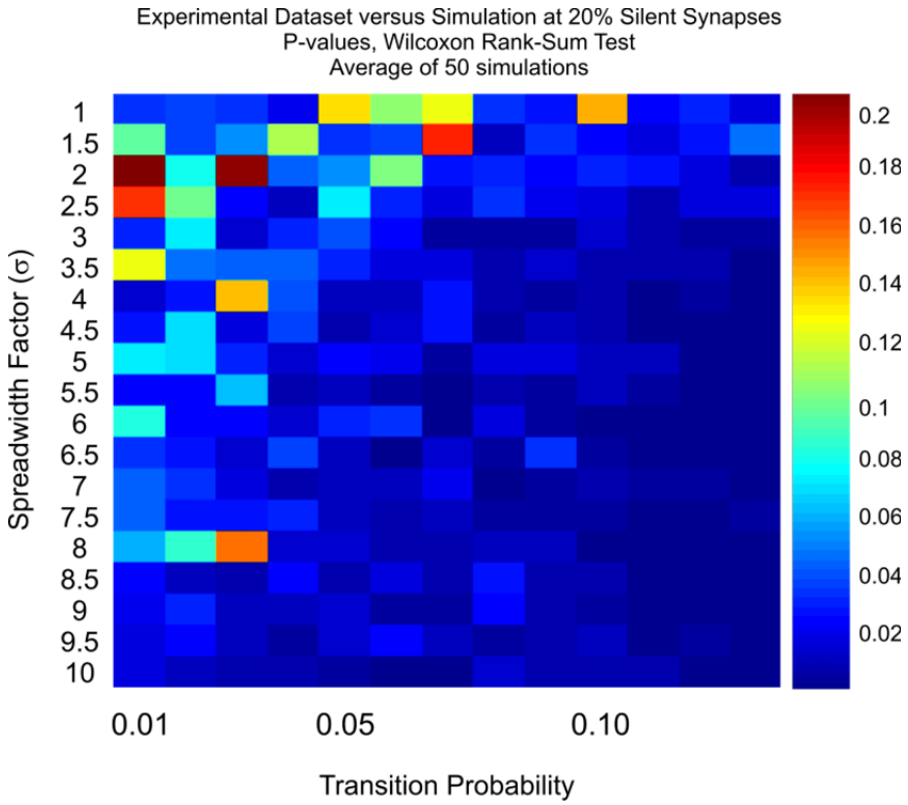

MSD Figure 4 – P-value matrix, simulated data compared to experimental data.

I ran the simulation with a range of baseline transition probabilities and σ-values (local dendritic influence). I used the Wilcoxon test to evaluate the goodness of fit between experimental and simulated synaptic weight distributions at a time point when 20% of synapses were *'silent'*. MSD Figure 4 shows the P-value matrix of these comparisons (average P-values from 50 simulations per condition pair). Hot colours (relatively high P-values) reflect the most optimal simulation parameters for matching experimental data.

Part 2: A Spiking Neuron Model

This improved model utilizes the same dendritic space described above (MSD Figure 1), but includes threshold-based 'spike' and simple spike-timing dependent plasticity rules (pre-post/post-pre) for LTP and LTD.

Conceptual changes:

- state transition probability becomes 'presynaptic release probability'
- the dendritic space receives stochastic inputs that follow a Poisson distribution around the mean presynaptic release probability of 0.1
- all synapses are initialized with a 'weight' of 1.0, and each state transition adds 0.1 to their weight.
- the neuron model sums the total weight of inputs on each iteration
- the neuron fires a 'spike' when the input weight exceeds a spike threshold of two times the standard deviation of mean input
- the spike is a global signal that is 'felt' throughout the dendritic arbor
- the spike gates plasticity (no state transitions can occur without a spike)
- the temporal influence of a spike spans only one iteration (*i.e.,* pre-post and post-pre rules only span one iteration before or after a given spike)

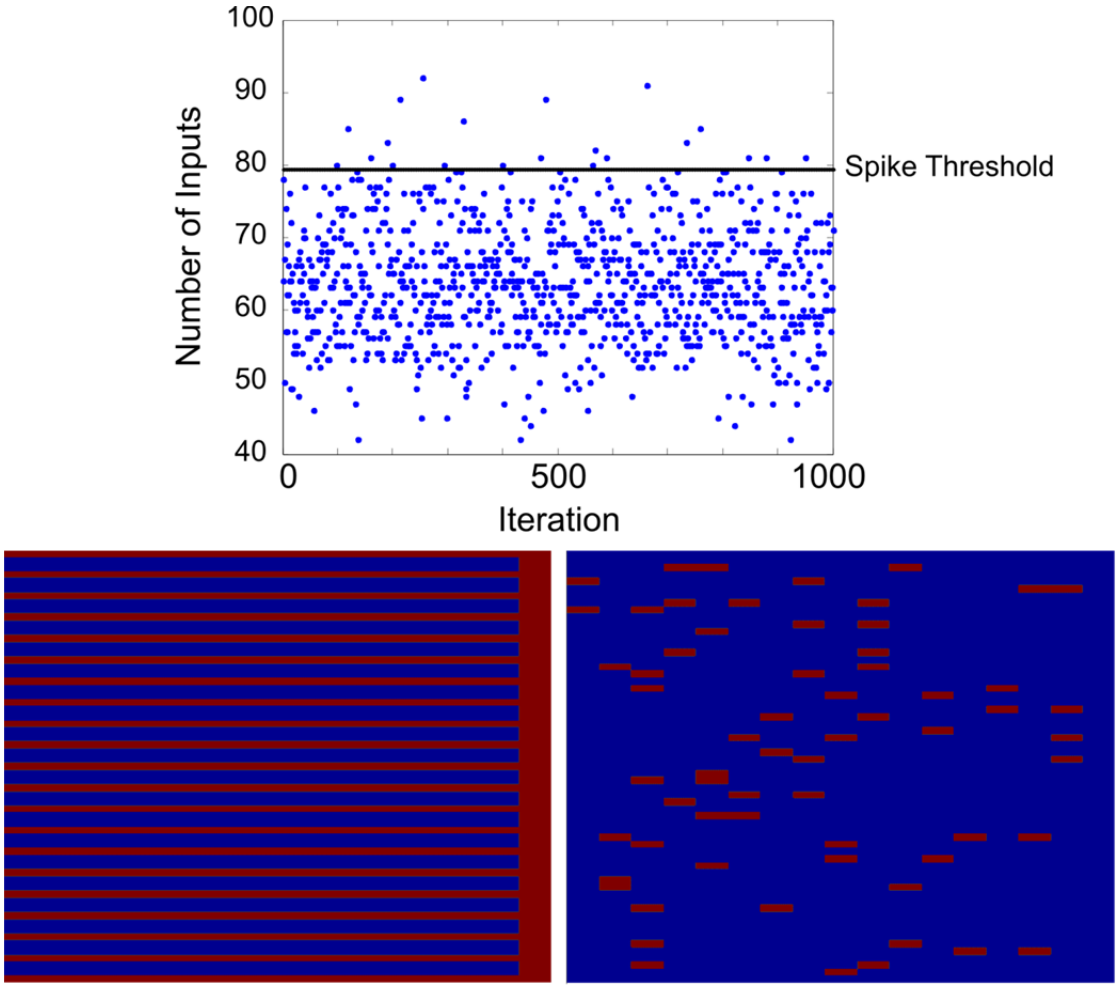

MSD Figure 5 – Poisson inputs delivered to the spiking neuron model. *Top panel* shows an example Poisson train of inputs (0.1 release probability per synapse) impinging on the neuron model. Inputs that exceed the spike threshold generate a 'spike'. *Bottom left* shows the dendritic space as in MSD Figure 1. *Bottom right* shows one iteration of synaptic inputs in the dendritic field. Red rectangles reflect activated synapses.

The spike is the global signal that gates synaptic plasticity, which follows STDP-like rules. I graded the spike influence in the dendritic arbor to simulate the attenuation of back-propagating action potentials (bAPs) as they travel into the dendritic arbor (Stuart et al. TINS 1997). Therefore distal synapses are less likely to be influenced by bAPs compared to proximal synapses. See MSD Figure 6.

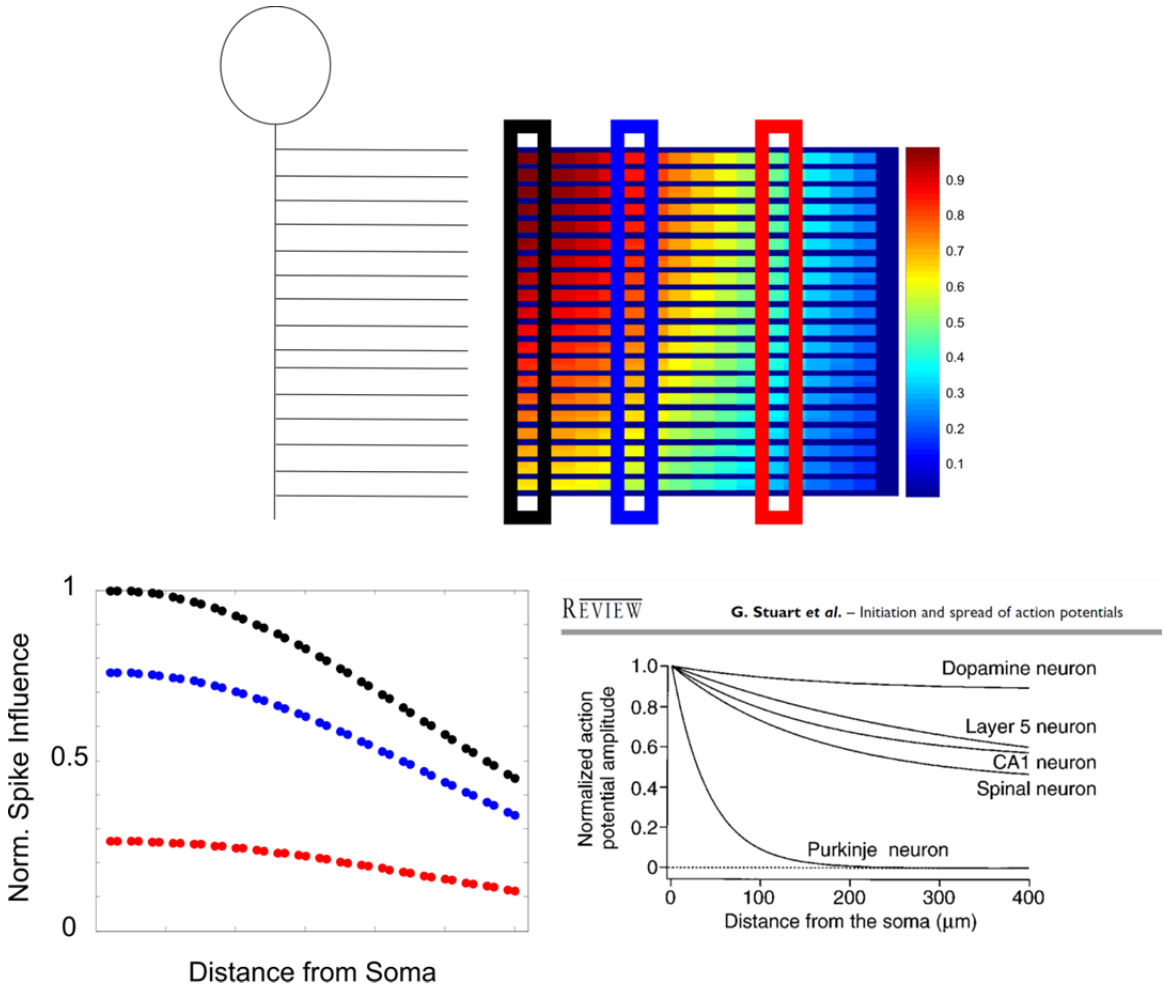

MSD Figure 6 – Graded influence of backpropagating action potentials (bAP) along the proximal distal axis of the model neuron. *Top panel* shows the influence of the bAP overlaid onto the dendritic space shown in MSD Figure 1 and 5. *Bottom left panel* shows the normalized spike influence for the three regions outlined by rectangles (colour-coded) in the *top panel*. *Bottom right panel* is taken from Stuart et al. TINS 1997 to show normalized bAP amplitudes for different types of neurons. The spike influence in the model neuron roughly matches cortical and hippocampal pyramidal cells.

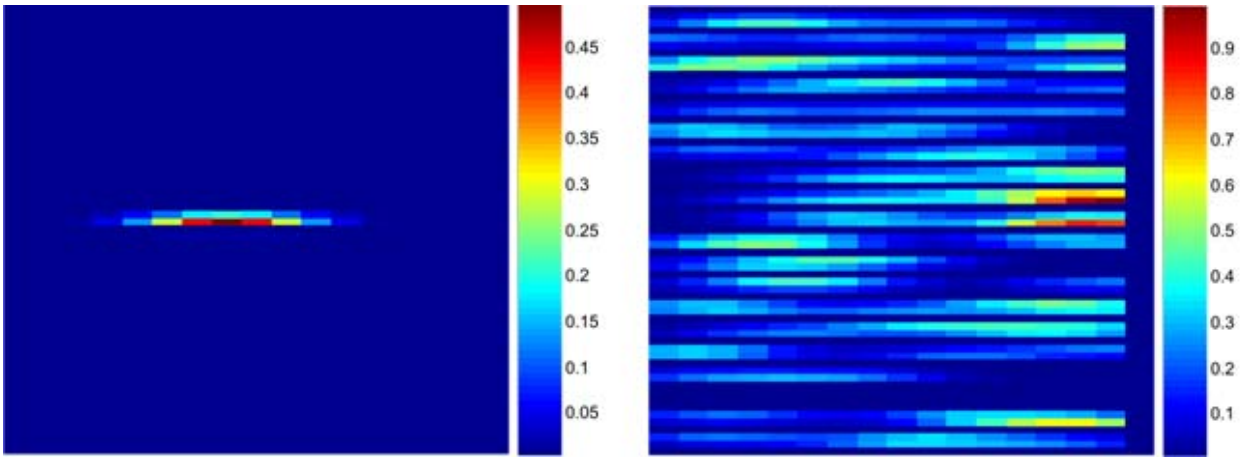

MSD Figure 7 – The local plasticity signal along dendrites. *Left panel* shows an example of the spatial extent of the local plasticity signal exerted by activation of a single synaptic site. The spreadwidth factor σ dictates the spatial extent of the local influence along the dendrite. *Right panel* shows the normalized cumulative influence of all local plasticity signals in the dendritic arbor in one iteration of simulation after a spike. The net influence of any plasticity signal is the sum of global and local factors.

Synaptic Plasticity Rules

The plasticity rules in the model are akin to spike-timing dependent plasticity rules based on the relative timing of pre- and postsynaptic spiking. LTP occurs when the sum of synaptic input exceeds the spike threshold. The synapses that participated in the spike are selected to undergo a probabilities-based transition to the next (stronger) synaptic state. The probability of synaptic state transition is dictated by the sum of the global and local plasticity signals. Conversely, LTD occurs at synapses that are activated in the iteration *following* a spike event. These synapses are selected to undergo a probabilities-based transition to a weaker state dictated entirely by the global spiking influence (no local rules).

Results

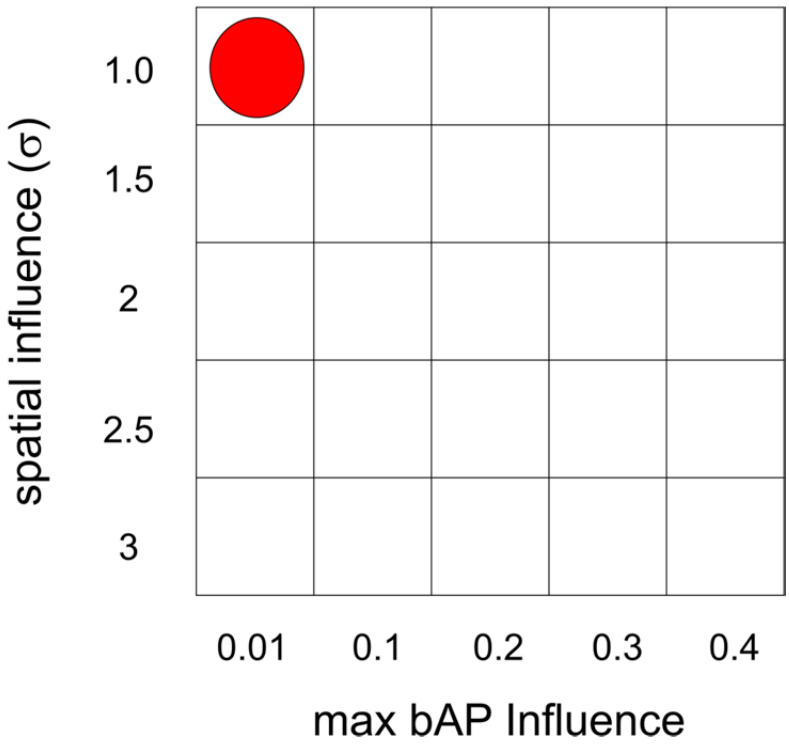

MSD Figure 8 – Spiking model synapse development parameter space. The spiking model was run systematically stepping through different combinations of global (spike) and local plasticity signals. For example, the red circle indicates a spatial influence of 1.0 (lowest influence) and a maximum spike influence of 0.01 (lowest influence).

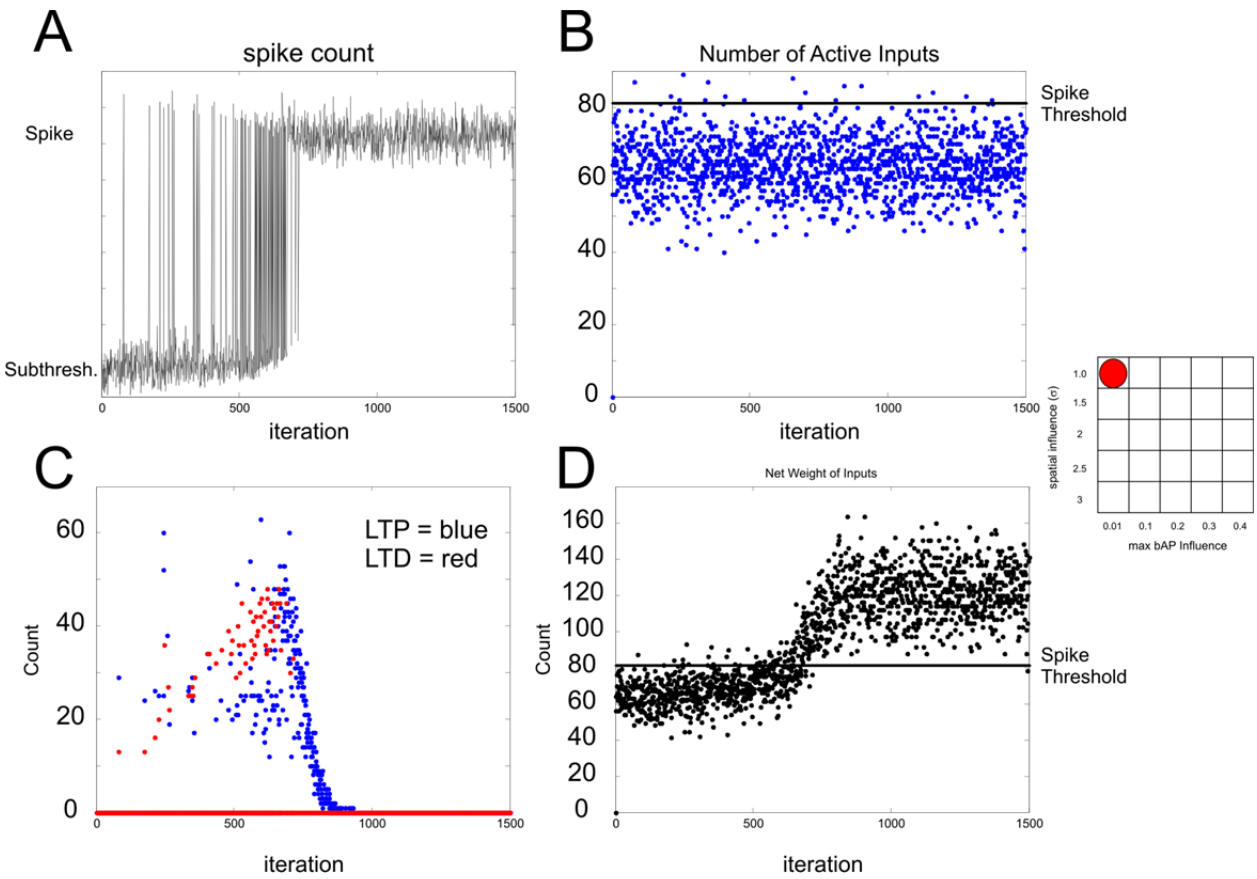

MSD Figure 9 – Dynamic behavior of the spiking neuron model. This example utilizes the plasticity parameters shown in MSD Figure 8, shown again to the right of the figure. (A) Spiking behavior of the neuron. As the simulation evolved and synapses were strengthened, the neuron spiked more frequently, eventually spiking on every iteration. (B) Constant number of synaptic inputs were delivered following a Poisson distribution throughout the simulation (presynaptic release probability of 0.1). The spike threshold is shown and was constant. The neuron spiked more frequently than expected by the given number of inputs because synapses were strengthened (gained 'weight') by LTP mechanisms. (C) Count of LTP and LTD events as the simulation evolved. LTP events were recorded, but eventually ceased as synapses reached their maximum weights. LTD events were rare at the start because synapses initialized at the weakest state and therefore could not be further depressed. Once the neuron began spiking non-stop (iteration ~700), LTD no longer occurred since there were no iterations free from spikes. (D) Net weight of all synaptic inputs at each iteration. Synaptic input was strengthened by LTP until synaptic inputs persistently exceeded spiking threshold. Note that the total number of synaptic inputs did not change (B). This is an example of 'runaway excitation' in a neuron model with unconstrained Hebbian plasticity mechanisms.

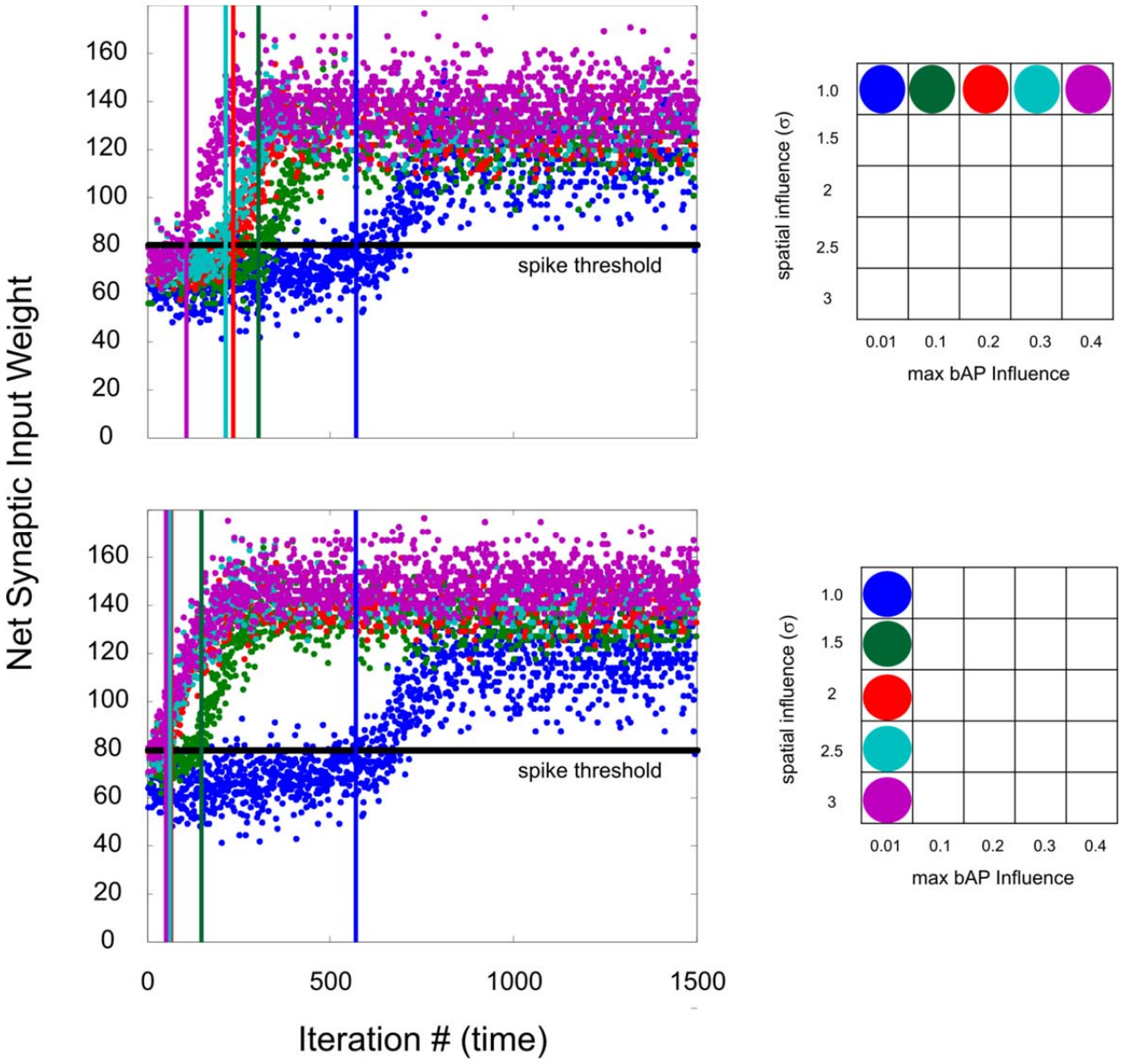

MDS Figure 10 – Evolution of synaptic weights under different plasticity parameters. *Top,* Increasing global spike influence while keeping the local plasticity signal minimal resulted in progressively faster synapse maturation. *Bottom*, Increasing the local plasticity signal while keeping the global spike influence minimal also resulted in progressively faster synapse maturation. Vertical lines mark the time point where 20% silent synapses was reached in each condition. The spike threshold was kept constant. Neurons received the same Poisson input trains as shown in MDS Figures 5 and 9.

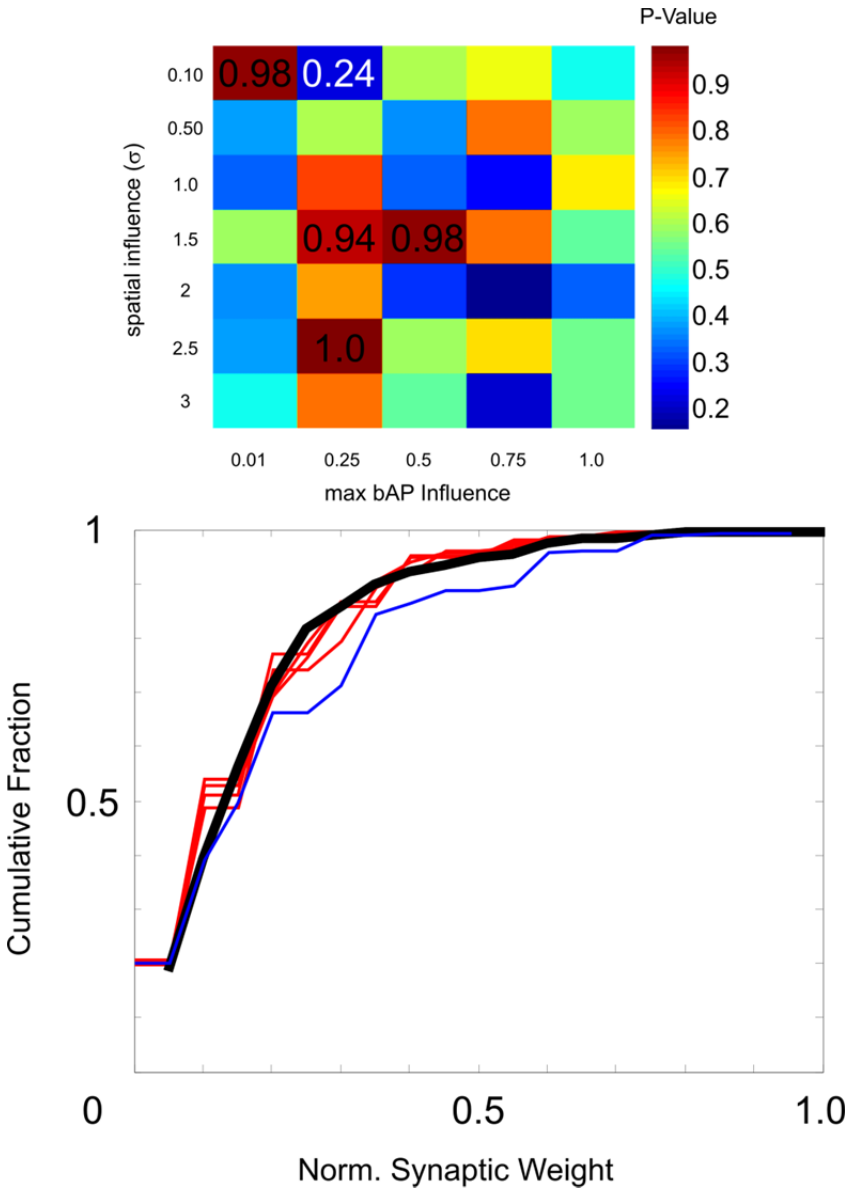

MDS Figure 11 – Comparing overall synaptic weight distributions between experiment and model at a developmental epoch with 20% silent synapses. *Top,* P-value matrix (average from 20 simulations) for comparisons is overall synaptic weight distributions between experimental data and results from the model at different positions in the plasticity parameter space. The four highest P-values (best fits) are indicated along with the lowest P-value (poorest fit). *Bottom*, Cumulative distribution of experimental synaptic weight distribution (black) with the best (red) and worst (blue) fitting distributions from the spiking model.

So far, I have demonstrated that the simple spiking model of synapse development can generate overall synaptic weight distributions that closely match experimental data at a time point when 20% of synapses are silent/immature. This overall synaptic weight distribution does not account for the spatial positions of mature and immature synapses on the dendrites.

To determine whether the model can recapitulate features of clustered synapse development, we must spatially map the synaptic weights along individual dendritic segments in the model neuron as I have done experimentally. To reiterate, I used 2P glutamate uncaging and whole-cell electrophysiological recordings to probe the AMPAR function of neighbouring synapses on dendritic segments ~16 µm in length. To obtain a measure for the developmental state of each dendritic segment, I calculated the fraction of silent/immature synapses on each dendritic segment. This can be referred to as the Clustering Index, as illustrated in MDS Figure 12. The results of this analysis is shown in MDS Figure 13.

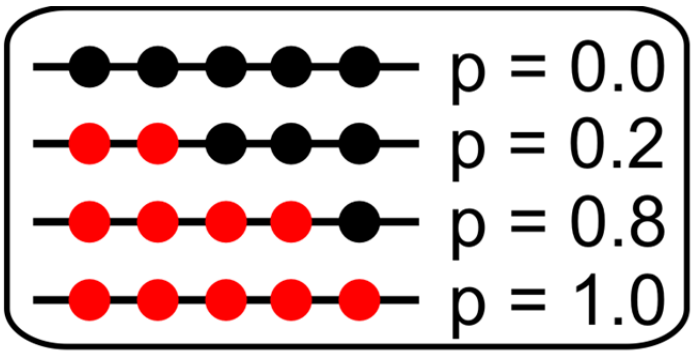

MDS Figure 12 – The clustering index. Silent/immature synapses are depicted as red circles while mature synapses are black. The fraction of silent/immature synapses is the clustering index.

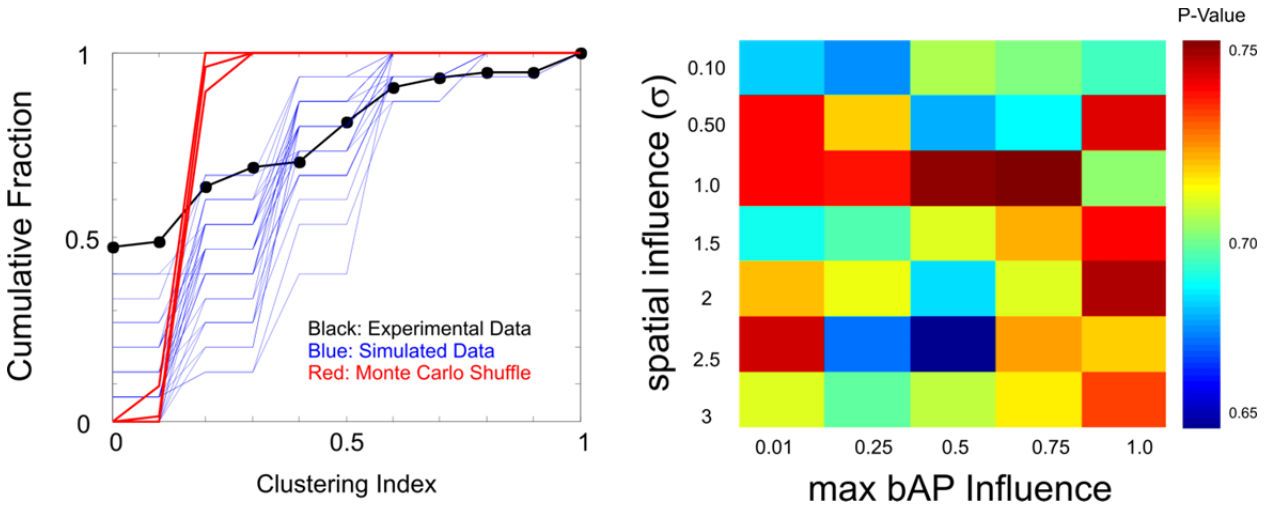

MDS Figure 13 – The clustering index comparison between experiment and model. *Left,* Cumulative distribution of Cluster Index values for individual dendritic segments. Experimental data (black), shuffled data (red, with 95% confidence intervals), and spike model data (blue) are shown. The spike model approaches experimental distributions under some conditions. *Right,* P-value matrix for comparisons at different positions in the plasticity parameter space

Discussion & Concluding Remarks

I have generated two rudimentary model neurons to simulate synapse development. The first model is based on Markov Chain principles using only probabilities to dictate synaptic 'state transitions' toward synapse maturity. The second model is an improvement toward a simple integrate-and-fire neuron model that uses spiking events to define bidirectional spike-timing dependent plasticity-like rules for synapse maturation. In both models, I attempted to incorporate local plasticity rules that operate along individual dendrites, akin to the local calcium propagation events I discovered in developing CA1 pyramidal neurons (Manuscript V). In the spiking model, I attempted to shape the bAP influence to reflect the distance-dependent attenuation of bAP invasion into the dendritic arbor. I compared the simulated synaptic weight distributions to experimental data across a range of global (bAP) and local plasticity rule parameters.

I found that the spiking model could faithfully replicate overall (cell-wide) experimental synaptic weight distributions, but was not good at capturing the clustering of synaptic weights along individual dendrites. It is likely that the model requires significant refinement before it is able to recapitulate the fine-scale dynamics of synapse development detected experimentally in the dendritic arbor (Manuscript V). Nevertheless, these attempts at modeling synapse development were my very first experiences in computational modeling and were enriching experiences, significantly enhancing my MATLAB literacy at the very least.

One interesting observation from the spiking neuron model is the development of runaway excitation that is well known to occur in neuron models that implement solely Hebbian forms of plasticity (LTP/LTD) without constraints. During the evolution of the simulation, the neuron increased its firing rate as a result of increasing synaptic weights due to LTP and quickly became over-excited, spiking non-stop toward the end of the simulation. This runaway excitation occurred despite a constant number of inputs in the Poisson train. This suggests that this simple spiking model could be useful for exploring homeostatic plasticity mechanisms that normalize synaptic weights. However, there are significantly more sophisticated computer models currently being reported on in the literature, so it remains unlikely that this simple spiking model will be of significant publication value.

Shortly after assembling the results of these simulations, which I invented from scratch, I took the course on Computational Neuroscience (NSC8104) coordinated by Drs. Len Maler and Andre Longtin. During this course, I was able to develop an integrate-and-fire (IF) neuron model of spike-timing dependent plasticity to replicate core findings from the lab of Larry Abbott (Song et al. Nat Neurosci 2000). For future modeling work, it will likely be more useful to utilize this IF neuron model as a starting platform rather than the models that I described above.

Dendritic simulation space

--

```
% Make dendrite simulation space

oneline_dendrite = ones(60,16);
save 'oneline_dendrite'

k = 1;

dens_perlength = 3;
denlengths = [16 16 16 16 16 16 16 16 16 16 16 16 16 16 16 16 16 16 16 16];
denwidth = 2;

for i = 1:length(denlengths);
    dendrite_mask(k+1:k+denwidth,1:denlengths(i)) = 0;
    k = k+denwidth+1;
end

keep dendrite_mask
save 'dendrite_mask'

imagesc(dendrite_mask)
```

--

Markov Chain Model

--

```
load ('dendrite_mask')
% Simulation Initialization
% % Frame resolution
    [L W] = size(dendrite_mask);
%     L = 70;
%     W = 50;
% % Number of States
    S = 10;
% % Number of iterations per simulation
    T = 150;
% % Number of simulations
%     simrep = 5;

mask_raw = dendrite_mask;
mask = imresize(mask_raw, [L W], 'nearest');
%Markov matrix of transition probabilities
M = zeros(S);
% Single transition probability
transprob = 0.1;
for i = 1:S-1
    M(i,i+1) = transprob;
end
```

```
% For state-dependent transitions
% M(1,2) = 0.1;
% M(2,3) = 0.1;
% M(3,4) = 0.1;
% M(4,5) = 0.1;
% M(5,6) = 0.1;
% M(6,7) = 0.1;
% M(7,8) = 0.1;
% M(8,9) = 0.1;
% M(9,10) = 0.1;

% 'eye(S)' returns the identity matrix of size S
% an identity matrix is square matrix with 1's along its diagonal
M = M+eye(S)*0.9; %0.9, probability of staying in the same state

%state initialization
sites = zeros(L,W,T)+1; % allocating space
storeSites = zeros(L,W,T)+1; % allocating space
h = zeros(T,5);

for t = 2:T
    disp(t)
    z = t-1;
    for w = 1:W
        for l = 1:L
            m = M(storeSites(l,w,z),:);
            v=[];
            for k = 1:length(m)
                v = [v (zeros(m(k).*10,1)+k)'];
            end
            r = randperm(length(v));
            sites(l,w,z) = v(r(1));
            storeSites(l,w,t) = sites(l,w,z);
        end
    end
%     Apply mask here: reset all non-object pixels back to State 1
%     Check mask, ensure non-object pixels == 1 and object pixels == 0
    [rows,cols] = find(mask == 1);
    for i = 1:length(rows)
        rr = rows(i);
        cc = cols(i);
        storeSites(rr,cc,t) = 1;
        storeSites(rr,cc,t+1) = S+1; % to identify the outline of structure
in analysis
        moviemovie = storeSites;
    end
end

moviemovie = storeSites;
--
```

Spiking Neuron Model

```
--

% clear all;
% clc;

% % % % % 'spiking_LTPLTD_simulation'
% %
% state-transition simulation of spike-depedent LTP and LTD
% Poisson dist of synaptic inputs according to 'release probability'
% Threshold-based spiking activity (2*STD of input_dist)
% Spike-driven probabilistic transitions (1:10)
% Plasticity requires spike
% 1-iteration spike influence
% i) pre-post ii)post-pre iii) spike-spike(x2)
% % % % %

load ('dendrite_mask')
% Set simulation parameters frame
% Simulation Initialization

% % Frame resolution
    [W L] = size(dendrite_mask);
%     L = 70;
%     W = 50;
% % Number of States
    S = 10;
% % Number of iterations per simulation
    T = 1500;
% % %
% % Spatial influence spread width (NO LOCAL INFLUENCE HERE)
%     spreadwidth = 1;
% % %
% % % % % % % % % % %
mask_raw = dendrite_mask;
mask = imresize(mask_raw, [W L], 'nearest');
numpix = (dendrite_mask == 0);

% TOTAL number of synaptic sites in the model neuron
total_sites = sum(sum(numpix));

% % % % % % % % % % % % % % % % % %
% Presynaptic Release Probability
releaseprob = 0.1;
% % % % % % % % % % % % % % % % % %

%Markov matrix of transition (release) probabilities
M = zeros(S);
for i = 1:S-1
    M(i,i+1) = releaseprob;
end
M = M+eye(S)*(1-releaseprob);

% Poisson distribution of input around the
```

```
% expected mean, releaseprob*input_density
expected_active = releaseprob*total_sites;
input_dist = poissrnd(expected_active,1000,1);
spike_threshold = mean(input_dist) + 2*std(input_dist);

% % % Normalized Threshold for Weight Normalization
% norm_input_dist = poissrnd(expected_active,1000,1)./expected_active;
% norm_spike_threshold = mean(norm_input_dist) + 2*std(norm_input_dist);

% % % % % % % % % % %
%State Initialization
sites = zeros(W,L)+1;
storeSites = zeros(W,L,T)+1;
spike_count = zeros(T,1);
[r c d] = size(storeSites);

% Identify "primary apical branchpoint"; ie/ beginning of each dendrite
[rows cols] = size(storeSites(:,:,1));
rowstart = [2:3:59];
rowend = [rowstart+1];
RR = [rowstart rowend];
branchpoints = sort(RR)';

% Global bAP signal for plasticity
% bAP influence shrinks with increasing dist from soma
% % two different bAP probability matrices
% - standard versus enhanced (for successive spikes)

% spreadunit = 1;
% spreadwidth = 2;
Iapical = zeros(W,L)+1;
proximal_start = branchpoints(1,1);
for IW = 1:W
    for IL = 1:L
        IBAP(IW,IL) =
1000000*Multivariate(IW,IL,proximal_start,1,spreadunit*(round(W)),spreadunit*
(round(L/2)),0);
    end
end
for IW = 1:W
    for IL = 1:L
        IBAPplus(IW,IL) =
1000000*Multivariate(IW,IL,proximal_start,1,spreadunit*(round(W*1.5)),spreadu
nit*(round(L)),0);
    end
end
%     Apply mask to bAP probability/influence matrix
[rows,cols] = find(mask == 1);
for i = 1:length(rows)
rr = rows(i);
cc = cols(i);
%     Iproject(rr,cc) = 0;
IBAP(rr,cc) = 0;
IBAPplus(rr,cc) = 0;
end
% % % % %
```

```
BAP1 = normalize(IBAP);
BAP2 = BAP1 >= 0.1;
% % SET bAP influence
[r c] = size(BAP1);
bAP = zeros(r,c,5)+1;
bAP_influences = [0.01;0.1;0.2;0.3;0.4];
r = length(bAP_influences);
for i = 1:r
    BAP(:,:,i) = (BAP1.*BAP2).*(bAP_influences(i,1));
end
% % %
% % bAP_influence = 1,2,3,4,5
% bAP_influence = 5;
% % 1=0.01; 2=0.1; 3=0.2; 4=0.3; 5=0.4;
% % %
% bAPplus for consecutive activations
BAPplus1 = normalize(IBAPplus);
BAPplus2 = BAPplus1 >= 0.1;
bAPplus = BAPplus1.*BAPplus2;

% % % keep track of number of spines undergoing LTP(:,1) and LTD(:,2) and
% enhanced-LTP(:,3)
LTPvsLTD = zeros(T,3); % number of sites that transitioned

% % %
% ITERATE
% % % % %
for t = 2:T
    disp(t)
    z = t-1;
    storeSites(:,:,t) = storeSites(:,:,z);
    [rows,cols] = find(mask == 1);
    for i = 1:length(rows)
    rr = rows(i);
    cc = cols(i);
    storeSites(rr,cc,z) = 1;
    storeSites(rr,cc,t) = 1;
    storeSites(rr,cc,t+1) = S+1;
    end
%     STEP 1: purely probabilistic presynaptic release
    for w = 1:W
        for l = 1:L
            m = M(storeSites(w,l,1),:);
            v = [];
            for k = 1:length(m)
                v = [v (zeros(m(k).*100,1)+k)'];
            end
            K = randperm(length(v));
            sites(w,l) = v(K(1));
        end
    end
    inputs = sites;

    [rows,cols] = find(mask == 1);
    for i = 1:length(rows)
    rr = rows(i);
```

```
    cc = cols(i);
    inputs(rr,cc) = 1;
    storeSites(rr,cc,z) = 1;
    storeSites(rr,cc,t) = 1;
    storeSites(rr,cc,t+1) = S+1;
    end

%     STEP 2: find sites that received input
    [rows cols] = find(inputs(:,:) > storeSites(:,:,1));
    insyn = [rows cols];
    input_synapses(1:length(insyn),1:2,t) = insyn;

%     current iteration of active synapses
    active_synapses = input_synapses(:,:,t);
    limit = find(active_synapses == 0);
    if limit > 1
        lim = limit(1);
        active_synapses = active_synapses(1:lim-1,:);
    end
%     count number of active synapses
    num_inputs = length(active_synapses);
    active_inputs(:,t) = num_inputs';

%     previous iteration of active synapses
    prev_synapses = input_synapses(:,:,z);
    limit = find(prev_synapses == 0);
    if limit > 1
        lim = limit(1);
        prev_synapses = prev_synapses(1:lim-1,:);
    end


%     Use synaptic weights of inputs to drive spike activity
% Provide global bAP signal for plasticity, distance-dependent influence

    for w = 1:length(active_synapses)
        weights(w,t) =
0.1*(storeSites(active_synapses(w,1),active_synapses(w,2),z)) + 0.9;
    end
    synaptic_input(:,t) = sum(weights(:,t));
% % % % % % % % % %
% % % % % % % % % % % % % % % % % %
% % % % % % % % % % % % % % % % % % % % % % % % % % % %
% % % % % % % % % % % % % % % % % % % % % % % % % % % % % % % % % % % % % % %
% %     Threshold-based Spike Discharge

% % IF NO SPIKE
    if synaptic_input(:,t) <= spike_threshold
        spike_count(t,1) = -num_inputs;
        storeSites(:,:,t) = storeSites(:,:,z);
        downsites = nonZeroVec(prev_synapses);
        num_downsites = downsites > 0;
        LTDsites = sum(num_downsites(:,1));
        prev_synapses = prev_synapses(1:LTDsites(1),:);
        [r c] = size(prev_synapses);
```

```
        newstates1 = storeSites(:,:,t);

% % % >>>SPIKE-DEPENDENT DEPRESSION
% % if previous iteration spiked, LTD for these failure synapses
% % % % Turn off LTD mechanism here (LTDon = 1 is ON)
        if spike_count(z,1) > 0
            LTDon = 1;
            if LTDon == 1;
                for ind = 1:r
                    spine = [prev_synapses(ind,1) prev_synapses(ind,2)];
                    tt = BAP(spine(1,1),spine(1,2),bAP_influence);  %
distance-dependent bAP influence
                    MM = zeros(S);
                    for iii = 1:length(MM)-1
                        MM(iii,iii+1) = tt;
                    end
                    MM = MM+eye(S)*(1-tt); % probability of staying in the
same state
                    if storeSites(spine(1,1),spine(1,2),z) ~= S
                        mm = MM(storeSites(spine(1,1),spine(1,2),t),:);
                        vv = [];
                        for kk = 1:length(mm)
                            vv = [vv (zeros(round(mm(kk).*100),1)+kk)'];
                        end
                        KK = randperm(length(vv));
                    % % for floor states (1:2)
                        if vv(KK(1)) == 2
                            if vv(KK(1)) == max(vv)
                                newstates1(spine(1,1),spine(1,2)) = 1;
                            else
                                newstates1(spine(1,1),spine(1,2)) = 2;
                            end
                        end
                    % % for all other states (3:10)
                        if vv(KK(1)) > 2
                            if vv(KK(1)) == max(vv)
                                newstates1(spine(1,1),spine(1,2)) =
newstates1(spine(1,1),spine(1,2))-1;
                            else
                                newstates1(spine(1,1),spine(1,2)) = min(vv);
                            end
                        end
                        if newstates1(spine(1,1),spine(1,2)) ~=
storeSites(spine(1,1),spine(1,2),z)
                            LTPvsLTD(t,2) = LTPvsLTD(t,2)+1;
                        else
                            LTPvsLTD(t,2) = LTPvsLTD(t,2)+0;
                        end
                        transitSites = newstates1;
                    end
                end
            end
        end
% % % IF SPIKE SUCCESS
    else
        spike_count(t,1) = num_inputs;
        LTPvsLTD(t,:) = 0;
```

```
        transitSites = storeSites(:,:,z);
%  >>>>>> SPIKE-DEPENDENT POTENTIATION
% %for synapses that contributed to the spike

%  ISOLATED SPIKES (no spike in previous iteration)
% % % % % % % % % % % % % % % % % % % % % % % % % % % % % % % % % % %
        if spike_count(z,1) < 0
            upsites = nonZeroVec(active_synapses);
            num_upsites = upsites > 0;
            LTPsites = sum(num_upsites(:,1));
            active_synapses = active_synapses(1:LTPsites(1),:);
            [r c] = size(active_synapses);
% % % % % % % % % % % % % % % % % % % % % % % % % % % % % % % % % % %
% % % % % % LOCAL SPATIAL INFLUENCE
            %     impose spatial influence here
%             spreadunit = 1;
            Imat = zeros(W,L)+1;
            [r c] = size(active_synapses);
            for f = 1:r
                xcoord = active_synapses(f,1);
                ycoord = active_synapses(f,2);
        %         centre the "cone of influence" on successfully-transitioned
sites
                for IW = 1:W
                    for IL = 1:L
                        Ipremat(IW,IL) =
1000000*Multivariate(IW,IL,xcoord,ycoord,spreadunit,spreadunit*spreadwidth,0)
;
                    end
                end
                Imat(:,:,f) = Ipremat;
            end
            Iproject = sum(Imat,3);
            Iproject = normalize(Iproject)./2;
            %     Apply mask to probability matrix
            [rows,cols] = find(mask == 1);
            for i = 1:length(rows)
            rr = rows(i);
            cc = cols(i);
            Iproject(rr,cc) = 0;
            end
% % % % % % % % % % % % % % % % % % % % % % % % % % % % % % % % % % %
% % % % % % % % % % % % % % % % % % % % % % % % % % % % % % % % % % %
            bAP = BAP(:,:,bAP_influence)+Iproject;

            newstates2 = transitSites;
            for ind = 1:r
                spine = [active_synapses(ind,1) active_synapses(ind,2)];
                tt = bAP(spine(1,1),spine(1,2));  % distance-dependent bAP
influence
                MM = zeros(S);
                for iii = 1:length(MM)-1
                    MM(iii,iii+1) = tt;
                end
                MM = MM+eye(S)*(1-tt); % probability of staying in the same
state
```

```
                if storeSites(spine(1,1),spine(1,2),t) ~= S
                    mm = MM(storeSites(spine(1,1),spine(1,2),t),:);
                    vv = [];
                    for kk = 1:length(mm)
                        vv = [vv (zeros(round(mm(kk).*100),1)+kk)'];
                    end
                    KK = randperm(length(vv));
                    newstates2(spine(1,1),spine(1,2)) = vv(KK(1));
                end
                if newstates2(spine(1,1),spine(1,2)) ~=
storeSites(spine(1,1),spine(1,2),z)
                    LTPvsLTD(t,1) = LTPvsLTD(t,1)+1;
                else
                    LTPvsLTD(t,1) = LTPvsLTD(t,1)+0;
                end
            end
            storeSites(:,:,t) = newstates2;
        else

% % CONSECUTIVE SPIKES ('RAPID' FIRING)
% % Find synaptic sites that participated in both spines
% % % % enhanced influence for common sites
            cmn = intersect(prev_synapses,active_synapses,'rows');
            [r c] = size(cmn);
            storeCommon(1:r,1:2,t) = cmn;
            common = nonZeroVec(storeCommon(:,:,t));
            num_common = common > 0;
            commonsites(t,1) = sum(num_common(:,1));
            common = common(1:commonsites(1),:);
            [r c] = size(common);
            newstates1 = storeSites(:,:,z);
            for ind = 1:r
                spine = [common(ind,1) common(ind,2)];
                tt = bAPplus(spine(1,1),spine(1,2));  % ENHANCED INFLUENCE
%                 tt = bAP(spine(1,1),spine(1,2));  % STANDARD INFLUENCE
                MM = zeros(S);
                for iii = 1:length(MM)-1
                    MM(iii,iii+1) = tt;
                end
                MM = MM+eye(S)*(1-tt); % probability of staying in the same
state
                if storeSites(spine(1,1),spine(1,2),t) ~= S
                    mm = MM(storeSites(spine(1,1),spine(1,2),t),:);
                    vv = [];
                    for kk = 1:length(mm)
                        vv = [vv (zeros(round(mm(kk).*100),1)+kk)'];
                    end
                    KK = randperm(length(vv));
                    newstates1(spine(1,1),spine(1,2)) = vv(KK(1));
                end
                if newstates1(spine(1,1),spine(1,2)) ~=
storeSites(spine(1,1),spine(1,2),z)
                    LTPvsLTD(t,3) = LTPvsLTD(t,3)+1;
                else
                    LTPvsLTD(t,3) = LTPvsLTD(t,3)+0;
                end
            end
```

```
% %
            upsites = nonZeroVec(active_synapses);
            num_upsites = upsites > 0;
            LTPsites = sum(num_upsites(:,1));
            active_synapses = active_synapses(1:LTPsites(1),:);
            [r c] = size(active_synapses);

% % % % % % % LOCAL SPATIAL INFLUENCE
            %     impose spatial influence here
%             spreadunit = 1;
            Imat = zeros(W,L)+1;
            [r c] = size(active_synapses);
            for f = 1:r
                xcoord = active_synapses(f,1);
                ycoord = active_synapses(f,2);
        %         centre the "cone of influence" on successfully-transitioned
sites
                for IW = 1:W
                    for IL = 1:L
                        Ipremat(IW,IL) =
1000000*Multivariate(IW,IL,xcoord,ycoord,spreadunit,spreadunit*spreadwidth,0)
;
                    end
                end
                Imat(:,:,f) = Ipremat;
            end
            Iproject = sum(Imat,3);
            Iproject = normalize(Iproject);
            %     Apply mask to probability matrix
            [rows,cols] = find(mask == 1);
            for i = 1:length(rows)
            rr = rows(i);
            cc = cols(i);
            Iproject(rr,cc) = 0;
            end
% % % % % % % % % % %
            bAP = BAP(:,:,bAP_influence)+Iproject;

            newstates2 = newstates1;
            for ind = 1:r
                spine = [active_synapses(ind,1) active_synapses(ind,2)];
                tt = bAP(spine(1,1),spine(1,2));  % distance-dependent bAP
influence
                MM = zeros(S);
                for iii = 1:length(MM)-1
                    MM(iii,iii+1) = tt;
                end
                MM = MM+eye(S)*(1-tt); % probability of staying in the same
state
                if storeSites(spine(1,1),spine(1,2),t) ~= S
                    mm = MM(storeSites(spine(1,1),spine(1,2),t),:);
                    vv = [];
                    for kk = 1:length(mm)
                        vv = [vv (zeros(round(mm(kk).*100),1)+kk)'];
                    end
                    KK = randperm(length(vv));
```

```
                    newstates2(spine(1,1),spine(1,2)) = vv(KK(1));
                end
                if newstates2(spine(1,1),spine(1,2)) ~=
storeSites(spine(1,1),spine(1,2),z)
                    LTPvsLTD(t,1) = LTPvsLTD(t,1)+1;
                else
                    LTPvsLTD(t,1) = LTPvsLTD(t,1)+0;
                end
            end
            storeSites(:,:,t) = newstates2;
        end
    end
    %     Reapply mask
    [rows,cols] = find(mask == 1);
    for i = 1:length(rows)
    rr = rows(i);
    cc = cols(i);
    storeSites(rr,cc,t) = 1;
    storeSites(rr,cc,t+1) = S+1;
    end
end

simulation = storeSites;

% % Some post-processing

APs = spike_count > 0;
ind = find(APs == 1);
for i = 1:length(ind)-1
    ISI(i) = ind(i+1) - ind(i);
end

% Log of LTP(:,1), LTD(:,2), LTPplus(:,3), LTP(all)-LTPplus(:,4)
% LTPvsLTD(:,4) = LTPvsLTD(:,1)-LTPvsLTD(:,3);

% save 'Spike Dep March 12 LTP plus LTD'

--
```

Appendix F

Integrate-and-fire model of spike-timing dependent plasticity: A course report for NSC8104, replicating the results from a theoretical study on STDP by Song & Abbott (Nature Neuroscience, 2000)

Stabilizing synaptic weight distributions through spike-timing dependent plasticity

A study of Song, Miller & Abbott (Nature Neuroscience, 2000)

Computational Neuroscience Summer School
NSC 8104

University of Ottawa

June 9-21, 2013

Report prepared by:
Kevin F.H. Lee
Neuroscience, University of Ottawa

Project partner:
Caitlyn Parmelee
Mathematics, University of Nebraska-Lincoln

Synaptic plasticity as a cellular substrate for neural circuit development and memory

The brain is faced with the complicated task of processing an immense amount of sensory stimuli to appropriately coordinate behaviour. These processes involve the rapid transfer of information within and between brain regions. The majority of fast excitatory neurotransmission between neurons takes place at specialized chemical junctions called synapses. Over the past four decades, a major framework has emerged for understanding how – at the cellular level – the brain is capable of adapting its functions to the environment, as occurs during learning and memory (Malenka & Bear, 2004). This framework is centred on the active regulation of the strength of synaptic transmission, in response to patterned neural activity, termed 'synaptic plasticity'. Synaptic plasticity can powerfully modulate the routing of neural information flow in the brain by strengthening specific synaptic connections, while weakening others, in an activity-dependent manner. The most widely studied forms of synaptic plasticity are long-term potentiation and long-term depression (LTP and LTD, respectively; Malenka & Bear, 2004). As key features of LTP and LTD are consistent with a prescient hypothesis posed by Donald Hebb more than fifty years ago, these forms of synaptic plasticity are now broadly referred to as "Hebbian" forms of synaptic plasticity.

Among the numerous insights into Hebbian-type plasticity uncovered over the past decades, one particularly important finding is that the relative timings of presynaptic and postsynaptic activity can dictate the direction of synaptic changes (potentiation/strengthening or depression/weakening; Bell et al. 1997; Markram 1997; Bi & Poo 1998; Bi & Poo 2001). Specifically, LTP is induced when presynaptic input precedes postsynaptic firing ('pre-post'), whereas LTD occurs when presynaptic input follows postsynaptic firing (post-pre). These 'spike-timing dependent plasticity' (STDP) rules require that pre- and postsynaptic events (Δt) occur

within approximately 50ms of one another to elicit measureable synaptic changes, with the most robust synaptic changes occurring with the shortest Δt (for review, see Bi & Poo 2001). These plasticity rules therefore favor the strengthening of synapses that are causal to postsynaptic spike activity and the weakening of synapses that do not contribute to postsynaptic spiking. Thus, STDP provides a plausible and intuitive physiological means for neurons to store information, by sensitizing postsynaptic neurons to specific presynaptic inputs.

Insights at the intersection of experimental and theoretical investigations

Experiments in neurobiology are perpetually limited by the technological state of experimental tools. In many cases, some questions are nearly impossible to investigate in a wet lab due do feasibility. For instance, it technically difficult to explore the long-term consequences of STDP experimentally due to the strict conditions required to reveal it (although this may now be possible in neurons cultured on multi-electrode arrays; Muller et al. 2013). As such, questions of whether STDP can support stable neuronal firing and efficient information-processing, or whether other mechanisms must exist, are difficult to test. In this respect, theoretical works using computer models have been instrumental in exploring these hypothetical avenues and has generated important mechanistic insights to help bridge relationships between observed phenomena.

Early observations of ocular dominance columns development in the kitten visual cortex led to the hypothesis that 'synaptic competition' must exist, where some synapses stabilize at the expense of others (Hubel & Wiesel 1965; Blakemore 1976). Similar observations were later reported using other developing nervous systems (Rubel et al 1990; Shatz 1990; Fraser 1990; Lo & Poo 1991; Zhang 1998). For instance, synaptic competition was demonstrated using cultured

muscle cells innervated by two competing motor afferents to show that potentiation of one afferent pathway led to the depression of the other (Lo & Poo 1991). Despite demonstrating experimental control over the phenomenon, the mechanism underlying competition remained elusive. The discovery of STDP (Markram 1997, Bi 1998) provided an interesting potential mechanism for synaptic competition. The first experimental observation indicating that STDP could provide a basis for synaptic competition came from a study in the Xenopus tadpole tectal system *in vivo* where presynaptic activity from two convergent afferent pathways exhibited differential degrees of plasticity depending on the timing of their activity with respect to postsynaptic spiking (Zhang et al. 1998). Although this experimental work suffered the same limitations as the *in vitro* demonstrations described above, STDP provided an attractive framework that could be modeled numerically, and therefore manipulated and studied *in silico* with relative ease. The subsequent years witnessed a flurry of both experimental and theoretical work on STDP and synaptic competition, yielding lively debate.

A classic study published in 2000 by the group of Larry F. Abbott at Brandeis University found that the simple implementation of STDP in a neuron model forces synaptic competition (Song et al. 2000). In doing so, STDP resulted in a stable steady-state synaptic weight distribution and it was thus argued that STDP carries inherent stabilizing properties to neuronal function. In this report, we will examine a classic computer model of STDP from Song et al. (2000), which was our topic of study during the 6th Computational Neuroscience Summer School at the University of Ottawa (NSC8104; June 9-21, 2013). The strengths and limitations of the model will be discussed, and we will also contrast with experimental data and different variations of STDP models now in the literature.

Modeling Synaptic Competition and Spike-Timing Dependent Plasticity

Song et al. (2000) modeled an integrate-and-fire (IF) neuron that included basic STDP rules in line with previously described experimental data (Markram et al. 1997; Bi & Poo 1998). The IF model maintains fundamental features of synaptic integration and spike generation, but is unlike the Hodgkin-Huxley or FitzHugh-Nagumo neuron models because action potential dynamics are reduced to instantaneous delta-like function events. When the membrane potential of the IF neuron reaches action potential threshold, the membrane potential is reset to some subthreshold value. In this way, the subthreshold temporal relationships between synaptic input and postsynaptic spiking can be efficiently studied. Since the core questions surrounding STDP are centred on subthreshold events (that is, the precise timing of presynaptic input relative to postsynaptic spiking), the IF neuron model provides a simple and computationally efficient foundation for addressing such questions. Being a simplified model, however, the IF neuron requires important overarching assumptions. One assumption is that all action potentials are equal, and that complex action potential firing, such as bursts, can be ignored. It is also assumed that the action potential interacts equally with every synapse in the model, and that all synapses influence spike activity with zero attenuation. These are considerable oversimplifications given the cable properties of dendrites and the diverse spiking behaviour known to exist in neurons. Nevertheless, the IF neuron serves as a useful starting point for exploring questions of STDP.

Song et al. (2000) found that synaptic competition arising from STDP tends to push synaptic weights towards upper and lower extremes, resulting in a bimodal distribution of synaptic weights. It was argued that this stable weight distribution provides a balanced regime of excitatory and inhibitory input and ultimately sensitizes the postsynaptic neuron to respond to correlated bursts of input with shorter latency. The authors therefore concluded that synaptic

competition via STDP mechanisms provide a basis for stable neuronal function. Here, I discuss our efforts to replicate this STDP model.

Methods & Results

As described by Song et al. (2000), we constructed an IF neuron model that received 1000 excitatory and 200 inhibitory synaptic inputs and was stimulated by independent Poisson spike trains. Excitatory input was tested with constant average rates of 6-40 Hz. Inhibitory input was constant at a rate of 10 Hz. We focused our study using only independent Poisson inputs and did not explore correlated input bursts, which was also investigated by Song et al. (2000).

The membrane potential of the neuron was given by

$$\tau_m \frac{dV}{dt} = V_{rest} - V + g_{ex}(t)(E_{ex} - V) + g_{in}(t)(E_{in} - V)$$

To implement this in our model, we approximated V through time using the Euler method with a time step dt = 1.0 msec by

$$V(t+1) = V(t) + dt/\tau_m \cdot [V_{rest} - V(t) + g_{ex}(t)(E_{ex} - V(t)) + g_{in}(t)(E_{in} - V(t))]$$

Membrane potential is therefore dictated by the sum of inhibitory (g_{in}) and excitatory (g_{ex}) inputs, and a tendency to relax to (V_{rest}) according to the membrane time constant (τ_m). Membrane potential fluctuations are shown in **Figure 1**. When the membrane voltage exceeds the action potential threshold, a spike is said to occur, and V is set to -60 mV. In contrast to so-called leaky-integrate-and-fire (LIF) neuron models, this IF model does not explicitly include a leak conductance (typically modeling a potassium conductance). The constant inhibitory input at 10 Hz does, however, serve impart a leaky property to this model.

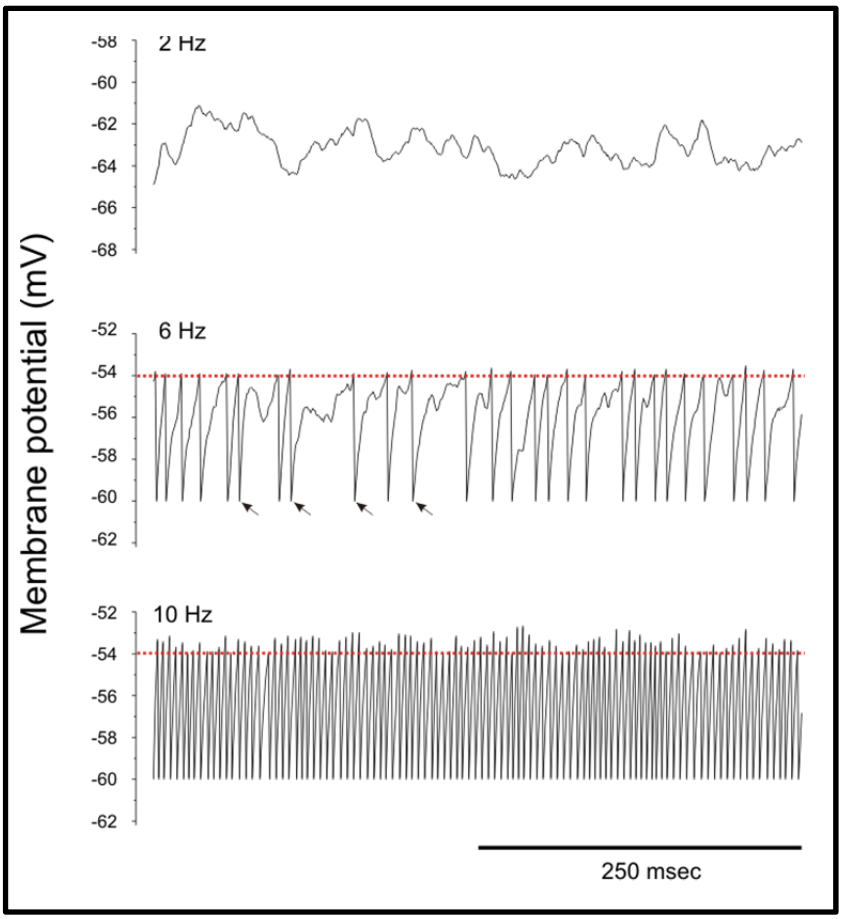

Figure 1. Dynamic membrane voltage fluctuations and action potential discharge in an Integrate-and-Fire (IF) neuron model.

Top: Subthreshold membrane potential fluctuations at the onset of simulation in response to 2 Hz Poisson input.

Middle: Increasing the stimulus frequency to 6 Hz causes action potential discharge, represented by a membrane potential reset to -60 mV (arrows: 4 example spikes)

Bottom: The postsynaptic neuron fires at high frequency at the beginning of the simulation in response to 10Hz Poisson input.

We used the values of the membrane time constant, τ_m= 20 msec; resting membrane potential, V_{rest} = -70 mV; action potential threshold = -54 mV; excitatory synaptic reversal potential, E_{ex} = 0 mV; inhibitory synaptic reversal potential, E_{in} = -70 mV, as described (Song et al. 2000). Individual inhibitory synaptic conductances were fixed at $\bar{g}_{in} = 0.05$. The excitatory conductance of each synapse *a* was modifiable according to STDP rules but was bounded by $0 \leq \bar{g}_a \leq \bar{g}_{max}$ with $\bar{g}_{max} = 0.015$. According to calculations by Song et al. (2000), $\bar{g}_{max} = 0.015$ corresponds to a peak synaptic conductance of 150 pS for a neuron with 100 MΩ input resistance.

Because inhibitory synapses were fixed at $\bar{g}_{in}$ and did not exhibit plasticity, we calculated inhibitory input at each time step by $g_{in} \rightarrow \bar{g}_{in} \cdot N$, where N is the number of active inhibitory synapses during the time step. Since excitatory synapses were not fixed and exhibited plasticity, it was necessary to actively track and update each excitatory synapse individually. Excitatory synaptic input was the sum of individual synaptic conductances, $g_{ex} \rightarrow \sum g_a$, where a is the index of each synapse active during the time step. Both excitatory and inhibitory synaptic inputs decay exponentially with the time constants, $\tau_{in} = \tau_{ex} = 5$ msec, and were approximated at each time step using the Euler method by,

$$g_{in}(t+1) = g_{in}(t) \cdot e^{-\left(\frac{dt}{\tau_{in}}\right)} + g_{in}$$

$$g_{ex}(t+1) = g_{ex}(t) \cdot e^{-\left(\frac{dt}{\tau_{ex}}\right)} + g_{ex}$$

According to these dynamics, synaptic events are summed linearly and decay with a single exponential time course described by τ_{in} and τ_{ex}. This implies that, given equal synaptic weights, all synapses will equally influence membrane potential and therefore action potential output. We therefore assume no filtering of synaptic potentials by dendritic cable properties.

As discussed in the *Results* section of the paper (Song et al. 2000), STDP followed a rule whereby the function $F(\Delta t)$ determines the amount of potentiation or depression for each presynaptic-postsynaptic spike pair (**Figure 2**).

$$F(\Delta t) = \begin{cases} A_+ \cdot e^{\left(\frac{\Delta t}{\tau_+}\right)} & if\ \Delta t < 0 \\ -A_- \cdot e^{\left(\frac{-\Delta t}{\tau_-}\right)} & if\ \Delta t \geq 0 \end{cases}$$

The parameters τ_+ and τ_- reflect the STDP window and were both set to 20 msec; A_+ and A_- reflect the maximum amount of synaptic modification when $\Delta t \approx 0$. Song et al. (2000) determined the values of A_+ and A_- by dividing the total amount of synaptic modification observed experimentally by the total number of pre-post spike pairings used to induce the modifications. Song et al. (2000) therefore established that $A_+ = 0.005$ and $A_- = 1.05 \cdot A_+ = 0.0053$, with the assumption that synaptic depression is a slightly stronger process than synaptic potentiation during STDP. The effect of each pre-post spike pair is determined by $\bar{g}_{max} \cdot F(\Delta t)$ such that the maximum amount of potentiation per spike pair is 0.5% of peak synaptic conductance $\bar{g}_{max}$. If a potentiation event at synapse a makes $\bar{g}_a$ greater than $\bar{g}_{max}$ then $\bar{g}_a = \bar{g}_{max}$. Similarly, $\bar{g}_a = 0$ if a weakening event at synapse a brings $\bar{g}_a$ below 0.

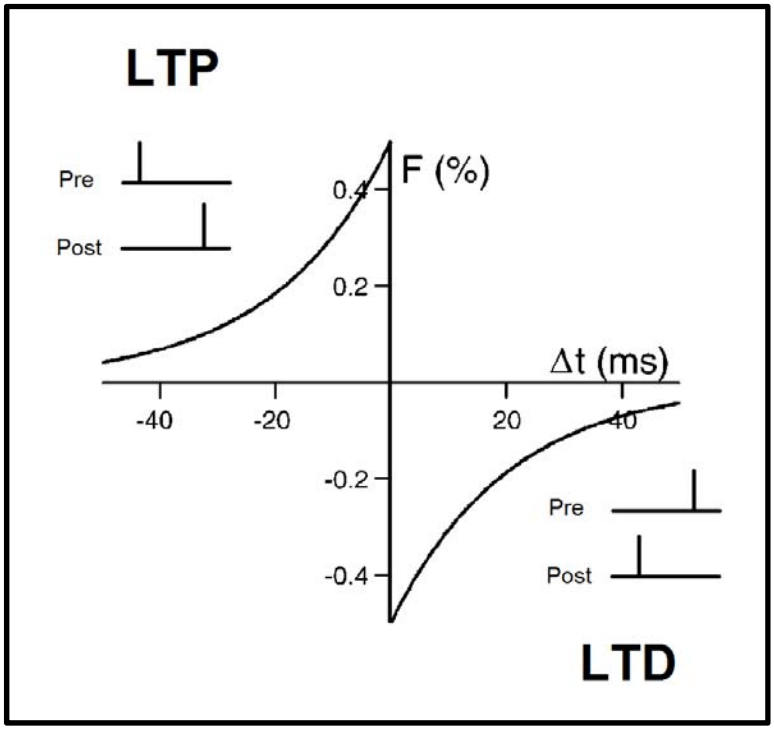

Figure 2. Spike-timing dependent plasticity synaptic modification rule

When presynaptic activation precedes a postsynaptic action potential spike, the active synapses undergo synaptic potentiation (LTP).

If presynaptic activation takes place after a postsynaptic spike, the active synapses undergo LTD.

The amount of synaptic strengthening that occurs with each spike pair depends on the relative timing of pre- and postsynaptic spikes. Pre-post pairs that exceed Δt of approximately 50 msec will not induce plasticity.

In general, this rule establishes that a synapse can strengthen with a maximum change of $A_+ \cdot \bar{g}_{max}$ and weaken with a maximum change of $A_- \cdot \bar{g}_{max}$. Given that $\bar{g}_{max}$ is fixed, the synaptic weights in this model are hard bounded by 0 and $\bar{g}_{max}$. Changes in synaptic weight are

assumed to be independent of the starting synaptic weight. These assumptions will be considered in further detail in the *Discussion*.

Although conceptually straightforward, we faced considerable challenges in implementing these plasticity rules in our model. The *Methods* section of Song et al. (2000) described two variables M and P_a that were used to dictate synaptic depression and potentiation, respectively. However, it was not immediately clear how to make use of these variables. As such, we ignored M and P_a during our first attempt and instead decided to interpret the function $F(\Delta t)$, as described in the *Results* (Song et al. 2000), to implement the STDP rules in our model. We reasoned that we could correctly modify synaptic weights if the time of each synaptic input and each postsynaptic spike was actively tracked. We therefore designed the model such that upon a postsynaptic spike, each synapse potentiates according to the Δt between the spike and their respective synaptic activation times leading up to the spike. Synaptic depression was set to occur at each time step for all active synapses based on Δt since the time of the last postsynaptic spike. In principle, this method of implementing the STDP rule appeared sound. However, we soon found that implementing such a rule in MATLAB was computationally inefficient (*horribly* inefficient!). In fact, our TA Mr. Stephen Clarke offered to run our model on his personal computer, which he touted as a sort of demi-supercomputer. It was not long before Mr. Clarke emailed to notify us that his computer became rather upset when attempting to run our model, and informed us that our script was computationally burdensome. We were provided with some basic strategies to pre-allocate memory, but these changes did little to facilitate the running of our model – it simply was not the proper computational strategy. Therefore, we returned to the *Methods* section of Song et al. (2000) to study the M and P_a variables more closely. Song et al. (2000) describe M and P_a as exponentially decaying variables:

$$\tau_- \frac{dM}{dt} = -M \qquad \text{and} \qquad \tau_+ \frac{dP_a}{dt} = -P_a$$

Upon closer inspection and contemplation, and to our general relief, it became clear how M and P_a were used to carry out synaptic modifications. As described by Song et al. (2000), the variable M dictates the amount of synaptic depression and was a single value that was applied across all synapses. The variable P_a determines the amount of synaptic potentiation and is specific for each synapse a. All values of P_a can be stored in the vector P and therefore updated quite easily with each time step dt. We set initial values of M and P_a to zero and their values were determined using the Euler method as follows:

For each postsynaptic spike at time t, M is decremented by A_-

$$M(t+1) = M(t) \cdot e^{-\left(\frac{dt}{\tau_-}\right)} - A_-$$

Otherwise, the value of M decays exponentially with each time step by

$$M(t+1) = M(t) \cdot e^{-\left(\frac{dt}{\tau_-}\right)}$$

Upon each presynaptic spike at synapse a, P_a is incremented by A_+

$$P_a(t+1) = P_a(t) \cdot e^{-\left(\frac{dt}{\tau_+}\right)} + A_+$$

Otherwise, the value of P_a for all synapses decays exponentially with each time step by

$$P_a(t+1) = P_a(t) \cdot e^{-\left(\frac{dt}{\tau_+}\right)}$$

Together, M and P_a provide computationally effective means to track and apply the correct amount of synaptic modification in a synapse-specific manner, consistent with the function $F(\Delta t)$. Synaptic plasticity was therefore carried out as follows:

Each postsynaptic spike served as a signal for synaptic potentiation at synapse *a* according to

$$g_a(t) = g_a(t-1) + g_{max} \cdot P_a(t)$$

Synaptic depression occurred for each synapse *a* at every time step *t* according to

$$g_a(t) = g_a(t-1) - g_{max} \cdot M(t)$$

Surprisingly, however, we found that our model did not behave as described by Song et al. (2000), across all input frequencies that were tested (10-40 Hz). Specifically, it was stated that "*...a steady-state condition was achieved in which the firing rate of the postsynaptic neuron and the distribution of peak synaptic conductances remained constant*" (**Figure 3**). It was further noted that "*...there is no stable equilibrium state with a uniform distribution* [of synaptic conductances]" (Song et al. 2000). In every simulation we performed, we achieved a steady-state firing rate of 0 Hz (**Figure 4**) and uni-modal distributions of synaptic conductances (**Figure 5**). This was in stark contrast to the reported bimodal distribution of synaptic weights we originally sought to replicate. Since we observed a qualitatively similar trend whereby higher input frequencies tended to shift the synaptic conductance distribution toward lower values, we first considered whether the model simply required more simulation time for the weight distributions to evolve. However, because postsynaptic spiking gradually ceased in our model, it was unlikely that longer simulation times could rescue our results because synaptic plasticity was completely dependent on spiking activity. Thus, although we felt confident in our MATLAB code, we were

still short of our goal of replicating a core finding of the study. We began to explore alternative reasons for the discrepancies.

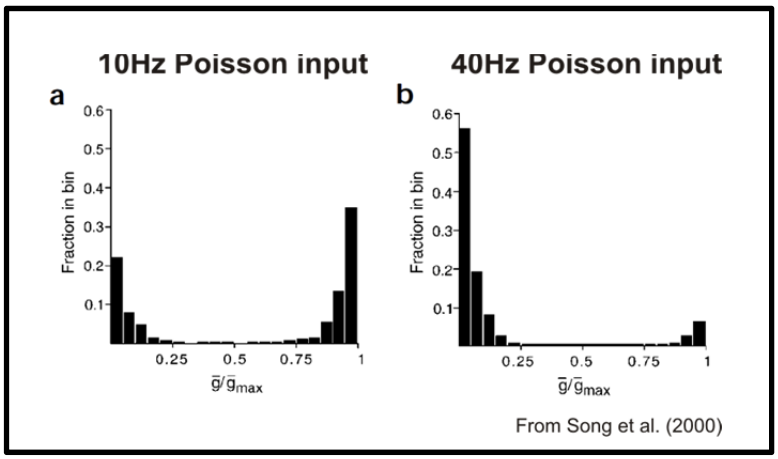

Figure 3. STDP induces synaptic competition and generates stable bimodal distributions of synaptic weights.

Stable bimodal synaptic weight distributions were shown develop from STDP. These steady-state distributions were suggested to balance excitation and inhibition and therefore promote stable neuronal function.

Adapted from Song et al. (2000)

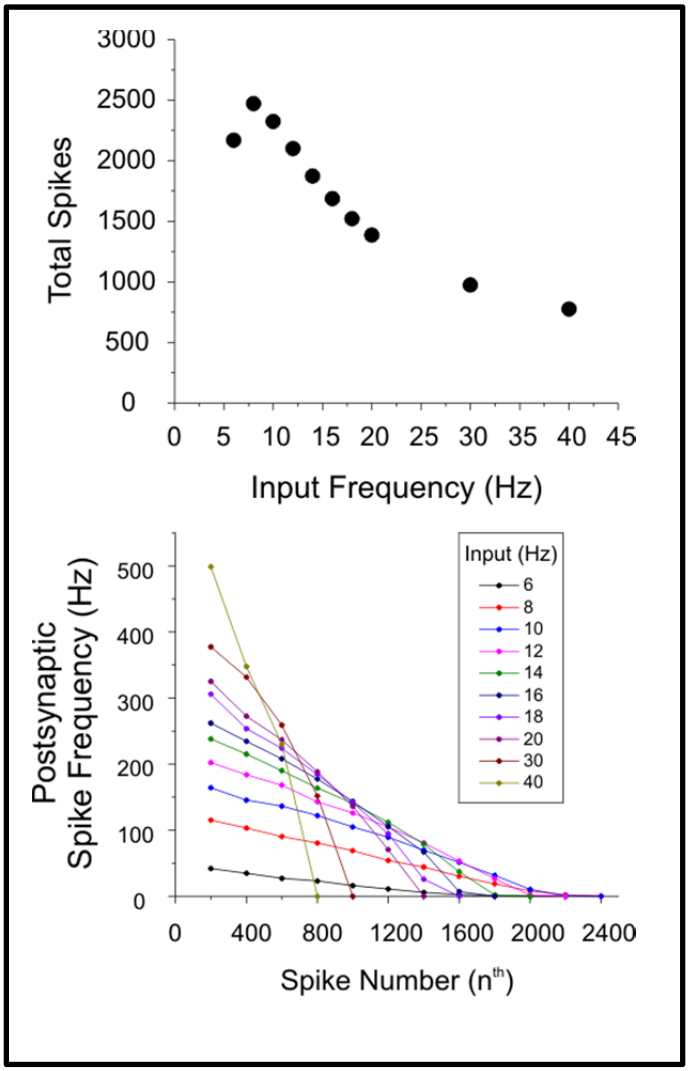

Figure 4. Initial attempts at replicating the model of Song et al. (2000) failed.

Steady-state postsynaptic activity.

Across all input frequencies tested, our model neuron gradually ceased to fire action potentials. Here, a total of 60 minutes were simulated at ten different input frequencies (6, 8 10, 12, 14, 16, 18, 20, 30, 40 Hz).

Top: Total number of postsynaptic spikes after 60 minutes of simulated time. Total spike count decreases with increasing stimulus frequency.

Bottom: Average postsynaptic spike frequency was calculated in 200-spike bins. All input frequencies led to a complete cessation of postsynaptic firing. Cessation of postsynaptic firing was achieved more quickly with higher stimulus frequencies.

First, we recalled that the accuracy of the Euler method in solving discrete-time ordinary differential equations is highly dependent on step size, with its error proportional to step size. Therefore, we entertained the idea that a time step of 1 msec was perhaps too long, leading to the unexpected behaviour of our model. At first, it was difficult to understand this possibility since the shortest decay time constant in our model was 5 msec. By drawing an analogy from the Nyquist sampling theorem, a time step of 1 msec should provide a reasonable 'sampling rate' to account for the behaviour in the model. Nevertheless, we reduced the time step by one order of magnitude from 1 msec to 0.1 msec and re-tested the model. Our results were unchanged by this adjustment across a range of synaptic input frequencies, indicating that the original 1 msec time step did not play a role in distorting the behaviour of our model (not shown).

Since the synapses in our model were weakening until postsynaptic spiking could no longer be sustained, we next wondered whether the balance between synaptic depression and potentiation was in some way distorted. While reviewing our MATLAB script, we identified a small error whereby the potentiation variable P_a was not properly decaying with time. Since this error would in principle serve to elevate potentiation in the simulations, it was unlikely to underlie the primary problem of strong synaptic depression. As expected, correcting this error did not change our results (not shown).

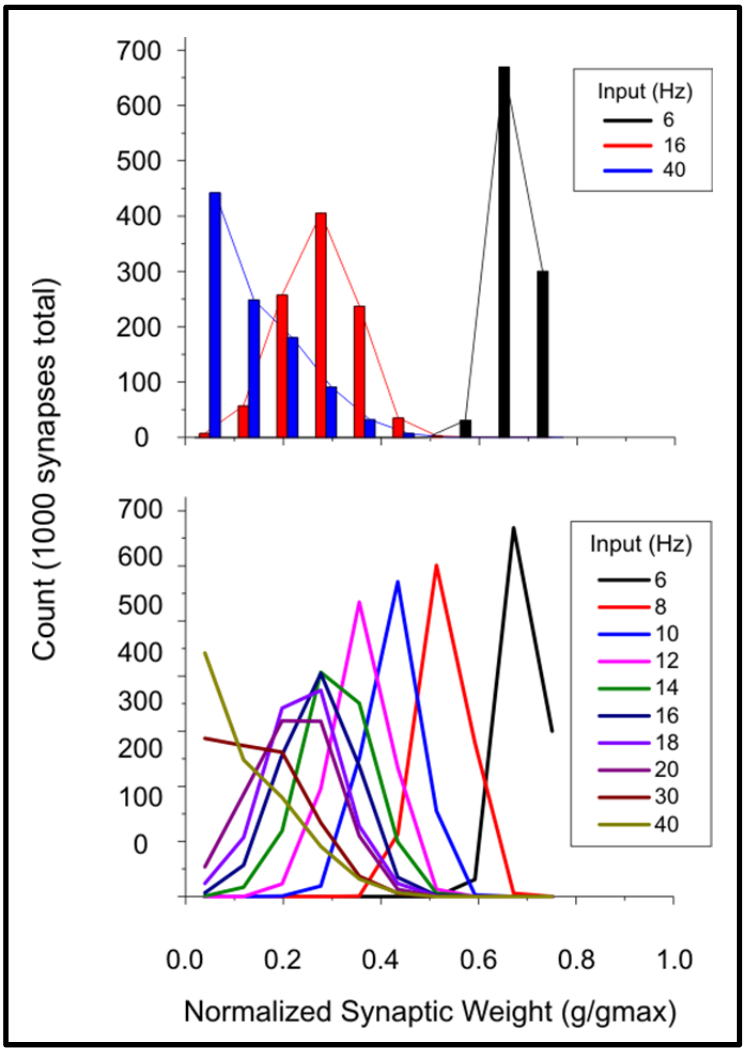

Figure 5. Initial attempts at replicating the model of Song et al. (2000) failed.

Steady-state synaptic weight distributions.

Top: Steady-state synaptic weight histograms after 60 minutes of simulated time with 6, 16 and 40 Hz synaptic stimulation. Unlike the expected bimodal distributions (Figure 3), steady-state weight distributions were unimodal in the model and no longer sustained postsynaptic activity in response to the stimulus (Figure 4). Increasing the stimulation frequency causes a left shift in the distribution, toward lower synaptic weights.

Bottom: As above, but shown for all ten input frequencies tested (Figure 4).

We next noted that Song et al. (2000) investigated the effects of manipulating the ratio of depression and potentiation by testing various A_-/A_+ ratios. It was shown that elevating the A_-/A_+ ratio to 1.10 resulted in a steady-state postsynaptic firing rate of 0 Hz, while A_-/A_+ ratios close to 1.00 maintain high rates of postsynaptic firing (Song et al. 2000). Although our model initialized with an A_-/A_+ ratio of 1.05 as described by Song et al. (2000), we decided to reduce the A_-/A_+ ratio to 1.00 and tested our model once again, expecting to see a robust change in the behaviour of the model. To our surprise, this change did not alter our results significantly (not shown).

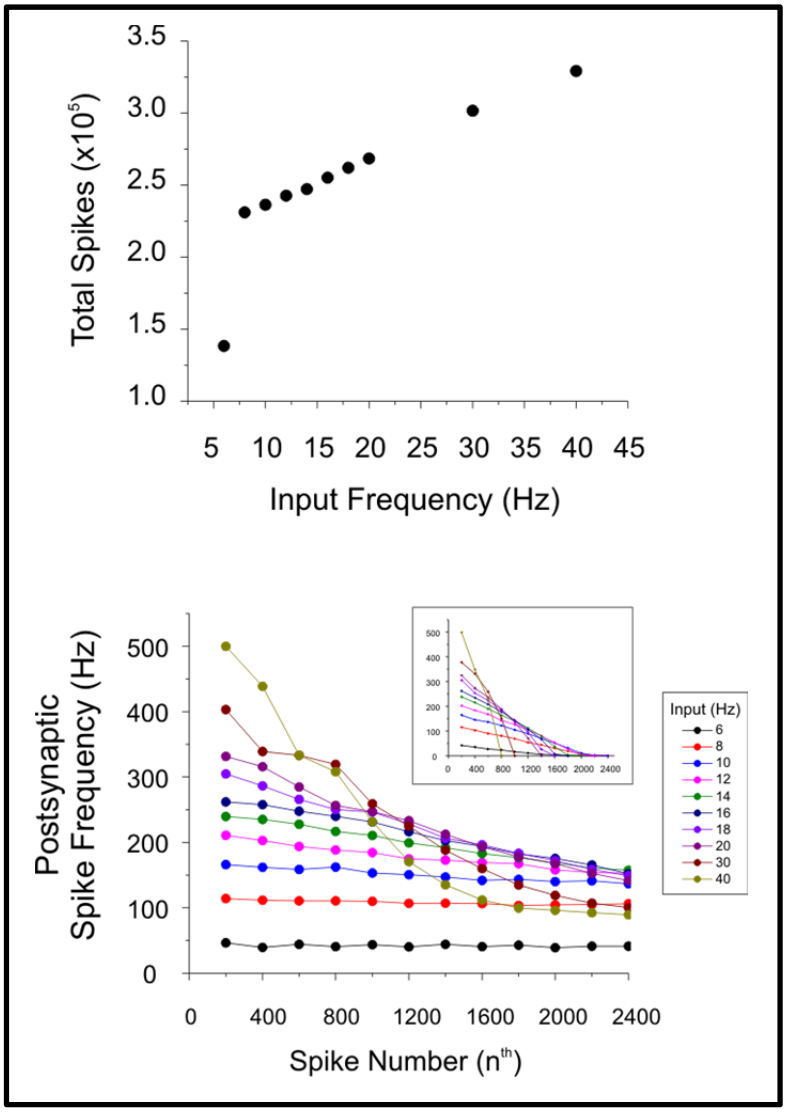

Figure 6. Success in replicating the core STDP model of Song et al. (2000).

Steady-state postsynaptic activity.

Same as Figure 4, but with revised/improved model (see text). The neuron model achieves a stable non-zero rate of firing across all input frequencies.

Top: Total number of postsynaptic spikes after 60 minutes of simulated time. Increasing input frequency causes an elevation in the average steady-state firing rate and total spike count.

Bottom: Postsynaptic spike frequency was calculated in 200-spike bins. The model neuron achieves a steady-state non-zero firing rate. *Inset*: Initial uncorrected behaviour of the model.

On the morning of our scheduled project presentation (June 21), I spoke with Dr. John Lewis about our difficulties replicating results from Song et al. (2000). I described the behaviour of our model and our attempts to correct it. Again, the potentiation rules roused suspicion since the propensity for synaptic depression was clearly dominating our simulations. While sitting in the lecture hall with my mind fixated on our model, Dr. Georg Northoff lecturing on brain imaging studies, it dawned on me – our code was written such that only a small fraction of all synapse were strengthened with each postsynaptic spike! Whereas the *every* synapse should have

potentiated upon each postsynaptic spike at time *t*, our code was written such that only synapses activated at time *t* were strengthened. This can be understood by considering the potentiation factor P_a of each synapse *a*. As described above, the value of P_a is specific for each synapse and is actively adjusted based on the time of previous synaptic events. The vector *P* that contains the values of P_a for each synapse therefore tracks synapse 'history' such that the appropriate amount of potentiation occurs for each synapse *a* whenever the postsynaptic neuron spikes. After making the necessary adjustments to ensure that *each* synapse potentiated according to their respective P_a with each postsynaptic spike, we were finally able to replicate that "*…a steady-state condition was achieved in which the firing rate of the postsynaptic neuron and the distribution of peak synaptic conductances remained constant*" (Song et al. 2000). These (triumphant!) simulations were performed less than two hours before our scheduled presentation and we were fortunate to demonstrate our success in replicating a core finding of Song et al. (2000) – that STDP produces synaptic competition, which drives the formation of a stable bimodal distribution of synaptic weights and steady-state postsynaptic firing rate (**Figures 6 & 7**).

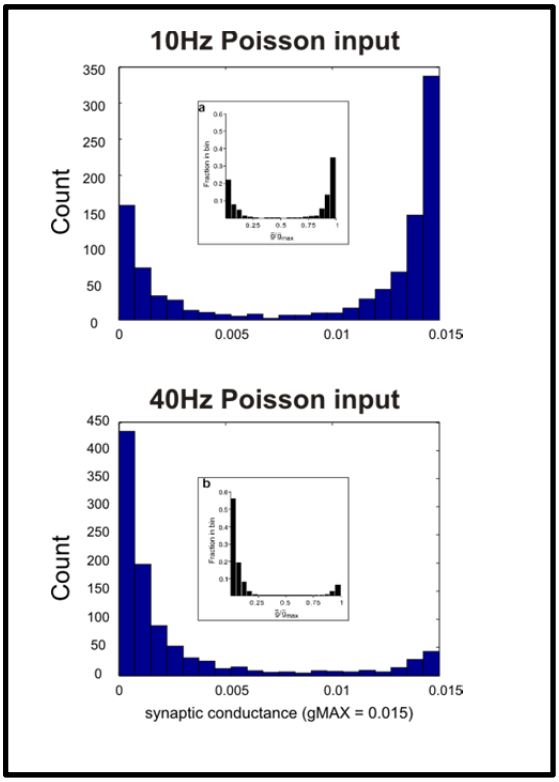

Figure 7. Success in replicating the core STDP model of Song et al. (2000).

The neuron model achieves a stable bimodal synaptic weight distribution.

Synaptic weight distributions after 60 minutes of simulated time in response to 10 Hz (Top) and 40 Hz (Bottom) Poisson spike trains. *Inset* shows the corresponding data from Song et al. (2000).

Notice that our model replicates the left-shift in synaptic weight distribution observed by the original study (*Inset*).

Discussion

Synaptic plasticity has served as the theoretical cellular basis of learning and memory for decades. STDP enables the strengthening of synaptic inputs that drive postsynaptic spiking, and weakening of synapses that are less predictive of postsynaptic activity. The study of Song et al. (2000) provides interesting theoretical insights into the stabilizing features of STDP, demonstrating that STDP *per se* can impose competition between synapses. Their model showed that synaptic competition allows the neuron to achieve a stable bimodal distribution of synaptic weights. This acts to balance the ratio of inhibition and excitation, and reduces the latency of postsynaptic firing in response to presynaptic inputs. We developed an integrate-and-fire STDP model in MATLAB that well replicates core findings of Song et al. (2000) – that STDP drives the emergence of a bimodal steady-state distribution of synaptic weights in response to independent Poisson input trains, across a wide range of input frequencies. We did not pursue

more detailed aspects of the study, such as the effects of correlated bursts of synaptic input. Nevertheless, the fundamental notion of synaptic competition by STDP has received interesting debate since the publication of this report. Specifically, there exists an apparent discrepancy between this STDP model and experimental data regarding synaptic weight distributions. One potential solution to this problem might be found by re-examining the study by Song et al. (2000), and we will formulate a novel prediction that can be tested in the future. Finally, alternative models of STDP and challenges to the notion of synaptic competition will be considered.

First, it is pertinent to ask how the bimodal synaptic weight distributions described by Song et al. (2000) compare to synaptic weights measured experimentally. Although Song et al. (2000) suggest that the weight distributions derived from their model "*...matches the experimentally observed distribution of spontaneous synaptic (mini) potentials"*, citing Bekkers & Stevens (1996), we feel that re-examination of these data do not support this claim. Instead, I contend that the data reported by Bekkers & Stevens (1996) show unimodal synaptic weight distributions, with an apparent skew simply arising from effects of cable filtering by dendrites. Such a skew cannot be compared to that observed in this IF STDP model since cable properties are not accounted for. Examination of additional studies that have performed recordings of spontaneous synaptic events further supports the notion that synaptic weight distribution are unimodal around some mean value (Turrigiano 1998, Beique et al. 2006, Goel & Lee 2007, Soares et al. 2013, resubmitted). Given the data presented by Song et al. (2000), a reinterpretation may help reconcile this discrepancy with experimental literature.

One key notion from the model described by Song et al. (2000) is that STDP forces *competition* between synapses. Competition is difficult to conceptualize when the synaptic input consists of

persistent independent Poisson trains across the entire synaptic population, but can be better understood when STDP is studied in response to discrete bursts of synaptic input. Consider a postsynaptic neuron receiving a 20 msec burst of input from multiple presynaptic partners, as in Figure 4 of the paper (Song et al. 2000). As outlined by Song and colleagues, if the postsynaptic neuron spikes sometime during the burst, STDP rules will effectively separate 'pre-post' and 'post-pre' pairings and induce synaptic strengthening and weakening among the synapses, accordingly. Thus, a subset of synapses active during the burst is potentiated while others are depressed, and it is relatively easy to see how a bimodal synaptic weight distribution emerges from STDP. But why is the bimodal synaptic weight distribution not observed experimentally? It is likely that the bimodal distribution simply does not reflect the entire synaptic population of a neuron, but rather the tug-of-war that exists at an individual subset of competing synapses. One can thus consider a neuron that receives many different patterns of synaptic input in the form of correlated bursts, with specific temporal sequences of unique subsets of synapses that comprise these bursts. Here, we can assume flexibility in this synaptic code such that synapses may participate in multiple bursts, albeit at different relative latencies. Under these circumstances, the synapses that lead in the burst order will strengthen while others weaken, and this competition can exist across multiple distinct subsets of synapses. In this way, the bimodal distribution that theoretically arises from competition within a single burst does not represent a cell-wide synaptic weight distribution, which could acquire an entirely different shape, and the notion of a 'steady-state' bimodal distribution may be misleading. It is tempting to therefore speculate that the phenomenon of synaptic competition described by Song et al. (2000) could exist between many subsets of synapses, each encoding different pieces of neural information. In this way, STDP

might lead to a global unimodal weight distribution as found experimentally. Future computer simulations can readily test this hypothesis.

The hypothesis presented above introduces a simple change that could provide new perspectives on the results of Song et al. (2000). However, this reformulation of the model still necessitates the same set of assumptions as the original model, which may not accurately reflect biology. One important assumption is that the amount of synaptic modification at each synapse is independent of its synaptic weight. This idea is challenged by experimental work showing that the propensity for synaptic potentiation may be weaker for strong synapses (Debanne 1996, 1999; Bi and Poo1998). Furthermore, different models have questioned the necessity of synaptic competition for maintaining a stable distribution of synaptic weights. For example, van Rossum et al. (2000) described a model of STDP which included weight-dependent synaptic plasticity. This weight-dependence rendered synaptic potentiation self-limiting and therefore circumvented the need for a hard upper bound to synaptic weight. Importantly, a stable, unimodal synaptic weight distribution that more closely matched the experimental distributions described above was achieved (van Rossum et al. 2000). It was further noted that synaptic competition was relatively weak, leading to the conclusion that competition was not necessary for achieving a stable synaptic weight distributions. This study was therefore in direct opposition to the results of Song et al. (2000) which can be explained by differences in the design and complexity of the models. A review of these differences was later published by authors of the conflicting studies (Kepecs et al. 2002).

Recall that during our first attempts to replicate the core STDP model of Song et al. (2000), we encountered difficulty generating a bimodal distribution of synaptic weight. Instead, our distributions were largely unimodal. After presenting our results, Dr. John Lewis asked whether

our troubleshooting experience could tell us something about how a unimodal distribution of weights might arise from STDP. He pointed out that our old 'bugged' model simply had fewer synapses potentiating, and asked whether that could perhaps better reflect the situation in a 'real' neuron. I immediately caught on to this line of thought and recalled that indeed, due to cable properties of dendrites, the signal for STDP (back-propagating action potentials) likely does not reach all synapses equally. Altogether, there is good evidence to suggest that the bimodal weight distribution demonstrated by Song et al. (2000) is not likely representative of the weight distributions of a neuron, and perhaps should not be interpreted as such – although some groups have (van Rossum et al. 2000).

Instead, the bimodal weight distribution emerging from the model is perhaps better situated to demonstrate the basic phenomenon of synaptic competition by spike-timing dependent plasticity. Given the thousands of synapses that impinge on individual neurons, such competition – with winners and losers – could take place among many different subsets of synapses (innumerable combinations), each participating in different ensembles of input with different relative temporal lags. This idea is, to the best of knowledge, very different from a recent compartmental model of a L5 pyramidal cell (Bar Ilan et al. 2010). This model segregated the neuron into different subcellular STDP territories (ie/proximal vs distal dendrites), and found that competition resulted in territory-specific bimodal weight distributions. Contrary to this model, we propose that a more realistic neuron model should face 'decisions' between multiple, distinct, patterns of input *perhaps within distinct subcellular domains*, that STDP could help encode information across a stable, overall unimodal, weight distribution. Other models have provided alternative mechanisms to achieve stable unimodal weight distributions, including non-linear forms of

STDP (Gilson & Fukai 2011) and inclusion of weight-dependence (van Rossum et al. 2000; but see Bonfill-i-Petit & Murray 2004).

Many models of STDP, at both single-cell and network levels, now exist, with varying degrees of complexity between them (Song et al. 2000; van Rossum et al. 2000; Song & Abbott 2001; Bonfill-i-Petit & Murray 2004; Appleby & Elliott 2006; Lazar et al. 2007, 2009; Watt & Desai 2010; Gilson & Fukai 2011; Zheng et al. 2013). At present, theoretical studies are not able to account for the immense amount of experimental data published on STDP since its discovery. Thus, despite the advances in model complexity, fundamental notions such as how and/or whether synaptic competition can arise from STDP rules, and whether synaptic competition is even necessary to maintain stable synaptic weight distributions to support balanced neuronal function, are still uncertain. Future theoretical work should revisit these fundamental ideas to better match modeling data with experimental observations. Nevertheless, mechanisms of synaptic competition and the regulation of synaptic weight are likely much more complicated than the simple model originally proposed by Song et al. (2000). Given the different forms of plasticity that neurons exhibit, the regulation of synaptic weight and stable neuronal function likely involves a combination of other forms of plasticity in addition to STDP, such as intrinsic and homeostatic plasticity, that operate on both a global cell-wide, as well as a more local synapse-specific, scale (Zhang & Linden 2003; Lee et al. 2013).

Concluding Remarks & Acknowledgments

Over the course of the 6th Computational Neuroscience Summer School, we have generated an integrate-and-fire neuron model that includes classic STDP rules as described by Song et al. (2000). Numerous thought experiments were provoked by this project, and considerable

troubleshooting in MATLAB was accomplished – all within the short time that the Summer School was in session. Since the presentation of this work on June 21, a more thorough literature review during the writing of this report has generated several refinements to our understanding of the relationship between STDP and the regulation of synaptic weights. We hope to explore these ideas using our new computational tools in future work. We extend thanks to course TAs Stephen Clarke, Dave Houtman and Jorge Mejias for their assistance in the evening hours.

Post script.

During the preparation of this report, I noticed that the potentiation factor P_a was still incorrectly updating. We had inadvertently based our decay on the elapsed time since last spike rather than dt. This had the effect of shortening the -Δt window for synaptic potentiation, thereby reducing overall potentiation. This caused a higher postsynaptic steady-state firing rate in our revised model (shown in Figure 6, bottom) than reported in Figure 2c of Song et al. (2000). Overall, this has the qualitative effect of increasing the A_-/A_+ ratio shown in Figure 2e of Song et al. (2000). Therefore, the behaviour of the model is not expected to change drastically and I have included the corrected MATLAB script in the Appendix.

References

Appleby PA, Elliott T. (2006) Stable competitive dynamics emerge from multispike interactions in a stochastic model of spike-timing-dependent plasticity. Neural Computation 18:2414-2464

Bar Ilan L, Gidon A, Segev I. (2011) Interregional synaptic competition in neurons with multiple STDP-inducing signals. J Neurophysiol 105:989-998

Beique JC, Lin DT, Kang MG, Aizawa H, Takamiya K, Huganir RL. (2006) Synapse-specific regulation of AMPA receptor function by PSD-95. Proc Natl Acad Sci USA 103:19535-40

Bell CC, Han VZ, Sugawara Y, Grant K. (1997) Synaptic plasticity in a cerebellum-like structure depends on temporal order. Nature 387:278-281

Bekkers JM, Stevens CF. (1996) Cable properties of cultured hippocampal neurons determined from sucrose-evoked miniature EPSCs. J Neurophysiol 75:1250-1255

Bi GQ, Poo MM (1998) Synaptic modifications in cultured hippocampal neurons: dependence on spike timing, synaptic strength, and postsynaptic cell type. J Neurosci 18:10464-10472

Bi GQ, Poo MM (2001) Synaptic modification by correlated activity: Hebb's postulate revisited. Ann Rev Neurosci. 24:139-66

Blakemore C, van Sluyters RC, Movshon JA. (1976) Synaptic competition in the kitten's visual cortex. Cold Spring Harb Symp Quant Biol 40:601-609

Bonfill-i-Petit A, Murray AF. (2004) Synchrony detection and amplification by silicon neurons with STDP synapses. IEEE Transac Neural Netw 15:5

Debanne D, Gahwiler BH, Thompson SM (1996) Cooperative interactions in the induction of long-term potentiation and depression of synaptic excitation between hippocampal CA3-CA1 cell pairs in vitro. Proc Natl Acad Sci USA 93:11225-112230

Debanne D, Gahwiler BH, Thompson SM (1999) Heterogeneity of synaptic plasticity at unitary CA1-CA3 and CA3-CA3 connections in rat hippocampal slice cultures. J Neurosci 19:10664-10671

Fraser SE, Perkel DH. (1990) Competitive and positional cues in the patterning of nerve connections. J Neurobiol 21(1):51-72

Gilson M, Fukai T. (2011) Stability versus neuronal specialization for STDP: long-tail weight distributions solve the dilemma. PLoS One 6:10

Hubel DH, Wiesel TN (1965) Binocular interaction in the striate cortex of kittens reared with artificial squint. J Neurophysiol 28:1041.

Kepecs A, van Rossum MCW, Song S, Tegner J. (2002) Spike-timing-dependent plasticity: common themes and divergent vistas. Biological Cybernetics 87:446-458

Lazar A, Pipa G, Triesch J. (2007) Fading memory and time series prediction in recurrent networks with different forms of plasticity. Neural Netw 20:312-22

Lazar A, Pipa, G, Triesch J. (2009) SORN: a self-organizing recurrent neural network. Front Comput Neurosci. 3:23

Lee KF, Soares C, Beique JC. (2013) Tuning into diversity of homeostatic synaptic plasticity. Neuropharmacology [Epub ahead of print]

Lo YJ, Poo MM. (1991) Activity-dependent synaptic competition in vitro: heterosynaptic suppression of developing synapses. Science 254:1019-22

Malenka RC, Bear MF. (2004) LTP and LTD: an embarrassment of riches. Neuron 44:5-21

Markram H, Lubke J, Frotscher M, Sakmann B. (1997) Regulation of synaptic efficacy by coincidence of postsynaptic APs and EPSPs. Science 275:213-5

Miller KD. (1996) Synaptic economics: competition and cooperation in synaptic plasticity. Neuron 17:371-374

Muller J, Bakkum DJ, Hierlemann A. (2013) Sub-millisecond closed-loop feedback stimulation between arbitrary sets of individual neurons. Frontiers in Neural Circuits 6(21):1-11

Rubel EW, Hyson RL, Durham D. (1990) Afferent regulation of neurons in the brain stem auditory system. J Neurobiol 21(1):169-96

Soares C, Lee KF, Nassrallah W, Beique JC. (2013) Differential subcellular targeting of glutamate receptor subtypes during homeostatic synaptic plasticity. (J Neurosci, resubmitted)

Shatz CJ. (1990) Competitive interactions between retinal ganglion cells during prenatal development. J Neurobiol 21(1):197-211

Song S, Miller KD, Abbott LF (2000) Competitive Hebbian learning through spike-timing dependent plasticity. Nat Neurosci 3:919-926

Song S, Abbott LF. (2001) Cortical development and remapping through spike timing-dependent plasticity. Neuron 32:339-50.

Turrigiano GG, Leslie KR, Desai NS, Rutherford LC, Nelson SB. (1998) Activity-dependent scaling of quantal amplitude in neocortical neurons. Nature 391:892-6

Van Rossum MCW, Bi GQ, Turrigiano GG (2000) Stable Hebbian learning from spike timing-dependent plasticity. J Neurosci 20:8812-8821

Watt AJ, Desai NS. (2010) Homeostatic plasticity and STDP: Keeping a neuron's cool in a fluctuating world. Front Synaptic Neurosci 2:5

Zhang LI, Tao HW, Holt CE, Harris WA, Poo MM (1998) A critical window for cooperation and competition among developing retinotectal synapses. Nature 395(3):37-44

Zhang W, Linden DJ. (2003) The other side of the engram: experience-driven changes in neuronal intrinsic excitability. Nat Rev Neurosci. 4:885-900

Zheng P, Dimitrakakis C, Triesch J. (2013) Network self-organization explains the statistics and dynamics of synaptic connection strengths in cortex. PLoS Comp Biol 9:1

MATLAB code for the model

An integrate-and-fire (IF) model neuron for spike-timing dependent plasticity (STDP)

i) The integrate-and-fire STDP model (save as: STDP_Song2000.m)
ii) Initialization parameters for the IF-model (save as: in_STDP_mp.m)
iii) Meta-code used to automate simulations with different input frequencies iteratively (save as: iterate.m)

i) The integrate-and-fire STDP model (STDP_Song2000.m)

```
--

% % Spike-Timing Dependent Plasticity Model based on Song et al. 2000.
% for the 6th Computational Neuroscience Summer School (NSC8104)
% at the University of Ottawa, June 2013

% Authors
% Kevin F.H. Lee (Neuroscience, University of Ottawa)
% Caitlyn Parmelee (Mathematics, Univeristy of Nebraska-Lincoln)
% % % % % % % % % % %
% This is an integrate-and-fire neuron model based on the methods used by
% Song, Miller & Abbott (Nature Neuroscience, 2000)
% % % % % % % % % % %

% tSTART = tic; % start timer

% initialize
in_STDP_mp

% postsynaptic neuron
tau_m = 20; % membrane time constant
tau_stdp = 20; % STDP time constant
Vrest = -70; % resting Vm
Vthresh = -54; % threshold for spike
V = zeros(1,klokmax) + Vrest; % Vm
syn_weights = zeros(num_ex,1)+g_max;
spike_history = zeros(klokmax,1);
% STDP factors
Aplus = 0.005;
Aminus = 1.05*Aplus;
M = 0;
P = zeros(num_ex,1);
p_times = zeros(num_ex,1);
fspike = [];

% % %
% % %
% % %
for klok = 2:klokmax-1

%     Save half-run data
    if klok == round(klokmax/2)
        syn_weights_halfrun = syn_weights;
    end
```

```
    % Synaptic Input
    poisson_inputs; % Poisson inputs
    % identify currently-active excitatory synapses
    f = find(ex_spike == 1); % Identify active synapses
    gex = sum(syn_weights(f)); % summed weight of synaptic input

    % Action potentials
    if V(1,klok-1) > Vthresh
        V(1,klok) = -60; % 'spike' & reset to -60mV
        spike_time = klok;
        spike_history(klok) = 1;
        fspike = find(spike_history == 1);

%         INHIBITORY CONDUCTANCE
        g_INH = g_INH*exp(-(dt/tau_inh)) + (inh_input*g_inh);
        if g_INH < 0
            g_INH = 0;
        end
%         EXCITATORY CONDUCTANCE
        % total conductance (including residual from previous step)
        g_EX = g_EX*exp(-(dt/tau_ex)) + gex;
        if g_EX < 0
            g_EX = 0; % negative g_EX not possible
        end

% % M & P business
    % M is decremented upon each spike; used to decrease synaptic strength
        M = M*exp(-1/tau_stdp) - Aminus;
    % P is increased with synaptic activity; used to increase synaptic
strength
    % update (decay) P for current klok time
         for dep = 1:length(P)
            curr_P = P(dep);
            new_P = P(dep)*exp(-1/tau_stdp);
            P(dep) = new_P;
        end

    % % SYNAPTIC POTENTIATION
        for dep = 1:length(P)
            curr_weight = syn_weights((dep),1);
            new_weight = curr_weight + g_max*(P(dep));
            if new_weight > g_max
                new_weight = g_max;
            end
            syn_weights(dep) = new_weight;
        end
% % % % % %
    else
% % % % % %
%         ONGOING SYNAPTIC INPUT
%         INHIBITORY CONDUCTANCES
        g_INH = g_INH*exp(-(dt/tau_inh)) + (inh_input*g_inh);
        if g_INH < 0
            g_INH = 0;
        end
%         EXCITATORY CONDUCTANCES
```

```
        % total conductance (including residual from previous step)
        g_EX = g_EX*exp(-(dt/tau_ex)) + gex;
        if g_EX < 0
            g_EX = 0; % negative g_EX not possible
        end

% % % % Update membrane potential V(t)
        Vprev = V(1,klok-1);
        V(1,klok) = Vprev + dt*(1/tau_m)*(Vrest - Vprev + g_EX*(E_ex-Vprev) +
g_INH*(E_inh-Vprev));
%         V(1,klok) = V(1,klok-1) + (dt/tau_m)*(Vrest + g_EX*E_ex +
g_INH*E_inh - V(1,klok-1)*(1+g_EX+g_INH));
% % % %
% % M & P business
        % P(a) decay
        for dep = 1:length(P)
            curr_P = P(dep);
            new_P = P(dep)*exp(-1/tau_stdp);
            P(dep) = new_P;
        end
        % P(a) is incremented by Aplus when synapse(a) is active
        for dep = 1:length(f)
            curr_P = P(f(dep));
            new_P = curr_P + Aplus;
            P(f(dep)) = new_P;
        end

        % M is used to decrease strength of currently-active synapses
        % update (decay) M for current klok time
        M = M*exp(-1/tau_stdp);

%         % SYNAPTIC DEPRESSION
        for dep = 1:length(f)
            curr_weight = syn_weights(f(dep),1);
            new_weight = curr_weight + g_max*(M);
            if new_weight < 0
                new_weight = 0;
            end
            syn_weights(f(dep)) = new_weight;
        end

        % Synaptic input history (synapse-specific input times)
        p_times(f) = klok;
    end
end

% tELAPSED=toc(tSTART); % end timer
AP_times = find(spike_history > 0);
stdp_analysis
```

--

ii) Initialization parameters for the IF-model (in STDP_mp.m)

--

```
% initialize parameters for STDP model

% % time is in milliseconds
tmax = 1; % seconds
milliseconds = tmax*1000;
dt = 1; %  1msec timestep
klokmax = ceil(milliseconds/dt);
% number of excitatory and inhibitory synapses
num_ex = 1000;
num_inh = 200;

% % Synaptic input trains
seconds = tmax;
inh_freq = 10; % Hz
ex_freq = 10; % Hz

% excitatory
ex_spike = zeros(num_ex,1);
ex_lambda = ex_freq/1000; % expected spikes/1000msec
% inhibitory
inh_spike = zeros(num_inh,1);
inh_lambda = inh_freq/1000; % expected spikes/1000msec

% % % %
% equilibrium potentials
E_ex = 0; % excitatory
E_inh = -70; % inhibitory
% synaptic decay times
tau_ex = 5; % excitatory
tau_inh = 5; % inhibitory
% synaptic conductances
g_inh = 0.05; % inhibitory
g_max = 0.015; % excitatory synapse max conductance
% starting synaptic conductances
g_EX = 0;
g_INH = 0;

spike_time = 0;
```

--

iii) Generate Poisson Input Train

--

```
% % POISSON INPUTS
% uses variables created in in_stdp_model.m

% ex_lambda is spike probability per timestep (dt)
% % dt = 1msec
% % ex_lamba = Hz/(1/1000seconds)

% Excitatory synapses
ex_spike = poissrnd(ex_lambda,num_ex,1);
% Inhibitory synapses
inh_spike = poissrnd(inh_lambda,num_inh,1);
inh_input = sum(inh_spike);
```

--

iv) Meta-code used to automate simulations with different input frequencies iteratively (iterate.m)

--

```
% % Iterate STDP model

tSTART = tic; % start timer

frequency = [6;8;10;12;14;16;18;20;30;40];
% frequency = [8;12;16;30;40];
% frequency = 10;
reps = 1;
spike_output = {};
weight_dist = {};
weight_dist_halfrun = {};

% weight_dist = zeros(1000,reps,length(frequency));

for R = 1:reps
    for ifreq = 1:length(frequency)
        disp(R)
        disp(ifreq)

        ex_freq = frequency(ifreq);

        STDP_Song2000

        weight_dist{ifreq,R} = syn_weights;
        weight_dist_halfrun{ifreq,R} = syn_weights_halfrun;
        spike_output{ifreq,R} = AP_times';

        save ('June 21 weekend 2')  % edit save date as appropriate

%         save ('June 18 overnight weights', 'weight_dist');
%         save ('June 18 overnight weights halfrun', 'weight_dist_halfrun');
%         save ('June 18 overnight spike output', 'spike_output');
    end
    keep weight_dist weight_dist_halfrun spike_output frequency reps R ifreq
tSTART
end

tELAPSED=toc(tSTART); % end timer
tHOURS = tELAPSED/3600;

save ('June 21 weekend 2') % edit save date as appropriate
```

--

v) STDP analysis

This code is called at the end of **STDP_Song2000.m** to plot variable of interest.

--

```
% membrane potential Vm
timeaxis = 0:seconds/tmax:seconds-1;
figure(1);plot(1:length(V),V); xlim([0 klokmax]); ylim([-100 0]);
xlabel('Time (ms)')
title('membrane potential')
ylabel('Vm (mV)')
%
% % Postsynaptic spike times
APs = find(V > Vthresh);
ISIs = diff(APs)*dt;
xintervals = 1:max(ISIs)/50:max(ISIs);
histISIs = histc(ISIs,xintervals);
figure(2);bar(xintervals,histISIs)
% figure(2);bar(hist(ISIs,20))
title('ISIs')
xlabel('ISI (msec)')
ylabel('count')
figure(4);plot(ISIs)
title('ISIs')
xlabel('spike number')
ylabel('ISI (ms)')
%
% % Synaptic weight
figure(5);hist(syn_weights,20)
title('synaptic weight histogram')
xlim([0 g_max])
xlabel('synaptic conductance (gMAX = 0.015)')
ylabel('count')
```

--

Appendix G

Supplemental Data for MANUSCRIPT V

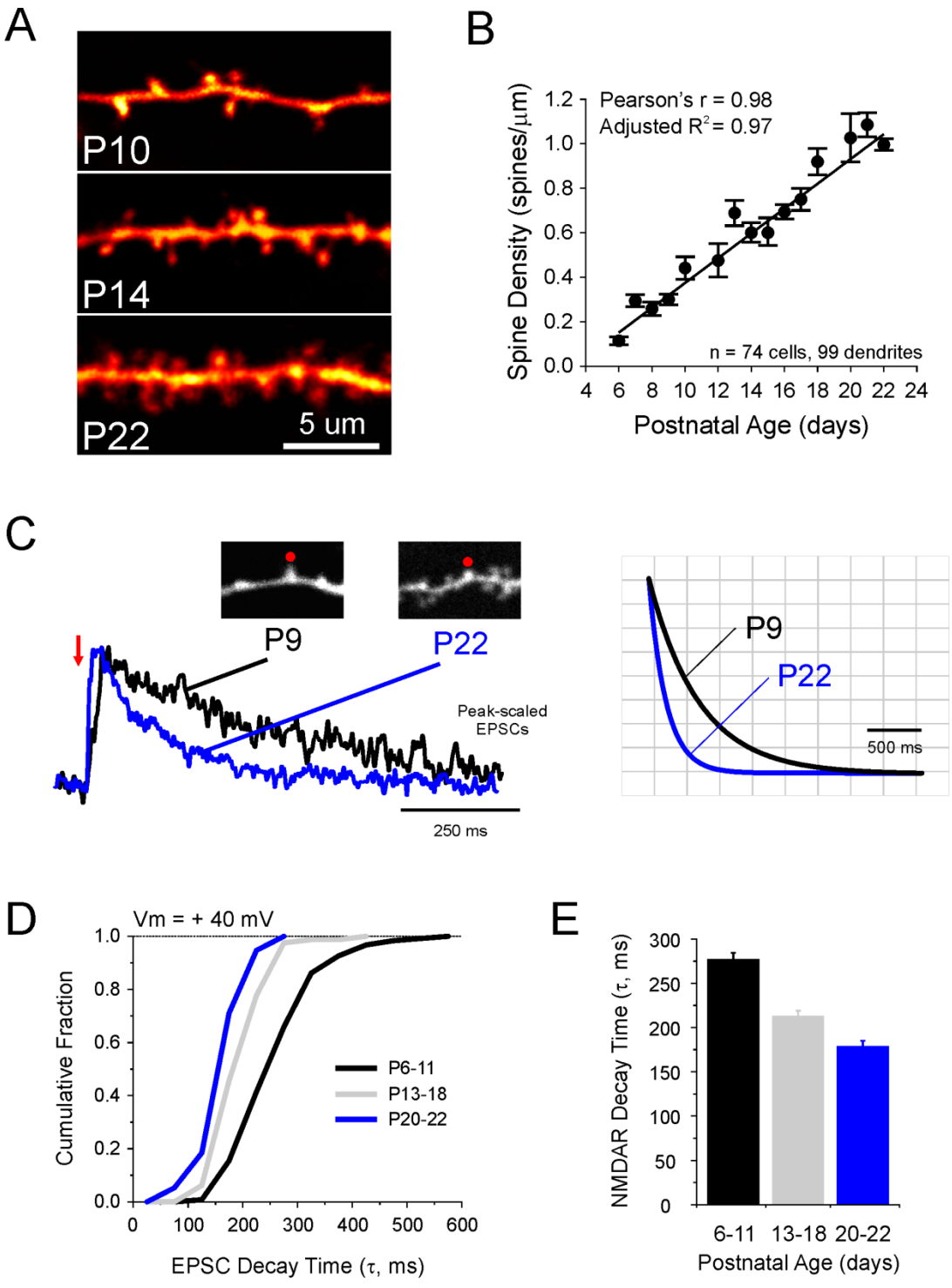

Figure S1

Figure S1. Spinogenesis and synapse development during the second and third postnatal weeks (A) Two-photon images of apical secondary dendrites of CA1 pyramidal neurons at different postnatal ages filled with 30 μM Alexa 594 during whole-cell recording. (B) Dendritic spine density during the second and third postnatal weeks of CA1 development. Dendritic spine density was measured by counting spines along segments of dendrite (> 20 μm) and dividing by the length of dendrite examined. Since we only counted dendritic protrusions in the *x-y* plane, our absolute measures likely underestimate the true spine density. A total of 99 dendrites from 74 cells were analyzed. (C-E) Developmental changes in the decay kinetics of NMDAR-mediated EPSCs. (C) *Left panel,* 2P glutamate uncaging at dendritic spines generated outward currents at V_m = +40 mV. Each trace is an average of 3 consecutive sweeps. *Right panel*, Peak-normalized monoexponential fits of the EPSCs shown in *left panel*. (D) Cumulative distribution and (E) bar graph showing summary data for decay kinetics of currents evoked by single-spine glutamate uncaging at V_m = +40 mV at three age-bins during early postnatal CA1 development (decay time τ: P6-11, 277.4 ± 7.1 ms, 123 spines; P13-17, 213.36 ± 5.6 ms, 81 spines; P20-26, 178.8 ± 6.4 ms, 38 spines). Data represented as mean ± SEM.

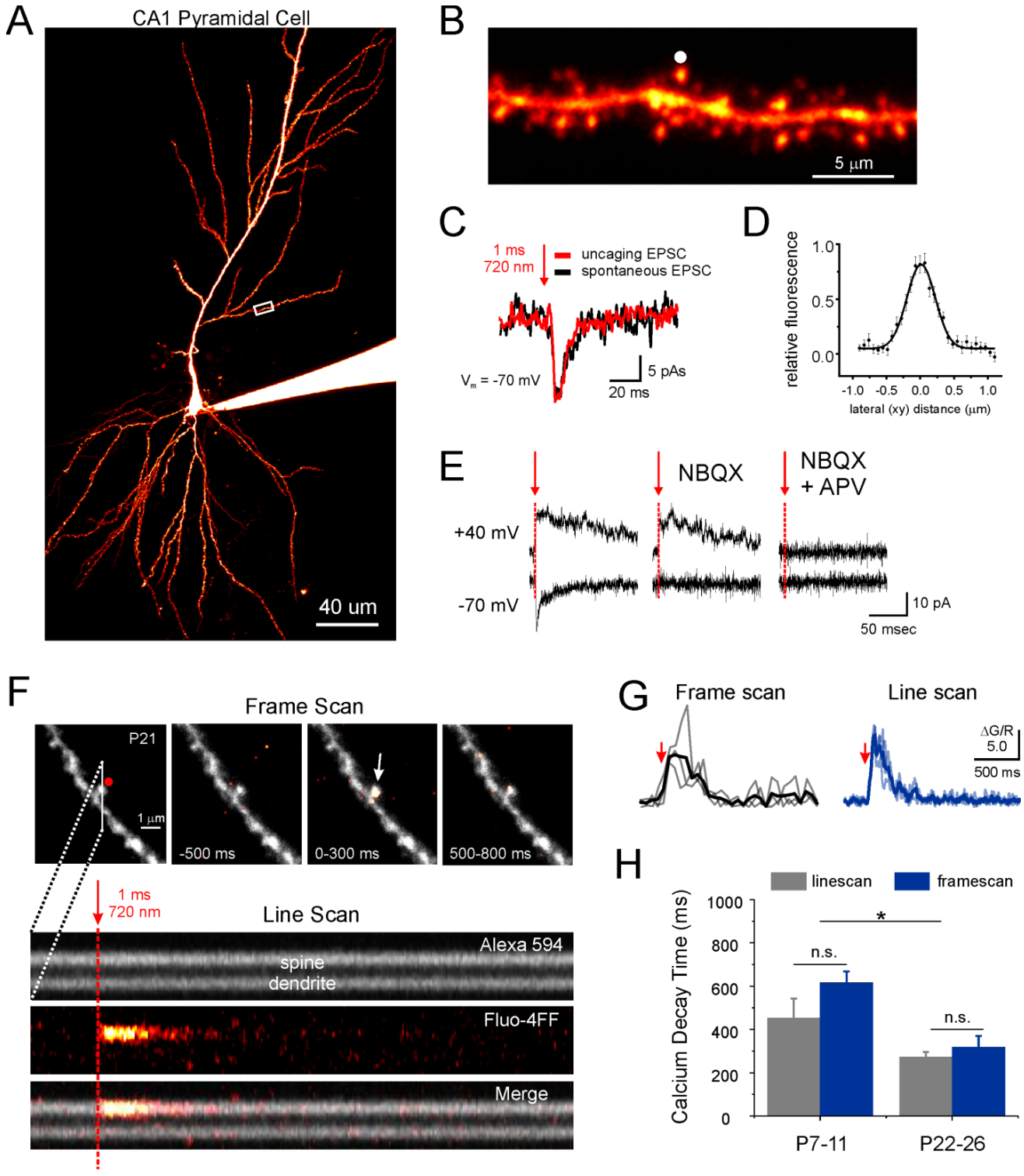
A
CA1 Pyramidal Cell
40 um
B
5 μm
C
1 ms
720 nm
uncaging EPSC
spontaneous EPSC
V_m = -70 mV
5 pAs
20 ms
D
relative fluorescence
1.0
0.5
0.0
-1.0 -0.5 0.0 0.5 1.0
lateral (xy) distance (μm)
E
NBQX
NBQX
+ APV
+40 mV
-70 mV
10 pA
50 msec
F
Frame Scan
P21
1 μm
-500 ms
0-300 ms
500-800 ms
1 ms
720 nm
Line Scan
Alexa 594
spine
dendrite
Fluo-4FF
Merge
G
Frame scan
Line scan
ΔG/R
5.0
500 ms
H
linescan
framescan
Calcium Decay Time (ms)
1000
800
600
400
200
0
*
n.s.
n.s.
P7-11
P22-26

Figure S2

Figure S2. Two-photon (2P) glutamate uncaging and calcium imaging. (A) *Z*-stack reconstruction of a P26 CA1 pyramidal neuron filled with 30 μM Alexa 594 in whole-cell recording. The dendritic segment outlined by the rectangle is shown in high magnification image in panel B. (B) 2P glutamate uncaging at the tip of an individual dendritic spine (red circle). (C) In voltage-clamp at V_m = -70 mV, 2P glutamate uncaging (arrow, 1 ms, 720 nm) evoked EPSCs that were indistinguishable from spontaneous EPSCs in the same recording. (D) Point spread function of 2P illumination under our imaging conditions in the lateral (xy) axis, measured from 0.1 μm fluorescent beads (n = 15 beads). (E) AMPA and NMDA receptor antagonists abolished glutamate uncaging-evoked EPSCs. *Left,* Under drug-free recording conditions, glutamate uncaging at spines generated inward EPSCs at V_m = -70 mV and outward EPSCs with long decay kinetics at V_m = +40 mV. *Middle*, 20 μM NBQX blocked the EPSC at V_m = -70mV, but not at V_m = +40. *Right,* Addition of 100 μM DL-APV abolished the outward EPSC at Vm = +40 mV. (F) An experiment performed at P21 where the fluorescent calcium indicator Fluo-4FF was included in the recording electrode to enable imaging of intracellular calcium signals. Glutamate uncaging was directed dendritic spines at V_m = 0 mV to activate NMDARs, and calcium signals were imaged in frame scan mode (256 x 256 frames, ~15 Hz acquisition), or in line scan mode along a line drawn across the spine and parent dendrite (4 kHz). *Upper panel*, time lapse images from an individual frame scan experiment. Calcium fluorescence was summed over the indicated time intervals and overlaid with the Alexa 594 signal. A brief calcium transient is observed at the stimulated spine (arrow). *Lower panel,* At the same spine, 2P calcium imaging was performed in line scan mode. Fluorescence signals were acquired along a line drawn through the spine and parent dendrite. Consistent with frame scan imaging, the uncaging-evoked calcium signal recorded in line scan mode was limited to the spine head compartment and not detected in the

parent dendrite. (G) Calcium fluorescence signals from 3 consecutive frame scans and 3 consecutive line scans at the spine shown in panel e, with the mean calcium signal in bold. (H) Summary data of monoexponential decay time constants of spine calcium transients acquired in both frame scan and line scan mode at early (P8-11; mean decay time: line scan, 454 ± 89 ms, n = 11 spines; frame scan, 617 ± 50 ms, n = 99 spines, p = 0.1087; Wilcoxon test) and late development (P22-26, mean decay time: line scan, 273 ± 24 ms, n = 21 spines; frame scan, 318 ± 52 ms, n = 12 spines, p = 1.0; Wilcoxon test). Spine calcium signals became faster with age (line scan and frame scan data pooled, P8-11, 596 ± 48 ms; P22-26, 324 ± 30 ms, p = 2.25e-04; Wilcoxon test). Data represented as mean ± SEM.

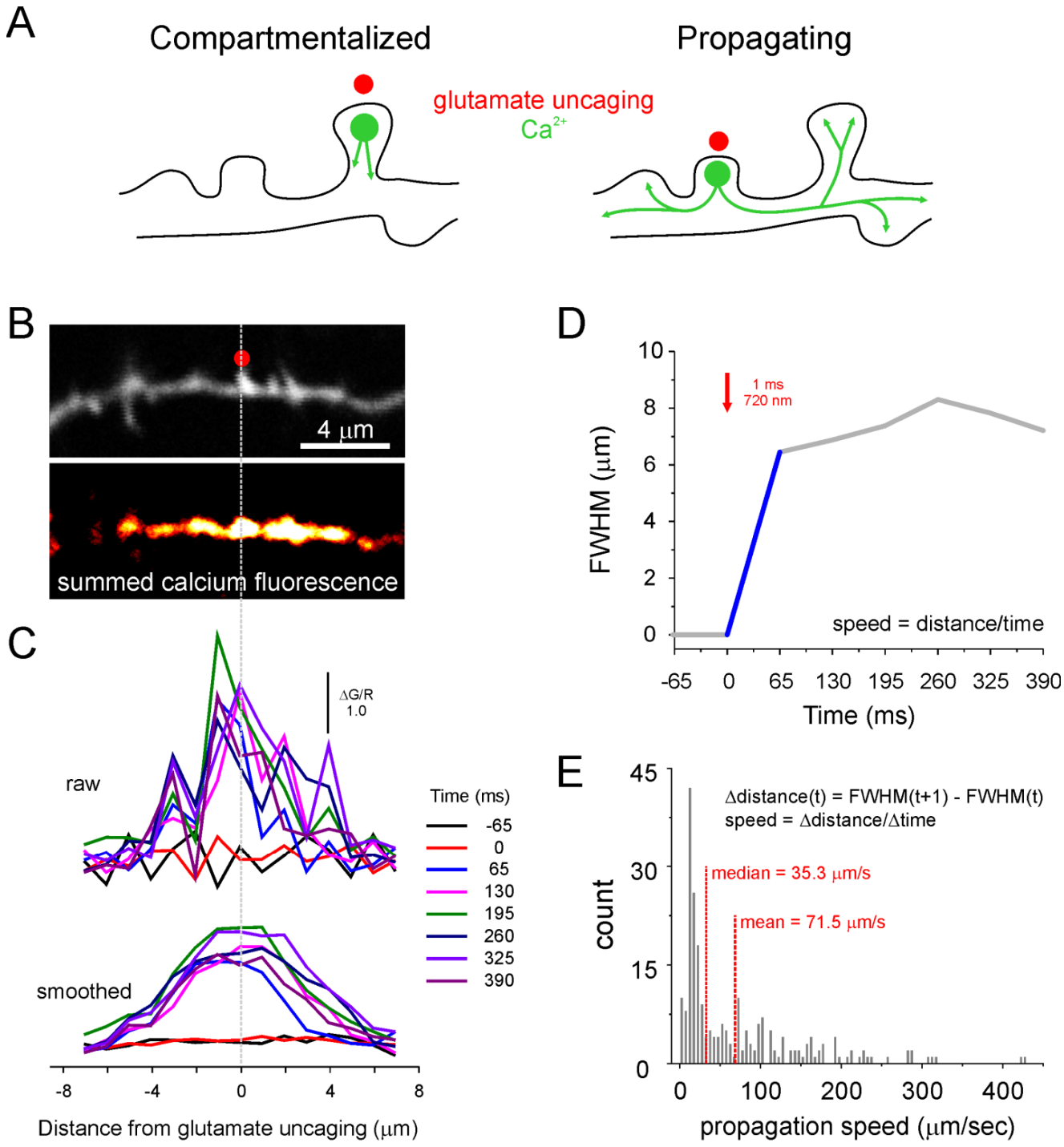
A
Compartmentalized
Propagating
glutamate uncaging
Ca2+
B
4 μm
summed calcium fluorescence
C
ΔG/R
1.0
raw
smoothed
Time (ms)
-65
0
65
130
195
260
325
390
-8
-4
0
4
8
Distance from glutamate uncaging (μm)
D
1 ms
720 nm
FWHM (μm)
10
8
6
4
2
0
speed = distance/time
-65
0
65
130
195
260
325
390
Time (ms)
E
Δdistance(t) = FWHM(t+1) - FWHM(t)
speed = Δdistance/Δtime
median = 35.3 μm/s
mean = 71.5 μm/s
count
45
30
15
0
0
100
200
300
400
propagation speed (μm/sec)

Figure S3

Figure S3, related to Figures 2 and 3. Spatial spread of calcium signals originating at dendritic spines. (A) Schematized behaviors of calcium signals (green) evoked by 2P glutamate uncaging at the tips of dendritic spines (red dot): 'Compartmentalized' calcium signals were largely restricted to the spine head, whereas 'propagating' calcium signals clearly exited the stimulated spine, spread locally along the dendrite and invaded neighboring spines. The dendritic segment shown in **Figure 2A** is used here to demonstrate how calcium propagation was analyzed. (B) Alexa 594 fluorescence (*upper*) and summed Fluo-4FF calcium fluorescence (715-975 ms after uncaging, *lower*). (C) Calcium fluorescence profiles along the length of the dendrite (1 μm ROIs) at 8 consecutive frames (uncaging stimulus at 0 ms). To objectively measure the spatial spread of calcium along the dendrite, full-width at half-maximum (FWHM) values were obtained from smoothed fluorescence profiles (*lower*). This measurement likely provides an underestimate of true calcium spread. (D) Plot of FWHM values for fluorescence profiles shown in panel C. The maximum change in FWHM (shown in blue) was divided by the time interval (one frame, 65 ms) to yield propagation speed. Given the 15Hz imaging rate in the framescan configuration and 1μm ROI segmentation of the dendrite for analysis, these measurements provide only simplified descriptions of local calcium behavior. (E) Histogram distribution of all computed propagation speeds with mean and median values indicated.

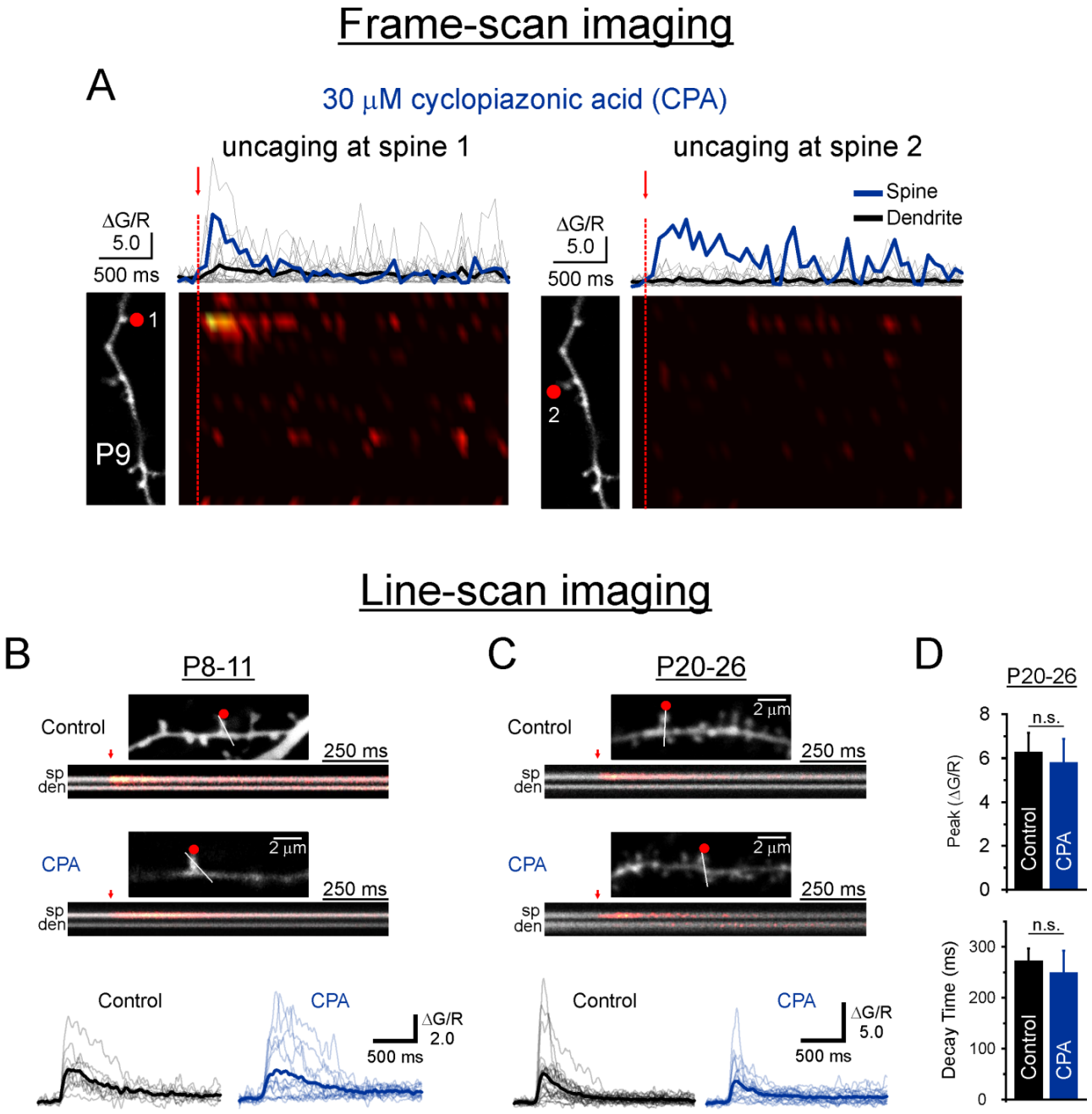
Frame-scan imaging
A
30 μM cyclopiazonic acid (CPA)
uncaging at spine 1
uncaging at spine 2
ΔG/R
5.0
500 ms
Spine
Dendrite
1
2
P9
Line-scan imaging
B
P8-11
C
P20-26
D
Control
CPA
250 ms
2 μm
sp
den
ΔG/R
2.0
5.0
n.s.
Peak (ΔG/R)
Decay Time (ms)

Figure S4

Figure S4, related to Figures 3. Summary data (mean ± SEM) for spine calcium transients recorded in CPA (> 1hr pretreatment). (A) Example calcium imaging experiment at P9 on two neighboring spines. Calcium transients from the stimulated spines (blue) and dendritic ROIs (gray, mean in black) are aligned to a corresponding dendritic calcium maps. Calcium propagation was reduced in the presence of CPA (**Figures 3D-3F**). (B) Line scan imaging revealed two major effects of CPA on spine calcium signals from young neurons (P8-11). Calcium signals from all line scan experiments are shown, with mean behavior shown in bold. At some young spines, CPA reduced the amplitude of uncaging-evoked calcium fluorescence, indicating a dominant role of intracellular calcium stores in spine calcium signals (see also ryanodine data in **Figure 3D**). At other spines we observed large, abnormally-shaped calcium elevations, indicating a role for endoplasmic reticulum (ER) Ca^{2+}-ATPase dependent extrusion mechanisms in controlling calcium kinetics (Pozzo-Miller et al., 1997; Majewska et al., 2000; Scheuss et al., 2006) at developing spines. Interestingly, these CPA-induced behaviors were not evident at older spines (P20-26). *Right panel,* Summary bar graphs show no effect of CPA on spine calcium amplitude (ΔG/R, control: 6.29 ± 0.86, N = 26 spines; CPA: 5.82 ± 1.06, N = 11 spines P = 0.7842, two-sided Student's t-test) or decay kinetics (decay time, ms; control: 272.9 ± 23.95; CPA: 250.2 ± 42.3, P = 0.6195, two-sided Student's t-test). Data are represented as mean ± SEM.

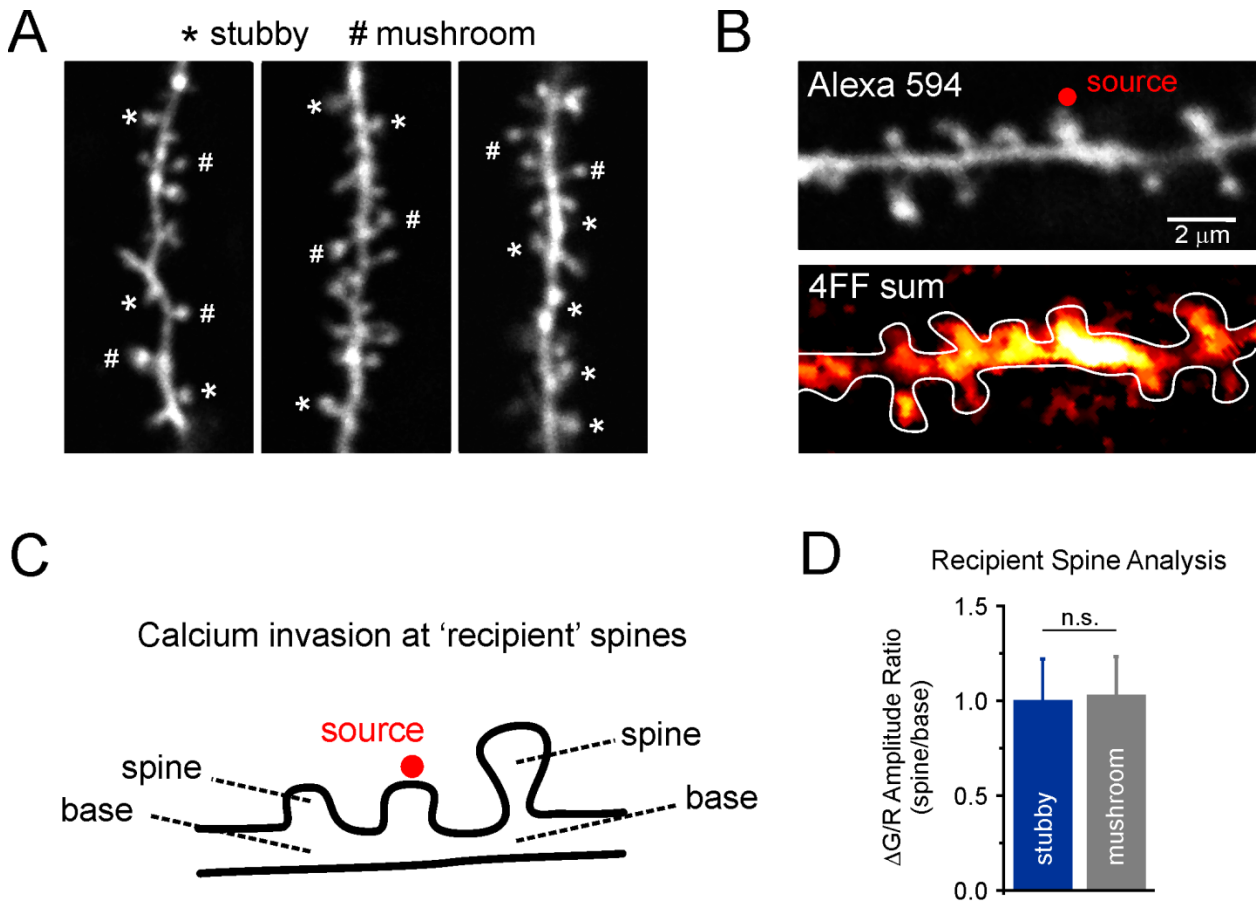

Figure S5

Figure S5, related to Figure 5. The relationship between spine morphology and spine calcium behaviour. (A) 2P images of 3 apical oblique dendrites from CA1 pyramidal cells (P13-17) filled with Alexa 594 during whole-cell recording. Spine morphology is heterogeneous. Visually-scored stubby and mushroom spines are marked with an asterisk (*) or hash (#) symbol, respectively. Spines that were difficult to classify were excluded from this analysis. (B) Calcium invasion at neighboring ('recipient') spines was pervasive, as seen from the summed Fluo-4FF fluorescence. (C) Calcium invasion at recipient spines was quantified by calculating calcium fluorescence amplitude ratios from the spine and base compartments. (D) Summary data of

spine/base amplitude ratios from recipient spines of stubby and mushroom morphologies. (Spine/base amplitude ratio: stubby, 1.00 ± 0.22, 15 spines; mushroom 1.03 ± 0.20, 16 spines; $P = 0.7158$; Wilcoxon test). This analysis suggests that stubby and mushroom spines are similarly invaded by propagating dendritic calcium signals. **See Figure 5A**. Data are represented as mean ± SEM.

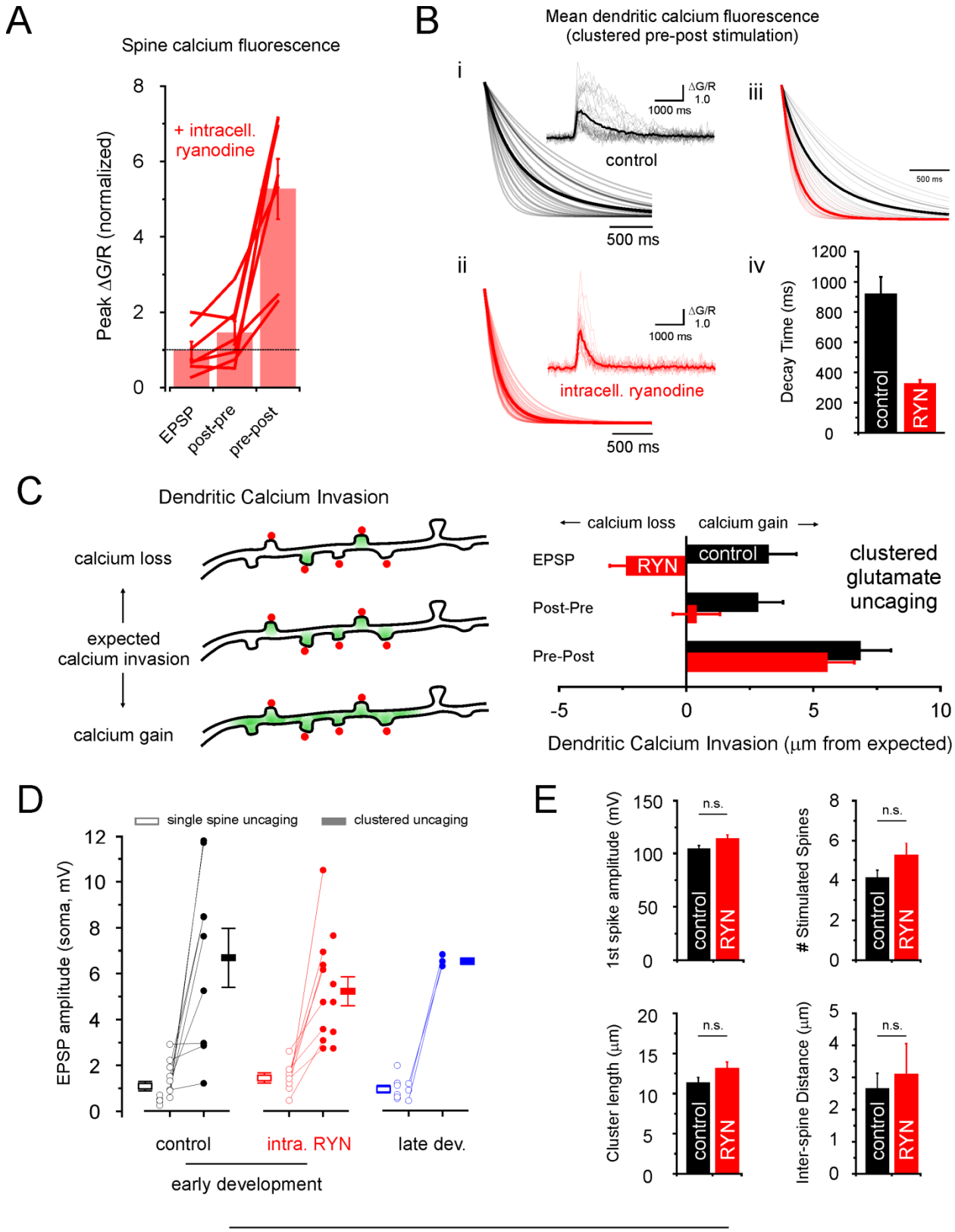
A
Spine calcium fluorescence
Peak ΔG/R (normalized)
+ intracell. ryanodine
EPSP
post-pre
pre-post
B
Mean dendritic calcium fluorescence
(clustered pre-post stimulation)
i
ΔG/R 1.0
1000 ms
control
500 ms
ii
intracell. ryanodine
iii
iv
Decay Time (ms)
control
RYN
C
Dendritic Calcium Invasion
calcium loss
expected calcium invasion
calcium gain
calcium loss
calcium gain
EPSP
Post-Pre
Pre-Post
RYN
control
clustered glutamate uncaging
Dendritic Calcium Invasion (μm from expected)
D
single spine uncaging
clustered uncaging
EPSP amplitude (soma, mV)
control
intra. RYN
late dev.
early development
E
1st spike amplitude (mV)
Stimulated Spines
Cluster length (μm)
Inter-spine Distance (μm)
n.s.
control
RYN

Figure S6

Figure S6, related to Figure 6. Activation of NMDAR-mediated CICR by spatially-clustered glutamate uncaging and spike-pairing at young dendrites. (A) Spine calcium fluorescence from seven experiments where dendrites were stimulated by clustered spike-paired glutamate uncaging in the presence of intracellular ryanodine. Spine calcium fluorescence was normalized to the mean fluorescence response to clustered uncaging alone (spine ΔG/R, fold-change relative to EPSP alone: EPSP, 1.0 ± 0.21; Post-Pre, 2.03 ± 0.64, p = 0.1253; Pre-Post, 6.23 ± 1.18, p = 0.0024. Post-pre vs pre-post, p = 0.00105). Only dendrites that received all three spike-pairing sequences (*i.e.,* EPSP alone, post-pre, pre-post) are shown. (B) Monoexponential fits of dendritic calcium fluorescence signals (*insets*) generated by clustered pre-post glutamate uncaging at (i) control and (ii) ryanodine-treated neurons. Traces from individual dendrites are shown (bold: population mean). (iii) Overlay of monoexponential fits. (iv) Summary data of dendritic calcium decay times (P8-9; control, 919.71 ± 113.40 ms; 100 μM intracellular ryanodine, 325.07 ± 26.14 ms, p = 4.43e-05). (C) To further analyze the role of CICR in NMDAR-dependent calcium signals, we compared the spatial extent of evoked calcium signals with 'expected' values given by assuming a 1:1 correspondence between the number of uncaging points to number of calcium-positive ROIs (1 μm each). Examples are shown in the *left panel*, where clustered glutamate uncaging at 5 points along a dendrite is expected to generate calcium signals in at least 5 ROIs (5 μm). The relative gain or loss of dendritic calcium can therefore be determined by deviations from the expected extent of calcium invasion. *Right panel* shows summary data of calcium gain and loss at control and ryanodine-treated dendrites. Control neurons exhibited a net gain in dendritic calcium in response to clustered EPSPs alone (*i.e.,* greater than expected) while ryanodine-treated dendrites showed apparent calcium loss (gain/loss in μm: EPSP, 3.24 ± 1.11; ryanodine: -2.33 ± 0.68, p = 5.7e-04). Consistent with NMDAR activation (panel A), dendritic

calcium signals were modulated by pairing clustered input with spikes and were completely rescued by pre-post stimulation (clustered glutamate uncaging; gain/loss in μm; Post-Pre: control, 2.81 ± 1.0; ryanodine, 0.4 ± 0.92, p = 0.2523; Pre-Post: control, 6.85 ± 1.20; ryanodine, 5.55 ± 1.10, p = 0.6630). Thus, the coupling of NMDARs to CICR mechanisms tunes local calcium signaling. (D) EPSPs triggered by glutamate uncaging at single-spines or spine clusters during early development (‘early dev.’ *left,* control; *middle,* ryanodine) and at P22-26 (*right*). Experiments from dendrites that received both single-spine and clustered input are shown as pairs. (E) *Clockwise from top left*, Bar graphs showing action potential amplitude (control, 104.5 ± 2.85 mV; ryanodine, 114.7 ± 3.5 mV, p = 0.2087), number of stimulated spines (control, 4.1 ± 0.4; ryanodine, 5.3 ± 0.6, p = 0.1732), distance between uncaging points (inter-spine distance; control, 2.7 ± 0.5 μm; ryanodine, 3.1 ± 1.0 μm, p = 0.1531), and total length of the spine cluster (distance between spines at either end of cluster; control, 11.4 ± 0.7 μm; ryanodine, 13.2 ± 0.8 μm, p = 0.1182) control and ryanodine-treated neurons. Wilcoxon tests; Data are represented as mean ± SEM.

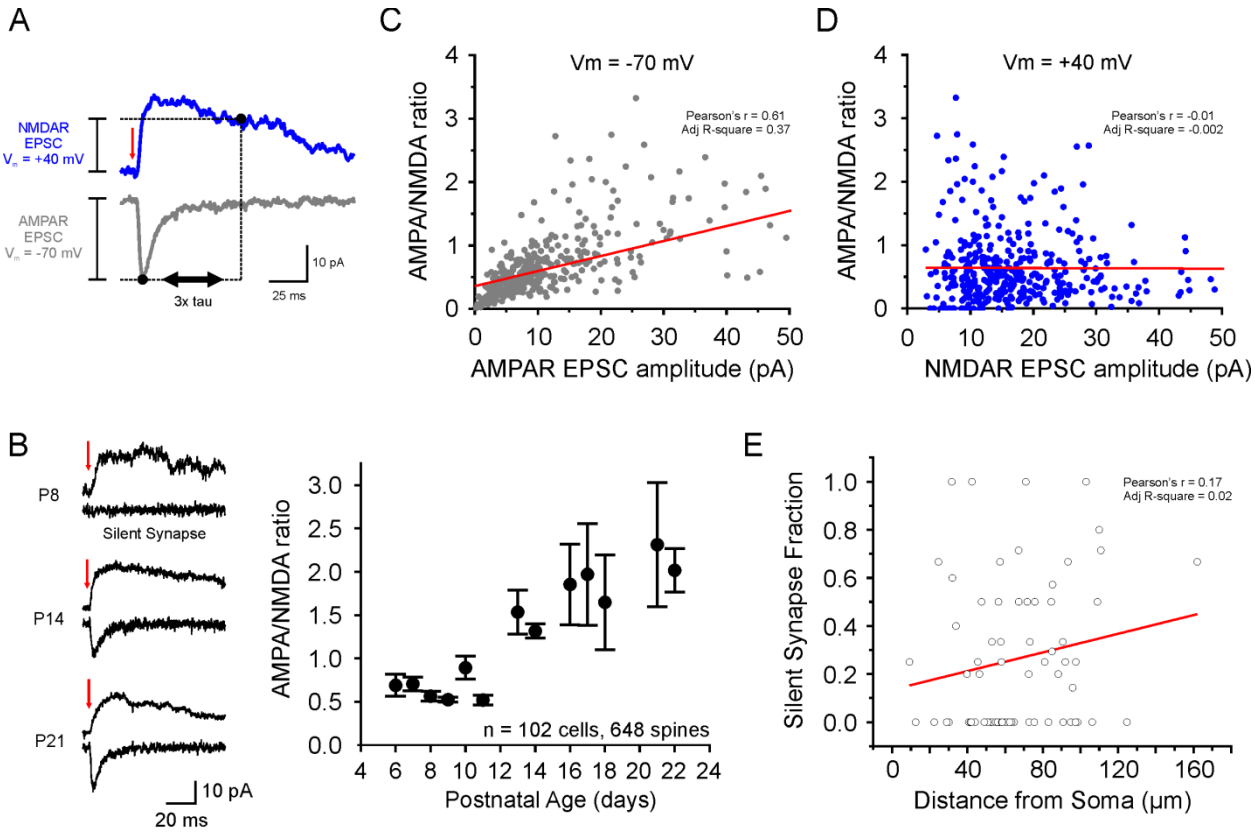

Figure S7

Figure S7, related to Figure 7. Probing the functional development of dendritic spines by measuring AMPA/NMDA ratios with 2P glutamate uncaging. (A) Measuring AMPA/NMDA ratios: example EPSCs evoked by 2P glutamate uncaging at V_m = -70 mV (gray) and +40 mV (blue) (average of at least 5 consecutive sweeps each). The AMPAR-mediated component was given by the peak amplitude of the EPSC at V_m = -70 mV and the NMDAR-mediated component was estimated by the peak amplitude of the EPSC measured at V_m = +40 mV, at a time when the EPSC at V_m = -70 mV has decayed (3x tau). Although space-clamp problems can distort AMPA/NMDA ratio measurements measured this way, these problems would bias the data toward high AMPA/NMDA ratios and mask the presence of silent/weak synapses. Thus, with respect to detecting silent spines, the rate of false negatives, rather than false positives, would

increase. (B) *Left panel,* Example ESPCs evoked by 2P glutamate uncaging at individual dendritic spines at V_m = -70 mV and +40 mV at P8, P14 and P21. A silent synapse is shown at P8. (Each trace is an average of at least 3 consecutive sweeps). *Right panel,* Uncaging-evoked AMPA/NMDA ratios outline the functional strengthening of AMPAR-mediated transmission at dendritic spines during postnatal development. (C) AMPA/NMDA ratios were correlated with glutamate uncaging-evoked EPSC amplitudes recorded at Vm = -70 mV (Pearson's r = 0.61), but not (D) EPSCs recorded at Vm = +40 mV (Pearson's r = -0.01). (E) Fraction of silent synapses at dendritic segments plotted against distance from soma. The prevalence of silent synapses was not dependent on distance from the soma. See also **Figure 7E**. (F) Data from **Figure 7J**, binned at 1 μm distance intervals. A tally of weight matched neighbor spines as a function of inter-spine distance (1 μm bins, *gray bars*) in the experimental dataset is plotted with summary of shuffled data (mean ± 95% C.I.; solid and dashed blue lines, respectively; 100 iterations). Weak spines and strong spines exhibited significantly more weight matching within 15 μm than expected from chance. These data outline the presence of mechanisms that locally regulate synaptic strengthening along short (~15 μm) dendritic segments, which is in the range of intracellular calcium elevations caused by NMDAR-mediated CICR. Intermediate-weight (*middle*) spines did not show the same degree of weight-matching with neighbors. It is interesting to consider the unique position held by intermediate-weight spines as a population of synapses with diverse histories (*i.e.,* synapses potentiated from a weak state, or depressed from a strong state), and speculate on the potential influence of homeostatic plasticity mechanisms to account for the apparent lack of clustering of intermediate-weight spines.

Supplemental Experimental Procedures

Whole-cell Electrophysiology, Two-Photon Imaging and Glutamate Uncaging

Coronal hippocampal slices were obtained in cutting solution containing (in mM): 119 choline chloride, 2.5 KCl, 4.3 $MgSO_4$–7 H_2O, 1.0 $CaCl_2$, 1.0 NaH_2PO_4–H_2O, 1.3 Na-ascorbate, 26.2 $NaHCO_3$, 11 glucose, saturated with 95% O_2 and 5% CO_2 (pH = 7.3; 295-310 mOsm/L). Slices were transferred to a recovery chamber containing an artificial cerebral spinal fluid (ACSF) composed of (in mM): 119 NaCl, 2.5 KCl, 1.3 $MgSO_4$–7 H_2O, 2.5-4.0 $CaCl_2$, 1.0 NaH_2PO_4–H_2O, 26.2 $NaHCO_3$, 11 glucose and saturated with 95% O_2 and 5% CO_2 (pH = 7.3; 295-310 mOsm/L). This standard ACSF was used in all whole-cell electrophysiology experiments. Additional drugs were included in the ACSF (0.01 mM NBQX, 0.1 mM APV, 0.03 mM cyclopiazonic acid (CPA), 0.5 mM MCPG; Abcam) as described in the text. For voltage clamp experiments (**Figures 1-5**), electrodes were filled with an intracellular solution (pH = 7.2-7.3; 270-290 mOsm/L) containing (in mM): 115 cesium methane-sulfonate, 0.4 EGTA, 5 tetraethylammonium-chloride (TEA-Cl), 6.7 NaCl, 20 HEPES, 3 ATP-Mg, 0.5 GTP, 10 Na-phosphocreatine (all purchased from Life Technologies), 5 QX-314 (Abcam). To probe AMPA/NMDA EPSCs at spines (**Figure 7**), the intracellular solution contained (in mM): 77 cesium methane-sulfonate, 10 tetracesium BAPTA, 4 TEA-Cl, 3 $CaCl_2$, 20 HEPES, 4 ATP-Mg, 0.5 GTP, 5 QX-314, 10 Na-phosphocreatine. For current-clamp experiments, electrodes were filled with a K-gluconate based solution containing (in mM): 115 K-gluconate, 20 KCl, 10 HEPES, 4 ATP-Mg, 0.5 GTP, 10 Na-phosphocreatine (pH = 7.2-7.3; 270-290 mOsm/L). Ryanodine (Abcam) was included in the intracellular solution (0.1 mM ryanodine dissolved in DMSO; 0.2% intracellular DMSO total) in some experiments (**Figures 3 and 6**). Intracellular solutions were supplemented with 0.03 mM Alexa Fluor-594 and 0.2 mM Fluo-4FF (Life

Technologies) to visualize morphology and image calcium, respectively. Reagents were purchased from Sigma-Aldrich unless otherwise specified.

Synaptic stimulation was carried out using a patch electrode positioned near an individual dendrite (**Figure 1**) or by 2P glutamate uncaging at visually identified dendritic spines (**Figures 2-7**). In voltage-clamp, electrical stimuli were adjusted to evoke small compound EPSCs (10-50 pA) at a holding potential of -70 mV, and the intensity of the uncaging laser was tuned to generate 5-20 pA AMPAR-mediated EPSCs from single spines. These stimuli were subsequently delivered at a holding potential of 0 mV to probe NMDAR-mediated calcium signals. Calcium imaging was performed in either frame scan or line scan mode (**Figure S2**). For frame scan imaging experiments, we surveyed the apical dendritic arbor for lengths of dendrite (>10 μm) that lay parallel to the imaging plane. Synaptic stimuli were delivered while acquiring image frames (256 x 256; <0.138 μm/pixel) at ~15 Hz (65 ms/frame). Line scan acquisitions were performed across individual dendritic spines and the parent dendrite at ~4 kHz (0.244 ms/line) and filtered at 500 Hz. Kalman-averaged (2 frames) images and small z-stack reconstructions were used for morphology analysis. Spine density was given by dividing the number of protrusions emanating from the dendrite in the *x-y* plane by the total length of dendrite examined (at least 20 μm), which likely provides an underestimate of the true spine density.

For current-clamp experiments, somatic current injection was used in some cases to maintain stable membrane potential between -60 and -70 mV, and cells were discarded if more than 50 pA of current was required. The uncaging laser was tuned to trigger ~1 mV EPSPs from individual spines at resting potential. Back-propagating action potentials (bAPs) were evoked by somatic current steps (100 ms, 100-200 pA) which generally elicited 3-5 spikes. Multi-site glutamate uncaging was delivered to spines with 5 ms inter-stimulus-interval and the sequence of inputs

was always applied in the forward-propagating direction (toward the soma) (Branco et al., 2010). The order of spike-timing sequences (*i.e.,* EPSP alone, pre-post, post-pre) was randomized between dendrites. The pre-post and post-pre spike-timing interval was < 50 ms (between uncaging time and start/end of somatic current injection) and the timing of these sequence patterns was controlled by external trigger from a Master-8 pulse generator (A.M.P.I., Israel).

Uncaging-evoked AMPA/NMDA ratios were used to infer synaptic weights at spines. In these experiments, the intensity of the uncaging laser was tuned to first generate 10-30 pA mixed AMPA and NMDA-mediated EPSCs at a holding potential of +40 mV, and the AMPA-mediated EPSC was subsequently measured at a holding potential of -70 mV using the same uncaging power. These experiments were carried out with 10 mM intracellular BAPTA. Only the spines sharing a dendritic segment in the same focal plane and probed with the same laser power were included in the synaptic weight clustering dataset to nominally ensure even uncaging laser power between neighboring spines. To minimize space-clamp problems, the vast majority of dendritic spines we probed were located on secondary and tertiary proximal apical dendrites (<100 μm from soma; **Figure 7E**).

Calcium imaging analysis

For frame scan experiments, the Alexa Fluor 594 signal was used to guide the placement of circular ROIs (1 μm diameter) along the length each dendrite and around dendritic spines. Average fluorescence time series were taken from both red (Alexa Fluor 594) and green (Fluo-4FF) channels, and a dual indicator approach was used to measure relative changes in calcium fluorescence (Higley and Sabatini, 2008). Since peak changes in intracellular [Ca^{2+}] through NMDARs (~1 μM) are significantly lower than the K_D of Fluo-4FF (~10 μM), calcium

fluorescence signals were assumed to track Δ [Ca^{2+}] in a linear manner (Higley and Sabatini, 2008). To quantify Δ [Ca^{2+}] along dendrites, we computed ΔG/R to minimize signal noise and accommodate for subtle differences in compartment size and/or *z*-position. For each ROI, the pre-stimulus fluorescence (G_o) was subtracted from the green signal (G), which was subsequently normalized to the mean red fluorescence signal through the time series: $\Delta G/R = (G - G_o) / R_{mean}$. Peak calcium fluorescence values were given by the average ΔG/R of three frames centered on the absolute peak. Calcium signals were considered detectable if the peak fluorescence exceeded the baseline signal noise by at least two standard deviations. Experiments where calcium fluorescence exhibited anomalous behavior such as delayed rise time or high resting calcium fluorescence were excluded from analysis.

Dendritic calcium wave-fronts were identified by the calcium fluorescence rise time at individual ROIs along the dendrite; time-to-half peak (**Figures 1D and 1E**) provided evidence for wave-front propagation by revealing a temporal lag in calcium rise as a function of distance from the stimulus. To measure the calcium propagation distance, we used the spatial profile of ΔG/R along the dendrite at each frame in the time series (**Figure S4**). The fluorescence profiles were smoothed using a moving average filter and propagation distance was approximated by full-width at half-maximum (FWHM), which provides an objective metric for propagation distance between experiments, although likely also underestimating the effective spread of calcium. A rough estimate of calcium propagation speed could be calculated by dividing the maximal change in FWHM (μm) by the intervening time-step (seconds, given by the number of intervening frames). However, the limited temporal resolution of frame scan imaging (~15 Hz acquisition) does not fully capture the dynamics of calcium propagation and thus, our propagation speeds likely underestimate and over-simplify the true behavior.

One principle observation was the reduction in dendritic calcium propagation frequency with development. To segregate propagating events from non-propagating events, a 2 μm threshold was used. This partitioning was guided the distribution of propagation distances (**Figure 2C**), and resulted in the expected separation of dendrite to spine fluorescence amplitude ratios (**Figures 4D and 4E**). In multi-spine stimulation experiments in current-clamp (**Figure 6**), we could not define calcium 'propagation' in the same way as uncaging at single spines since multiple uncaging points spanned variable dendritic lengths. We reasoned that spatially-restricted calcium signals evoked by uncaging are generally limited to ~ 1 μm regions around the stimulus (**Figures 2C and 3F**), the spatial extent of dendritic calcium invasion should not exceed the number of glutamate uncaging points, therefore providing an 'expected' degree of calcium invasion (*e.g.,* 4 uncaging points will generate only 4 μm of dendritic calcium; **Figure S6C**). We thus defined propagating dendritic calcium invasions as those which exceeded the expected invasion distance. Propagation probability was determined for each neuron by tallying the number of spines (or spine clusters) that generated $prop^+$ events, and dividing by the total number of spines (or spine clusters) probed. Summary data was computed from calcium propagation probabilities grouped for individual neurons. Calcium fluorescence signals acquired by line scan imaging (**Figures S2E-S2G and S4C**) were first reduced by a factor of ten (bilinear extrapolation) and then processed as described above (ΔG/R). A 20 Hz Butterworth filter was applied to line scan signals shown in the figures, which did not cause significant distortion to the fluorescence waveform.

For analysis of calcium decay kinetics, spine calcium signals were taken from single ROIs positioned on the stimulated spine. Dendritic calcium signals were given by the mean of all detectable signals from ROIs along the dendrite. Calcium signals were peak-normalized and

fitted with a single exponential in Origin to obtain a decay time constant. Only time constants that fitted with $R^2 > 0.5$ were included in the decay kinetics analysis. Visual inspection of poor-fitting calcium signals ($R^2 < 0.5$) showed long-decaying calcium signals that were incompletely captured by the imaging sweep, and these signals primarily occurred during early postnatal development when NMDAR-mediated CICR was most prevalent. As such, this selection criterion is not expected to change the interpretation of our data or conclusions.

Analysis of clustered synaptic weights

To analyze the spatial clustering of synaptic weights, we compared our experimental data to a shuffled dataset using Monte Carlo-type experiments on three independent measures: 1) synaptic weight variance; 2) dendritic branch strength; and 3) synaptic weight matching. Shuffling experiments were performed on an array of model dendrites matched for segment length, spine number and distance between spines to experimentally-probed segments. Experimentally-measured synaptic weights (AMPA/NMDA ratios) were pooled and drawn randomly without replacement to decorate the model dendrites, and measurements were taken from 100 iterations of shuffling. Results did not differ significantly when using 10 and 1000 shuffling iterations. For each dendritic segment where at least 3 spines were probed, the variance in synaptic weight (AMPA/NMDA ratio) was calculated. Experimentally-measured variance values were compared to shuffled data using the Wilcoxon test, and were corrected for multiple comparisons using the Benjamini & Hochberg procedure (Benjamini and Hochberg, 1995). Dendritic segment strength was given by the fraction of silent synapses on the dendritic segment and each segment was assigned to one of three categories: ‘strong’ segments exhibited zero silent spines; ‘intermediate’ segments showed ≤ 50% silent spines; and ‘weak’ dendrites had >50% silent spines. Last, we performed a weight matching analysis to determine the spatial bounds of synaptic weight

clustering. We divided the entire distribution of AMPA/NMDA ratios into three synaptic weight classes (weakest 33%, intermediate 33%, and strongest 33%) and for each experimentally-probed spine, we tallied the instances of weight-matching between neighbor spines (*i.e.,* weak spines neighboring weak spines, strong spines neighboring strong spines) to generate weight-matching counts as a function of distance between spines. Experimental weight-matching counts were significantly difference from shuffled data (95% confidence intervals) within a range of ~15 μm (**Figure 7J**).

Supplemental References

Benjamini Y, Hochberg Y (1995) Controlling the false discovery rate: a practical and powerful approach to multiple testing. Journal of the Royal Statistical Society Series B (Methodological) 57:289-300.

Branco T, Clark BA, Hausser M (2010) Dendritic discrimination of temporal input sequences in cortical neurons. Science 329:1671-1675.

Higley MJ, Sabatini BL (2008) Calcium signaling in dendrites and spines: practical and functional considerations. Neuron 59:902-913.

Pozzo-Miller LD, Pivovarova NB, Leapman RD, Buchanan RA, Reese TS, Andrews SB (1997) Activity dependent sequestration in dendrites of hippocampal neurons in brain slices. J Neurosci 17:8729-8738.

Scheuss V, Yasuda R, Sobczyk A, Svoboda K (2006) Nonlinear [Ca2+] signaling in dendrites and spines caused by activity-dependent depression of Ca2+ extrusion. J Neurosci 26:8183-8194.